Shaping the synapse

The molecular architecture and dynamics of the postsynaptic endocytic zone

Lisa A.E. Catsburg

ISBN: 978-94-6416-901-0

The studies described in this thesis were performed at the department of Cell Biology, Neurobiology and Biophysics at the Faculty of Science of Utrecht University in Utrecht, the Netherlands

Cover design: Lisa Catsburg & Mitch Hartog
Layout: Lisa Catsburg

Printed by Ridderprint
Copyright © Lisa Adrianne Elisabeth Catsburg, 2021
All rights reserved

Shaping the synapse
The molecular architecture and dynamics of the postsynaptic endocytic zone

De synapse vormgeven
De moleculaire architectuur en dynamiek van de postsynaptische endocytische zone
(met Nederlandse samenvatting)

Proefschrift

ter verkrijging van de graad van doctor aan de Universiteit Utrecht
op gezag van de rector magnificus, prof. dr. H.R.B.M. Kummeling,
ingevolge het besluit van het college voor promoties in het openbaar
te verdedigen op

woensdag 8 december 2021
des middags te 12.15 uur

door

Adrianne Elisabeth Catsburg

geboren op 26 augustus 1993 te Zeist

Promotor: Prof. dr. L. Kapitein
Copromotor: Dr. H.D. MacGillavry

Dit proefschrift werd medemogelijk gemaakt met financiële steun van Nederlandse Organisatie voor Wetenschappelijk Onderzoek (NWO-ALWOP. 191)

CONTENT

Chapter 1: General introduction 8

Chapter 2: AMPA receptor trafficking in the developing and mature glutamatergic synapse 30

Chapter 3: Shank proteins couple the endocytic zone to the postsynaptic density to control trafficking and signaling of metabotropic glutamate receptors 62

Chapter 4: Dynamics and nanoscale organization of the postsynaptic endocytic zone 98

Chapter 5: Activity-dependent alterations in the molecular organization of the postsynaptic endocytic zone 132

Chapter 6: General discussion 148

Addendum 160

1

General introduction

Lisa A.E. Catsburg

Department of Cell Biology, Neurobiology and Biophysics at the Faculty of
Science of Utrecht University in Utrecht, the Netherlands

The brain is an immensely complex organ containing over a 100 billion individual neurons. Each neuron contacts hundreds to thousands other neurons, creating complex networks and circuits (Azevedo et al., 2009). Within a network neurons communicate by sending information via the axon and receive information at their dendrites. The site where neurons make contact and communicate with each other, is called a synapse (Figure 1). Here, neurons communicate using neurotransmitters, that are released from presynaptic intracellular vesicles into the synaptic cleft. Neurotransmitters are then detected by receptors at the postsynaptic site, allowing the signal to be transduced. Perhaps the most fascinating aspect of the brain is the ongoing ability to adapt and change neuronal networks and circuits (Shepherd and Huganir, 2007). Changes in the network are modulated at the synaptic level, where low signal transduction weakens the synapse, while high signal transduction strengthens the connection, thereby modulating synaptic transmission and changing the network. This weakening or strengthening of individual synaptic connections is called synaptic plasticity, and forms the foundation of many brain functions, particularly learning and memory.

The most prevalent model regarding the regulation of synaptic plasticity, states that the number and location of postsynaptic receptors determines synaptic strength. At glutamatergic synapses, the synapse is formed on dendritic spines that isolate it from the main dendritic branch (Figure 1). Here, glutamate receptors mediate synaptic transmission and facilitate synaptic plasticity. Fast transmission is mediated by ionotropic receptors, that are divided into three classes based on their agonist selectivity: N-methyl-D-aspartate (NMDA), α-amino3-hydroxy-5-methyl-4-isoxazole proprionic acid (AMPA) and kainate (KA) receptors (Anggono and Huganir, 2012; Shepherd and Huganir, 2007). The ionotropic glutamate receptors are enriched in the postsynaptic density (PSD), a densely packed network of proteins closely attached to the postsynaptic membrane (Figure 1). In contrast to the ionotropic receptors, the metabotropic glutamate receptors 1 and 5 (mGluR1/5) are G-protein coupled receptors (GPCR) that act on longer timescales (Volk et al., 2015), and are enriched in the perisynaptic domain surrounding the PSD (Sheng and Kim, 2011; Tu et al., 1999; Tu et al., 1998). Both ionotropic and metabotropic glutamate receptors undergo dynamic membrane trafficking to control the number of receptors at the synaptic membrane, thereby regulating synaptic plasticity.

Membrane trafficking of glutamate receptors can be divided into multiple processes: exocytosis, lateral diffusion, endocytosis, sorting and recycling. Because excitatory synapses are isolated from the main dendritic branch, local mechanisms are in place to facilitate efficient membrane trafficking. As such, endocytosis of synaptic glutamate receptors is mediated by the postsynaptic endocytic zone (EZ). The EZ is a clathrin-marked structure stably associated with the PSD, and is thought to allow local endocytosis of glutamate receptors. Receptors internalized via the EZ, enter a local recycling mechanism, that retains receptors in intracellular pools and can recycle back to the synaptic membrane (Park et al., 2006; Petrini et al., 2009). The EZ plays a vital role in synaptic plasticity as loss of the EZ results in a depletion of glutamate receptors at the synaptic membrane and thereby hampers plasticity (Lu et al., 2007; Petrini et al., 2009; Scheefhals et al., 2019).

Even though the EZ plays a critical role in synaptic plasticity, we know little about how the EZ is built to sustain local endocytosis of synaptic receptors. Moreover, the mechanisms that control the molecular composition and organization of the EZ are poorly understood. Revealing the organization of the EZ would greatly contribute to our understanding of how the EZ could allow local endocytosis of synaptic glutamate receptors. In the current thesis, we use a multitude of fluorescence microscopy techniques to visualize the architecture and dynamics of the EZ. We primarily focus on clathrin, that thus far is described to be the main protein of the EZ. As clathrin is the key component of clathrin-mediated endocytosis (CME), we and others assume that this is the mechanism of endocytosis at the EZ. While clathrin structures and function have been studied in great depth in non-neuronal cells, what types of clathrin structures are present in neurons, let alone their dynamics, architecture and involvement in receptor trafficking and plasticity are poorly understood. In the following chapters, we reveal the architecture of the EZ and the mechanisms that allow local capture and endocytosis of glutamate receptors that is so important for synaptic functioning.

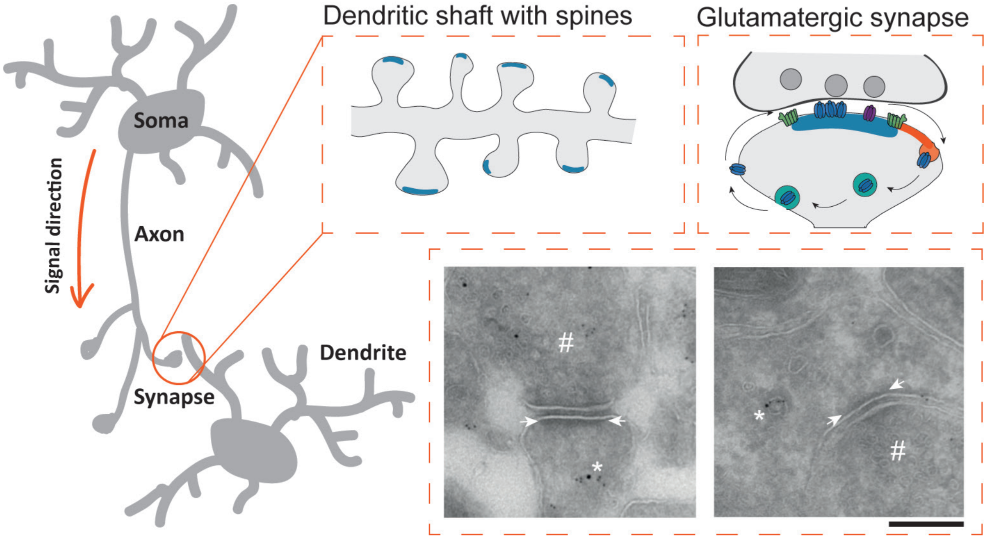

Figure 1: Neuronal communication at glutamatergic synapses. On the left: neurons send information through their axon and receive information at their dendrites. Glutamatergic synapses are often formed on dendritic spines (middle upper panel) characterized as dendritic protrusions, and thereby isolate the synapse from the dendritic shaft. A glutamatergic synapse is characterized by a PSD (blue) that is often associated with an endocytic zone (orange). In the PSD the ionotropic AMPA (blue receptor) and NMDA (purple receptor) receptors are located, while mGluR (green receptor) is enriched at perisynaptic sites. Endocytosis of these receptors is mediated by the EZ, that functions as a hub for local glutamate receptor recycling (right upper panel). In the lower panel the pre -and postsynaptic side of DIV16 neurons are visualized using electronmicroscopy (curtesy of J. van der Beek, Klumperman group). The presynaptic side, indicated with a hash, is filled with vesicles containing neurotransmitters that are released into the synaptic cleft and received by receptors that reside in the PSD (between the arrows). Clathrin-coated vesicles are present inside the spine, close to the PSD (asterisk). Scalebar: 200 nm.

CLATHRIN STRUCTURE AND ASSEMBLY

Clathrin is a highly conserved proteins among organisms. A single clathrin molecule consists of a heavy chain (~190kDa) and a smaller light chain (~25kDa), that selfassemble into a trimeric clathrin triskelion. Within a triskelion the heavy chains interact with each other in the central hub, and extent their legs outwards, to contact other triskelia. Light chains bind the heavy chain at their proximal end, and reach to the heavy chain knee, where they regulate the characteristics and bending capacity of the heavy chain (Figure 2) (Dannhauser et al., 2015; Kirchhausen et al., 1983; Ungewickell, 1983). Under physiological conditions, clathrin triskelia polymerize into spheres, which is the energetically favored conformation (Ahle and Ungewickell, 1986; Ungewickell and Ungewickell, 1991; Van Jaarsveld et al., 1981; Wilbur et al., 2010). These spheres are composed of a mix of clathrin pentagons and hexagons that physically force the clathrin triskelia into a dome-like structure. In contrast to these prototypical clathrin cages, large hexagonal clathrin assemblies have also been observed. These hexagonal assemblies are flat, a conformation that can only be obtained in the presence of clathrin adaptor proteins or at low pH, causing the light chain to retract from the heavy chain knee, thereby changing bending capacity and allowing hexagonal clathrin assemblies.

During clathrin-mediated endocytosis, clathrin polymerizes into a pentagon-containing spherical structure at the plasma membrane, ultimately resulting in closed clathrin-coated vesicles. These assemblies are small (<30,000 nm^2) and transient: rapid assembly and disassembly of clathrin-coated vesicles typically takes place in <120 sec. In contrast, hexagonal assemblies are described as flat lattices or plaques that lie directly under the plasma membrane (Grove et al., 2014). Flat lattices are large (>100,000 nm^2) and exceptionally stable, with lifetimes reported up to one hour (Grove et al., 2014; Saffarian et al., 2009). Their function has been a matter of heavy debate, as a hexagonal conformation of clathrin physically hampers the formation of spheres that is needed for vesicle formation. However, recent studies show the presence of clathrin adaptor proteins at the edge of lattices that allow the formation of vesicles from the edge (Sochacki et al., 2017). Moreover, several studies show the endocytic capacity of flat lattices (Grove et al., 2014; Leyton-Puig et al., 2017), which has led to the current hypothesis that flat lattices function as endocytic hubs that allow for specific internalization of membrane components.

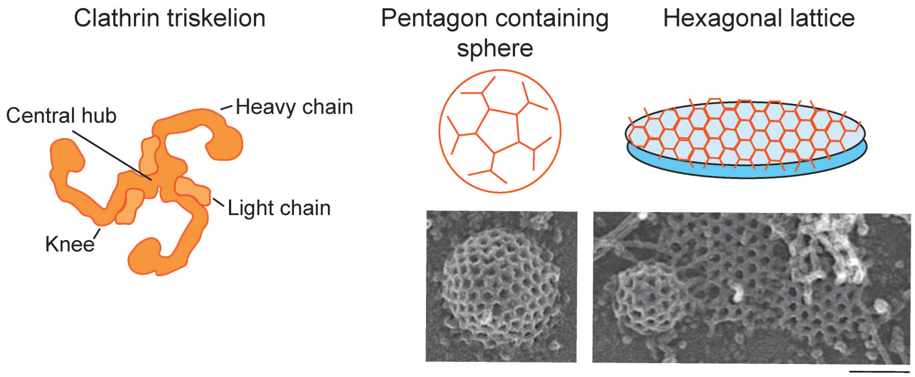

Figure 2: Structure and assembly of clathrin. Illustration of a clathrin triskelion containing three heavy chains and three light chains (left). Clathrin triskelia assemble into a pentagon containing structure (middle), while flat lattices are built from hexagonal clathrin assemblies (right). The lower panel represents an example image obtained from cryo-electron microscopy (EM) in HeLa cells, showing vesicle formation (lower left) and a flat lattice where vesicles are formed from the edge area (lower right). The EM image was copied from Sochacki et al. 2017 (Sochacki et al., 2017).

MECHANISMS OF ENDOCYTOSIS

Clathrin-mediated endocytosis

Clathrin-mediated endocytosis (CME) is the primary route for the internalization of membrane components and nutrients and is highly conserved among cells. Although the name originates from its key component clathrin, tens of other endocytic proteins are involved in the formation of clathrin-coated vesicles, including clathrin-adaptors and scaffolding proteins.

CME consist of five sequential yet partially overlapping steps: initiation, cargo selection, coat assembly, scission and uncoating. Each step is highly organized and requires precise temporal recruitment of multiple endocytic proteins to the site of membrane nucleation. Clustering at the membrane can occur random, but most often specific membrane sites are repeatedly used, suggesting the presence of hotspots (Merrifield et al., 2005; Nunez et al., 2011). Especially in neuronal cells, such localized endocytosis is often observed (Blanpied et al., 2002). It might be suggested that specific membrane content (e.g. lipids), or other membrane domains are in place to facilitate the favoring of CME. For example, any endocytic proteins have phosphatidylinositol 4,5-bisphosphate (PIP2) binding domains, which was shown to be necessary to initiate CME, suggesting that PIP2 enriched membranes might be favored for CME (Antonescu et al., 2011; Zoncu et al., 2007).

Among the early adaptors that bind PIP2 is adaptor protein 2 (AP2). AP2 is considered a key component of CME and recruits other scaffolds like clathrin, epidermal growth factor receptor substrate 15 (Eps15) and intersectin to endocytic sites (Beacham et al., 2019; Gaidarov and Keen, 1999; Kadlecova et al., 2017; Mettlen et al., 2018; Owen et al., 2000; Shih et al., 1995; Traub et al., 1999). In parallel, F-BAR domain containing only protein 1 (FCHO) is recruited to facilitate membrane curvature. FCHO, Eps15, intersectin and AP2 are known as the ‘pioneer module’ that are responsible for the initiation of pits. Even though the temporal recruitment of endocytic proteins is well established (Cocucci et al., 2012; Taylor et al., 2011), which of these proteins is the absolute first is not entirely understood. Several studies suggest that FCHO is the first, recruiting AP2, Eps15 and clathrin to the membrane (Henne et al., 2010). However, other studies show that pit initiation is not affected in the absence of FCHO, but further growth is halted (Cocucci et al., 2012), suggesting that FCHO might be part of a complex that facilitates endocytosis. Indeed, FCHO, Eps15, intersectin and epsins form a complex to stabilize membrane curvature (Cocucci et al., 2012; Henne et al., 2010; Saffarian et al., 2009; Tebar et al., 1996). Intriguingly, at flat clathrin structures endocytic proteins are stably maintained, similar as clathrin (Grove et al., 2014). This further raises the question what signal initiates endocytosis, as the presence of endocytic proteins does not necessarily induce endocytosis.

Some studies suggest that receptor activation initiates endocytosis. However, it remains unclear whether specific cargoes contribute to initiation, or are simply passengers that are recruited after initiation. It is likely that initiation and cargo selection happen at the same time as most early arriving endocytic proteins have a dual function in pit initiation and cargo selection. For example, FCHO also has a cargo binding domain (Reider et al., 2009) and clathrin assembly lymphoid myeloid leukemia protein (CALM), another early-arriving protein, binds PIP2, facilitates membrane bending and binds specific cargo (Chidambaram et al., 2008). Moreover, while Eps15 and epsins specifically recognize ubiquitinated cargo (Sorkina et al., 2006; Traub, 2009; Wendland, 2002), ß-arrestin is known to selectively bind specific phosphorylated motifs (Ferguson et al., 1996; Goodman et al., 1996), suggesting that posttranslational modifications of cargo contribute to selectivity.

After initiation and cargo recruitment the clathrin coat is assembled and coupled to AP2. Initially, it was assumed that clathrin polymerization mediates further membrane bending and induces higher curvature (Hinrichsen et al., 2006). However, the force generated by clathrin is insufficient to deform the membrane, and it is more likely that clathrin senses membrane curvature rather than deforming it (Zeno et al., 2021). Another mechanism promoting maturation of the budding vesicle involves the actin cytoskeleton that generates a pulling and pushing force to facilitate vesicle maturation (Boulant et al., 2011; Ferguson et al., 2009). This force is generated by local actin polymerization that generates a flow from the base of the invagination to the budding vesicle. The coupling of actin to clathrin, for example by Hip1R, then transmits this force to bend the membrane and push the vesicle into the cytosol (Kaksonen and Roux, 2018; Mooren et al., 2012). Interestingly, inhibiting the clathrin-Hip1R interaction results in loss of lattices, but transient pit formation remains unaffected (Saffarian et al., 2009). Similarly, the Hip1R binding protein cortactin, that stimulates branching of actin, is very abundant at lattices but the overall levels at pits is very low (Saffarian et al., 2009), showing that the actin cytoskeleton and adaptors have differential roles in pit formation and at lattices. While at transient pits, actin facilitates vesicle maturation, at lattices actin most likely has a dual function in the maintenance of the clathrin structure and perhaps facilitating endocytosis (Leyton-Puig et al., 2017; Saffarian et al., 2009).

When budding of the vesicle is almost completed, N-BAR domain-containing proteins, like amphiphysin, endophilin and sorting nexin 9 (SNX9) are recruited to form the neck of the vesicle. Finally, dynamin-2, a GTPase, polymerizes around the neck and severs the vesicle from the membrane. The now detached clathrin-coated vesicle, is rapidly uncoated, and clathrin disassembles into triskelia mediated by heat shock cognate 70 (HSC70) and auxilin. The naked vesicle fuses with endosomal compartments, from where the cargo is either sorted for degradation or recycling. In mammalian cells, two pathways of recycling have been described, the so called ‘long loop’ where vesicles are transported to, and fused with intracellular endosomal compartments, and the ‘short loop’ where vesicles are locally redirected to the membrane (Li and DiFiglia, 2012; Moretto and Passafaro, 2018). It has been proposed that in such a short-loop recycling pathway, the acidity of the vesicles drops to around pH 6, which is sufficient to dissociate the majority of ligands from the receptor, without damaging the cargo itself (Maxfield and McGraw, 2004). However, what exactly determines the fate of specific cargoes is not yet fully understood.

Clathrin-independent pathways (CIE)

Apart from the classic CME pathway, also other, clathrin-independent pathways mediating the uptake of membrane components have been described. Caveolar-type endocytosis (CTE) was long thought to be the second most common route for the endocytosis of nutrients and membrane components. The main protein in CTE is caveolin, that unlike clathrin, is embedded in the membrane where it adopts a hairpin-like structure with both the N- and C-terminus exposed to the cytoplasm. This

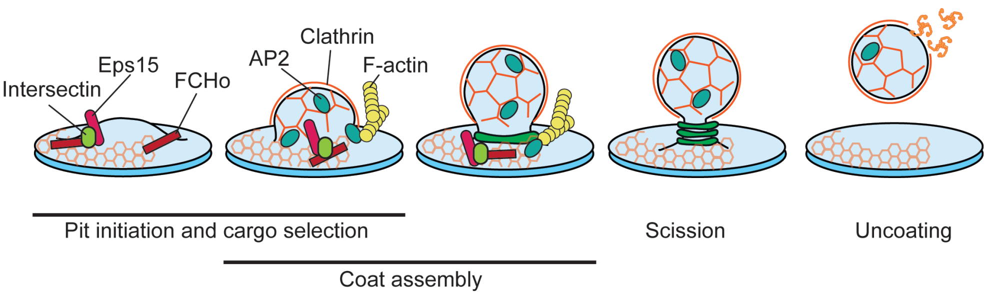

Figure 3: The five steps of clathrin-mediated endocytosis. In the early stages the pioneer module that includes AP2, FCHO, Eps15 and intersectin are present at the membrane and facilitate initial membrane curvature and cargo selection. Next, the clathrin coat is assembled and various adaptor proteins and the actin cytoskeleton facilitate further membrane bending and vesicle formation. The vesicle is released from the plasma membrane after scission, mediated by dynamin-2. The clathrin coat is then disassembled and the vesicle fuses with other endosomal compartments.

conformation contributes to the typical spike-like coat found on caveolae (Doherty and McMahon, 2009b). Caveolin oligomers are stabilized by binding to cholesterol and sphingolipids. Therefore, caveolae are often associated with lipid rafts and were thought to regulate lipid homeostasis, but other functions like signal transduction have been shown as well (Parton, 2018). However, this signal transduction is most likely not due to endocytosis, but rather the result of membrane stretching. Recent studies proposed that caveolae function as mechano-sensing membrane domains, rather than an endocytic pathway (Sinha et al., 2011). Upon membrane stretching caveolae flatten and thereby release inhibited receptors that are localized in caveolae. These receptors then diffuse laterally over the membrane and start signaling. Moreover, upon membrane stretching, cavins, that are binding partners of caveolin, are released into the cytosol and initiate intracellular responses (Ferreira and Boucrot, 2018; Lamaze et al., 2017; Sinha et al., 2011). Interestingly, although caveolin is expressed in neurons, and is important for development, cell migration and intracellular signaling, caveolae have never been observed in neurons (Breuer et al., 2020; Parton, 2018; Stern and Mermelstein, 2010).

Similar to CTE, clathrin-independent carrier/GPI-AP-enriched early endosome compartment (CLIC/GEEC) -type endocytosis is associated with lipid-based cargo and is involved in the regulation of plasma membrane homeostasis. CLIC/GEEC adopts a long tubular-like morphology, but seems to lack a clear coat (Kirkham et al., 2005). CLIC/GEEC is both clathrin -and dynamin independent, but heavily depends on the RhoGTPase Cdc42, BAR domain containing proteins and the actin cytoskeleton (Chadda et al., 2007; Ferreira and Boucrot, 2018). Among these BAR proteins is GRAF1 that marks and controls CLIC/GEEC formation, and even though GRAF1 binds dynamin-2, the budding of CLIC/GEEC is independent of dynamin and rather relies on forces generated by the actin cytoskeleton. As such, it is believed that friction generated by actin and BAR proteins are responsible for budding and scission from the membrane. Interestingly, CLIC/GEEC is solely a constitutive process and content endocytosed via CLIC/GEEC rapidly recycles back to the plasma membrane (Kirkham et al., 2005).

Another mode of clathrin-independent endocytosis is Arf6-associated endocytosis. Arf6 is a small GTPase that regulates trafficking between the plasma membrane and endosomal compartments. Arf6 undergoes constant cycling between an active and inactive state, which stimulates the generation of PIP2 at the plasma membrane, and it should therefore be noted that Arf6 can indirectly affect CME, that critically relies on PIP2 (Van Acker et al., 2019). Moreover, Arf6 is activated by dynamin-2 and binds AP2 in clathrin-coated pits to facilitate fast recycling after endocytosis (Montagnac et al., 2011; Van Acker et al., 2019). This close connection to CME makes it difficult to distinguish between the two pathways. Nevertheless, Arf6-associated endocytosis is clathrin -and dynamin independent, but highly depends on cholesterol and the actin cytoskeleton. Moreover, cargo internalized via Arf6-associated endocytosis is distinct from that obtained from CME (Grant and Donaldson, 2009; Mayor et al., 2014; Naslavsky et al., 2003). How Arf6-associated endocytosis is regulated is yet to be determined. Interestingly, Arf6-mediated endocytosis shares many commonalities with the CLIC/GEEC pathway. Although, CLIC/GEEC and Arf6-associated endocytosis are considered as separate, clear evidence is lacking and it is possible that Arf6 regulates CLIC/GEEC subtypes (Doherty and McMahon, 2009).

Finally, fast endophilin mediated endocytosis (FEME) is a clathrin-independent but dynamin-dependent pathway. Similar to CME, FEME regulates the internalization of specific cargoes, including adrenergic -and dopaminergic receptors and potentially AMPA receptors (Casamento and Boucrot, 2020). However, FEME is much faster than CME (<10 seconds) and is therefore often associated with receptor hyperstimulation, hormone release and stress reactions that require immediate response. As the name suggests, FEME heavily depends on endophilins, a group of BAR domain containing proteins, that sense, stabilize and promote membrane curvature (Casamento and Boucrot, 2020). Even though, endophilins are also involved in CME, they only have a supporting role, while during FEME they are essential. FEME is not constitutively active, and requires a pre-enrichment of endophilin at the plasma membrane. Moreover, while clathrin-coated vesicles rapidly uncoat after being released from the membrane, endophilins remain attached to FEME generated vesicles until they fuse with endosomes (Boucrot et al., 2015).

GLUTAMATE RECEPTOR ENDOCYTOSIS

At glutamatergic synapses, endocytosis has an important regulatory role controlling the number of receptors at the synaptic membrane that are available for activation. Internalization of glutamate receptors is primarily clathrin -and dynamin dependent, although evidence for clathrin-independent glutamate receptor endocytosis is emerging (Anggono and Huganir, 2012; Carroll et al., 1999; Dale et al., 2001; Fourgeaud et al., 2003; Francesconi et al., 2009; Glebov et al., 2015; Man et al., 2000; Pula et al., 2004). It is assumed that CME of glutamate receptors is facilitated by the EZ, as glutamate receptors are preferentially internalized in close proximity to the PSD (Rosendale et al., 2017), and the EZ is marked by clathrin (Blanpied et al., 2002). Interestingly, receptors internalized at this specific location are sorted for recycling rather than degradation, indicating a regulatory role for the EZ. However, whether endocytosis at the EZ is indeed CME, or if CIE is also facilitated by this structure has never been shown. Moreover, it is unclear what initiates CME versus

CIE, and whether the route of internalization contributes to receptor recycling or degradation is not known.

Constitutive endocytosis

Constitutive trafficking refers to the trafficking of receptors between the plasma membrane and intracellular endosomal compartments under basal conditions and occurs independent of ligand activation. Both ionotropic and metabotropic glutamate receptors undergo constitutive endocytosis. While AMPA receptors traffic rapidly and constitutively between the plasma membrane and intracellular stores to regulate fast changes at the synaptic membrane (Lira et al., 2020), constitutive endocytosis of NMDA receptors is minimal. The metabotropic glutamate receptor mGluR5 traffics constitutively, but to what extent is not clear (Fourgeaud et al., 2003; Trivedi and Bhattacharyya, 2012). Constitutive endocytosis of both receptor classes can occur independent of clathrin and dynamin (Anggono and Huganir, 2012; Carroll et al., 1999; Dale et al., 2001; Fourgeaud et al., 2003; Francesconi et al., 2009; Glebov et al., 2015; Man et al., 2000; Pula et al., 2004). For both the ionotropic and metabotropic glutamate receptors Arf6-associated endocytosis has been suggested to mediate constitutive internalization in spines (Glebov et al., 2015; Lavezzari and Roche, 2007; Zheng et al., 2015). Moreover, constitutive trafficking of mGluR5 has been suggested to be mediated by caveolin (Francesconi et al., 2009). Nevertheless, clathrin-mediated constitutive endocytosis has been shown as well (Bredt and Nicoll, 2003; Malinow and Malenka, 2002; Man et al., 2000; Sheng and Kim, 2002). A commonly used receptor to study this process is the transferrin receptor (TfR), that traffics constitutively via CME. In neurons, endocytosis of the TfR does not seem to be localized to a specific location but randomly occurs in both spine and dendrite. In contrast, AMPA receptors were preferentially internalized in close proximity to the PSD (Rosendale et al., 2017). Moreover, candidate plasticity gene 2 (CPG2) regulates constitutive endocytosis of AMPA receptors and is specifically localized to the EZ, suggesting that constitutive endocytosis of AMPA receptor is indeed mediated by the EZ (Cottrell et al., 2004). Interestingly, constitutive endocytosis of glutamate receptors often results in fast recycling, thereby contributing to the maintenance of the synaptic membrane (Petrini et al., 2009; Trivedi and Bhattacharyya, 2012). To this date, the mechanisms of recycling remain elusive, and whether recycling and exocytosis are constitutive or agonist-induced processes is not fully understood. However, some key players in recycling have been identified. For example, constitutive recycling of AMPA receptors is regulated by cortactin. Removing cortactin results in lysosomal targeting, suggesting that cortactin regulates endo-lysosomal targeting of AMPA receptors during constitutive trafficking (Parkinson et al., 2018).

Activity-dependent endocytosis

Changes in synaptic strength are mediated by the trafficking of AMPA receptors to and from the PSD. While during long-term depression (LTD) AMPA receptors are removed from the PSD resulting in decreased synaptic strength, long-term potentiation (LTP) enhances synaptic strength and coincides with the recruitment and clustering of AMPA receptors in the PSD. There are two major forms of LTD: NMDA receptor dependent LTD (NMDA-LTD) and metabotropic glutamate receptor LTD (mGluR-LTD), that both lead to the internalization of AMPA receptors. Both types

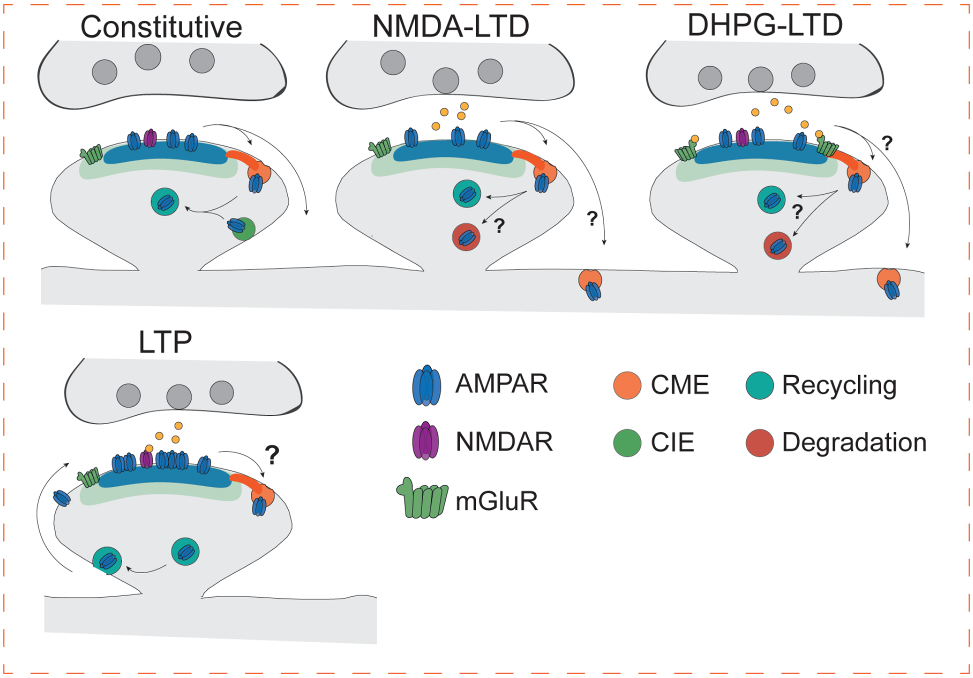

Figure 4: Constitutive and activity-induced glutamate receptor trafficking at the glutamatergic synapse. Glutamatergic synapse is characterized by a PSD (blue area), where ionotropic receptors are located, surrounded by the perisynaptic region (light green area), where metabotropic receptors are enriched. The EZ (orange area) is coupled to the PSD. During constitutive trafficking, endocytosis is most likely mediated by the EZ, but other CIE mechanisms inside the spine have been described as well. Constitutive endocytosis often leads to recycling of receptors (upper left). During LTD, receptors are endocytosed via CME, however the location of CME after specific types of LTD is not fully understood and might occur in the EZ but also at the dendritic shaft (upper middle and right panel). Moreover, different types of stimuli determine recycling or degradation. During LTP, exocytosis of AMPARs takes place, but whether and where endocytosis also occurs during LTP is not fully understood (lower panel).

of LTD can be induced by low frequency stimulation or selective agonists such as NMDA and DHPG, to activate NMDA -and mGluR receptors, respectively. This type of stimulation results in a modest rise in intracellular calcium, triggering LTD (Kang and Kaang, 2016; Luscher and Malenka, 2012; Moult et al., 2006; Snyder et al., 2001). LTD is often described to induce regulated clathrin -and dynamin-dependent endocytosis of AMPA receptors (Carroll et al., 1999; Ehlers, 2000; Luscher et al., 1999; Tao-Cheng et al., 2011), that are sorted to endosomal compartments for recycling (Ehlers, 2000). Moreover, NMDA-LTD induces endocytosis near the PSD at clathrin marked structures, suggesting that NMDA-LTD results in EZ-mediated endocytosis (Rosendale et al., 2017). On the other hand, application of AMPA, that also induces AMPA receptor endocytosis, leads to lysosomal targeting and degradation, suggesting that different stimuli affect the trafficking pathway (Beattie et al., 2000; Ehlers, 2000). However, whether endocytosis after AMPA application is mediated by the EZ is not known. Compared to NMDA-LTD, the mechanisms of endocytosis after mGluR-LTD are less well studied, although mGluR-LTD was recently shown to be mediated by myosin6, which binds AP2 after DPHG application, suggesting that mGluR-LTD is regulated by CME (Wagner et al., 2019). However, whether endocytosis occurs at the EZ or at the dendritic shaft was not determined.

While LTD is triggered in response to low levels of calcium, high calcium levels result in the induction of LTP. Originally, LTP research focused on the involvement of exocytosis and recruitment of AMPA receptors to the PSD. Indeed, exocytosis was shown to occur around the PSD (Kennedy et al., 2010), and recruitment and capture of lateral diffusing AMPA receptors in the PSD is necessary for efficient LTP induction (Chen et al., 2015; Opazo and Choquet, 2011; Opazo et al., 2010). However, recent studies suggest that during LTP not only exocytosis takes place, but endocytosis is increased as well (Sumi and Harada, 2020). Indeed, an earlier study showed that upon LTP the number of clathrin-coated pits inside the spine increases, suggesting enhanced CME (Puchkov et al., 2011). Moreover, LTP increased dynamin-dependent endocytosis of AMPA receptors (Zheng et al., 2015). Also, the small-conductance calcium-activated potassium channel 2 (SK2), that resides in the PSD, was shown to be internalized in response to LTP (Lin et al., 2010). Interestingly, SK2 endocytosis was hampered when exocytosis of AMPA receptors was blocked. These findings suggest that activity-dependent endocytosis and exocytosis in spines highly are coupled processes. However, the mechanisms underlying LTP-induced endocytosis and how this is coupled to exocytosis remain undetermined.

THE POSTSYNAPTIC ENDOCYTIC ZONE

The EZ is marked by a clathrin assembly that is stably associated with the PSD (Blanpied et al., 2002) via a Shank-Homer1c-Dynamin3 interaction, that retains the EZ in close proximity to the PSD (Lu et al., 2007). PSD-EZ coupling is crucial for glutamate receptor trafficking as removing either one of these proteins uncouples the EZ from the PSD and depletes the number of glutamate receptors at the synapse (Lu et al., 2007; Scheefhals et al., 2019). Interestingly, a nonsense mutation in Shank2 that is associated with autism spectrum disorder, was unable to rescue PSD-EZ coupling after Shank knock down (Scheefhals et al., 2019). Moreover, a mutation in OPHN1 that is associated with X-linked mental retardation, inhibits Homer1c binding and uncouples the EZ from the PSD (Nakano-Kobayashi et al., 2014), implying the crucial role of the EZ and PSD coupling in brain functioning. The tight coupling of the EZ to the PSD most likely facilitates the local capture of receptors from the synapse. Indeed, a study showed that receptors that are uncoupled from the PSD diffuse across the membrane until they contact the EZ, where they are rapidly immobilized, suggesting that the presence of an EZ adjacent to the PSD allows efficient capture and immobilization of receptors (Petrini et al., 2009). The mechanisms that target receptors to the EZ are only starting to emerge. For example, PICK1 a proteins that was previously described to regulate AMPA receptor trafficking is now known to specifically direct AMPA receptors from the PSD to the EZ upon NMDA-LTD and constitutively (Maria Fiuza et al., 2017). Moreover, PICK1 promotes dynamin-2 polymerization, and remains bound to the receptor after internalization to facilitates recycling (Anggono et al., 2013; Widagdo et al., 2016). Interestingly, while some studies show that PICK1 is involved in lysosomal targeting of AMPA receptors (Koszegi et al., 2017; Madsen et al., 2012), other studies show that PICK1 targets

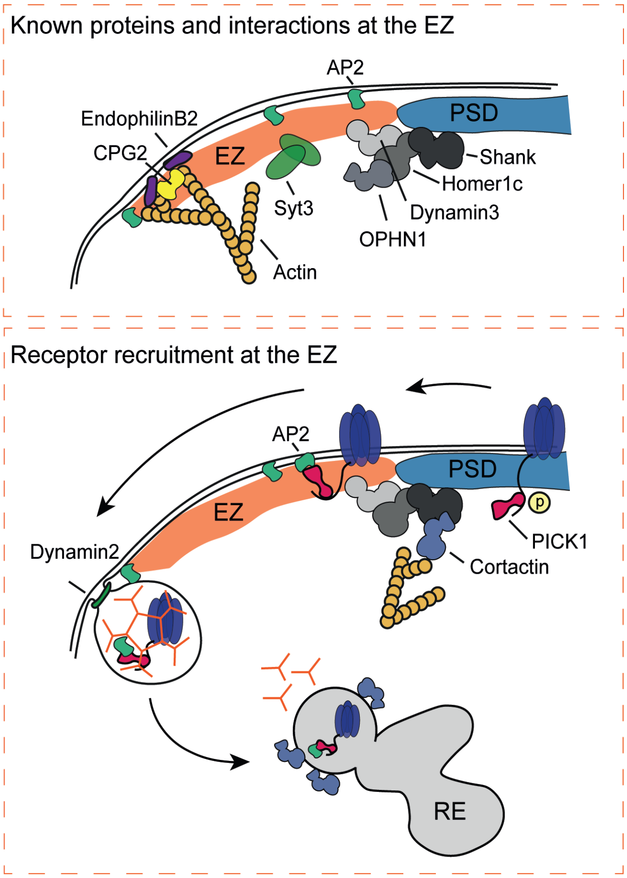

Figure 5: Known interactions and proteins involved in coupling, maintenance and receptor recruited at the EZ. The EZ (orange area) is physically coupled to the PSD (blue area) via a Shank-Homer1c-Dynamin3 interaction. Recently, OPHN1 was also identified to couple the EZ to the PSD. Other proteins localized to the EZ are CPG2, EndophilinB2 and Synaptotagmin3 (syt3). Also PICK1 localized to the EZ and directs synaptic receptors to the EZ by binding to AP2. Moreover, PICK1 and cortactin facilitate recycling

AMPA receptors to recycling compartments (Anggono et al., 2013; Lin and Huganir, 2007), suggesting that PICK1 has a more general role in regulating endocytosis, and third parties are involved to determine recycling or degradation.

Even though EZ-mediated endocytosis is well acknowledged, the lack of clathrin dynamics at the EZ has been a long-standing dilemma, as disappearance of clathrin from endocytic sites had long been a hallmark of vesicle formation. However, LTD induction does not change clathrin stability at the EZ (Blanpied et al., 2002). Therefore the question was raised whether actual endocytosis takes place at the EZ. However, early EM studies show clathrin-coated pits and vesicle formation inside the spine at approximately 200-600 nm distance from the PSD, that coincides with other endocytic proteins like dynamin-2 and AP2 (Rácz et al., 2004). Moreover, a study using high temporal resolution imaging together with pH-sensitive fluorophores showed that AMPA receptors are internalized in close proximity to the PSD, and coincide with the location of clathrin-coated structures (Rosendale et al., 2017). Together these studies indicate that even though the EZ remains optically stable and clathrin remains tightly coupled to the EZ upon internalization, multiple rounds of endocytosis can take place at the EZ.

Apart from clathrin, only a few other proteins have been found to colocalize with the EZ. Among those are CPG2 (Cottrell et al., 2004), PICK1 (Maria Fiuza et al., 2017) and syntaptotagmin-3 (Awasthi et al., 2018). CPG2 was identified as a specific marker of the EZ that regulates both activity-induced and constitutive internalization of glutamate receptors. CPG2 knockdown resulted in reduced internalization of AMPA receptors, most likely due to a defect in clathrin uncoating, thereby halting further endocytosis (Cottrell et al., 2004). Later, it was found that PKA-dependent activation of CPG2 anchors the endocytic machinery to the actin cytoskeleton to regulate endocytosis (Loebrich et al., 2016; Loebrich et al., 2013). Recently, synaptotagmin-3 was also shown to facilitate endocytosis of AMPA receptors at the EZ. Synaptotagmin-3-mediated internalization is calcium-dependent and only occurs during agonist stimulation (Awasthi et al., 2018). Together, these results suggest that both constitutive and agonist-induced trafficking are mediated by the EZ, but specific adaptors are in place to facilitate these specific processes, and perhaps downstream sorting.

Once receptors are endocytosed via the EZ they are thought to enter a local recycling mechanism, where receptors are stored in intracellular endosomal compartments to recycle back to the membrane in a constitutive or agonist-induced manner. Indeed, using an inactive form of Rab11, a marker of recycling endosomes, blocked AMPA receptor recycling and resulted in a loss of synaptic receptors (Petrini et al., 2009). Moreover, induced removal of recycling endosomes from spines decreased the number of AMPA receptors in the synapse (Esteves da Silva et al., 2015), indeed suggesting that local endocytosis facilitates local recycling. However, whether EZ-mediated endocytosis always leads to recycling, or whether some receptors are still targeted for degradation is not known.

SCOPE OF THE THESIS

The EZ is a clathrin-marked structure that is tightly coupled to the PSD, to facilitate local endocytosis and recycling of glutamate receptors. Without the EZ, glutamate receptors are lost from the PSD. Therefore, the EZ plays a vital role in facilitating efficient synaptic plasticity and is essential for proper brain functioning. Although the function of the EZ is evident, how the EZ is built to sustain endocytosis is not known. For example, whether other endocytic proteins are enriched at the EZ has never been studied. Moreover, the dynamics and nanoscale organization of the EZ have never been resolved. This spatiotemporal information about the architecture of the EZ was previously inaccessible due to limited resolution imaging techniques. Recent advances in fluorescence microscopy have allowed for greater temporal and spatial resolution. For example, super-resolution techniques such as stimulated emission depletion and single-molecule localization microscopy allow us to visualize distinct features that are 50-200 nm apart (Sahl et al., 2017).This high spatial resolution is needed to properly resolve cellular structures such as the EZ.

In the current thesis, we took advantage of these super-resolution techniques to explore the dynamics and architecture of the EZ. Combined with live-cell imaging we were able to visualize critical cellular processes that have been hidden for a long time. Therefore, this work provides new insights into the organization, function and mechanisms that underlie EZ function. These novel fundamental observations greatly contribute to our understanding of synapse biology and opens up many possibilities for future research. In the past decades, many studies looked into the mechanisms of AMPA receptor trafficking. In **chapter 2** we discuss these mechanisms in the developing and mature glutamatergic synapse. This chapter extensively reviews our current understanding of glutamatergic synapse formation, and how AMPA receptor trafficking is regulated throughout development. Moreover, we discuss the mechanisms at mature synapses, that are crucial for the maintenance of the synaptic membrane.

Unlike AMPA receptors, the mechanisms of mGluR endocytosis are poorly understood. In **chapter 3** we reveal that agonist-induced internalization of mGluR5 is mediated by the EZ. Moreover, we show that Shank proteins control mGluR trafficking and signaling, by coupling essential components of the endocytic machinery to the PSD. We propose that Shank proteins anchor the EZ to allow local mGluR trafficking and recycling, thereby balancing the surface expression of mGluRs and modulating synaptic functioning. These findings provide novel insights into the spatial and temporal control of mGluR activity, that is critical for the regulation of synaptic plasticity.

In **chapter 4**, we reveal the dynamics and nanoscale organization of the EZ. We show that the EZ is a stable, highly organized endocytic machinery that contains a multitude of endocytic proteins. We reveal that these endocytic proteins are differentially retained at the EZ and are in part coupled to the PSD. These novel insights provide strong support that the EZ is specifically organized to optimize efficient capture of synaptic components. This local uptake of synaptic components ensures the maintenance and composition of the synaptic membrane via local recycling. As such, these finding have a significant impact on our understanding on how the EZ facilitates local receptor trafficking, that underlie synaptic transmission and plasticity.

In **chapter 5** we show that the EZ reorganizes in an activity-dependent manner. In this chapter we show that the EZ splits after LTP resulting in long-lasting structural alterations. Intriguingly, NMDA-LTD did not change EZ characteristics, while DHPG-LTD induced rapid increase in the number of CCSs per PSD. Although the nature of this second structure is not yet determined, these novel results greatly aid our understanding of synaptic plasticity mechanisms. Moreover, new questions are raised: does endocytosis support LTP and if so, what are the functional implications? Also, how does reorganization of synaptic and perisynaptic structures that accompany synaptic activity impact or facilitate synaptic functioning?

This thesis will we concluded with a general discussion (**chapter 6**), in which I discuss the key findings of this thesis, place them in broader context and provide recommendations for future research and perspectives.

REFERENCES

Ahle, S., and Ungewickell, E. (1986). Purification and properties of a new clathrin assembly protein. EMBO J 5, 3143-3149.

Anggono, V., and Huganir, R.L. (2012). Regulation of AMPA receptor trafficking and synaptic plasticity. Curr Opin Neurobiol 22, 461-469.

Anggono, V., Koc-Schmitz, Y., Widagdo, J., Kormann, J., Quan, A., Chen, C.M., Robinson, P.J., Choi, S.Y., Linden, D.J., Plomann, M., et al. (2013). PICK1 interacts with PACSIN to regulate AMPA receptor internalization and cerebellar long-term depression. Proc Natl Acad Sci U S A 110, 13976-13981.

Antonescu, C.N., Aguet, F., Danuser, G., and Schmid, S.L. (2011). Phosphatidylinositol-(4,5)-bisphosphate regulates clathrin-coated pit initiation, stabilization, and size. Mol Biol Cell 22, 2588-2600.

Awasthi, A., Ramachandran, B., Ahmed, S., Benito, E., Shinoda, Y., Nitzan, N., Heukamp, A., Rannio, S., Martens, H., Barth, J., et al. (2018). Synaptotagmin-3 drives AMPA receptor endocytosis, depression of synapse strength, and forgetting. Science, eaav1483-eaav1483.

Azevedo, F.A., Carvalho, L.R., Grinberg, L.T., Farfel, J.M., Ferretti, R.E., Leite, R.E., Jacob Filho, W., Lent, R., and Herculano-Houzel, S. (2009). Equal numbers of neuronal and nonneuronal cells make the human brain an isometrically scaled-up primate brain. J Comp Neurol 513, 532-541.

Beacham, G.M., Partlow, E.A., and Hollopeter, G. (2019). Conformational regulation of AP1 and AP2 clathrin adaptor complexes. Traffic 20, 741-751.

Beattie, E.C., Carroll, R.C., Yu, X., Morishita, W., Yasuda, H., von Zastrow, M., and Malenka, R.C. (2000). Regulation of AMPA receptor endocytosis by a signaling mechanism shared with LTD. Nat Neurosci 3, 1291-1300.

Blanpied, T.A., Scott, D.B., and Ehlers, M.D. (2002). Dynamics and regulation of clathrin coats at specialized endocytic zones of dendrites and spines. Neuron 36, 435-449.

Boucrot, E., Ferreira, A.P., Almeida-Souza, L., Debard, S., Vallis, Y., Howard, G., Bertot, L., Sauvonnet, N., and McMahon, H.T. (2015). Endophilin marks and controls a clathrin-independent endocytic pathway. Nature 517, 460-465.

Boulant, S., Kural, C., Zeeh, J.C., Ubelmann, F., and Kirchhausen, T. (2011). Actin dynamics counteract membrane tension during clathrin-mediated endocytosis. Nat Cell Biol 13, 1124-1131.

Bredt, D.S., and Nicoll, R.A. (2003). AMPA receptor trafficking at excitatory synapses. Neuron 40, 361-379.

Breuer, M., Berger, H., and Borchers, A. (2020). Caveolin 1 is required for axonal outgrowth of motor neurons and affects Xenopus neuromuscular development. Sci Rep 10, 16446.

Carroll, R.C., Beattie, E.C., Xia, H., Luscher, C., Altschuler, Y., Nicoll, R.A., Malenka, R.C., and von Zastrow, M. (1999). Dynamin-dependent endocytosis of ionotropic glutamate receptors. Proc Natl Acad Sci U S A 96, 14112-14117.

Casamento, A., and Boucrot, E. (2020). Molecular mechanism of Fast Endophilin-Mediated Endocytosis. Biochem J 477, 2327-2345.

Chadda, R., Howes, M.T., Plowman, S.J., Hancock, J.F., Parton, R.G., and Mayor, S. (2007). Cholesterol-sensitive Cdc42 activation regulates actin polymerization for endocytosis via the GEEC pathway. Traffic 8, 702-717.

Chen, X., Levy, J.M., Hou, A., Winters, C., Azzam, R., Sousa, A.A., Leapman, R.D., Nicoll, R.A., and Reese, T.S. (2015). PSD-95 family MAGUKs are essential for anchoring AMPA and NMDA receptor complexes at the postsynaptic density. Proc Natl Acad Sci U S A 112, E6983-6992.

Chidambaram, S., Zimmermann, J., and von Mollard, G.F. (2008). ENTH domain proteins are cargo adaptors for multiple SNARE proteins at the TGN endosome. J Cell Sci 121, 329-338.

Cocucci, E., Aguet, F., Boulant, S., and Kirchhausen, T. (2012). The first five seconds in the life of a clathrin-coated pit. Cell 150, 495-507.

Cottrell, J.R., Borok, E., Horvath, T.L., and Nedivi, E. (2004). CPG2: A brain- and synapse-specific protein that regulates the endocytosis of glutamate receptors. Neuron 44, 677-690.

Dale, L.B., Bhattacharya, M., Seachrist, J.L., Anborgh, P.H., and Ferguson, S.S. (2001). Agonist-stimulated and tonic internalization of metabotropic glutamate receptor 1a in human embryonic kidney 293 cells: agonist-stimulated endocytosis is beta-arrestin1 isoform-specific. Mol Pharmacol 60, 1243-1253.

Dannhauser, P.N., Platen, M., Böning, H., Ungewickell, H., Schaap, I.A.T., and Ungewickell, E.J. (2015). Effect of Clathrin Light Chains on the Stiffness of Clathrin Lattices and Membrane Budding. Traffic 16, 519-533.

Doherty, G.J., and McMahon, H.T. (2009a). Mechanisms of Endocytosis. Annual Review of Biochemistry 78, 857-902.

Doherty, G.J., and McMahon, H.T. (2009b). Mechanisms of endocytosis. Annu Rev Biochem 78, 857-902.

Ehlers, M.D. (2000). Reinsertion or Degradation of AMPA Receptors Determined by Activity-Dependent Endocytic Sorting. Neuron 28, 511-525.

Esteves da Silva, M., Adrian, M., Schätzle, P., Lipka, J., Watanabe, T., Cho, S., Futai, K., Wierenga, Corette J., Kapitein, Lukas C., and Hoogenraad, Casper C. (2015). Positioning of AMPA Receptor-Containing Endosomes Regulates Synapse Architecture. Cell Reports 13, 933-943.

Ferguson, S.M., Raimondi, A., Paradise, S., Shen, H., Mesaki, K., Ferguson, A., Destaing, O., Ko, G., Takasaki, J., Cremona, O., et al. (2009). Coordinated actions of actin and BAR proteins upstream of dynamin at endocytic clathrin-coated pits. Dev Cell 17, 811-822.

Ferguson, S.S., Downey, W.E., 3rd, Colapietro, A.M., Barak, L.S., Menard, L., and Caron, M.G. (1996). Role of beta-arrestin in mediating agonist-promoted G protein-coupled receptor internalization. Science 271, 363-366.

Ferreira, A.P.A., and Boucrot, E. (2018). Mechanisms of Carrier Formation during Clathrin-Independent Endocytosis. Trends Cell Biol 28, 188-200.

Fourgeaud, L., Bessis, A.S., Rossignol, F., Pin, J.P., Olivo-Marin, J.C., and Hemar, A. (2003). The metabotropic glutamate receptor mGluR5 is endocytosed by a clathrin-independent pathway. J Biol Chem 278, 12222-12230.

Francesconi, A., Kumari, R., and Zukin, R.S. (2009). Regulation of group I metabotropic glutamate receptor trafficking and signaling by the caveolar/lipid raft pathway. J Neurosci 29, 3590-3602.

Gaidarov, I., and Keen, J.H. (1999). Phosphoinositide-AP-2 interactions required for targeting to plasma membrane clathrin-coated pits. J Cell Biol 146, 755-764.

Glebov, O.O., Tigaret, C.M., Mellor, J.R., and Henley, J.M. (2015). Clathrin-independent trafficking of AMPA receptors. J Neurosci 35, 4830-4836.

Goodman, O.B., Jr., Krupnick, J.G., Santini, F., Gurevich, V.V., Penn, R.B., Gagnon, A.W., Keen, J.H., and Benovic, J.L. (1996). Beta-arrestin acts as a clathrin adaptor in endocytosis of the beta2-adrenergic receptor. Nature 383, 447-450.

Grant, B.D., and Donaldson, J.G. (2009). Pathways and mechanisms of endocytic recycling. Nat Rev Mol Cell Biol 10, 597-608.

Grove, J., Metcalf, D.J., Knight, A.E., Wavre-Shapton, S.T., Sun, T., Protonotarios, E.D.,

Griffin, L.D., Lippincott-Schwartz, J., and Marsh, M. (2014). Flat clathrin lattices: stable features of the plasma membrane. Molecular biology of the cell 25, 3581-3594.

Henne, W.M., Boucrot, E., Meinecke, M., Evergren, E., Vallis, Y., Mittal, R., and McMahon, H.T. (2010). FCHo proteins are nucleators of clathrin-mediated endocytosis. Science 328, 1281-1284.

Hinrichsen, L., Meyerholz, A., Groos, S., and Ungewickell, E.J. (2006). Bending a membrane: how clathrin affects budding. Proc Natl Acad Sci U S A 103, 8715-8720.

Kadlecova, Z., Spielman, S.J., Loerke, D., Mohanakrishnan, A., Reed, D.K., and Schmid, S.L. (2017). Regulation of clathrin-mediated endocytosis by hierarchical allosteric activation of AP2. J Cell Biol 216, 167-179.

Kaksonen, M., and Roux, A. (2018). Mechanisms of clathrin-mediated endocytosis. Nature Reviews Molecular Cell Biology 19, 313-326.

Kang, S.J., and Kaang, B.K. (2016). Metabotropic glutamate receptor dependent long-term depression in the cortex. Korean J Physiol Pharmacol 20, 557-564.

Kennedy, M.J., Davison, I.G., Robinson, C.G., and Ehlers, M.D. (2010). Syntaxin-4 defines a domain for activity-dependent exocytosis in dendritic spines. Cell 141, 524-535.

Kirchhausen, T., Harrison, S.C., Parham, P., and Brodsky, F.M. (1983). Location and distribution of the light chains in clathrin trimers. Proc Natl Acad Sci U S A 80, 2481-2485.

Kirkham, M., Fujita, A., Chadda, R., Nixon, S.J., Kurzchalia, T.V., Sharma, D.K., Pagano, R.E., Hancock, J.F., Mayor, S., and Parton, R.G. (2005). Ultrastructural identification of uncoated caveolin-independent early endocytic vehicles. J Cell Biol 168, 465-476.

Koszegi, Z., Fiuza, M., and Hanley, J.G. (2017). Endocytosis and lysosomal degradation of GluA2/3 AMPARs in response to oxygen/glucose deprivation in hippocampal but not cortical neurons. Sci Rep 7, 12318.

Lamaze, C., Tardif, N., Dewulf, M., Vassilopoulos, S., and Blouin, C.M. (2017). The caveolae dress code: structure and signaling. Curr Opin Cell Biol 47, 117-125.

Lavezzari, G., and Roche, K.W. (2007). Constitutive endocytosis of the metabotropic glutamate receptor mGluR7 is clathrin-independent. Neuropharmacology 52, 100-107.

Leyton-Puig, D., Isogai, T., Argenzio, E., Van Den Broek, B., Klarenbeek, J., Janssen, H., Jalink, K., and Innocenti, M. (2017). Flat clathrin lattices are dynamic actin-controlled hubs for clathrin-mediated endocytosis and signalling of specific receptors. Nature Communications 8.

Li, X., and DiFiglia, M. (2012). The recycling endosome and its role in neurological disorders. Progress in Neurobiology 97, 127-141.

Lin, D.T., and Huganir, R.L. (2007). PICK1 and phosphorylation of the glutamate receptor 2 (GluR2) AMPA receptor subunit regulates GluR2 recycling after NMDA receptor-induced internalization. J Neurosci 27, 13903-13908.

Lin, M.T., Lujan, R., Watanabe, M., Frerking, M., Maylie, J., and Adelman, J.P. (2010). Coupled activity-dependent trafficking of synaptic SK2 channels and AMPA receptors. J Neurosci 30, 11726-11734.

Lira, M., Mira, R.G., Carvajal, F.J., Zamorano, P., Inestrosa, N.C., and Cerpa, W. (2020). Glutamatergic Receptor Trafficking and Delivery: Role of the Exocyst Complex. Cells 9.

Loebrich, S., Benoit, M.R., Konopka, J.A., Cottrell, J.R., Gibson, J., and Nedivi, E. (2016). CPG2 recruits endophilin B2 to the cytoskeleton for activity-dependent endocytosis of synaptic glutamate receptors. Current Biology 26, 296-308.

Loebrich, S., Djukic, B., Tong, Z.J., Cottrell, J.R., Turrigiano, G.G., and Nedivi, E. (2013). Regulation of glutamate receptor internalization by the spine cytoskeleton is mediated by its PKA-dependent association with CPG2. Proceedings of the National Academy of Sciences of the United States of America 110, E4548-4556.

Lu, J., Helton, T.D., Blanpied, T.A., Rácz, B., Newpher, T.M., Weinberg, R.J., and Ehlers, M.D. (2007). Postsynaptic Positioning of Endocytic Zones and AMPA Receptor Cycling by Physical Coupling of Dynamin-3 to Homer. Neuron 55, 874-889.

Luscher, C., and Malenka, R.C. (2012). NMDA receptor-dependent long-term potentiation and long-term depression (LTP/LTD). Cold Spring Harb Perspect Biol 4.

Luscher, C., Xia, H., Beattie, E.C., Carroll, R.C., von Zastrow, M., Malenka, R.C., and Nicoll, R.A. (1999). Role of AMPA receptor cycling in synaptic transmission and plasticity. Neuron 24, 649-658.

Madsen, K.L., Thorsen, T.S., Rahbek-Clemmensen, T., Eriksen, J., and Gether, U. (2012). Protein interacting with C kinase 1 (PICK1) reduces reinsertion rates of interaction partners sorted to Rab11-dependent slow recycling pathway. J Biol Chem 287, 12293-12308.

Malinow, R., and Malenka, R.C. (2002). AMPA receptor trafficking and synaptic plasticity. Annu Rev Neurosci 25, 103-126.

Man, H.Y., Lin, J.W., Ju, W.H., Ahmadian, G., Liu, L., Becker, L.E., Sheng, M., and Wang, Y.T. (2000). Regulation of AMPA receptor-mediated synaptic transmission by clathrin-dependent receptor internalization. Neuron 25, 649-662.

Maria Fiuza, C.M.R.G.T.P.A.M.B.N.H., Marcio Baptista, I.M., and Jonathan, G.H. (2017). PICK1 regulates AMPA receptor endocytosis via direct interaction with AP2 a-appendage and dynamin. The Rockefeller University Press J Cell Biol.

Maxfield, F.R., and McGraw, T.E. (2004). Endocytic recycling. Nat Rev Mol Cell Biol 5, 121-132.

Mayor, S., Parton, R.G., and Donaldson, J.G. (2014). Clathrin-independent pathways of endocytosis. Cold Spring Harb Perspect Biol 6.

Merrifield, C.J., Perrais, D., and Zenisek, D. (2005). Coupling between clathrin-coated-pit invagination, cortactin recruitment, and membrane scission observed in live cells. Cell 121, 593-606.

Mettlen, M., Chen, P.H., Srinivasan, S., Danuser, G., and Schmid, S.L. (2018). Regulation of Clathrin-Mediated Endocytosis. Annu Rev Biochem 87, 871-896.

Montagnac, G., de Forges, H., Smythe, E., Gueudry, C., Romao, M., Salamero, J., and Chavrier, P. (2011). Decoupling of activation and effector binding underlies ARF6 priming of fast endocytic recycling. Curr Biol 21, 574-579.

Mooren, O.L., Galletta, B.J., and Cooper, J.A. (2012). Roles for Actin Assembly in Endocytosis. Annu Rev Biochem 81, 661-686.

Moretto, E., and Passafaro, M. (2018). Recent Findings on AMPA Receptor Recycling. Frontiers in Cellular Neuroscience 12, 286-286.

Moult, P.R., Gladding, C.M., Sanderson, T.M., Fitzjohn, S.M., Bashir, Z.I., Molnar, E., and Collingridge, G.L. (2006). Tyrosine phosphatases regulate AMPA receptor trafficking during metabotropic glutamate receptor-mediated long-term depression. J Neurosci 26, 2544-2554.

Nakano-Kobayashi, A., Tai, Y., Nadif Kasri, N., and Van Aelst, L. (2014). The X-linked mental retardation protein OPHN1 interacts with Homer1b/c to control spine endocytic zone positioning and expression of synaptic potentiation. The Journal of neuroscience : the official journal of the Society for Neuroscience 34, 8665-8671.

Naslavsky, N., Weigert, R., and Donaldson, J.G. (2003). Convergence of non-clathrin- and clathrin-derived endosomes involves Arf6 inactivation and changes in phosphoinositides. Mol Biol Cell 14, 417-431.

Nunez, D., Antonescu, C., Mettlen, M., Liu, A., Schmid, S.L., Loerke, D., and Danuser, G. (2011). Hotspots organize clathrin-mediated endocytosis by efficient recruitment and retention of nucleating resources. Traffic 12, 1868-1878.

Opazo, P., and Choquet, D. (2011). A three-step model for the synaptic recruitment of AMPA receptors. Mol Cell Neurosci 46, 1-8.

Opazo, P., Labrecque, S., Tigaret, C.M., Frouin, A., Wiseman, P.W., De Koninck, P., and Choquet, D. (2010). CaMKII triggers the diffusional trapping of surface AMPARs through phosphorylation of stargazin. Neuron 67, 239-252.

Owen, D.J., Vallis, Y.F., Pearse, H.T., McMahon, and Evans, P.R. (2000). Structure and function of the B2-adaptin appendage domain.

Park, M., Salgado, J.M., Ostroff, L., Helton, T.D., Robinson, C.G., Harris, K.M., and Ehlers, M.D. (2006). Plasticity-induced growth of dendritic spines by exocytic trafficking from recycling endosomes. Neuron 52, 817-830.

Parkinson, G.T., Chamberlain, S.E.L., Jaafari, N., Turvey, M., Mellor, J.R., and Hanley, J.G. (2018). Cortactin regulates endo-lysosomal sorting of AMPARs via direct interaction with GluA2 subunit. Scientific Reports 8, 4155-4155.

Parton, R.G. (2018). Caveolae: Structure, Function, and Relationship to Disease. Annu Rev Cell Dev Biol 34, 111-136.

Petrini, E.M., Lu, J., Cognet, L., Lounis, B., Ehlers, M.D., and Choquet, D. (2009). Endocytic trafficking and recycling maintain a pool of mobile surface AMPA receptors required for synaptic potentiation. Neuron 63, 92-105.

Puchkov, D., Leshchyns’ka, I., Nikonenko, A.G., Schachner, M., and Sytnyk, V. (2011). NCAM/spectrin complex disassembly results in PSD perforation and postsynaptic endocytic zone formation. Cereb Cortex 21, 2217-2232.

Pula, G., Mundell, S.J., Roberts, P.J., and Kelly, E. (2004). Agonist-independent internalization of metabotropic glutamate receptor 1a is arrestin- and clathrin-dependent and is suppressed by receptor inverse agonists. J Neurochem 89, 1009-1020.

Rácz, B., Blanpied, T.A., Ehlers, M.D., and Weinberg, R.J. (2004). Lateral organization of endocytic machinery in dendritic spines. Nature Neuroscience 7, 917-918.

Reider, A., Barker, S.L., Mishra, S.K., Im, Y.J., Maldonado-Baez, L., Hurley, J.H., Traub, L.M., and Wendland, B. (2009). Syp1 is a conserved endocytic adaptor that contains domains involved in cargo selection and membrane tubulation. EMBO J 28, 3103-3116.

Rosendale, M., Julli, D., Choquet, D., and Perrais, D. (2017). Spatial and Temporal Regulation of Receptor Endocytosis in Neuronal Dendrites Revealed by Imaging of Single Vesicle Formation. Cell Reports 18, 1840-1847.

Saffarian, S., Cocucci, E., and Kirchhausen, T. (2009). Distinct Dynamics of Endocytic Clathrin-Coated Pits and Coated Plaques. PLoS Biology 7, e1000191-e1000191.

Sahl, S.J., Hell, S.W., and Jakobs, S. (2017). Fluorescence nanoscopy in cell biology. Nature Publishing Group.

Scheefhals, N., Catsburg, L.A.E., Westerveld, M.L., Blanpied, T.A., Hoogenraad, C.C., and MacGillavry, H.D. (2019). Shank Proteins Couple the Endocytic Zone to the Postsynaptic Density to Control Trafficking and Signaling of Metabotropic Glutamate Receptor 5. Cell Rep 29, 258-269 e258.

Sheng, M., and Kim, E. (2011). The postsynaptic organization of synapses. Cold Spring Harb Perspect Biol 3.

Sheng, M., and Kim, M.J. (2002). Postsynaptic signaling and plasticity mechanisms. Science 298, 776-780.

Shepherd, J.D., and Huganir, R.L. (2007). The cell biology of synaptic plasticity: AMPA receptor trafficking. Annu Rev Cell Dev Biol 23, 613-643.

Shih, W., Gallusser, A., and Kirchhausen, T. (1995). A clathrin-binding site in the hinge of the beta 2 chain of mammalian AP-2 complexes. J Biol Chem 270, 31083-31090.

Sinha, B., Koster, D., Ruez, R., Gonnord, P., Bastiani, M., Abankwa, D., Stan, R.V., Butler-

Browne, G., Vedie, B., Johannes, L., et al. (2011). Cells respond to mechanical stress by rapid disassembly of caveolae. Cell 144, 402-413.

Snyder, E.M., Philpot, B.D., Huber, K.M., Dong, X., Fallon, J.R., and Bear, M.F. (2001). Internalization of ionotropic glutamate receptors in response to mGluR activation. Nat Neurosci 4, 1079-1085.

Sochacki, K.A., Dickey, A.M., Strub, M.-P., and Taraska, J.W. (2017). Endocytic proteins are partitioned at the edge of the clathrin lattice in mammalian cells. Nature Cell Biology 19.

Sorkina, T., Miranda, M., Dionne, K.R., Hoover, B.R., Zahniser, N.R., and Sorkin, A. (2006). RNA interference screen reveals an essential role of Nedd4-2 in dopamine transporter ubiquitination and endocytosis. J Neurosci 26, 8195-8205.

Stern, C.M., and Mermelstein, P.G. (2010). Caveolin regulation of neuronal intracellular signaling. Cell Mol Life Sci 67, 3785-3795.

Sumi, T., and Harada, K. (2020). Mechanism underlying hippocampal long-term potentiation and depression based on competition between endocytosis and exocytosis of AMPA receptors. Sci Rep 10, 14711.

Tao-Cheng, J.H., Crocker, V.T., Winters, C.A., Azzam, R., Chludzinski, J., and Reese, T.S. (2011). Trafficking of AMPA receptors at plasma membranes of hippocampal neurons. J Neurosci 31, 4834-4843.

Taylor, M.J., Perrais, D., and Merrifield, C.J. (2011). A High Precision Survey of the Molecular Dynamics of Mammalian Clathrin-Mediated Endocytosis. 9.

Tebar, F., Sorkina, T., Sorkin, A., Ericsson, M., and Kirchhausen, T. (1996). Eps15 Is a Component of Clathrin-coated Pits and Vesicles and Is Located at the Rim of Coated Pits. Journal of Biological Chemistry 271, 28727-28730.

Traub, L.M. (2009). Tickets to ride: selecting cargo for clathrin-regulated internalization. Nat Rev Mol Cell Biol 10, 583-596.

Traub, L.M., Downs, M.A., Westrich, J.L., and Fremont, D.H. (1999). Crystal structure of the alpha appendage of AP-2 reveals a recruitment platform for clathrin-coat assembly. Proc Natl Acad Sci U S A 96, 8907-8912.

Trivedi, R.R., and Bhattacharyya, S. (2012). Constitutive internalization and recycling of metabotropic glutamate receptor 5 (mGluR5). Biochem Biophys Res Commun 427, 185-190.

Tu, J.C., Xiao, B., Naisbitt, S., Yuan, J.P., Petralia, R.S., Brakeman, P., Doan, A., Aakalu, V.K., Lanahan, A.A., Sheng, M., et al. (1999). Coupling of mGluR/Homer and PSD-95 complexes by the Shank family of postsynaptic density proteins. Neuron 23, 583-592.

Tu, J.C., Xiao, B., Yuan, J.P., Lanahan, A.A., Leoffert, K., Li, M., Linden, D.J., and Worley, P.F. (1998). Homer binds a novel proline-rich motif and links group 1 metabotropic glutamate receptors with IP3 receptors. Neuron 21, 717-726.

Ungewickell, E. (1983). Biochemical and immunological studies on clathrin light chains and their binding sites on clathrin triskelions. EMBO J 2, 1401-1408.

Ungewickell, E., and Ungewickell, H. (1991). Bovine brain clathrin light chains impede heavy chain assembly in vitro. J Biol Chem 266, 12710-12714.

Van Acker, T., Tavernier, J., and Peelman, F. (2019). The Small GTPase Arf6: An Overview of Its Mechanisms of Action and of Its Role in Host(-)Pathogen Interactions and Innate Immunity. Int J Mol Sci 20.

Van Jaarsveld, P.P., Nandi, P.K., Lippoldt, R.E., Saroff, H., and Edelhoch, H. (1981). Polymerization of clathrin protomers into basket structures. Biochemistry 20, 4129-4135.

Volk, L., Chiu, S.L., Sharma, K., and Huganir, R.L. (2015). Glutamate synapses in human cognitive disorders. Annu Rev Neurosci 38, 127-149.

Wagner, W., Lippmann, K., Heisler, F.F., Gromova, K.V., Lombino, F.L., Roesler, M.K., Pechmann, Y., Hornig, S., Schweizer, M., Polo, S., et al. (2019). Myosin VI Drives Clathrin-Mediated AMPA Receptor Endocytosis to Facilitate Cerebellar Long-Term Depression. Cell Rep 28, 11-20 e19.

Wendland, B. (2002). Epsins: adaptors in endocytosis? Nat Rev Mol Cell Biol 3, 971-977.

Widagdo, J., Fang, H., Jang, S.E., and Anggono, V. (2016). PACSIN1 regulates the dynamics of AMPA receptor trafficking. Nature Publishing Group.

Wilbur, J.D., Hwang, P.K., Ybe, J.A., Lane, M., Sellers, B.D., Jacobson, M.P., Fletterick, R.J., and Brodsky, F.M. (2010). Conformation switching of clathrin light chain regulates clathrin lattice assembly. Dev Cell 18, 841-848.

Zeno, W.F., Hochfelder, J.B., Thatte, A.S., Wang, L., Gadok, A.K., Hayden, C.C., Lafer, E.M., and Stachowiak, J.C. (2021). Clathrin Senses Membrane Curvature. Biophys J.

Zheng, N., Jeyifous, O., Munro, C., Montgomery, J.M., and Green, W.N. (2015). Synaptic activity regulates AMPA receptor trafficking through different recycling pathways. Elife 4.

Zoncu, R., Perera, R.M., Sebastian, R., Nakatsu, F., Chen, H., Balla, T., Ayala, G., Toomre, D., and De Camilli, P.V. (2007). Loss of endocytic clathrin-coated pits upon acute depletion of phosphatidylinositol 4,5-bisphosphate. Proc Natl Acad Sci U S A 104, 3793-3798.

2

AMPA receptor trafficking at the developing and mature glutamatergic synapse

Lisa A.E. Catsburg, Harold D. MacGillavry

Department of Cell Biology, Neurobiology and Biophysics at the Faculty of Science of Utrecht University in Utrecht, the Netherlands

Elsevier (2019), Comprehensive developmental neuroscience, Synapse development and maturation (chapter 23, pages 507-518)

ABSTRACT

The proper development of excitatory synapses is fundamental for the formation of neuronal circuits in the brain. Newly formed glutamatergic synapses undergo a characteristic series of developmental changes that prime synapses to efficiently transmit and encode information in neuronal circuits. One of the most prominent and functionally relevant changes at synapses, is the increase in the number of functional AMPA receptors early in development. Over the past decades, important aspects of the cellular processes that govern the assembly, intracellular trafficking and targeting to synapses of AMPA receptors have been uncovered. Here, we provide an overview of these molecular mechanisms that are fundamental for the proper development of excitatory synapses.

INTRODUCTION

Development of the mammalian central nervous system critically relies on the proper formation of neuronal circuits. Neuronal circuits are formed by a complex interplay of biological processes, guided by extracellular cues and intrinsic growth programs. In particular, the formation and maturation of synaptic contacts between neurons is arguably one of the most critical steps, endowing neuronal circuits with the ability to efficiently transmit and process information. The formation of synapses, a process termed synaptogenesis, peaks during early brain development before birth, but continues into early postnatal life and persists in adulthood, albeit at low levels. An initial period of synapse overproduction is followed by a period of synaptic pruning during which a significant amount of synapses is eliminated in a competitive manner, leading to the refinement of connectivity in neuronal circuits. Newly formed synapses that persist, follow a characteristic sequence of developmental changes leading to the maturation of a fully functional synapse. These changes involve a coordinated series of activity-dependent alterations in composition and physiology of the synapse to allow for the proper integration into neuronal circuits. Indeed, subtle disruptions in these processes are broadly held to underlie the development of human cognitive and behavioral disorders.

The vast majority of synapses in the mature brain are glutamatergic. At these synapses, the release of glutamate into the synaptic cleft triggers a postsynaptic response that is mediated by the concerted action of diverse types of glutamate receptors. Ionotropic glutamate receptors, including the AMPA, kainate, and NMDA receptors, are ligand-gated ion channels that evoke rapid excitatory currents, and work in concert with metabotropic glutamate receptors (mGluRs) that control postsynaptic responses via G-protein signalling (D'Angelo et al., 1993; Reiner and Levitz, 2018; Scheefhals and MacGillavry, 2018). The AMPA-type glutamate receptors (AMPARs) in particular, are the workhorse in excitatory synaptic transmission, carrying the majority of fast excitatory synaptic transmission in the mature brain. AMPARs are ligand-gated ion channels comprised of different combinations of four subunits (GluA1-GluA4). AMPARs respond extremely fast, producing excitatory currents within less than a millisecond in response to glutamate release. Activation of NMDA-type glutamate receptors (NMDARs) on the other hand, is more complex. At resting membrane potentials, the pore of the NMDAR is blocked by extracellular magnesium ions binding specific sites in the channel, which is only relieved by strong depolarization of the membrane (Nowak et al., 1984). Thus, NMDARs are conductive only when both glutamate is bound and the membrane is depolarized. As such, NMDARs are thought to act as molecular coincidence detectors gating the induction of processes that underlie developmental and plastic changes in synaptic efficacy. Importantly, the mechanisms for synaptic efficacy involve dynamic trafficking of AMPARs to and from synapses, thereby mediating the ability of synapse to efficiently carry transmission (Anggono and Huganir, 2012).

Over the course of development, the molecular composition of synapses changes dramatically (figure 1). Perhaps the most pronounced defining hallmark of excitatory synapse maturation is the selective recruitment and stabilization of AMPARs at the synaptic membrane during the first postnatal weeks (figure 2). Indeed, a developmental increase in the contribution of AMPAR-mediated currents relative to NMDAR-mediated currents is a common hallmark for excitatory synapses maturation in different brain regions (Crair and Malenka, 1995; Hestrin, 1992; Ramoa and McCormick, 1994). Initially, most newly formed synapses express NMDARs only, but lack functional AMPARs (figure 1) (Gomperts et al., 1998; Liao et al., 1999; Nusser et al., 1998; Petralia et al., 1999). Because NMDARs are not conductive at resting membrane potentials, these synapses are unable to transmit signals, and have been termed “silent synapses” accordingly. Importantly, coordinated pre- and postsynaptic activity can “unsilence” these synapses, a process that critically relies on the regulated trafficking of AMPARs to the postsynaptic membrane (Hanse et al., 2013; Isaac et al., 1995; Liao et al., 1995). The processes that regulate the trafficking of AMPARs to and from synapses is best understood in the context of synaptic plasticity at mature synapses. Most notably, the regulated insertion and removal of AMPARs from the synapse is broadly held to underlie the expression of long-term potentiation (LTP) and long-term depression (LTD) respectively (Huganir and Nicoll, 2013; Malenka and Bear, 2004; Malinow and Malenka, 2002). However, while the mechanisms of activity-dependent trafficking of AMPARs underlying synaptic plasticity are quite well understood, these trafficking rules do not necessarily apply to the developmental recruitment of AMPARs to synapses. Given that the molecular composition of synapses, including the abundance of specific signalling and scaffolding molecules that hold these receptors in place, differ significantly between mature and immature synapse, it is likely that the molecular rules that control the synaptic recruitment of AMPARs differ between mature and immature synapses. Indeed, extensive investigation over the past decades has elucidated the fundamental principles of AMPAR trafficking in developing and mature synapses, and mechanistic differences between developmental stages. Insight in the mechanisms that control AMPAR assembly and trafficking to synaptic sites is important to better understand the sequential steps in healthy brain development. Given that many neurodevelopmental disorders are associated with dysfunction of excitatory synapses (Henley and Wilkinson, 2016; Volk et al., 2015), understanding these processes also holds promise for the development of treatments that can interfere with the maldevelopment of synapses in these diseases. In this chapter, we will focus on the molecular mechanisms underlying synaptogenesis with a particular emphasis on AMPAR trafficking during the development and maturation of glutamatergic synapses. We will highlight new insights and technological advances that can be used to study AMPAR trafficking in the greatest detail.

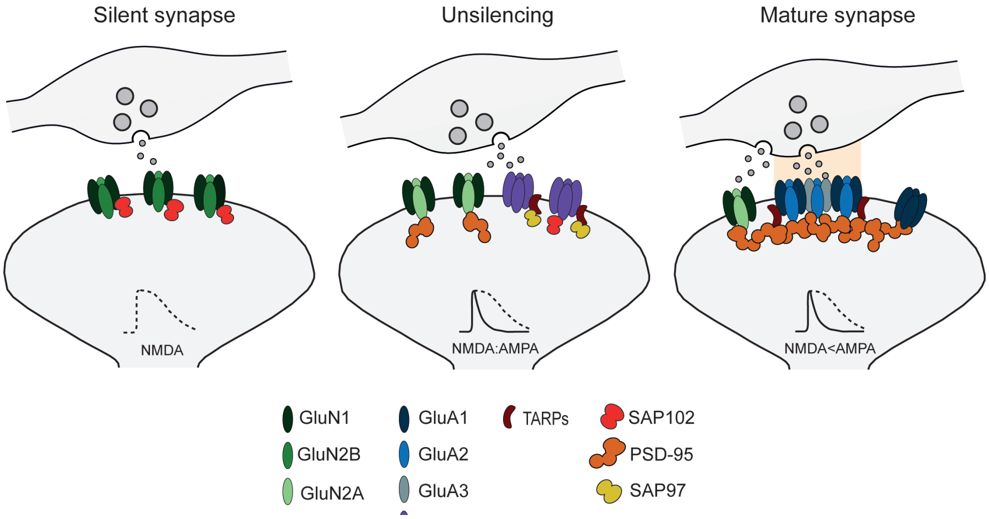

Figure 1. Developmental stages of the glutamatergic synapse. Schematic representation of the postsynaptic organization during maturation. GluN1 and GluN2B heteromers are recruited in parallel with SAP102 (left panel) resulting in NMDAR-mediated currents, rendering the synapse silent (dashed line). A developmental switch from GluN1/GluN2B to GluN1/GluN2A heteromers and the recruitment of GluA4 homomers to the synapse by SAP97 initiates AMPAR-mediated activity (black line) thereby unsilencing the synapse (middle panel). In mature neurons PSD-95 is the most abundant synaptic scaffold protein, capturing receptors at the synapse and forming nanodomains that directly oppose the presynaptic release site (right panel).

GLUTAMATERGIC SYNAPTOGENESIS DURING DEVELOPMENT

In developing circuits, most of the initial axon-dendrite contacts are very short-lived, and only a few contacts will remain and stabilize to form functional synapses. Thus, for a synapse to form, contacts between axons and dendrites have to be stabilized before these can develop and mature. Stabilization of the initial axon-dendritic contact is largely mediated by trans-synaptic adhesion proteins that bridge the axon-dendrite contact sites and provide bidirectional signals that instruct the recruitment of pre- and postsynaptic protein assemblies. Many of such synaptogenic adhesion molecules have been identified. For instance, the neurexin-neuroligin adhesion pair, the trans-synaptic EphrinB/EphB receptor pathways, and LRRTM and cadherin protein families have been described to have such synaptogenic effects. For a more elaborate discussion on the role of adhesion complexes in synapse initiation, maturation and maintenance we refer to recent reviews on this topic (de Wit and Ghosh, 2016; Sudhof, 2017). Importantly, through intracellular interactions, clustering of adhesion complexes such as neuroligin is sufficient to trigger the accumulation of components of the postsynaptic machinery (Graf et al., 2004; Heine et al., 2008b). The exact time course of recruitment of synaptic components during synaptogenesis however remains elusive. Early live-cell imaging experiments on cultured hippocampal neurons suggested that presynaptic components accumulate within ~30 minutes after initial axon-dendritic contact, and that assembly of the postsynaptic compartment occurs gradually with post synaptic density scaffold proteins appearing first (~45 minutes after contact), followed by AMPAR and

NMDAR (Friedman et al., 2000). Later studies in cultured cortical neurons however, found that NMDARs were almost immediately (within ~10 minutes) recruited to new synapses, coinciding with the recruitment of presynaptic components, while AMPARs followed later (~1 hour) (Barrow et al., 2009; Washbourne et al., 2002; Washbourne et al., 2004). More recent imaging studies in hippocampal slice cultures showed that newly formed dendritic spines contain AMPAR and NMDARs almost instantly after formation (Kwon and Sabatini, 2011; Zito et al., 2009), and show a delayed accumulation of synaptic scaffolds (Lambert et al., 2017). Thus, the exact timing and sequence of molecular events during synaptogenesis seem to vary between synapses, but generally the arrival of AMPARs is a relatively late event following the initial formation of synaptic contacts.

Consistent with the late arrival of AMPARs, is the transformation of synapses from silent, non-conducting synapses to functional, current-conducting synapses observed during the first postnatal weeks (figure1) (Durand et al., 1996; Liao et al., 1995). Two explanations for this phenomenon of silent synapses have been postulated. The first attributed this phenomenon to a postsynaptic mechanism, stating that silent synapses initially only contain NMDARs and only later recruit AMPARs, ‘unsilencing’ the synapse. The second proposed a presynaptic mechanism, and stated that the low release probability at newly formed synapses is not sufficient to activate postsynaptic AMPARs due to their low affinity to glutamate (Choi et al., 2000; Hanse et al., 2013). There is experimental evidence for both mechanisms, but strong support for a postsynaptic mechanism comes from glutamate uncaging experiments demonstrating that a fraction of the neonatal synapses indeed showed NMDAR-mediated currents only (Ashby and Isaac, 2011; Busetto et al., 2008; Zhu et al., 2000). Moreover, immuno-labeling confirmed that at postnatal day 2 NMDARs are present at most synapses, while AMPARs remain largely absent until postnatal day 10 (Gomperts et al., 1998; Nusser et al., 1998; Petralia et al., 1999). Thus, although several mechanisms could explain silent synapses, the developmental switch from predominantly NMDAR-mediated to AMPAR-mediated transmission is a prominent phenomenon occurring during the first two postnatal weeks of development and seems to be key to synapse maturation (Shi et al., 2001a).

While in mature neurons NMDAR activity usually positively regulates trafficking of AMPARs to synapses, at newly formed synapses NMDARs seem to actively suppress the insertion of AMPARs (Adesnik et al., 2008; Hall and Ghosh, 2008; Hall et al., 2007; Lu et al., 2011). NMDARs are heteromeric receptors formed from the assembly of two obligatory GluN1 subunits with two regulatory subunits, usually GluN2 subunits of which there are four isoforms (GluN2A, GluN2B, GluN2C, and GluN2D). The GluN2 subunits each confer unique functional properties to the NMDAR and influence channel kinetics, and the coupling to downstream signaling pathways. The subunit composition of NMDARs gradually changes throughout synapse maturation with a predominant expression of GluN2B-containing NMDARs during early development that declines and becomes dominated by GluN2A-containing receptors at mature stages (figure 2) (Flint et al., 1997; Monyer et al., 1994; Sheng et al., 1994). This developmental switch from GluN2B to GluN2A-dominant NMDARs has been shown to be critical for synapse maturation. While GluN2A knockout mice are fully viable (Sakimura et al., 1995), GluN2B knockout mice die soon after birth (Kutsuwada et al., 1996), similar to GluN1 knockouts

(Forrest et al., 1994). In a more recent study, conditional GluN2A and GluN2B knockouts were generated to dissect the differential contribution of each these subunits during development (Gray et al., 2011). This study found that while deletion of GluN2B increased the number of functional synapses, deletion of GluN2A resulted in increased synaptic strength, but did not change the number of synapses. Thus, while GluN2B primarily functions to maintain the number of silent synapses, GluN2A dampens synaptic potentiation by preventing recruitment of functional AMPARs to nascent synapses. These results add to earlier notions that both GluN2A and GluN2B negatively regulate AMPAR recruitment, but via distinct mechanisms (Kim et al., 2005). Thus, at early developmental stages, coordinated expression of GluN2B and GluN2A seems to act to suppress AMPAR insertion and maintain synapses in a silent state. This mechanism would ensure that newly formed synapses only mature and recruit AMPARs upon strong, or correlated activity patterns, and that synapses that lack these inputs are lost during the course of development.

The correlated activity patterns that trigger the NMDAR-dependent potentiation of synaptic activity in developing synapses is comparable to LTP in mature neurons, but differs in two important aspects. First, while LTP at mature synapses relies on activity of CaMKII, the expression levels of this kinase are low early in development and CaMKII activity only becomes required for LTP after the second postnatal week (Yasuda et al., 2003). Instead, activity of PKA is required for developmental LTP, and is in fact sufficient to drive AMPARs to silent synapses and unsilence these (figure 2) (Esteban et al., 2003; Luchkina et al., 2014; Zhu et al., 2000). Second, there is a developmental switch in the preference for which AMPAR subunit is recruited to the synapse. While in mature neurons AMPARs containing the GluA1 subunit are preferentially incorporated in response to LTP, at developing synapses the early expressed GluA4 subunit and the long splice variant of the GluA2 subunit (GluA2L) can be recruited by spontaneous activity or PKA activation (Esteban et al., 2003; Kolleker et al., 2003; Zhu et al., 2000). This subunit preference was also shown in vivo during experience-dependent plasticity in the barrel cortex, where whisker stimulation at postnatal day 8-10 induces the synaptic delivery of GluA4, but not GluA1. In contrast, a few days later (postnatal day 12-14), GluA1-containing receptors were preferentially inserted upon whisker stimulation (Miyazaki et al., 2012).

It is important to note that in seeming contrast to this prevailing model in which synaptic maturation is controlled by synaptic activity patterns, several studies found that assembly of excitatory synapses can occur in the absence of neurotransmission. Mouse models in which release of glutamate-containing vesicles is almost absent developed morphologically normal synapses in the postnatal hippocampus (Sando et al., 2017; Sigler et al., 2017; Verhage et al., 2000). Also, in hippocampal neurons lacking ionotropic glutamate receptors morphology of the dendrites and spine synapses was unaffected (Lu et al., 2013). Thus, it seems that intrinsic developmental programs are sufficient to set up the morphological development of synapses, but that the correct formation and maturation of synapses is finely tuned by synaptic activity patterns.

Apart from AMPARs and NMDARs, synaptic proteins are gradually recruited to the developing synapse (figure 2). The membrane-associated guanylate kinases (MAGUK) are a family of scaffolding proteins that can bind and anchor AMPARs and

NMDARs at synapses. Together with other structural components of the synapse like GKAP, Shank, Homer and SynGAP they are present at the synapse by postnatal day 2 (Foa and Gasperini, 2009; Petralia et al., 2005), and could thus be involved in instructing receptor trafficking during synapse maturation. In particular, the two MAGUKs, SAP102 and PSD-95, seem to be critical for receptor trafficking, but act at different developmental stages. SAP102 is already present during early stages of development, but is gradually replaced by PSD-95 (figure 2) (Sans et al., 2000; Zheng et al., 2010), suggesting that SAP102 supports synaptic maturation, but is not crucial for synaptic transmission at later stages. Indeed, it was found that knockdown of SAP102 in developing neurons reduces both NMDAR and AMPAR-mediated currents, while PSD-95 knockdown has no effect at this early stage (Elias et al., 2008; Elias et al., 2006). In mature neurons, overexpression of PSD-95 results in strongly enhanced synaptic function, while knockdown of PSD-95 reduces AMPAR-mediated currents (Ehrlich and Malinow, 2004; Elias et al., 2008; Stein et al., 2003). In contrast, overexpression of SAP102 in mature hippocampal neurons has minimal effects on AMPAR-mediated currents, and knockdown does not affect transmission (Elias et al., 2008; Elias et al., 2006). Interestingly, the expression levels of SAP102 and PSD-95 accurately follow the expression levels of GluN2B and GluN2A respectively (Sans et al., 2000), and biochemical studies showed that PSD-95 and SAP102 can bind both GluN2A and GluN2B-containing NMDARs. However, while SAP102 can recruit both GluN2A and GluN2B-containing NMDARs, PSD-95 seems to specifically recruit GluN2A-containing NMDARs (Elias et al., 2008). Thus, synaptic scaffolding proteins, in particular the MAGUKs SAP102 and PSD-95, seem to have instructive roles in the developmental recruitment of NMDARs and AMPARs.

In summary, over the course of development newly formed synapses undergo dramatic changes in their structure, molecular composition and function. Starting from the initial axon-dendrite contact, synapses sequentially recruit different molecular assemblies that ultimately form the functional synaptic machinery. The blueprint of these molecular changes seems to be embedded in intrinsic developmental programs, but is critically modulated by activity patterns that instruct the maturation and refinement of synaptic connections. In particular, a relatively late, but critical step in synapse maturation, is the activity-dependent recruitment of AMPARs, and defines the transition of silent, immature synapses to fully matured synapses. Given that AMPARs play such a central role in the development and maturation of glutamatergic synapses, we will now consider the functional diversity of AMPAR complexes (section 3), the assembly and intracellular trafficking of AMPARs (section 4), and the molecular processes that maintain and alter the expression of AMPARs at the neuronal membrane.

AMPAR SUBUNIT SPECIFIC STRUCTURE, LOCALIZATION AND FUNCTION

AMPARs are homo- or hetero–tetrameric ligand-gated ion channels formed by different combinations of four core subunits, GluA1-GluA4, encoded by four different genes (Gria1-4) (Rosenmund et al., 1998). A multitude of stoichiometries is possible, dependent on cell type-specific subunit expression and developmental stage, and can be modulated by synaptic activity. Because each of these subunits differ in their contribution to channel kinetics, ion selectivity, and ability to interact with specific protein complexes that control the trafficking of AMPARs, hetero-tetramerization

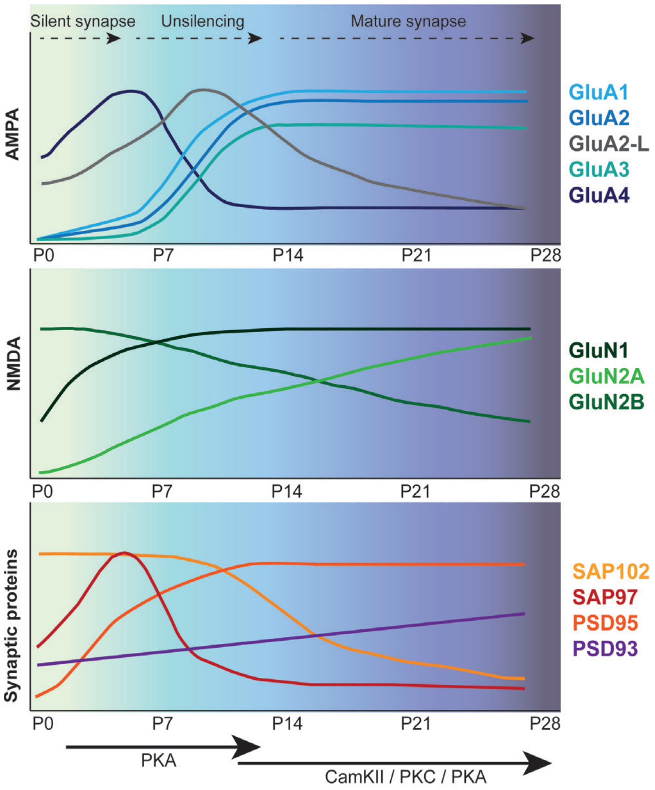

Figure 2. Relative time resolved recruitment of synaptic components.
A schematic representation of the temporal recruitment of postsynaptic proteins during postnatal development in a hippocampal synapse. Black dashed arrows above represent the different stages of synaptic development. The black arrows below illustrate the differential kinase dependency during development. The GluA4 subunit is most abundant during early stages of development and is gradually replaced by GluA1, 2 and 3 (upper panel). While GluN1A expression gradually increases over time, GluN2B levels decrease as GluN2A-containing NMDARs increase. Expression pattern of other postsynaptic proteins correlate to the specific subunit specific recruitment. SAP97 patterns follows the recruitment of GluA4, while SAP102 mimics GluN2A expression. Both PSD-95 and PSD-93 expression increases over time with PSD-95 being the most abundant MAGUK in mature synapses. Data based on (Petralia et al., 2005; Sans et al., 2000; Schwenk et al., 2014; Zhu et al., 2000) and see references in main text.

gives rise to a functional variety of AMPAR types. Functional diversity is further conferred by alternative splicing and RNA editing (Seeburg and Hartner, 2003). Each of the four subunits can exist in two forms, the “flip” and “flop” variants that arise through alternative splicing of two exons that encode part of the ligand binding domain (Sommer et al., 1990). This alternative splicing event greatly impacts the pharmacology and channel kinetics of the receptor. In general, the “flop” versions desensitize much more rapidly than the “flip” versions and are less sensitive to the desensitization blocker cyclothiazide (Sommer et al., 1990). Alternative splicing of the subunits is developmentally regulated. While mRNAs encoding the “flip” variant are expressed throughout development, “flop” versions are expressed at low levels early in development, and only start to increase from postnatal day 8 on, reaching peak levels at postnatal day 14 (Monyer et al., 1991). At mature synapses, AMPARs thus generally desensitize faster than at immature synapse. Unlike the other subunits, the GluA2 subunit undergoes RNA editing of a single residue in the pore region of the ion channel (Sommer et al., 1991). This specific modification has multiple significant implications for receptor functioning. Editing of the glutamine to the positively charged arginine at position 607 (Q/R editing) in one GluA2 subunit is sufficient to render the entire channel impermeable for calcium, altering the rectification of the ion channel (Burnashev et al., 1992; Hollmann et al., 1991; Hume et al., 1991). Importantly, this editing event also severely restricts receptor exit from the ER, dramatically increasing the dwell time of the edited GluA2 subunit in the ER (Greger et al., 2002). Already early in embryonic development, the vast majority of GluA2 transcripts is in the edited form (Burnashev et al., 1992; Jacobs et al., 2009), and impaired editing in transgenic mice leads to epileptic seizures and death within three weeks after birth (Brusa et al., 1995).

The AMPAR complex displays a modular organization, consisting of four distinct domain layers: an extracellular N-terminal domain (NTD), a ligand-binding domain (LBD), a transmembrane domain (TMD) and an intracellular C-terminal domain (CTD) (Herguedas et al., 2016; Sobolevsky et al., 2009). The extracellular region of the AMPAR containing the NTD and LBD forms the bulk of the receptor. The four subunits have virtually identical TMDs, but principally authenticate by their CTD and glutamate binding affinity. The CTD varies extensively in length and sequence between the different subunits. The CTD is also subject to alternative splicing and contains posttranslational modification sites that tune the ability of subunit-specific protein-protein interactions. The GluA1, GluA4, and GluA2L (long splice variant of GluA2) subunits have long CTDs, while GluA2, GluA3, and GluA4S (short splice variant of GluA4) have relatively short tails. These differences confer specificity in interactions and posttranslational modifications. The subunit specificity of the intracellular CTD has long been considered to be the principal determinant of synaptic trafficking, and has been subject of intense investigation in the context of subunit-specific trafficking to the synapse, particularly in the context of synaptic plasticity (Shepherd and Huganir, 2007). From these studies, the general notion emerged that GluA1 is dominant in instructing activity-dependent recruitment of AMPARs to synapses, and that once at the synapse, GluA2-containing receptors are inserted by a constitutive process (Kessels and Malinow, 2009; Shepherd and Huganir, 2007; Shi et al., 2001b). However, while CTD-mediated interactions are most likely instructive, the exact differential contribution of these interactions to activity-dependent synaptic trafficking of AMPARs remains to be established (Granger et al., 2013; Zhou et al., 2018).

The composition and expression patterns of AMPAR complexes change drastically over the course of development. At birth, the expression levels of GluA1, GluA2 and GluA3 are still very low, and GluA4 is the predominantly expressed subunit (figure 2) , suggesting that at this stage, synapses contain AMPARs composed almost exclusively of GluA4 subunits. Consistently, it has been shown that low, spontaneous activity patterns are sufficient to traffic GluA4 homomers into synapses (Zhu et al., 2000). GluA4 levels rapidly decline after birth to undetectable levels in the first two weeks (Akaneya, 2007; Zhu et al., 2000). In contrast, during the first two weeks the levels of the other subunits start to increase in parallel, reaching adult levels three weeks after birth (Petralia et al., 1999; Petralia et al., 2005; Zhu et al., 2000). The levels of the GluA2L also increase during this period, but only briefly peak in the second week after birth, and return to low levels in the mature hippocampus (Kolleker et al., 2003). In the adult hippocampus, the GluA2 subunit is most abundant, with GluA1/2 and GluA2/3 heterotetrameric AMPAR complexes being the most prominent receptor types, and GluA1 homomeric AMPARs making up only a small population (figure 2) (Lu et al., 2009; Schwenk et al., 2014; Wenthold et al., 1996).

Importantly, the assembly, trafficking and biophysical properties of AMPARs are not solely determined by subunit assembly. Unlike other ionotropic glutamate receptors, AMPAR complexes are coupled to a variety of auxiliary subunits that significantly influence receptor kinetics, conductance and trafficking properties. The entire AMPAR complex is estimated to consist of >30 different proteins forming a large, multi-molecular signalling machine. The first auxiliary protein discovered was Stargazin, which belongs to a larger family of transmembrane AMPAR regulatory proteins (TARPs: γ2, γ-3, γ-4, γ-5, γ-7, γ-8), which differ in brain region expression and functional properties (Jackson and Nicoll, 2011; Kato et al., 2010; Nicoll et al., 2006; Tomita et al., 2003). Stargazin was identified as a mutant gene in the Stargazer mouse, which exhibits severe cerebellar ataxia and epilepsy (Chen et al., 1999; Hashimoto et al., 1999). TARPs can directly interact with each of the AMPAR subunits and promote their surface expression, synaptic retention, and modulate channel function (Straub and Tomita, 2012). More recently, quantitative mass spectrometry studies on isolated AMPARs have identified additional families of auxiliary proteins (Schwenk et al., 2012). Together with the TARPs, the cornichons (CNIH2 and 3), and GSG1l protein have been proposed to consist of the "core" of the AMPAR (Schwenk et al., 2014; Schwenk et al., 2012; Schwenk et al., 2009; Shanks et al., 2012). Apart from these core components, the AMPAR complex can additionally recruit a number of satellite components including cysteine-knot AMPAR modulating proteins (CKAMP44 and 52), proline-rich transmembrane proteins PRRT1 (also known as SynDIG4) and PRRT2, neuritin, Noelins1-3, leucine-rich repeat transmembrane neuronal protein 4 (LRRTM4), carnitine O-palmitoyltransferase 1c (CPT1c), and ferric-chelate reductase 1-like (FRRS1l, or C9Orf4) (Brechet et al., 2017; Chen et al., 2014; de Wit et al., 2013; Kalashnikova et al., 2010; Schwenk et al., 2014; Schwenk et al., 2012; von Engelhardt et al., 2010). These include various types of proteins including transmembrane, cytoplasmic, and secreted proteins. While our understanding of how these peripheral components affect the assembly, trafficking and physiology of the AMPAR is increasing (Jacobi and von Engelhardt, 2018), the precise function for most of these components has not been elucidated yet. Interestingly, the expression of these AMPAR-interacting proteins is highly regulated over the course of development (Schwenk et al., 2014). It is thus conceivable that developmental changes in the properties of synaptic AMPARs are in large part mediated by the differential action of this diverse set of AMPAR complex proteins and it would be of interest to investigate how each of these components contribute to the developmental maturation of excitatory synapses.

AMPAR ASSEMBLY AND INTRACELLULAR TRAFFICKING ALONG THE SECRETORY PATHWAY

Like the majority of membrane proteins, AMPAR complexes are assembled in the endoplasmic reticulum (ER). The exact mechanisms of AMPAR assembly are not fully understood, but assembly occurs in two consecutive steps where individual subunits dimerize followed by the dimerization of these dimers into a tetrameric complex (Greger et al., 2007). The first dimerization step relies primarily on interactions between the NTDs of the individual subunits, while the second step, the dimerization of dimers into tetramers, involves interactions between the LBD and transmembrane domains (Ayalon and Stern-Bach, 2001). Selective NTD-mediated interactions in principle allow a wide variety of potential subunit-specific associations, but due to differences in affinity, heteromerization is dominant with preferential incorporation of the GluA2 subunit (Rossmann et al., 2011). Formation of GluA2-containing receptors is further favored by Q/R editing which limits GluA2 homotetramerization, and thereby promotes the dimerization of GluA2 dimers with other subunits (Greger et al., 2006; Greger et al., 2002).

A principal function of the ER is to prevent the exit and delivery of not correctly folded, non-functional transmembrane proteins. Indeed, mutations in the AMPAR LBD that prevent glutamate binding, or in the pore region that block ion permeation lead to retention of receptors in the ER and severely hampers surface delivery (Grunwald and Kaplan, 2003). Moreover, TARPs and CNIHs associate with the AMPAR in the ER and are thought to act as chaperones that facilitate the assembly of AMPARs and export from the ER (Bedoukian et al., 2006; Brockie et al., 2013; Shi et al., 2010). Other AMPAR interactors such as FRRS1L (C9Orf4) and CPT1c also act as chaperones, but are retained in the ER, indicating that sequential binding of such components guide AMPAR assembly and ER exit (Brechet et al., 2017). Conventionally, after assembly in the ER, transmembrane proteins accumulate at specialized ER exit sites to be transported to the ER-Golgi intermediate compartment (ERGIC) via COPII-mediated transport. From the ERGIC, cargoes are sorted to the Golgi apparatus (GA) or return to the ER (figure 3). Transmembrane proteins pass through the GA and trans Golgi network (TGN) to undergo further post-translational processing such as glycosylation, and to be packaged in transport vesicles for membrane delivery. While the ER forms a continuous, complex reticular structure that extends throughout the somatodendritic compartment (Cui-Wang et al., 2012; Spacek and Harris, 1997), the GA is primarily localized in the cell body close to the nucleus. It has thus remained unclear how receptors that are synthesized locally in dendrites are processed and trafficked to the membrane and the question whether these locally synthesized AMPARs follow the conventional pathway emerged. Initially, cargoes that leave the dendritic ER were found to travel back to the somatic GA (Horton and Ehlers, 2003), or through Golgi-like structures, termed Golgi outposts, present in dendrites (Horton and Ehlers, 2003; Mikhaylova et al., 2016; Pierce et al., 2001). However, it remains controversial whether these Golgi outposts are fully operational similar to the conventional GA. Also, Golgi outposts have only been found in a subset of all dendrites, and the identification is dependent on experimental approaches. In support for the presence of local processing organelles of AMPAR in dendrites, recent studies found that newly synthesized receptors are locally trapped at dendritic ERGIC structures (Bowen et al., 2017; Hanus et al., 2014). Moreover, for

AMPARs, ER exit is a rate limiting step in synapse delivery (Penn et al., 2008), and is modulated by synaptic activity (Pick and Ziff, 2018), supporting the notion for local storage in the ERGIC. Indeed, newly synthesized AMPARs that exited the ER were found to accumulate preferentially in nearby dendritic ERGICs before they were further transported by recycling endosomes (REs) (figure 3) (Bourke et al., 2018; Bowen et al., 2017). Even in neurons treated with Brefeldin A, almost completely disrupting the somatic GA, AMPARs were still trafficked by REs and a significant portion of the receptors could still reached the membrane (Hanus et al., 2016). This suggests that a substantial pool of newly synthesized AMPARs can bypass the somatic GA, consistent with findings that a significant portion of receptors on the neuronal membrane display a glycosylation patterns that are reminiscent of immature, core-glycosylated proteins (Hanus et al., 2016). Together, these data suggest two possible routes for intracellular AMPAR trafficking, one via conventional trafficking involving passage through the GA and a second alternative pathway independent of the GA (figure 3).

Finally, once processed, AMPAR-containing transport vesicles are transported to the correct subcellular location via motor-based transport over the microtubule and actin cytoskeleton (Hirokawa et al., 2010; Kapitein and Hoogenraad, 2015). Long-range transport of AMPARs in dendrites is mediated by the molecular motor kinesin KIF5 that recruits GluA2/3 receptor via the GRIP1 adaptor protein (Hoogenraad et al., 2005; Setou et al., 2002), or KIF1 via the adaptor protein liprin-α(Shin et al., 2003; Wyszynski et al., 2002). Since most spines lack microtubules, and are therefore most likely not, or only infrequently, visited by microtubule motors, actin-based motors are involved in the final step of synaptic delivery. Indeed, motors of the myosin family, in particular myosin-V and –VI, have are thought to be key in driving cargo into spines (Wagner et al., 2011; Wang et al., 2008).

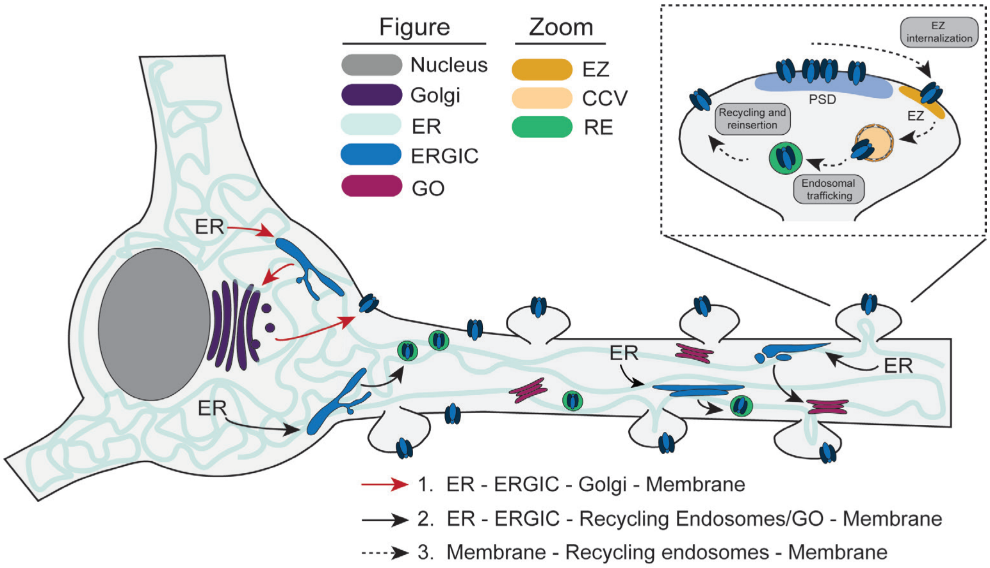
Figure
Nucleus
Golgi
ER
ERGIC
GO
Zoom
EZ
CCV
RE
EZ internalization
PSD
Recycling and reinsertion
EZ
Endosomal trafficking
ER
ER
ER
ER
1. ER - ERGIC - Golgi - Membrane
2. ER - ERGIC - Recycling Endosomes/GO - Membrane
3. Membrane - Recycling endosomes - Membrane

Figure 3. Intracellular and surface trafficking of AMPARs. Different routes for intracellular AMPAR trafficking have been described. The classical route for transmembrane proteins involves assembly

in the ER, and passage through the ERGIC to the GA to undergo posttranslational glycosylation. From the GA, membrane proteins are transported and inserted in the membrane (pathway 1: red line). Locally synthesized AMPARs have been shown to bypass the GA. These receptors are transported from the ER to the ERGIC and then enter recycling endosomes (pathway 2: black line), or pass through Golgi outposts (GOs) before insertion in the membrane. Surface trafficking of AMPARs (zoom) involves the insertion of AMPARs through exocytosis, that travel to the synapse via lateral diffusion where they are captured by synaptic scaffolds. Synaptic AMPARs can be uncoupled and recruited to the EZ for internalization. AMPARs endocytosed at the EZ enter a pathway for fast and local recycling to return to the membrane (pathway 3: dashed line). ER: endoplasmic reticulum, ERGIC: ER Golgi intermediate compartment, GO: Golgi outpost, EZ: endocytic zone, CCV: clathrin-coated vesicle, RE: recycling endosome, PSD: postsynaptic density.

SURFACE TRAFFICKING OF AMPARs

Once sorted to the correct subcellular compartment, AMPARs undergo constitutive and activity-dependent membrane trafficking events that can be divided into multiple steps: 1) exocytosis of AMPAR from intracellular pools, 2) lateral diffusion across the membrane, 3) capture at synaptic sites, 4) endocytosis, and 5) endosomal recycling (figure 3, zoom, figure 4). Together these processes maintain the steady-state levels of receptors at synaptic, extrasynaptic and intracellular sites, and allow developmental and plasticity-associated activity patterns to promote the exchange of receptors between these different locations. Thus, to properly regulate the density of receptors at individual synapses, these processes require complex regulatory mechanisms.

Exocytosis from intracellular pools

Endosomes containing AMPARs can fuse with the membrane by both constitutive and activity-dependent exocytosis to supply newly synthesized or recycle AMPARs to the neuronal membrane. However, the exact subcellular location of AMPAR exocytosis, is a long-debated question in the field of neuronal cell biology. Several studies have suggested that AMPARs are inserted in the plasma membrane of the soma or at the dendritic shaft before they reach the synapse via lateral diffusion (Adesnik et al., 2005; Lu et al., 2001; Makino and Malinow, 2009), while other studies suggested that exocytosis of receptors takes place both in dendrites and spines (figure 4) (Kennedy et al., 2010; Park et al., 2006; Patterson et al., 2010; Wang et al., 2008; Yudowski et al., 2006), or even directly into the PSD (Gerges et al., 2006). Thus, it seems most likely that AMPAR exocytosis can take place at distinct sites, both in spines and the somatodendritic compartment, but that the exact location is dependent on developmental stage, synaptic activity, endosomal source, and subunit composition (Passafaro et al., 2001). Based on imaging studies using fluorescently tagged AMPAR subunits, it has been estimated that under baseline conditions exocytosis rates are ~0.1 events/min in spines and ~0.03 events/min in the dendrite. However, upon LTP stimulation at single spines, these AMPAR exocytosis rates increased ~5-fold and then rapidly returned to baseline levels within 1 minute after stimulus onset (Patterson et al., 2010). Interestingly, exocytosis seemed restricted to an area of ~3 μm away from the stimulated synapse. The activity-induced increase in synaptic AMPARs can however not be solely explained by exocytic activity. In fact, it has been estimated that 70 - 90% of AMPARs entering the synapse during LTP originate from preexisting surface receptors supplied from adjacent areas, leaving only 10 -

30% of receptors to be exocytosed (Kopec et al., 2006; Makino and Malinow, 2009; Patterson et al., 2010). Also, the relative slow time-course of exocytosis (minutes) is not compatible with the rapid onset of synaptic potentiation observed with LTP-inducing stimuli (seconds). Accordingly, activity-dependent trafficking of AMPARs to synapses has been proposed to be a multi-step process, where initially AMPARs are recruited to the PSD via lateral diffusion from a pre-existing extrasynaptic pool, that is then further supplied by exocytosis from intracellular reserve pools (Opazo and Choquet, 2011). Indeed, blocking lateral diffusion prohibits expression of both early and late phases of LTP, while blocking exocytosis prohibits the expression of late LTP only (Penn et al., 2017).

Exocytosis is generally mediated by the SNARE complex and Sec1/Munc-18-like (SM) proteins that undergo a characteristic cycle of assembly and disassembly that catalyzes the fusion of the endosomal cargo-containing vesicle with the plasma membrane (Sudhof, 2013). Indeed, early experiments showing that activity-induced exocytosis of AMPARs is blocked by intracellular tetanus toxin (Lledo et al., 1998; Lu et al., 2001) formed the first indication that SNARE-dependent exocytosis mediates the fusion of AMPAR-containing endosomes with the membrane. However, while detailed information is available about the composition and regulation of the presynaptic machinery that mediates release of neurotransmitter vesicles, the molecular identities of the complexes in dendrites that mediate exocytosis are only beginning to be defined (Jurado, 2014). Targeted knockdown studies have confirmed the role of specific SNARE proteins in activity-induced fusion of AMPAR-containing endosomes (Jurado et al., 2013; Kennedy et al., 2010). Apart from SNARE proteins, the small complexin proteins that bind the SNARE complex and modulate SNARE-dependent membrane fusion in different cellular systems (McMahon et al., 1995), have been implicated in activity-dependent AMPAR exocytosis (figure 4) (Ahmad et al., 2012). Both complexin-1 and -2 are located in dendritic spines, and NMDAR-mediated delivery of AMPARs is impaired in complexin-1 and complexin-2 knockdown neurons (Ahmad et al., 2012). Complexins have been shown to function as co-factors for the calcium sensor synaptotagmin-1 in calcium-induced exocytosis, but initially no essential role for synaptotagmin-1 during AMPAR recruitment was observed (Ahmad et al., 2012). However, more recently, it was found that knockdown of both synaptotagmins-1 and 7 simultaneously, but not separately, abolished LTP (Wu et al., 2017), suggesting that both synaptotagmin-1 and synaptotagmin-7 act as redundant calcium-sensing mediators of AMPAR exocytosis during LTP in hippocampal CA1 region.

Lateral diffusion and capture at synaptic sites

After fusion with the membrane, endosomes release their cargo and the newly inserted extrasynaptic AMPARs are essentially free to diffuse through the membrane before insertion into the synaptic membrane (figure 4). Indeed, several methods have demonstrated that extrasynaptic receptors are highly mobile but become restricted in their diffusion at synaptic sites (Adesnik et al., 2005; Choquet and Triller, 2013; Ehlers et al., 2007; Heine et al., 2008a; Kerr and Blanpied, 2012; Opazo and Choquet, 2011). Thus, at synapses, mechanisms have to be in place that can effectively counteract free diffusion and anchor and position receptors in close opposition to the presynaptic release site. At glutamatergic synapses, AMPARs are concentrated in the PSD, a dense accumulation of scaffolding proteins, signaling molecules and adhesion complexes (Sheng and Kim, 2011). At mature synapses, the prototypical MAGUK PSD-95 is one of the core components of the PSD that anchors AMPARs at the synapse via binding to TARPs (Bats et al., 2007; Ehrlich and Malinow, 2004; Elias et al., 2006; Schnell et al., 2002). The bidirectional effects of PSD-95 overexpression and depletion on AMPAR-mediated transmission (see section 2), and the relative high abundance of PSD-95 in the PSD gave rise to the “slot-hypothesis” (Lisman and Raghavachari, 2006). This model postulates that potentiation of synaptic transmission involves the addition of binding sites for AMPARs, provided by PSD-95 and perhaps other scaffolds. However, changes in scaffold levels do not seem to precede LTP-induced synapse insertion of AMPARs, or the maturation of newly formed synapses. Rather, posttranslational modification of TARPs by CaMKII increases the affinity of AMPAR complexes for PSD-95, effectively stabilizing receptors at the PSD (Bats et al., 2007; Chetkovich et al., 2002; Sumioka et al., 2010). Apart from intracellular interactions, recent studies demonstrated that the extracellular NTD is required for proper AMPAR trafficking to synapses (Diaz-Alonso et al., 2017; Watson et al., 2017). The differential contribution of CTD- and NTD-mediated interactions of individual AMPAR subunits remains to be investigated, but it becomes clear that AMPARs are subject to a dynamic interplay of molecular interactions that control their lateral diffusion and capture at synaptic sites.

Once at the synapse, the subsynaptic positioning of AMPARs relative to the presynaptic release site ultimately determines the efficacy of synaptic transmission. Because the affinity of AMPARs for glutamate is relatively low, single release events generally activate only a subset of the postsynaptic pool of receptors (Franks et al., 2003; MacGillavry et al., 2011; Raghavachari and Lisman, 2004). Based on computational studies and physiological evidence that postsynaptic receptors are not saturated by single release events (Liu et al., 1999), it has been proposed that concentrating AMPARs close to the presynaptic release site increases synaptic efficacy. Consistent with this idea, recent super-resolution imaging studies have demonstrated that AMPARs are concentrated in subsynaptic PSD-95 nanodomains of approximately 80 nm (figure 4) (MacGillavry et al., 2013; Nair et al., 2013), that are often closely aligned with the presynaptic release site (Tang et al., 2016). This unprecedented level of subsynaptic organization has important consequences for how synaptic strength and plasticity can be regulated (Chen et al., 2018). Yet, how this distinct subsynaptic organization is established over the course of synapse development has not been studied yet and it will be of interest to address this more systematically.

Endocytosis and endosomal trafficking

The principal mechanism for the regulated removal of postsynaptic AMPARs from the postsynaptic membrane is clathrin-mediated endocytosis (figure 4) (Carroll et al., 1999; Man et al., 2000). AMPARs undergo continual cycles of endocytosis, but activity-regulated endocytosis of AMPARs is particularly important for the expression of LTD (Beattie et al., 2000; Luscher et al., 1999). The molecular players in clathrin-mediated endocytosis have been well characterized in other systems (Kaksonen and Roux, 2018), and for most of the core endocytic proteins, including adaptor molecules such as AP-2, endophilins and dynamins that regulate endosome formation and budding, it has been shown that these are localized at postsynaptic sites and are involved in AMPAR endocytosis (Chowdhury et al., 2006; Loebrich et al., 2016; Luscher et al., 1999; Racz et al., 2004). In mature, but not developing neurons, endocytosis of AMPARs preferentially occurs at a specialized site adjacent to the PSD that is enriched in clathrin, Eps15, and Dynamin-3 (Blanpied et al., 2002; Petrini et al., 2009; Racz et al., 2004; Rosendale et al., 2017). These endocytic zones (EZs) are physically coupled to the PSD via Shank/Homer/dynamin-3 interactions, and removal of either one of these components results in uncoupling of the EZ from the PSD. This particular localization of the EZ is thought to form a site for preferential capture and internalization of synaptic receptors to retain a local population of receptors in recycling endosomes. Indeed, uncoupling of the EZ from the PSD results in decreased receptor recycling and consequently depletes surface levels of synaptic receptors (Lu et al., 2007; Petrini et al., 2009). The EZ seems to be a characteristic feature of mature synapses (Blanpied et al., 2002; Blanpied et al., 2003), and it remains to be investigated how the EZ develops and what processes control the formation and maintenance of this structure.

Another key regulator in receptor trafficking is the actin cytoskeleton that regulates important aspects of AMPAR endocytosis and endosomal sorting. Several actin-binding proteins such as N-WASP, Arc/Arg3.1, candidate plasticity gene 2 (CPG2) and Cortactin (Chowdhury et al., 2006; Cottrell et al., 2004; DaSilva et al., 2016; Loebrich et al., 2016; Parkinson et al., 2018), as well as the actin-based motor protein Myosin VI (Osterweil et al., 2005) have been shown to directly affect AMPAR internalization via regulation of actin dynamics. For example, the activity-regulated protein CPG2 was identified as a mediator of endocytosis coupling filamentous actin (F-actin) to Endophilin-B2 (Cottrell et al., 2004; Loebrich et al., 2016; Loebrich et al., 2013). Knockdown of Endophilin-B2 inhibits activity-dependent internalization of AMPARs, and CPG2 knockdown resulted in an accumulation of clathrin coated vesicles in spines, hampering the recycling process (Cottrell et al., 2004). Another immediate early gene product, Arc/Arg3.1, that is locally translated, interacts with Dynamin and Endophilin to accelerate endocytosis of AMPARs (Chowdhury et al., 2006). Interestingly, these effects are selective for AMPARs, suggesting that Arc might act as a specific adaptor protein targeting AMPARs for endocytosis (figure 4). Recently, a similar role for PICK1 has been suggested. PICK1 binds GluA2-containing AMPARs in an activity-dependent manner (Citri et al., 2010), and promotes the rate of AMPAR endocytosis by coupling to AP2, promoting dynamin polymerization, and regulation of actin dynamics (Fiuza et al., 2017; Rocca and Hanley, 2015; Rocca et al., 2008). The molecular intermediates that sort AMPAR-containing endosomes to the recycling compartment remain to be identified, but recent evidence suggests that specific proteins such as protein kinase C, casein kinase II substrate in neurons (PACSIN) and the actin-binding protein Cortactin promotes sorting of AMPARs to recycling endosomes and prevent sorting to the lysosomal degradation system (figure 4) (Parkinson et al., 2018; Widagdo et al., 2016).

After endocytosis into early endosomes, receptors can undergo selective sorting to either the endocytic recycling compartment (ERC) for reinsertion into the membrane, or to late endosomes and lysosomes for degradation (figure 4) (Anggono and Huganir, 2012; Ehlers, 2000). The endosomal trafficking steps are guided by distinct members of the Rab family of small GTPases (Anggono and Huganir, 2012). For instance, Rab5-dependent trafficking of early endosomes is required for NMDAR-dependent LTD (Brown et al., 2005), while Rab7-dependent trafficking of late endosomes underlies the targeting of AMPARs to lysosomes for proteolytic degradation (figure 4) (Fernandez-Monreal et al., 2012). Importantly, live-cell imaging experiments have shown that Rab11-dependent recycling of AMPARs maintains a recycling pool that is required for the maintenance of synaptic receptor levels, as well as for the rapid supply of AMPARs during LTP induction (Park et al., 2004; Park et al., 2006). Recently, retromer-associated endosomes have been implicated in the delivery of AMPAR-containing vesicles in response to activity specifically (Choy et al., 2014; Temkin et al., 2017). Thus, it seems that different pools of AMPAR-containing endosomes might co-exist in dendrites and spines that can be recruited by different molecular mechanisms to differentially sustain constitutive and activity-dependent exocytosis of AMPARs.

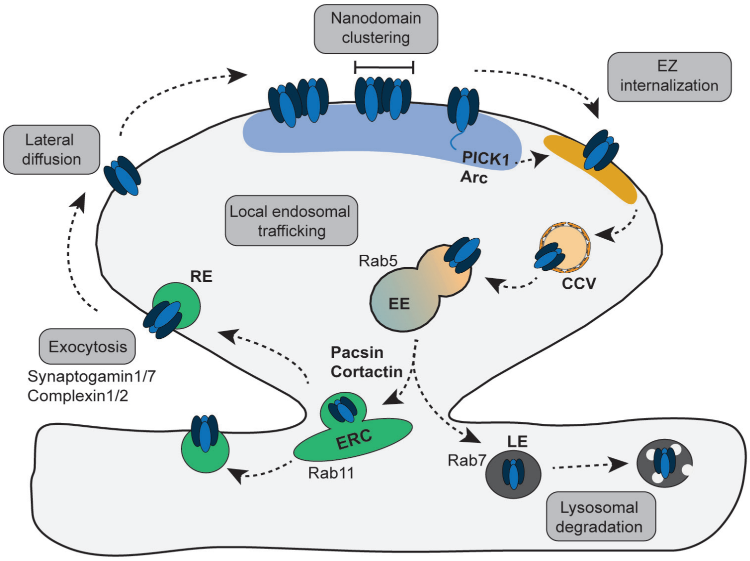

Figure 4. Surface and local endosomal trafficking of AMPARs. AMPARs undergo a sequence of trafficking events to retain a local pool of recycling endosomes, that can be readily exocytosed during LTP. AMPARs are recruited to the PSD (blue zone) via lateral diffusion, where they are captured and cluster into 80nm nanodomains. After uncoupling, receptors are internalized at the endocytic zone (orange zone) via clathrin mediated endocytosis. Clathrin coated vesicles (CCV) release their coat and fuse with early endosomes (EE). From there receptors are either degraded by entering late endosomes (LE), or transported to the endocytic recycling compartment (ERC) where they are released into recycling endosomes that are retained, and exocytosed at the dendritic shaft and spines.

CONCLUSION AND FUTURE PERSPECTIVE

The regulated recruitment of AMPARs to the postsynaptic membrane is a defining step in the development and maturation of synaptic contacts. In the past few decades, extensive investigations have shed light on the composition and function of AMPARs, and the mechanisms that control the sorting and trafficking of receptors to synapses during development and in mature neurons. Yet, while the dynamic, activity-dependent changes in synapse composition and function during development have been identified at a global level, it becomes clear that AMPAR trafficking is highly regulated on the level of single synapses. It will thus be important to study the developmental processes that govern synapse maturation at higher spatial and temporal resolution to reveal synapse-specific mechanisms. Encouragingly, exciting recent advances in microscopy techniques now enable live-cell imaging at much higher spatial and temporal resolution. Together with rapid advances in labeling techniques, and new optogenetic tools to manipulate receptor trafficking, these approaches now allow the study of AMPAR trafficking in much greater detail (Bourke et al., 2018; Reiner and Levitz, 2018). In particular, with super-resolution microscopy the composition and organization of the postsynaptic membrane can be studied on the nanoscale level. For instance, using single-molecule localization and tracking microscopy, an unprecedented level of subsynaptic organization of AMPARs has been revealed (MacGillavry et al., 2013; Nair et al., 2013). Moreover, gene editing technologies based on the CRISPR/Cas9 system has now been established for deletion of synaptic proteins (Incontro et al., 2014), and to introduce fluorescent tag sequences in the genome of post-mitotic neurons (Nishiyama et al., 2017; Suzuki et al., 2016). Such genetic knock-in strategies could be used to localize and track the dynamics of synaptic components in live cells. These strategies are arguably preferred over overexpression studies, as exogenous expression of AMPAR subunits, or other synaptic proteins can have unfavorable side effects on synapse formation and function. As a complement to these labeling methods, several new techniques manipulating AMPAR trafficking have been described, such as refined assays to visualize endocytic events (Rosendale et al., 2017), and light-inducible systems to temporally control receptor recruitment to synapses (Sinnen et al., 2017), or receptor endocytosis (Wood et al., 2017). These approaches will greatly contribute to our understanding of the mechanisms of receptor trafficking at individual synapses. For instance, while the relatively late recruitment of functional AMPARs to synapses has consistently been observed, it remains unclear whether silent synapses do not contain AMPARs at all, or rather contain non-responsive, silent AMPARs. And, importantly, the exact molecular mechanisms underlying the maintenance of silent synapses and their transition to mature, functional synapses remain poorly identified. Also, whether these mechanisms vary between different brain regions and different developmental stages is unknown. Further studies combining advanced imaging techniques in combination with molecular biological tools to precisely label and manipulate receptor levels at synapses would clarify these aspects at single synapses in different brain regions and at different developmental stages. Intriguingly, glutamatergic synapses appear to develop normally in the absence of synaptic transmission, suggesting that intrinsic programs can drive the core developmental steps of excitatory synapses in the absence of activity. Nevertheless, synaptic activity patterns are critical for guiding the development of neuronal networks. How does synaptic activity impinge on this intrinsic molecular blueprint? Even further, how is the development of synapses tuned by experience-dependent changes in neuronal activity that shape synaptic connectivity of neuronal circuits.

In this chapter we highlighted the current understanding of AMPAR trafficking during development and in mature neurons. Intriguingly, AMPAR trafficking defects have been implicated in a wide variety of neurodevelopmental disorders such as autism spectrum disorder, schizophrenia, Fragile X syndrome, and bipolar disease.

Indeed, these disorders are associated with severe defects in synapse development and synaptic functioning. Thus, identifying how the spatiotemporal control of AMPAR trafficking is established during synapse development and maturation would greatly contribute to our understanding of synaptic transmission and plasticity, but will also provide a basis for understanding disease mechanisms.

References

Adesnik, H., G. Li, M.J. During, S.J. Pleasure, and R.A. Nicoll. 2008. NMDA receptors inhibit synapse unsilencing during brain development. Proceedings of the National Academy of Sciences of the United States of America. 105:5597-5602.

Adesnik, H., R.A. Nicoll, and P.M. England. 2005. Photoinactivation of native AMPA receptors reveals their real-time trafficking. Neuron. 48:977-985.

Ahmad, M., J.S. Polepalli, D. Goswami, X. Yang, Y.J. Kaeser-Woo, T.C. Sudhof, and R.C. Malenka. 2012. Postsynaptic complexin controls AMPA receptor exocytosis during LTP. Neuron. 73:260-267.

Akaneya, Y. 2007. Activity regulates the expression of AMPA receptor subunit GluR4 in developing visual cortex. Eur J Neurosci. 25:1641-1646.

Anggono, V., and R.L. Huganir. 2012. Regulation of AMPA receptor trafficking and synaptic plasticity. Current Opinion in Neurobiology. 22:461-469.

Ashby, M.C., and J.T. Isaac. 2011. Maturation of a recurrent excitatory neocortical circuit by experience-dependent unsilencing of newly formed dendritic spines. Neuron. 70:510-521.

Ayalon, G., and Y. Stern-Bach. 2001. Functional assembly of AMPA and kainate receptors is mediated by several discrete protein-protein interactions. Neuron. 31:103-113.

Barrow, S.L., J.R. Constable, E. Clark, F. El-Sabeawy, A.K. McAllister, and P. Washbourne. 2009. Neuroligin1: a cell adhesion molecule that recruits PSD-95 and NMDA receptors by distinct mechanisms during synaptogenesis. Neural Dev. 4:17.

Bats, C., L. Groc, and D. Choquet. 2007. The interaction between Stargazin and PSD-95 regulates AMPA receptor surface trafficking. Neuron. 53:719-734.

Beattie, E.C., R.C. Carroll, X. Yu, W. Morishita, H. Yasuda, M. von Zastrow, and R.C. Malenka. 2000. Regulation of AMPA receptor endocytosis by a signaling mechanism shared with LTD. Nat Neurosci. 3:1291-1300.

Bedoukian, M.A., A.M. Weeks, and K.M. Partin. 2006. Different domains of the AMPA receptor direct stargazin-mediated trafficking and stargazin-mediated modulation of kinetics. J Biol Chem. 281:23908-23921.

Blanpied, T.A., D.B. Scott, and M.D. Ehlers. 2002. Dynamics and regulation of clathrin coats at specialized endocytic zones of dendrites and spines. Neuron. 36:435-449.

Blanpied, T.A., D.B. Scott, and M.D. Ehlers. 2003. Age-related regulation of dendritic endocytosis associated with altered clathrin dynamics. Neurobiol Aging. 24:1095-1104.

Bourke, A.M., A.B. Bowen, and M.J. Kennedy. 2018. New approaches for solving old problems in neuronal protein trafficking. Molecular and Cellular Neuroscience.

Bowen, A.B., A.M. Bourke, B.G. Hiester, C. Hanus, and M.J. Kennedy. 2017. Golgi-independent secretory trafficking through recycling endosomes in neuronal dendrites and spines. Elife. 6.

Brechet, A., R. Buchert, J. Schwenk, S. Boudkkazi, G. Zolles, K. Siquier-Pernet, I. Schaber, W. Bildl, A. Saadi, C. Bole-Feysot, P. Nitschke, A. Reis, H. Sticht, N. Al-Sanna'a, A.

Rolfs, A. Kulik, U. Schulte, L. Colleaux, R. Abou Jamra, and B. Fakler. 2017. AMPA-receptor specific biogenesis complexes control synaptic transmission and intellectual ability. Nat Commun. 8:15910.

Brockie, P.J., M. Jensen, J.E. Mellem, E. Jensen, T. Yamasaki, R. Wang, D. Maxfield, C. Thacker, F. Hoerndli, P.J. Dunn, S. Tomita, D.M. Madsen, and A.V. Maricq. 2013. Cornichons control ER export of AMPA receptors to regulate synaptic excitability. Neuron. 80:129-142.

Brown, T.C., I.C. Tran, D.S. Backos, and J.A. Esteban. 2005. NMDA receptor-dependent activation of the small GTPase Rab5 drives the removal of synaptic AMPA receptors during hippocampal LTD. Neuron. 45:81-94.

Brusa, R., F. Zimmermann, D.S. Koh, D. Feldmeyer, P. Gass, P.H. Seeburg, and R. Sprengel. 1995. Early-onset epilepsy and postnatal lethality associated with an editing-deficient GluR-B allele in mice. Science. 270:1677-1680.

Burnashev, N., H. Monyer, P.H. Seeburg, and B. Sakmann. 1992. Divalent ion permeability of AMPA receptor channels is dominated by the edited form of a single subunit. Neuron. 8:189-198.

Busetto, G., M.J. Higley, and B.L. Sabatini. 2008. Developmental presence and disappearance of postsynaptically silent synapses on dendritic spines of rat layer 2/3 pyramidal neurons. J Physiol. 586:1519-1527.

Carroll, R.C., E.C. Beattie, H. Xia, C. Luscher, Y. Altschuler, R.A. Nicoll, R.C. Malenka, and M. von Zastrow. 1999. Dynamin-dependent endocytosis of ionotropic glutamate receptors. Proc Natl Acad Sci U S A. 96:14112-14117.

Chen, H., A.H. Tang, and T.A. Blanpied. 2018. Subsynaptic spatial organization as a regulator of synaptic strength and plasticity. Curr Opin Neurobiol. 51:147-153.

Chen, L., S. Bao, X. Qiao, and R.F. Thompson. 1999. Impaired cerebellar synapse maturation in waggler, a mutant mouse with a disrupted neuronal calcium channel gamma subunit. Proc Natl Acad Sci U S A. 96:12132-12137.

Chen, N., N.J. Pandya, F. Koopmans, V. Castelo-Szekelv, R.C. van der Schors, A.B. Smit, and K.W. Li. 2014. Interaction proteomics reveals brain region-specific AMPA receptor complexes. J Proteome Res. 13:5695-5706.

Chetkovich, D.M., L. Chen, T.J. Stocker, R.A. Nicoll, and D.S. Bredt. 2002. Phosphorylation of the postsynaptic density-95 (PSD-95)/discs large/zona occludens-1 binding site of stargazin regulates binding to PSD-95 and synaptic targeting of AMPA receptors. J Neurosci. 22:5791-5796.

Choi, S., J. Klingauf, and R.W. Tsien. 2000. Postfusional regulation of cleft glutamate concentration during LTP at ‘silent synapses’. Nat Neurosci. 3:330-336.

Choquet, D., and A. Triller. 2013. The dynamic synapse. Neuron. 80:691-703.

Chowdhury, S., J.D. Shepherd, H. Okuno, G. Lyford, R.S. Petralia, N. Plath, D. Kuhl, R.L. Huganir, and P.F. Worley. 2006. Arc/Arg3.1 interacts with the endocytic machinery to regulate AMPA receptor trafficking. Neuron. 52:445-459.

Choy, R.W., M. Park, P. Temkin, B.E. Herring, A. Marley, R.A. Nicoll, and M. von Zastrow. 2014. Retromer mediates a discrete route of local membrane delivery to dendrites. Neuron. 82:55-62.

Citri, A., S. Bhattacharyya, C. Ma, W. Morishita, S. Fang, J. Rizo, and R.C. Malenka. 2010. Calcium binding to PICK1 is essential for the intracellular retention of AMPA receptors underlying long-term depression. J Neurosci. 30:16437-16452.

Cottrell, J.R., E. Borok, T.L. Horvath, and E. Nedivi. 2004. CPG2: a brain- and synapse-specific protein that regulates the endocytosis of glutamate receptors. Neuron. 44:677-690.

Crair, M.C., and R.C. Malenka. 1995. A critical period for long-term potentiation at thalamocortical synapses. Nature. 375:325-328.

Cui-Wang, T., C. Hanus, T. Cui, T. Helton, J. Bourne, D. Watson, K.M. Harris, and M.D. Ehlers. 2012. Local zones of endoplasmic reticulum complexity confine cargo in neuronal dendrites. Cell. 148:309-321.

D’Angelo, E., P. Rossi, and V. Taglietti. 1993. Different proportions of N-methyl-D-aspartate and non-N-methyl-D-aspartate receptor currents at the mossy fibre-granule cell synapse of developing rat cerebellum. Neuroscience. 53:121-130.

DaSilva, L.L., M.J. Wall, P.d.A. L, S.C. Wauters, Y.C. Januario, J. Muller, and S.A. Correa. 2016. Activity-Regulated Cytoskeleton-Associated Protein Controls AMPAR Endocytosis through a Direct Interaction with Clathrin-Adaptor Protein 2. eNeuro. 3.

de Wit, J., and A. Ghosh. 2016. Specification of synaptic connectivity by cell surface interactions. Nat Rev Neurosci. 17:22-35.

de Wit, J., M.L. O'Sullivan, J.N. Savas, G. Condomitti, M.C. Caccese, K.M. Vennekens, J.R. Yates, 3rd, and A. Ghosh. 2013. Unbiased discovery of glypican as a receptor for LRRTM4 in regulating excitatory synapse development. Neuron. 79:696-711.

Diaz-Alonso, J., Y.J. Sun, A.J. Granger, J.M. Levy, S.M. Blankenship, and R.A. Nicoll. 2017. Subunit-specific role for the amino-terminal domain of AMPA receptors in synaptic targeting. Proc Natl Acad Sci U S A. 114:7136-7141.

Durand, G.M., Y. Kovalchuk, and A. Konnerth. 1996. Long-term potentiation and functional synapse induction in developing hippocampus. Nature. 381:71-75.

Ehlers, M., M. Heine, L. Groc, M. Lee, and D. Choquet. 2007. Diffusional trapping of GluR1 AMPA receptors by input-specific synaptic activity. Neuron. 54:447-460.

Ehlers, M.D. 2000. Reinsertion or degradation of AMPA receptors determined by activity-dependent endocytic sorting. Neuron. 28:511-525.

Ehrlich, I., and R. Malinow. 2004. Postsynaptic density 95 controls AMPA receptor incorporation during long-term potentiation and experience-driven synaptic plasticity. J Neurosci. 24:916-927.

Elias, G.M., L.A.B. Elias, P.F. Apostolides, A.R. Kriegstein, and R.A. Nicoll. 2008. Differential trafficking of AMPA and NMDA receptors by SAP102 and PSD-95 underlies synapse development. Proceedings of the National Academy of Sciences. 105:20953-20958.

Elias, G.M., L. Funke, V. Stein, S.G. Grant, D.S. Bredt, and R.A. Nicoll. 2006. Synapse-specific and developmentally regulated targeting of AMPA receptors by a family of MAGUK scaffolding proteins. Neuron. 52:307-320.

Esteban, J.A., S.H. Shi, C. Wilson, M. Nuriya, R.L. Huganir, and R. Malinow. 2003. PKA phosphorylation of AMPA receptor subunits controls synaptic trafficking underlying plasticity. Nat Neurosci. 6:136-143.

Fernandez-Monreal, M., T.C. Brown, M. Royo, and J.A. Esteban. 2012. The balance between receptor recycling and trafficking toward lysosomes determines synaptic strength during long-term depression. J Neurosci. 32:13200-13205.

Fiuza, M., C.M. Rostosky, G.T. Parkinson, A.M. Bygrave, N. Halemani, M. Baptista, I. Milosevic, and J.G. Hanley. 2017. PICK1 regulates AMPA receptor endocytosis via direct interactions with AP2 alpha-appendage and dynamin. J Cell Biol. 216:3323-3338.

Flint, A.C., U.S. Maisch, J.H. Weishaupt, A.R. Kriegstein, and H. Monyer. 1997. NR2A subunit expression shortens NMDA receptor synaptic currents in developing neocortex. J Neurosci. 17:2469-2476.

Foa, L., and R. Gasperini. 2009. Developmental roles for Homer: more than just a pretty scaffold. J Neurochem. 108:1-10.

Forrest, D., M. Yuzaki, H.D. Soares, L. Ng, D.C. Luk, M. Sheng, C.L. Stewart, J.I. Morgan, J.A. Connor, and T. Curran. 1994. Targeted disruption of NMDA receptor 1 gene abolishes NMDA response and results in neonatal death. Neuron. 13:325-338.

Franks, K.M., C.F. Stevens, and T.J. Sejnowski. 2003. Independent sources of quantal variability at single glutamatergic synapses. J Neurosci. 23:3186-3195.

Friedman, H.V., T. Bresler, C.C. Garner, and N.E. Ziv. 2000. Assembly of New Individual Excitatory Synapses. Neuron. 27:57-69.

Gerges, N.Z., D.S. Backos, C.N. Rupasinghe, M.R. Spaller, and J.A. Esteban. 2006. Dual role of the exocyst in AMPA receptor targeting and insertion into the postsynaptic membrane. EMBO J. 25:1623-1634.

Gomperts, S.N., A. Rao, A.M. Craig, R.C. Malenka, and R.A. Nicoll. 1998. Postsynaptically Silent Synapses in Single Neuron Cultures. Neuron. 21:1443-1451.

Graf, E.R., X. Zhang, S.X. Jin, M.W. Linhoff, and A.M. Craig. 2004. Neurexins induce differentiation of GABA and glutamate postsynaptic specializations via neuroligins. Cell. 119:1013-1026.

Granger, A.J., Y. Shi, W. Lu, M. Cerpas, and R.A. Nicoll. 2013. LTP requires a reserve pool of glutamate receptors independent of subunit type. Nature. 493:495-500.

Gray, J.A., Y. Shi, H. Usui, M.J. During, K. Sakimura, and R.A. Nicoll. 2011. Distinct Modes of AMPA Receptor Suppression at Developing Synapses by GluN2A and GluN2B: Single-Cell NMDA Receptor Subunit Deletion In Vivo. Neuron. 71:1085-1101.

Greger, I.H., P. Akamine, L. Khatri, and E.B. Ziff. 2006. Developmentally regulated, combinatorial RNA processing modulates AMPA receptor biogenesis. Neuron. 51:85-97.

Greger, I.H., L. Khatri, and E.B. Ziff. 2002. RNA editing at arg607 controls AMPA receptor exit from the endoplasmic reticulum. Neuron. 34:759-772.

Greger, I.H., E.B. Ziff, and A.C. Penn. 2007. Molecular determinants of AMPA receptor subunit assembly. Trends Neurosci. 30:407-416.

Grunwald, M.E., and J.M. Kaplan. 2003. Mutations in the ligand-binding and pore domains control exit of glutamate receptors from the endoplasmic reticulum in C. elegans. Neuropharmacology. 45:768-776.

Hall, B.J., and A. Ghosh. 2008. Regulation of AMPA receptor recruitment at developing synapses. Trends in Neurosciences. 31:82-89.

Hall, B.J., B. Ripley, and A. Ghosh. 2007. NR2B Signaling Regulates the Development of Synaptic AMPA Receptor Current. Journal of Neuroscience. 27:13446-13456.

Hanse, E., H. Seth, and I. Riebe. 2013. AMPA-silent synapses in brain development and pathology. Nature Reviews Neuroscience. 14:839-850.

Hanus, C., H. Geptin, G. Tushev, S. Garg, B. Alvarez-Castelao, S. Sambandan, L. Kochen, A.S. Hafner, J.D. Langer, and E.M. Schuman. 2016. Unconventional secretory processing diversifies neuronal ion channel properties. Elife. 5.

Hanus, C., L. Kochen, S. Tom Dieck, V. Racine, J.B. Sibarita, E.M. Schuman, and M.D. Ehlers. 2014. Synaptic control of secretory trafficking in dendrites. Cell Rep. 7:1771-1778.

Hashimoto, K., M. Fukaya, X. Qiao, K. Sakimura, M. Watanabe, and M. Kano. 1999. Impairment of AMPA receptor function in cerebellar granule cells of ataxic mutant mouse stargazer. J Neurosci. 19:6027-6036.

Heine, M., L. Groc, R. Frischknecht, J.-C. Béïque, B. Lounis, G. Rumbaugh, R.L. Huganir, L. Cognet, and D. Choquet. 2008a. Surface mobility of postsynaptic AMPARs tunes synaptic transmission. Science (New York, N.Y.). 320:201-205.

Heine, M., O. Thoumine, M. Mondin, B. Tessier, G. Giannone, and D. Choquet. 2008b. Activity-independent and subunit-specific recruitment of functional AMPA receptors at neurexin/neuroligin contacts. Proc Natl Acad Sci U S A. 105:20947-20952. Henley, J.M., and K.A. Wilkinson. 2016. Synaptic AMPA receptor composition in development, plasticity and disease. Nat Rev Neurosci. 17:337-350.

Herguedas, B., J. Garcia-Nafria, O. Cais, R. Fernandez-Leiro, J. Krieger, H. Ho, and I.H. Greger. 2016. Structure and organization of heteromeric AMPA-type glutamate receptors. Science. 352:aad3873.

Hestrin, S. 1992. Developmental regulation of NMDA receptor-mediated synaptic currents at a central synapse. Nature. 357:686-689.

Hirokawa, N., S. Niwa, and Y. Tanaka. 2010. Molecular motors in neurons: transport mechanisms and roles in brain function, development, and disease. Neuron. 68:610-638.

Hollmann, M., M. Hartley, and S. Heinemann. 1991. Ca2+ permeability of KA-AMPA--gated glutamate receptor channels depends on subunit composition. Science. 252:851-853.

Hoogenraad, C.C., A.D. Milstein, I.M. Ethell, M. Henkemeyer, and M. Sheng. 2005. GRIP1 controls dendrite morphogenesis by regulating EphB receptor trafficking. Nat Neurosci. 8:906-915.

Horton, A.C., and M.D. Ehlers. 2003. Dual modes of endoplasmic reticulum-to-Golgi transport in dendrites revealed by live-cell imaging. J Neurosci. 23:6188-6199.

Huganir, R.L., and R.A. Nicoll. 2013. AMPARs and synaptic plasticity: the last 25 years. Neuron. 80:704-717.

Hume, R.I., R. Dingledine, and S.F. Heinemann. 1991. Identification of a site in glutamate receptor subunits that controls calcium permeability. Science. 253:1028-1031.

Incontro, S., C.S. Asensio, R.H. Edwards, and R.A. Nicoll. 2014. Efficient, complete deletion of synaptic proteins using CRISPR. Neuron. 83:1051-1057.

Isaac, J.T., R.A. Nicoll, and R.C. Malenka. 1995. Evidence for silent synapses: implications for the expression of LTP. Neuron. 15:427-434.

Jackson, A.C., and R.A. Nicoll. 2011. The expanding social network of ionotropic glutamate receptors: TARPs and other transmembrane auxiliary subunits. Neuron. 70:178-199.

Jacobi, E., and J. von Engelhardt. 2018. AMPA receptor complex constituents: Control of receptor assembly, membrane trafficking and subcellular localization. Mol Cell Neurosci. 91:67-75.

Jacobs, M.M., R.L. Fogg, R.B. Emeson, and G.D. Stanwood. 2009. ADAR1 and ADAR2 expression and editing activity during forebrain development. Dev Neurosci. 31:223-237.

Jurado, S. 2014. The dendritic SNARE fusion machinery involved in AMPARs insertion during long-term potentiation. Front Cell Neurosci. 8:407.

Jurado, S., D. Goswami, Y. Zhang, A.J. Molina, T.C. Sudhof, and R.C. Malenka. 2013. LTP requires a unique postsynaptic SNARE fusion machinery. Neuron. 77:542-558.

Kaksonen, M., and A. Roux. 2018. Mechanisms of clathrin-mediated endocytosis. Nat Rev Mol Cell Biol. 19:313-326.

Kalashnikova, E., R.A. Lorca, I. Kaur, G.A. Barisone, B. Li, T. Ishimaru, J.S. Trimmer, D.P. Mohapatra, and E. Diaz. 2010. SynDIG1: an activity-regulated, AMPA- receptor-interacting transmembrane protein that regulates excitatory synapse development. Neuron. 65:80-93.

Kapitein, L.C., and C.C. Hoogenraad. 2015. Building the Neuronal Microtubule Cytoskeleton. Neuron. 87:492-506.

Kato, A.S., M.B. Gill, H. Yu, E.S. Nisenbaum, and D.S. Bredt. 2010. TARPs differentially decorate AMPA receptors to specify neuropharmacology. Trends Neurosci. 33:241-248.

Kennedy, M.J., I.G. Davison, C.G. Robinson, and M.D. Ehlers. 2010. Syntaxin-4 defines a domain for activity-dependent exocytosis in dendritic spines. Cell. 141:524-535.

Kerr, J.M., and T.A. Blanpied. 2012. Subsynaptic AMPA receptor distribution is acutely regulated by actin-driven reorganization of the postsynaptic density. J Neurosci. 32:658-673.

Kessels, H.W., and R. Malinow. 2009. Synaptic AMPA receptor plasticity and behavior. Neuron. 61:340-350.

Kim, M.J., A.W. Dunah, Y.T. Wang, and M. Sheng. 2005. Differential roles of NR2A- and NR2B-containing NMDA receptors in Ras-ERK signaling and AMPA receptor trafficking. Neuron. 46:745-760.

Kolleker, A., J.J. Zhu, B.J. Schupp, Y. Qin, V. Mack, T. Borchardt, G. Kohr, R. Malinow, P.H. Seeburg, and P. Osten. 2003. Glutamatergic plasticity by synaptic delivery of GluR-B(long)-containing AMPA receptors. Neuron. 40:1199-1212.

Kopec, C.D., B. Li, W. Wei, J. Boehm, and R. Malinow. 2006. Glutamate receptor exocytosis and spine enlargement during chemically induced long-term potentiation. J

Neurosci. 26:2000-2009.

Kutsuwada, T., K. Sakimura, T. Manabe, C. Takayama, N. Katakura, E. Kushiya, R. Natsume, M. Watanabe, Y. Inoue, T. Yagi, S. Aizawa, M. Arakawa, T. Takahashi, Y. Nakamura, H. Mori, and M. Mishina. 1996. Impairment of suckling response, trigeminal neuronal pattern formation, and hippocampal LTD in NMDA receptor epsilon 2 subunit mutant mice. Neuron. 16:333-344.

Kwon, H.B., and B.L. Sabatini. 2011. Glutamate induces de novo growth of functional spines in developing cortex. Nature. 474:100-104.

Lambert, J.T., T.C. Hill, D.K. Park, J.H. Culp, and K. Zito. 2017. Protracted and asynchronous accumulation of PSD95-family MAGUKs during maturation of nascent dendritic spines. Dev Neurobiol. 77:1161-1174.

Liao, D., N.A. Hessler, and R. Malinow. 1995. Activation of postsynaptically silent synapses during pairing-induced LTP in CA1 region of hippocampal slice. Nature. 375:400-404.

Liao, D., X. Zhang, R. O’Brien, M.D. Ehlers, and R.L. Huganir. 1999. Regulation of morphological postsynaptic silent synapses in developing hippocampal neurons. Nat Neurosci. 2:37-43.

Lisman, J., and S. Raghavachari. 2006. A unified model of the presynaptic and postsynaptic changes during LTP at CA1 synapses. Sci STKE. 2006:re11.

Liu, G., S. Choi, and R.W. Tsien. 1999. Variability of neurotransmitter concentration and nonsaturation of postsynaptic AMPA receptors at synapses in hippocampal cultures and slices. Neuron. 22:395-409.

Lledo, P.M., X. Zhang, T.C. Sudhof, R.C. Malenka, and R.A. Nicoll. 1998. Postsynaptic membrane fusion and long-term potentiation. Science. 279:399-403.

Loebrich, S., M.R. Benoit, J.A. Konopka, J.R. Cottrell, J. Gibson, and E. Nedivi. 2016. CPG2 Recruits Endophilin B2 to the Cytoskeleton for Activity-Dependent Endocytosis of Synaptic Glutamate Receptors. Curr Biol. 26:296-308.

Loebrich, S., B. Djukic, Z.J. Tong, J.R. Cottrell, G.G. Turrigiano, and E. Nedivi. 2013. Regulation of glutamate receptor internalization by the spine cytoskeleton is mediated by its PKA-dependent association with CPG2. Proc Natl Acad Sci USA. 110:E4548-4556.

Lu, J., T.D. Helton, T.A. Blanpied, B. Rácz, T.M. Newpher, R.J. Weinberg, and M.D. Ehlers. 2007. Postsynaptic Positioning of Endocytic Zones and AMPA Receptor Cycling by Physical Coupling of Dynamin-3 to Homer. Neuron. 55:874-889.

Lu, W., E.A. Bushong, T.P. Shih, M.H. Ellisman, and R.A. Nicoll. 2013. The cell-autonomous role of excitatory synaptic transmission in the regulation of neuronal structure and function. Neuron. 78:433-439.

Lu, W., J.A. Gray, A.J. Granger, M.J. During, and R.A. Nicoll. 2011. Potentiation of synaptic AMPA receptors induced by the deletion of NMDA receptors requires the GluA2 subunit. J Neurophysiol. 105:923-928.

Lu, W., H. Man, W. Ju, W.S. Trimble, J.F. MacDonald, and Y.T. Wang. 2001. Activation of synaptic NMDA receptors induces membrane insertion of new AMPA receptors and LTP in cultured hippocampal neurons. Neuron. 29:243-254.

Lu, W., Y. Shi, A.C. Jackson, K. Bjorgan, M.J. During, R. Sprengel, P.H. Seeburg, and R.A. Nicoll. 2009. Subunit composition of synaptic AMPA receptors revealed by a single-cell genetic approach. Neuron. 62:254-268.

Luchkina, N.V., J. Huupponen, V.R.J. Clarke, S.K. Coleman, K. Keinänen, T. Taira, and S.E. Lauri. 2014. Developmental switch in the kinase dependency of long-term potentiation depends on expression of GluA4 subunit-containing AMPA receptors. Proceedings of the National Academy of Sciences of the United States of America. 111:4321-4326.

Luscher, C., H. Xia, E.C. Beattie, R.C. Carroll, M. von Zastrow, R.C. Malenka, and R.A. Nicoll. 1999. Role of AMPA receptor cycling in synaptic transmission and plasticity. Neuron. 24:649-658.

MacGillavry, H.D., J.M. Kerr, and T.A. Blanpied. 2011. Lateral organization of the postsynaptic density. Mol Cell Neurosci. 48:321-331.

MacGillavry, H.D., Y. Song, S. Raghavachari, and T.A. Blanpied. 2013. Nanoscale scaffolding domains within the postsynaptic density concentrate synaptic AMPA receptors. Neuron. 78:615-622.

Makino, H., and R. Malinow. 2009. AMPA receptor incorporation into synapses during LTP: the role of lateral movement and exocytosis. Neuron. 64:381-390.

Malenka, R.C., and M.F. Bear. 2004. LTP and LTD: an embarrassment of riches. Neuron. 44:5-21.

Malinow, R., and R.C. Malenka. 2002. AMPA receptor trafficking and synaptic plasticity. Annu Rev Neurosci. 25:103-126.

Man, H.Y., J.W. Lin, W.H. Ju, G. Ahmadian, L. Liu, L.E. Becker, M. Sheng, and Y.T. Wang. 2000. Regulation of AMPA receptor-mediated synaptic transmission by clathrin-dependent receptor internalization. Neuron. 25:649-662.

McMahon, H.T., M. Missler, C. Li, and T.C. Sudhof. 1995. Complexins: cytosolic proteins that regulate SNAP receptor function. Cell. 83:111-119.

Mikhaylova, M., S. Bera, O. Kobler, R. Frischknecht, and M.R. Kreutz. 2016. A Dendritic Golgi Satellite between ERGIC and Retromer. Cell Rep. 14:189-199.

Miyazaki, T., M. Kunii, H. Tada, A. Sano, Y. Kuroiwa, T. Goto, R. Malinow, and T. Takahashi. 2012. Developmental AMPA receptor subunit specificity during experience-driven synaptic plasticity in the rat barrel cortex. Brain Res. 1435:1-7.

Monyer, H., N. Burnashev, D.J. Laurie, B. Sakmann, and P.H. Seeburg. 1994. Developmental and regional expression in the rat brain and functional properties of four NMDA receptors. Neuron. 12:529-540.

Monyer, H., P.H. Seeburg, and W. Wisden. 1991. Glutamate-operated channels: developmentally early and mature forms arise by alternative splicing. Neuron. 6:799-810.

Nair, D., E. Hosy, J.D. Petersen, A. Constals, G. Giannone, D. Choquet, and J.B. Sibarita. 2013. Super-resolution imaging reveals that AMPA receptors inside synapses are dynamically organized in nanodomains regulated by PSD95. J Neurosci. 33:13204-13224.

Nicoll, R.A., S. Tomita, and D.S. Bredt. 2006. Auxiliary subunits assist AMPA-type glutamate receptors. Science. 311:1253-1256.

Nishiyama, J., T. Mikuni, and R. Yasuda. 2017. Virus-Mediated Genome Editing via Homology-Directed Repair in Mitotic and Postmitotic Cells in Mammalian Brain. Neuron. 96:755-768 e755.

Nowak, L., P. Bregestovski, P. Ascher, A. Herbet, and A. Prochiantz. 1984. Magnesium gates glutamate-activated channels in mouse central neurones. Nature. 307:462-465.

Nusser, Z., R. Lujan, G. Laube, J.D.B. Roberts, E. Molnar, and P. Somogyi. 1998. Cell Type and Pathway Dependence of Synaptic AMPA Receptor Number and Variability in the Hippocampus. Neuron. 21:545-559.

Opazo, P., and D. Choquet. 2011. A three-step model for the synaptic recruitment of AMPA receptors. Molecular and Cellular Neuroscience. 46:1-8.

Osterweil, E., D.G. Wells, and M.S. Mooseker. 2005. A role for myosin VI in postsynaptic structure and glutamate receptor endocytosis. J Cell Biol. 168:329-338.

Park, M., E.C. Penick, J.G. Edwards, J.A. Kauer, and M.D. Ehlers. 2004. Recycling endosomes supply AMPA receptors for LTP. Science. 305:1972-1975.

Park, M., J.M. Salgado, L. Ostroff, T.D. Helton, C.G. Robinson, K.M. Harris, and M.D. Ehlers.

2006. Plasticity-induced growth of dendritic spines by exocytic trafficking from recycling endosomes. Neuron. 52:817-830.

Parkinson, G.T., S.E.L. Chamberlain, N. Jaafari, M. Turvey, J.R. Mellor, and J.G. Hanley. 2018. Cortactin regulates endo-lysosomal sorting of AMPARs via direct interaction with GluA2 subunit. Sci Rep. 8:4155.

Passafaro, M., V. Piech, and M. Sheng. 2001. Subunit-specific temporal and spatial patterns of AMPA receptor exocytosis in hippocampal neurons. Nat Neurosci. 4:917-926.

Patterson, M.A., E.M. Szatmari, and R. Yasuda. 2010. AMPA receptors are exocytosed in stimulated spines and adjacent dendrites in a Ras-ERK-dependent manner during long-term potentiation. Proc Natl Acad Sci U S A. 107:15951-15956.

Penn, A.C., S.R. Williams, and I.H. Greger. 2008. Gating motions underlie AMPA receptor secretion from the endoplasmic reticulum. EMBO J. 27:3056-3068.

Penn, A.C., C.L. Zhang, F. Georges, L. Royer, C. Breillat, E. Hosy, J.D. Petersen, Y. Humeau, and D. Choquet. 2017. Hippocampal LTP and contextual learning require surface diffusion of AMPA receptors. Nature. 549:384-388.

Petralia, R.S., J.A. Esteban, Y.X. Wang, J.G. Partridge, H.M. Zhao, R.J. Wenthold, and R. Malinow. 1999. Selective acquisition of AMPA receptors over postnatal development suggests a molecular basis for silent synapses. Nature Neuroscience. 2:31-36.

Petralia, R.S., N. Sans, Y.X. Wang, and R.J. Wenthold. 2005. Ontogeny of postsynaptic density proteins at glutamatergic synapses. Mol Cell Neurosci. 29:436-452.

Petrini, E.M., J. Lu, L. Cognet, B. Lounis, M.D. Ehlers, and D. Choquet. 2009. Endocytic trafficking and recycling maintain a pool of mobile surface AMPA receptors required for synaptic potentiation. Neuron. 63:92-105.

Pick, J.E., and E.B. Ziff. 2018. Regulation of AMPA receptor trafficking and exit from the endoplasmic reticulum. Mol Cell Neurosci. 91:3-9.

Pierce, J.P., T. Mayer, and J.B. McCarthy. 2001. Evidence for a satellite secretory pathway in neuronal dendritic spines. Curr Biol. 11:351-355.

Racz, B., T.A. Blanpied, M.D. Ehlers, and R.J. Weinberg. 2004. Lateral organization of endocytic machinery in dendritic spines. Nat Neurosci. 7:917-918.

Raghavachari, S., and J.E. Lisman. 2004. Properties of quantal transmission at CA1 synapses. J Neurophysiol. 92:2456-2467.

Ramoa, A.S., and D.A. McCormick. 1994. Enhanced activation of NMDA receptor responses at the immature retinogeniculate synapse. J Neurosci. 14:2098-2105.

Reiner, A., and J. Levitz. 2018. Glutamatergic Signaling in the Central Nervous System: Ionotropic and Metabotropic Receptors in Concert. Neuron. 98:1080-1098.

Rocca, D.L., and J.G. Hanley. 2015. PICK1 links AMPA receptor stimulation to Cdc42. Neurosci Lett. 585:155-159.

Rocca, D.L., S. Martin, E.L. Jenkins, and J.G. Hanley. 2008. Inhibition of Arp2/3-mediated actin polymerization by PICK1 regulates neuronal morphology and AMPA receptor endocytosis. Nat Cell Biol. 10:259-271.

Rosendale, M., D. Jullie, D. Choquet, and D. Perrais. 2017. Spatial and Temporal Regulation of Receptor Endocytosis in Neuronal Dendrites Revealed by Imaging of Single Vesicle Formation. Cell Rep. 18:1840-1847.

Rosenmund, C., Y. Stern-Bach, and C.F. Stevens. 1998. The tetrameric structure of a glutamate receptor channel. Science. 280:1596-1599.

Rossmann, M., M. Sukumaran, A.C. Penn, D.B. Veprintsev, M.M. Babu, and I.H. Greger. 2011. Subunit-selective N-terminal domain associations organize the formation of AMPA receptor heteromers. EMBO J. 30:959-971.

Sakimura, K., T. Kutsuwada, I. Ito, T. Manabe, C. Takayama, E. Kushiya, T. Yagi, S. Aizawa, Y. Inoue, H. Sugiyama, and M. Mishina. 1995. Reduced hippocampal LTP and spatial learning in mice lacking NMDA receptor ε1 subunit. Nature. 373:151-155.

Sando, R., E. Bushong, Y. Zhu, M. Huang, C. Considine, S. Phan, S. Ju, M. Uytiepo, M. Ellisman, and A. Maximov. 2017. Assembly of Excitatory Synapses in the Absence of Glutamatergic Neurotransmission. Neuron. 94:312-321 e313.

Sans, N., R.S. Petralia, Y.X. Wang, J. Blahos, 2nd, J.W. Hell, and R.J. Wenthold. 2000. A developmental change in NMDA receptor-associated proteins at hippocampal synapses. J Neurosci. 20:1260-1271.

Scheefhals, N., and H.D. MacGillavry. 2018. Functional organization of postsynaptic glutamate receptors. Mol Cell Neurosci. 91:82-94.

Schnell, E., M. Sizemore, S. Karimzadegan, L. Chen, D.S. Bredt, and R.A. Nicoll. 2002. Direct interactions between PSD-95 and stargazin control synaptic AMPA receptor number. Proc Natl Acad Sci U S A. 99:13902-13907.

Schwenk, J., D. Baehrens, A. Haupt, W. Bildl, S. Boudkkazi, J. Roeper, B. Fakler, and U. Schulte. 2014. Regional diversity and developmental dynamics of the AMPA-receptor proteome in the mammalian brain. Neuron. 84:41-54.

Schwenk, J., N. Harmel, A. Brechet, G. Zolles, H. Berkefeld, C.S. Muller, W. Bildl, D. Baehrens, B. Huber, A. Kulik, N. Klocker, U. Schulte, and B. Fakler. 2012. High-resolution proteomics unravel architecture and molecular diversity of native AMPA receptor complexes. Neuron. 74:621-633.

Schwenk, J., N. Harmel, G. Zolles, W. Bildl, A. Kulik, B. Heimrich, O. Chisaka, P. Jonas, U. Schulte, B. Fakler, and N. Klocker. 2009. Functional proteomics identify cornichon proteins as auxiliary subunits of AMPA receptors. Science. 323:1313-1319.

Seeburg, P.H., and J. Hartner. 2003. Regulation of ion channel/neurotransmitter receptor function by RNA editing. Curr Opin Neurobiol. 13:279-283.

Setou, M., D.H. Seog, Y. Tanaka, Y. Kanai, Y. Takei, M. Kawagishi, and N. Hirokawa. 2002. Glutamate-receptor-interacting protein GRIP1 directly steers kinesin to dendrites. Nature. 417:83-87.

Shanks, N.F., J.N. Savas, T. Maruo, O. Cais, A. Hirao, S. Oe, A. Ghosh, Y. Noda, I.H.
Greger, J.R. Yates, 3rd, and T. Nakagawa. 2012. Differences in AMPA and kainate receptor interactomes facilitate identification of AMPA receptor auxiliary subunit GSG1L. Cell Rep. 1:590-598.

Sheng, M., J. Cummings, L.A. Roldan, Y.N. Jan, and L.Y. Jan. 1994. Changing subunit composition of heteromeric NMDA receptors during development of rat cortex. Nature. 368:144-147.

Sheng, M., and E. Kim. 2011. The postsynaptic organization of synapses. Cold Spring Harbor perspectives in biology. 3:a005678.

Shepherd, J.D., and R.L. Huganir. 2007. The Cell Biology of Synaptic Plasticity: AMPA Receptor Trafficking. Annu. Rev. Cell Dev. Biol. 23:613-643.

Shi, J., S.M. Aamodt, M. Townsend, M. Constantine-Paton, M. Mishina, and T. Nabeshima. 2001a. Developmental depression of glutamate neurotransmission by chronic low-level activation of NMDA receptors. The Journal of neuroscience : the official journal of the Society for Neuroscience. 21:6233-6244.

Shi, S., Y. Hayashi, J.A. Esteban, and R. Malinow. 2001b. Subunit-specific rules governing AMPA receptor trafficking to synapses in hippocampal pyramidal neurons. Cell. 105:331-343.

Shi, Y., Y.H. Suh, A.D. Milstein, K. Isozaki, S.M. Schmid, K.W. Roche, and R.A. Nicoll. 2010. Functional comparison of the effects of TARPs and cornichons on AMPA receptor trafficking and gating. Proc Natl Acad Sci U S A. 107:16315-16319.

Shin, H., M. Wyszynski, K.H. Huh, J.G. Valtschanoff, J.R. Lee, J. Ko, M. Streuli, R.J. Weinberg, M. Sheng, and E. Kim. 2003. Association of the kinesin motor KIF1A with the multimodular protein liprin-alpha. J Biol Chem. 278:11393-11401.

Sigler, A., W.C. Oh, C. Imig, B. Altas, H. Kawabe, B.H. Cooper, H.B. Kwon, J.S. Rhee, and N. Brose. 2017. Formation and Maintenance of Functional Spines in the Absence of Presynaptic Glutamate Release. Neuron. 94:304-311 e304.

Sinnen, B.L., A.B. Bowen, J.S. Forte, B.G. Hiester, K.C. Crosby, E.S. Gibson, M.L. Dell'Acqua, and M.J. Kennedy. 2017. Optogenetic Control of Synaptic Composition and Function. Neuron. 93:646-660 e645.

Sobolevsky, A.I., M.P. Rosconi, and E. Gouaux. 2009. X-ray structure, symmetry and mechanism of an AMPA-subtype glutamate receptor. Nature. 462:745-756.

Sommer, B., K. Keinanen, T.A. Verdoorn, W. Wisden, N. Burnashev, A. Herb, M. Kohler, T. Takagi, B. Sakmann, and P.H. Seeburg. 1990. Flip and flop: a cell-specific functional switch in glutamate-operated channels of the CNS. Science. 249:1580-1585.

Sommer, B., M. Kohler, R. Sprengel, and P.H. Seeburg. 1991. RNA editing in brain controls a determinant of ion flow in glutamate-gated channels. Cell. 67:11-19.

Spacek, J., and K.M. Harris. 1997. Three-dimensional organization of smooth endoplasmic reticulum in hippocampal CA1 dendrites and dendritic spines of the immature and mature rat. J Neurosci. 17:190-203.

Stein, V., D.R.C. House, D.S. Bredt, and R.A. Nicoll. 2003. Postsynaptic density-95 mimics and occludes hippocampal long-term potentiation and enhances long-term depression. The Journal of neuroscience : the official journal of the Society for Neuroscience. 23:5503-5506.

Straub, C., and S. Tomita. 2012. The regulation of glutamate receptor trafficking and function by TARPs and other transmembrane auxiliary subunits. Curr Opin Neurobiol. 22:488-495.

Sudhof, T.C. 2013. Neurotransmitter release: the last millisecond in the life of a synaptic vesicle. Neuron. 80:675-690.

Sudhof, T.C. 2017. Synaptic Neurexin Complexes: A Molecular Code for the Logic of Neural Circuits. Cell. 171:745-769.

Sumioka, A., D. Yan, and S. Tomita. 2010. TARP phosphorylation regulates synaptic AMPA receptors through lipid bilayers. Neuron. 66:755-767.

Suzuki, K., Y. Tsunekawa, R. Hernandez-Benitez, J. Wu, J. Zhu, E.J. Kim, F. Hatanaka, M. Yamamoto, T. Araoka, Z. Li, M. Kurita, T. Hishida, M. Li, E. Aizawa, S. Guo, S. Chen, A. Goebl, R.D. Soligalla, J. Qu, T. Jiang, X. Fu, M. Jafari, C.R. Esteban, W.T. Berggren, J. Lajara, E. Nunez-Delicado, P. Guillen, J.M. Campistol, F. Matsuzaki, G.H. Liu, P. Magistretti, K. Zhang, E.M. Callaway, K. Zhang, and J.C. Belmonte. 2016. In vivo genome editing via CRISPR/Cas9 mediated homology-independent targeted integration. Nature. 540:144-149.

Tang, A.H., H. Chen, T.P. Li, S.R. Metzbower, H.D. MacGillavry, and T.A. Blanpied. 2016. A trans-synaptic nanocolumn aligns neurotransmitter release to receptors. Nature. 536:210-214.

Temkin, P., W. Morishita, D. Goswami, K. Arendt, L. Chen, and R. Malenka. 2017. The Retromer Supports AMPA Receptor Trafficking During LTP. Neuron. 94:74-82 e75.

Tomita, S., L. Chen, Y. Kawasaki, R.S. Petralia, R.J. Wenthold, R.A. Nicoll, and D.S. Bredt. 2003. Functional studies and distribution define a family of transmembrane AMPA receptor regulatory proteins. J Cell Biol. 161:805-816.

Verhage, M., A.S. Maia, J.J. Plomp, A.B. Brussaard, J.H. Heeroma, H. Vermeer, R.F. Toonen, R.E. Hammer, T.K. van den Berg, M. Missler, H.J. Geuze, and T.C. Sudhof. 2000. Synaptic assembly of the brain in the absence of neurotransmitter secretion. Science. 287:864-869.

Volk, L., S.-L. Chiu, K. Sharma, and R.L. Huganir. 2015. Glutamate Synapses in Human Cognitive Disorders. Annual Review of Neuroscience. 38:127-149.

von Engelhardt, J., V. Mack, R. Sprengel, N. Kavenstock, K.W. Li, Y. Stern-Bach, A.B. Smit, P.H. Seeburg, and H. Monyer. 2010. CKAMP44: a brain-specific protein attenuating short-term synaptic plasticity in the dentate gyrus. Science. 327:1518-1522.

Wagner, W., S.D. Brenowitz, and J.A. Hammer, 3rd. 2011. Myosin-Va transports the endoplasmic reticulum into the dendritic spines of Purkinje neurons. Nat Cell Biol. 13:40-48.

Wang, Z., J.G. Edwards, N. Riley, D.W. Provance, Jr., R. Karcher, X.D. Li, I.G. Davison, M. Ikebe, J.A. Mercer, J.A. Kauer, and M.D. Ehlers. 2008. Myosin Vb mobilizes recycling endosomes and AMPA receptors for postsynaptic plasticity. Cell. 135:535-548.

Washbourne, P., J.E. Bennett, and A.K. McAllister. 2002. Rapid recruitment of NMDA receptor transport packets to nascent synapses. Nat Neurosci. 5:751-759.

Washbourne, P., X.B. Liu, E.G. Jones, and A.K. McAllister. 2004. Cycling of NMDA receptors during trafficking in neurons before synapse formation. J Neurosci. 24:8253-8264.

Watson, J.F., H. Ho, and I.H. Greger. 2017. Synaptic transmission and plasticity require AMPA receptor anchoring via its N-terminal domain. Elife. 6.

Wenthold, R.J., R.S. Petralia, J. Blahos, II, and A.S. Niedzielski. 1996. Evidence for multiple AMPA receptor complexes in hippocampal CA1/CA2 neurons. J Neurosci. 16:1982-1989.

Widagdo, J., H. Fang, S.E. Jang, and V. Anggono. 2016. PACSIN1 regulates the dynamics of AMPA receptor trafficking. Sci Rep. 6:31070.

Wood, L.A., G. Larocque, N.I. Clarke, S. Sarkar, and S.J. Royle. 2017. New tools for “hot-wiring” clathrin-mediated endocytosis with temporal and spatial precision. J Cell Biol. 216:4351-4365.

Wu, D., T. Bacaj, W. Morishita, D. Goswami, K.L. Arendt, W. Xu, L. Chen, R.C. Malenka, and T.C. Sudhof. 2017. Postsynaptic synaptotagmins mediate AMPA receptor exocytosis during LTP. Nature. 544:316-321.

Wyszynski, M., E. Kim, A.W. Dunah, M. Passafaro, J.G. Valtschanoff, C. Serra-Pages, M. Streuli, R.J. Weinberg, and M. Sheng. 2002. Interaction between GRIP and liprin-alpha/SYD2 is required for AMPA receptor targeting. Neuron. 34:39-52.

Yasuda, H., A.L. Barth, D. Stellwagen, and R.C. Malenka. 2003. A developmental switch in the signaling cascades for LTP induction. Nat Neurosci. 6:15-16.

Yudowski, G.A., M.A. Puthenveedu, and M. von Zastrow. 2006. Distinct modes of regulated receptor insertion to the somatodendritic plasma membrane. Nat Neurosci. 9:622-627.

Zheng, C., R. Petralia, Y. Wang, B. Kachar, and R. Wenthold. 2010. SAP102 is a highly mobile MAGUK in spines. J Neurosci. 30:4757-4766.

Zhou, Z., A. Liu, S. Xia, C. Leung, J. Qi, Y. Meng, W. Xie, P. Park, G.L. Collingridge, and Z. Jia. 2018. The C-terminal tails of endogenous GluA1 and GluA2 differentially contribute to hippocampal synaptic plasticity and learning. Nat Neurosci. 21:50-62.

Zhu, J.J., J.A. Esteban, Y. Hayashi, and R. Malinow. 2000. Postnatal synaptic potentiation: delivery of GluR4-containing AMPA receptors by spontaneous activity. Nat Neurosci 3:1098-1106.

Zito, K., V. Scheuss, G. Knott, T. Hill, and K. Svoboda. 2009. Rapid functional maturation of nascent dendritic spines. Neuron. 61:247-258.

3

Shank proteins couple the endocytic zone to the postsynaptic density to control trafficking and signalling of mGluRs

Nicky Scheefhals[1], Lisa A.E. Catsburg[1], Margriet L. Westerveld[1], Thomas A. Blanpied[2], Casper C. Hoogenraad[1], and Harold D. MacGillavry[1, 3]

[1]Department of Cell Biology, Neurobiology and Biophysics at the Faculty of Science of Utrecht University in Utrecht, the Netherlands
[2]Department of Physiology, Program in Neuroscience, University of Maryland School of Medicine, Baltimore, MD 21201, USA.

Cell Reports (2019), 29: 258-269

ABSTRACT

Activation of postsynaptic metabotropic glutamate receptors (mGluRs) modulates neuronal excitability and synaptic plasticity, while deregulation of mGluR signaling has been implicated in neurodevelopmental disorders. Importantly, overstimulation of mGluR is restricted by the rapid endocytosis of receptors after activation. However, how membrane trafficking of mGluRs at synapses is controlled remains poorly defined. We find that in hippocampal neurons, agonist-induced receptor internalization of synaptic mGluR5 is significantly reduced in Shank knockdown neurons. Interestingly, this is rescued by re-expression of wild-type Shanks, but not by mutants unable to bind Homer1b/c, Dynamin2 or Cortactin. Strikingly, these effects are paralleled by a reduction in synapses associated with an endocytic zone. Moreover, a mutation in SHANK2 found in ASD similarly disrupts these processes. Based on these findings, we propose that synaptic Shank scaffolds anchor the endocytic machinery to govern efficient trafficking of mGluR5 and to balance the surface expression of mGluRs to efficiently modulate neuronal functioning.

INTRODUCTION

At excitatory synapses of hippocampal neurons, the group I metabotropic glutamate receptors (mGluRs) mGluR1 and mGluR5 critically modulate synaptic transmission and plasticity (Scheefhals and MacGillavry, 2018). The contribution of mGluRs to glutamatergic signaling underlies cognitive functions and disrupted mGluR signaling has been implicated in neurological disorders including autism spectrum disorders (ASDs) (Lüscher and Huber, 2010). To prevent overstimulation, activated mGluRs are rapidly desensitized and internalized via clathrin-mediated endocytosis (Dhami and Ferguson, 2006). Despite the importance of controlled receptor trafficking at synapses, we know little about the mechanisms that control the endocytosis and recycling of synaptic mGluRs. Endocytosis of postsynaptic membrane proteins preferentially takes place at endocytic zones (EZs) (Rosendale et al., 2017). EZs are stable clathrin assemblies coupled to the postsynaptic density (PSD) via interactions with Homer1b/c and Dynamin3 (Blanpied et al., 2002; Lu et al., 2007; Racz et al., 2004). Disruption of PSD-EZ coupling reduces the synaptic population of AMPA receptors, and prevents plasticity-induced receptor insertion (Petrini et al., 2009). However, it remains untested whether mGluRs are locally endocytosed through EZs and recycle to the synaptic membrane. The Shank family (Shank1, 2 and 3) is an integral part of the PSD, interacting with a multitude of synaptic proteins, as well as endocytic proteins, such as Dynamin2, Cortactin, Syndapin I, and Abp1 (Kessels et al., 2001; McNiven et al., 2000; Naisbitt et al., 1999; Okamoto et al., 2001; Qualmann et al., 2004). Moreover, abrogated mGluR signaling has been found in Shank mutant models (Bariselli et al., 2016; Kouser et al., 2013; Lee et al., 2019; Verpelli et al., 2011), but how Shank proteins control mGluR function remains unknown. We hypothesized that Shank proteins recruit components of the endocytic machinery to facilitate local regulation of receptor internalization to control mGluR function. We found that agonist-induced internalization of mGluR5 is severely affected in Shank triple knockdown neurons and present evidence that mGluR5 is internalized through the EZ coupled to the PSD by Shank-mediated interactions. We propose that Shank proteins link the EZ to the PSD to control trafficking of synaptic membrane proteins and to balance the density of receptors at the membrane to modulate neuronal functioning.

RESULTS

Efficient internalization and intracellular sorting of activated mGluR5

To test whether activation of mGluR5 triggers endocytosis in hippocampal neurons, we live-labeled surface-expressed myc-mGluR5, and incubated neurons with the group I specific agonist DHPG. Surface expression of mGluR5 markedly decreased over time, which was best described by a single-exponential decay function with a rate constant of 0.077 ± 0.03 min^{-1}, reaching a plateau at 42 ± 7% reduction (Figures 1A and B), consistent with previous reports (Lee et al., 2008). Internalized mGluR5 puncta largely overlapped with the early and recycling endosome markers anti-EEA1, GFP-Rab5, GFP-Rab11, and mRFP-TfR, but much less with the late endosome marker GFP-Rab7, and lysosomal marker GFP-LAMP1 (EEA1: 70 ± 3%, Rab5: 80 ± 3%, Rab11: 76 ± 3%, TfR: 77 ± 4, Rab7: 38 ± 3%, LAMP1: 31 ± 5%, $P < 0.001$; Figure 1C and D). To image the surface expressed pool of mGluR5 in live cells, we tagged mGluR5 with an extracellular super-ecliptic pHluorin (SEP) tag (Figure 1E). We confirmed that fluorescence of this GFP variant is quenched at low pH, such as in endocytic vesicles, and only fluoresces at neutral pH (Supplementary Figure 1A). Application of DHPG induced a rapid decrease in SEP-mGluR5 intensity from dendritic spines (DHPG: 39.7 ± 2.2% at t = 28 minutes, vehicle: 14.0 ± 1.6%, $P < 0.001$; Figure 1F and G). Imaging at reduced frame rates revealed no significant difference in observed signal reduction both after vehicle (15.8 ± 3.1%; Supplementary Figure 1B) and DHPG application (37.8 ± 3.5%; Supplementary Figure 1C). Thus, the observed reduction of SEP-mGluR5 intensity in unstimulated spines is not due to photobleaching, but likely reflects ongoing receptor internalization, consistent with other studies that estimated ~20% agonist-independent internalization over 30 minutes (Francesconi et al., 2009; Lee et al., 2008). In some, but not all experiments we noted that DHPG or vehicle application induced a transient increase in SEP-mGluR5 fluorescence intensity (f.e. Figure 1G). If observed, it was independent of the experimental conditions, and could potentially be attributed to the opening of the imaging chamber, briefly affecting the pH of the imaging buffer.

In dendrites, the DHPG-induced decrease in SEP-mGluR5 signal in dendrites was not significantly different from the vehicle control (DHPG: 26.0 ± 4.7%, vehicle: 18.1 ± 2.6%; Figure 1H). However these measurements do not directly measure endocytosis, but also reflect ongoing recycling, and lateral exchange of receptors on the membrane. To more directly determine whether mGluR5 can be internalized in dendrites, we tagged mGluR5 with an extracellular Halo-tag to label with AcidiFluor ORANGE, which only fluoresces at low pH (pH 5 - 6) (Isa et al., 2014) (Supplementary Figure 1D). Application of DHPG induced distinct, local increases in Halo-mGluR5 signal intensity, reflecting acidification of Halo-mGluR5 containing endocytic vesicles, both in spines and dendrites (Supplementary Figure 1E, F, G and H).

To test whether dynamin activity is required for agonist-induced mGluR5 internalization in spines, we treated neurons with dynasore, a potent inhibitor of Dynamin GTPase activity (Macia et al., 2006) before addition of DHPG. Dynasore significantly reduced DHPG-induced mGluR5 internalization in spines (control: 46.9 ± 5.1%, dynasore: 20.1 ± 6.3%, $P < 0.05$; Figure 1I). Moreover, expression of a dominant-negative form of Dynamin2 (Dyn2), Dynamin2-K44A (Dyn2-K44A), also reduced DHPG-induced internalization of mGluR5 in spines internalization of mGluR5 in spines (Dyn2: 39.8 ± 4.3%, Dyn2-K44A: 18.0 ± 5.5%, $P < 0.05$; Figure 1J).

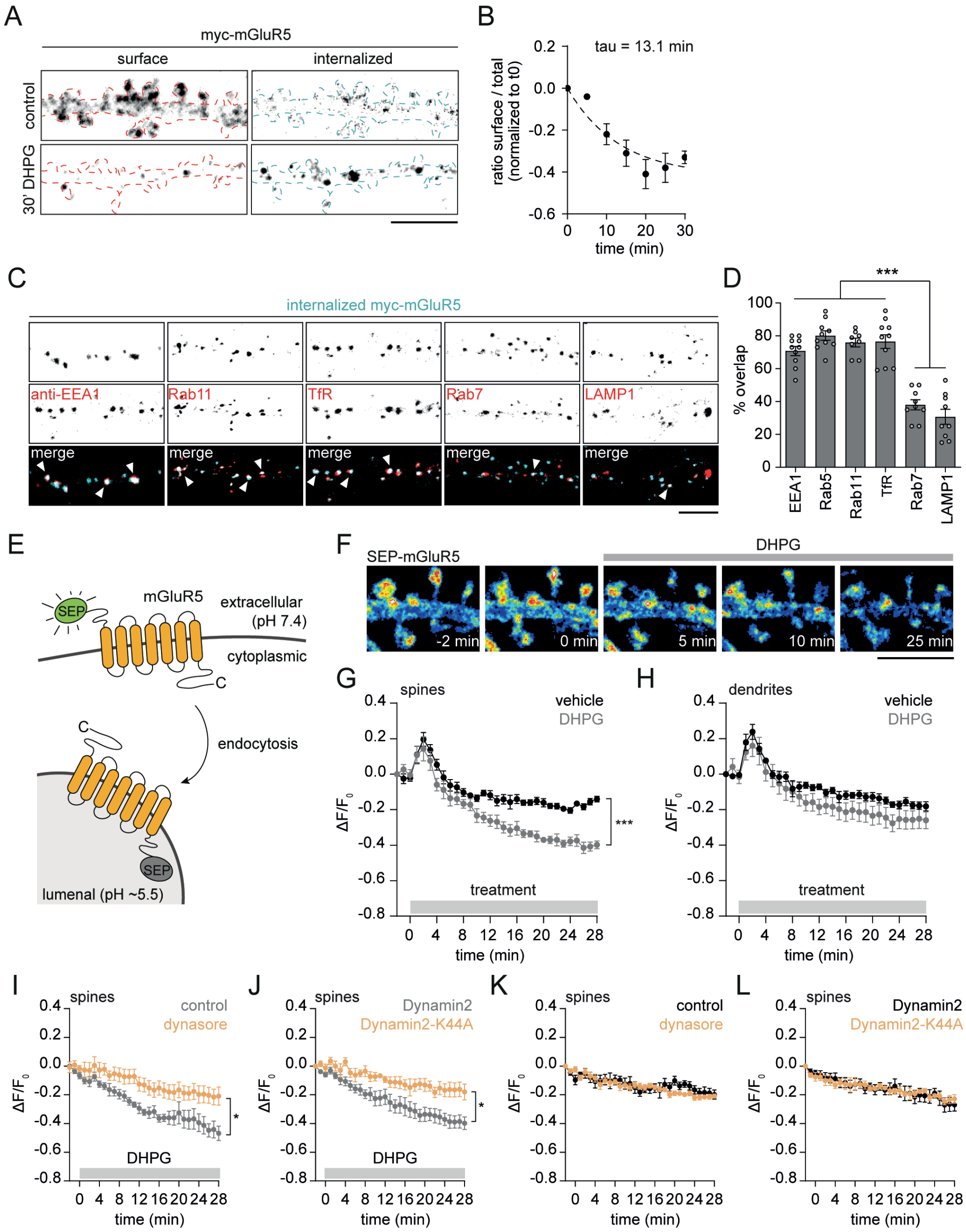

Figure 1. Efficient agonist-induced mGluR5 internalization in spines. (A) Dendrite stained for surface expressed (red outline) and internalized (cyan outline) myc-mGluR5 before (upper panels) and 30 minutes after (lower panels) DHPG treatment. Scale bar, 5 µm. (B) Quantification of the ratio of surface over total myc-mGluR5 intensity at different time points after DHPG stimulation (n = 8 – 20). Dashed line represents single exponential fit. (C) Co-localization of internalized myc-mGluR5 (cyan) and indicated endosomal- and lysosomal markers (red). Arrowheads indicate examples of overlapping puncta. Scale bar, 5 µm.

(D) Quantification of overlap between internalized myc-mGluR5 puncta and indicated markers (EEA1: n = 10, Rab5: n = 10, Rab11: n = 8, TfR: n = 10, Rab7: n = 9, LAMP1: n = 9). (E) Schematic of SEP-tag fused to mGluR5. (F) Live-cell time-lapse imaging of a dendrite expressing SEP-mGluR5 stimulated with DHPG at t = 0. Scale bar, 5 µm. (G) Quantification of SEP-mGluR5 intensity over a 30-minute time period comparing application of vehicle (black; n = 8) and DHPG (grey; n = 6) at t = 0 in spines (H) and dendrites. (I) Quantification of SEP-mGluR5 intensity in spines over time after DHPG stimulation comparing control neurons (grey; n = 6) with neurons pre-treated with dynasore (orange; n = 6) and (J) in neurons co-transfected with Dyn2 (grey; n = 6) with neurons co-transfected with Dyn2-K44A (orange, n = 6). (K) Quantification of SEP-mGluR5 intensity in spines over time without the addition of DHPG comparing control neurons (black; n = 6) with neurons pre-treated with dynasore (orange; n = 8) and (L) in neurons co-transfected with Dyn2 (grey; n = 6) with neurons co-transfected with Dyn2-K44A (orange; n = 6). Data are represented as mean ± SEM. * P < 0.05, *** P < 0.001.

The slow decrease in fluorescence intensity of SEP-mGluR5 observed in spines without the application of DHPG was similar in dynasore-treated neurons and neurons expressing Dyn2-K44A, and not different from control neurons (Figure 1K and L). In dendrites, the decrease in SEP-mGluR5 signal, in both unstimulated and DHPG-stimulated neurons, was not affected by dynasore, or expression of Dyn2-K44A (Supplementary Figure 1I, J, K and L), suggesting that internalization in dendrites is dynamin-independent. Together, these results indicate that in dendritic spines, receptor activation triggers rapid, dynamin-dependent endocytosis of mGluR5, and that internalized receptors preferentially enter the recycling compartment.

Shank proteins are required for agonist-induced internalization of mGluR5 in spines

To test whether Shank proteins contribute to mGluR5 endocytosis, we used a triple miRNA knockdown construct to simultaneously reduce the expression of Shank1, Shank2 and Shank3 (mirShank) (Supplementary Figure 2A) (MacGillavry et al., 2016). DHPG-induced mGluR5 internalization was significantly reduced in Shank triple knockdown (hereafter Shank knockdown) neurons compared to control neurons (control: 43.8 ± 2.2%, mirShank: 24.8 ± 2.9%, P < 0.001; Figure 2A and B). In contrast, in dendrites of both control and Shank knockdown neurons DHPG-induced mGluR5 internalization was similar (control: 22.8 ± 2.9%, mirShank: 18.8 ± 3.5%, Figure 2C). Importantly, DHPG-induced mGluR5 internalization in spines was completely restored to control levels by re-expression of miRNA-resistant Shank1, SHANK2 or SHANK3 in Shank knockdown neurons (control: 35.3 ± 1.8%, mirShank: 10.4 ± 4.4%, mirShank::SHANK2: 36.4 ± 2.6%, mirShank::SHANK3: 36.4 ± 2.4%; Figure 2A and D; and control: < 0.00144.5 ± 3.3%, mirShank: 24.8 ± 2.7%, mirShank::Shank1: 43.4 ± 2.9%; supplementary Figure 2B and C). We did not find a significant change in agonist-induced mGluR5 internalization in neurons overexpressing SHANK2 (control: 46.6 ± 4.0%, SHANK2 OE: 39.5 ± 2.7%; Figure 2E), suggesting that endogenous Shank levels are sufficient to sustain agonist-induced endocytosis of mGluR5. Also, SEP-mGluR5 intensity was unchanged over a period of 30 minutes in the absence of DHPG between control and Shank knockdown neurons in spines (control: 18.6 ± 1.7%, mirShank: 22.4 ± 2.8%; Figure 2F) and dendrites (control: 11.9 ± 2.7%, mirShank: 10.1 ± 3.9%, Supplementary Figure 2D). Similarly, agonist-induced internalization of mGluR1 was also reduced in

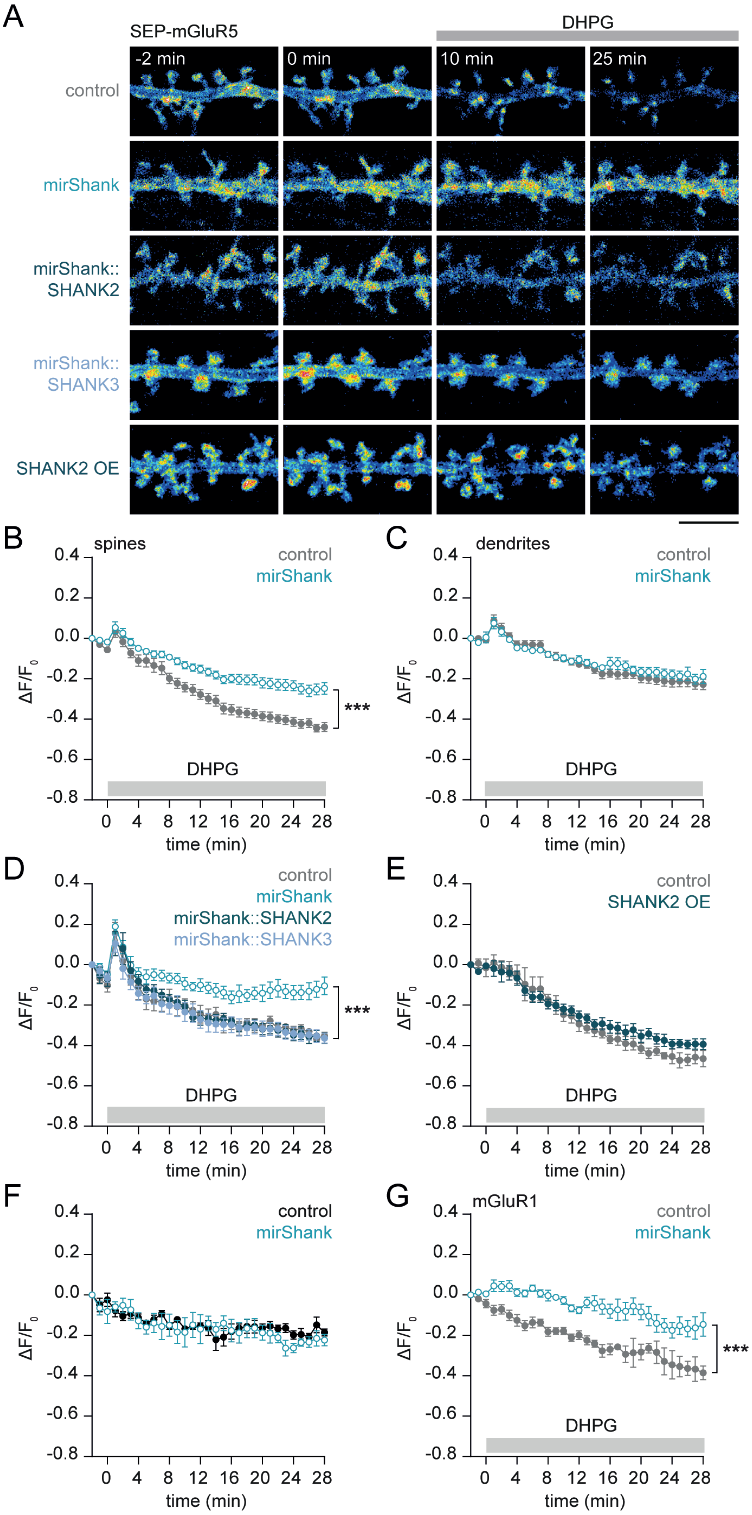
A
SEP-mGluR5
DHPG
-2 min
0 min
10 min
25 min
control
mirShank
mirShank::
SHANK2
mirShank::
SHANK3
SHANK2 OE
B
spines
control
mirShank
***
DHPG
ΔF/F0
0.4
0.2
0.0
-0.2
-0.4
-0.6
-0.8
0 4 8 12 16 20 24 28
time (min)
C
dendrites
control
mirShank
DHPG
ΔF/F0
0 4 8 12 16 20 24 28
time (min)
D
control
mirShank
mirShank::SHANK2
mirShank::SHANK3
***
DHPG
ΔF/F0
0 4 8 12 16 20 24 28
time (min)
E
control
SHANK2 OE
DHPG
ΔF/F0
0 4 8 12 16 20 24 28
time (min)
F
control
mirShank
ΔF/F0
0 4 8 12 16 20 24 28
time (min)
G
mGluR1
control
mirShank
***
DHPG
ΔF/F0
0 4 8 12 16 20 24 28
time (min)

Figure 2. Shank knockdown reduces agonist-induced mGluR5 internalization in spines. (A) Live-cell time-lapse images of SEP-mGluR5 before and after DHPG stimulation (added at t = 0 min) in control, mirShank, mirShank::SHANK2, mirShank::SHANK3 and SHANK2 overexpression (OE) neurons. The dendrites are color-coded for the fluorescence intensity of SEP-mGluR5. Scale bar, 5 μm. (B) Quantification of SEP-mGluR5 intensity over time after the addition of DHPG in spines (C) and dendrites of control (grey; n = 29) and mirShank neurons (blue; n = 34). (D) Quantification of SEP-mGluR5 intensity in spines over time after the addition of DHPG comparing control (grey; n = 7), mirShank (blue; open circles; n = 8) and the mirShank::SHANK2 (n = 6) and mirShank::SHANK3 (n = 8) rescue neurons (shades of blue; closed circles), and (E) in control (grey; n = 4) compared to SHANK2 overexpression (OE; blue; n = 6) neurons. (F) Quantification of SEP-mGluR5 intensity in spines over time without the addition of DHPG comparing control (black; n = 5) and mirShank neurons (blue; n = 5). (G) Quantification of SEP-mGluR1 intensity in spines over time after the addition of DHPG in control (grey; n = 8) and mirShank neurons (blue; n = 6). Data are represented as mean ± SEM. *** P

Shank knockdown neurons (control: 38.6 ± 3.4, mirShank: 14.6 ± 5.8%, $P < 0.001$; Figure 2G). Thus, agonist-induced internalization of mGluR1 and 5 in spines is modulated by synaptic Shank scaffolds.

Shank proteins couple the EZ to the PSD to mediate local endocytosis of mGluR5

We hypothesized that Shank proteins could play a central role in positioning the EZ by recruiting essential components of the endocytic machinery to the PSD (Figure 3A). As a first test, we measured the fraction of PSDs associated with an EZ in control and Shank knockdown neurons. Consistent with previous reports (Blanpied et al., 2002; Lu et al., 2007), we found that the majority of PSDs (72 ± 2%) were associated with an EZ marked by GFP-tagged clathrin light chain (GFP-CLC), but this was significantly reduced in Shank knockdown neurons (44 ± 2%, $P < 0.001$; Figure 3B and C). The density of GFP-CLC puncta along the dendrite was not different between control and Shank knockdown neurons (Supplementary Figure 3A). Also, immuno-labeled clathrin puncta were less frequently associated with synapses labeled with anti-Homer1b/c in Shank knockdown neurons compared to control neurons (untransfected: 72 ± 3%, control: 78 ± 3%, mirShank: 39 ± 5%; Figure 3D). Importantly, the synaptic distribution of Homer1c-mCherry was not altered in Shank knockdown neurons (Supplementary Figure 3B, C and D).

To test whether specific interaction motifs in SHANK2 are required for coupling the EZ to the PSD, we determined the fraction of EZ-positive synapses in Shank knockdown neurons co-expressing miRNA-resistant wild-type SHANK2 (mirShank::SHANK2-WT; WT) and mutant forms of SHANK2 that lack the Dynamin2 (mirShank::SHANK2-ΔDYN; ΔDYN), Cortactin (mirShank::SHANK2-ΔCOR; ΔCOR), or Homer1b/c (mirShank::SHANK2-P1035L; P1035L) bindings sites. All mutants were effectively targeted to the PSD and did not alter synapse density (Supplementary Figure 3E, F and G), and were used as a marker of the PSD. Interestingly, whereas re-expression of wild-type SHANK2 completely restored the fraction of EZ-associated PSDs to control levels, the Dynamin2, Cortactin, or Homer1c binding site mutants were all unable to rescue this (WT: 66 ± 3%, ΔDYN: 40.1 ± 3%, ΔCOR: 35.3 ± 3%, P1035L: 42.2 ± 2%, $P < 0.001$; Figure 3E and F).

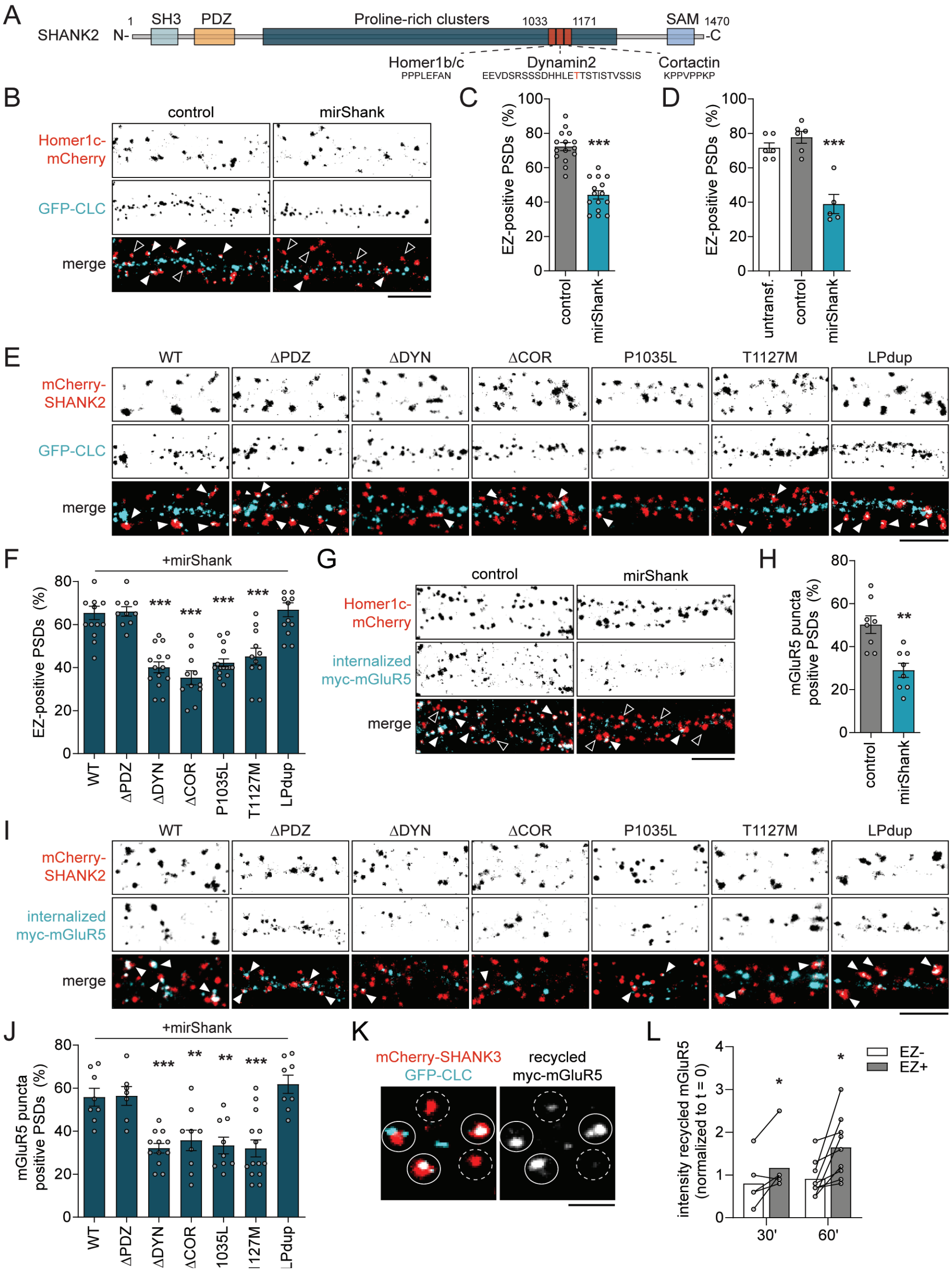

Figure 3. Shanks couple the EZ to the PSD to control mGluR5 trafficking in spines. (A) Domain structure of SHANK2. Proline-rich binding motifs for Homer1b/c, Dynamin2, and Cortactin are indicated. (B) Representative images of dendrites co-expressing GFP-CLC (cyan) and Homer1c-mCherry (red) in control and mirShank neurons. Indicated are examples of EZ-positive (filled arrowhead) and EZ-negative (open arrowheads) PSDs. Scale bar, 5 µm. (C) Quantification of the percentage of PSDs associated with a GFP-CLC marked EZ in control (n = 15) and mirShank (n = 15) neurons. (D) Quantification of

PSDs associated with endogenous anti-clathrin in untransfected (n = 6) and transfected control (n = 6) and mirShank (n = 5) neurons. (E) Representative images of dendrites co-expressing mCherry-tagged SHANK2 rescue constructs (red) and GFP-CLC (cyan). Scale bar, 5 µm. (F) Quantification of the percentage of EZ-positive PSDs in neurons co-expressing mCherry-tagged SHANK2 rescue constructs (WT: n = 14, Δ PDZ: n = 10, ΔDYN: n = 14, ΔCOR: n = 11, P1035L: n = 15, T1127M: n = 11, LPdup: n = 13). (G) Representative images showing internalized myc-mGluR5 (cyan) puncta 30 minutes after the application of DHPG in dendrites co-expressing Homer1c-mCherry (red) as a PSD-marker, in control and mirShank neurons. Indicated are examples of mGluR5 puncta positive PSDs (filled arrowhead) and mGluR5 puncta negative PSDs (open arrowheads). Scale bar, 5 µm. (H) Quantification of the percentage of mGluR5 puncta positive PSDs in control (n = 8) and mirShank (n = 8) neurons. (I) Representative images of dendrites co-expressing mCherry-tagged SHANK2 rescue constructs (red) and internalized myc-mGluR5 (cyan) 30 minutes after the application of DHPG. Scale bar, 5 µm. (J) Quantification of the percentage of mGluR5 puncta positive PSDs in neurons co-expressing mCherry-tagged SHANK2 rescue constructs (WT: n = 8, Δ PDZ: n = 7, ΔDYN: n = 12, ΔCOR: n = 9, P1035L: n = 9, T1127M: n = 14, LPdup: n = 8). (K) Representative image of recycled myc-mGluR5 (right panel) at EZ-positive PSDs (white circles) and at EZ-negative PSDs (white dashed circles). EZs are marked by GFP-CLC (cyan) and PSDs are marked by mCherry-SHANK3 (red) (left panel). Scale bar, 2 µm. (L) Quantification of signal intensity of recycled myc-mGluR5 at EZ-negative and EZ-positive synapses after 30 (n = 6) and 60 (n = 9) minutes recycling. Data is normalized to myc-mGluR5 intensity at t = 0 min. Data are represented as mean ± SEM. * P < 0.05, ** P < 0.01, *** P < 0.001.

On the other hand, complete removal of the SHANK2 PDZ domain (∆PDZ) did not alter the ability of SHANK2 to rescue the fraction of EZ-positive synapses (66.1 ± 2%, n = 10; Figure 3E and F). Also, the overall density of GFP-CLC puncta in dendrites was not different between conditions (Supplementary Figure 3H). Thus, these data indicate that SHANK2 binding to Homer1b/c, Cortactin, and Dynamin2 all contribute to positioning the EZ close to the PSD. Similar to SHANK2, re-expression of wild-type Shank1 and SHANK3 completely restored the fraction of EZ-associated PSDs (Shank1: 70.3 ± 3%, SHANK2: 73.6 ± 2%, SHANK3: 72.9 ± 2 %; Supplementary Figure 3I and J).

Among the numerous de novo mutations in the SHANK2 gene identified in individuals with ASD, one particular nonsense mutation in SHANK2 (T1127M) is located in the core of the Dynamin2 binding site (Berkel et al., 2010). We confirmed that this SHANK2 variant was efficiently targeted to synapses (Supplementary Figure S3E) (Berkel et al., 2012), but this single point mutation rendered SHANK2 unable to rescue the loss of EZ-associated PSDs (45.2 ± 4%, P < 0.001; Figure 3E and F). Another de novo mutation found in SHANK2 in an individual with autism (L1008P1009dup; LPdup) was still able to rescue the loss of EZ-associated PSDs (66.9 ± 3%; Figure 3E and F).

To further test whether Shank proteins promote the local endocytosis of mGluR5, we determined the localization of internalized myc-mGluR5 with respect to the PSD. Interestingly, the fraction of synapses that overlapped with internalized mGluR5 puncta was significantly reduced in Shank knockdown neurons (control: 50.2 ± 4%, mirShank: 29.0 ± 3%, P < 0.01; Figure 3G and H). In neurons re-expressing wild-type SHANK2 this was completely restored, while SHANK2 mutants deficient in binding Homer1b/c, Cortactin, or Dynamin2 were unable to rescue this (WT: 55.8 ± 4%, ΔDYN: 32.1 ± 2%, ΔCOR: 35.7 ± 5%, P1035L: 33.4 ± 4%, P < 0.001; Figure 3Iand J). Also, in neurons re-expressing the ASD-associated SHANK2-T1127M mutant there was a significant reduction in synapse-associated mGluR5 puncta

(32 ± 4%, $P < 0.001$; Figure 3I and J). On the other hand, re-expression of SHANK2-ΔPDZ and the ASD-associated SHANK2-LPdup mutant did not alter the ability of SHANK2 to rescue this (ΔPDZ: 56.4 ± 4%, LPdup: 61.8 ± 4%; Figure 3I and J). Thus, Shank proteins spatially restrict endocytosis of mGluR5 to perisynaptic sites by coupling the EZ to the PSD.

The EZ mediates local mGluR5 recycling

The reduction in EZ-associated synapses and the decrease in mGluR5 internalization in Shank knockdown neurons suggest that mGluR5 internalizes through the spine EZ coupled to the PSD via Shank intermediates. To further test whether mGluR5 can undergo recycling and whether this is facilitated by the EZ, we performed an antibody-based recycling assay to specifically label the recycled pool of receptors (Lu et al., 2007). Strikingly, the levels of recycled mGluR5 were significantly higher at EZ-positive synapses, with almost no detectable recycling at EZ-negative synapses (30’: EZ+: 1.2 ± 0.3, EZ-: 0.8 ± 0.2, 60’: EZ+: 1.6 ± 0.2, EZ-: 0.9 ± 0.1, $P < 0.05$; Figure 3K and L), consistent with the model that mGluR5 is internalized through the EZ to undergo local capture and recycling, reminiscent of AMPAR recycling (Lu et al., 2007).

Shank proteins control local trafficking of mGluR5 in spines

We found that Shank knockdown specifically reduced agonist-induced internalization of mGluR5 in spines, but not in dendrites and predicted that disrupting the coupling between the EZ and the PSD would favor mGluR5 internalization at extrasynaptic sites. The density of internalized mGluR5 puncta at the dendritic shaft under basal condition ($t = 0$ min) was similar in control and Shank knockdown neurons (Supplementary Figure 4A) and showed a similar increase 5 minutes after application of DHPG (Figure 4A and B). Strikingly, 10 minutes after treatment with DHPG the density of internalized mGluR5 puncta at the dendritic shaft was significantly increased in Shank knockdown neurons compared to $t = 0$ min (0’: 1 ± 0.09, 10’: 2.0 ± 0.2, $P < 0.001$) and significantly different from control neurons (10’: 1.2 ± 0.1, $P = 0.01$) (Figure 4A and B). This increase returned to control levels 20 minutes after treatment. Thus, in the absence of Shanks, activated receptors diffuse away from the synapse to internalize at extrasynaptic sites. This is expected to lead to a progressive reduction in surface mGluR5 levels at the synapse. Indeed, SEP-mGluR5 enrichment in spines was significantly reduced in Shank knockdown neurons, and fully rescued by re-expression of Shank1, SHANK2 and SHANK3 (control: 1.5 ± 0.1, mirShank: 1.1 ± 0.04, Shank1: 1.4 ± 0.04, SHANK2: 1.5 ± 0.1, SHANK3: 1.4 ± 0.04, $P < 0.001$; Supplementary Figure 4B). Immunoblotting showed no reduction in mGluR5 proteins levels in Shank knockdown neurons (Supplementary Figure 4C and D). However, immuno-labeling of mGluR5 showed that total levels of endogenous mGluR5 were reduced in Shank knockdown neurons (control: 1 ± 0.05, mirShank: 0.8 ± 0.03, $P < 0.01$; Supplementary Figure 4E and F), which has been previously reported in Shank3 knockdown neurons (Verpelli et al., 2011). Thus, disrupted mGluR5 recycling in Shank knockdown neurons leads to a reduction in the density of mGluR5 at the synaptic membrane. Shank proteins are large multi-domain scaffolding proteins and have been suggested to anchor mGluR5 at the synapse through interactions with Homer1b/c (Tu et al., 1999). The reduced surface levels of mGluR5 in spines, and total levels of endogenous mGluR5 in Shank knockdown neurons could thus also be explained by a reduction in receptor binding sites at the PSD modulating mGluR5 stability. However, using fluorescence recovery after photobleaching (FRAP) experiments, we found that the rate of recovery as well as the total recovery of Venus-mGluR5 were similar in control and Shank knockdown neurons (Figure 4C and D), suggesting that Shank proteins do not directly contribute to the anchoring of mGluR5 at synaptic sites.

mGluR5-mediated calcium and ERK1/2 signaling is abrogated in Shank knockdown neurons

The density of mGluR5 on the membrane controls the activation of downstream signaling pathways (Choi et al., 2011; Nash et al., 2002) that can trigger the oscillatory release of Ca^{2+} from internal stores (Kawabata et al., 1996) and activate the extracellular signal-regulated kinase (ERK1/2) pathway (Mao et al., 2005). To test the functional impact of the defect in mGluR5 trafficking in Shank knockdown neurons, we first measured DHPG-induced Ca^{2+} oscillations using the fluorescent Ca^{2+} reporter GCaMP6s (Chen et al., 2013). Consistent with previous reports, we found that DHPG triggered the immediate onset of robust Ca^{2+} oscillations (Figure 4E and F). DHPG-induced oscillations were completely blocked by addition of the specific mGluR5 antagonist MPEP (DHPG: 17.3 ± 1.3 mHz, and DHPG + MPEP: 3.5 ± 1.4 mHz, $P < 0.001$; Figure 4F and G), confirming that these oscillations are mediated by the activation of mGluR5. Importantly, we found that the frequency of DHPG-induced calcium peaks was significantly reduced in Shank knockdown neurons (control 21.6 ± 3.1 mHz, mirShank 12.6 ± 1.5 mHz, $P < 0.01$; Figure 4H, I and J). Furthermore, we compared DHPG-induced phosphorylation of ERK1/2 (pERK1/2) in control and Shank knockdown neurons. Incubation with DHPG for 10 and 30 minutes increased ERK1/2 phosphorylation shown by immuno-labeling of pERK1/2 in a population of control neurons, which was significantly reduced in Shank knockdown neurons after 30 minutes DHPG treatment (10’ DHPG: control: 1.4 ± 0.15, mirShank: 0.95 ± 0.08, and 30’ DHPG: control: 1.47 ± 0.16, mirShank: 0.89 ± 0.09, $P < 0.01$; Figure 4K and L). Importantly, under basal conditions (non-treated; NT) the levels of ERK1/2 phosphorylation were similar between control and Shank knockdown neurons (NT: control: 1.00 ± 0.10, mirShank: 0.94 ± 0.11; Figure 4J and K). These results indicate that Shank regulates mGluR5 signaling, substantiating an involvement of aberrant receptor trafficking in animal models of ASD with implicated deregulation of mGluR5 signaling.

DISCUSSION

Modulation of glutamatergic signaling by group I mGluRs is essential for proper synaptic transmission and plasticity, and deregulated mGluR signaling is broadly held to underlie the molecular pathology of neurodevelopmental disorders (Lüscher and Huber, 2010). However, fundamental aspects of mGluR signaling and trafficking at excitatory synapses are still poorly understood. Here we present a model in which coupling of the EZ to the PSD by Shank proteins enables local recycling of mGluRs, allowing the synapse to balance the density of mGluRs at the membrane to efficiently modulate neuronal functioning.

Our data show that Shank proteins selectively regulate activity-induced

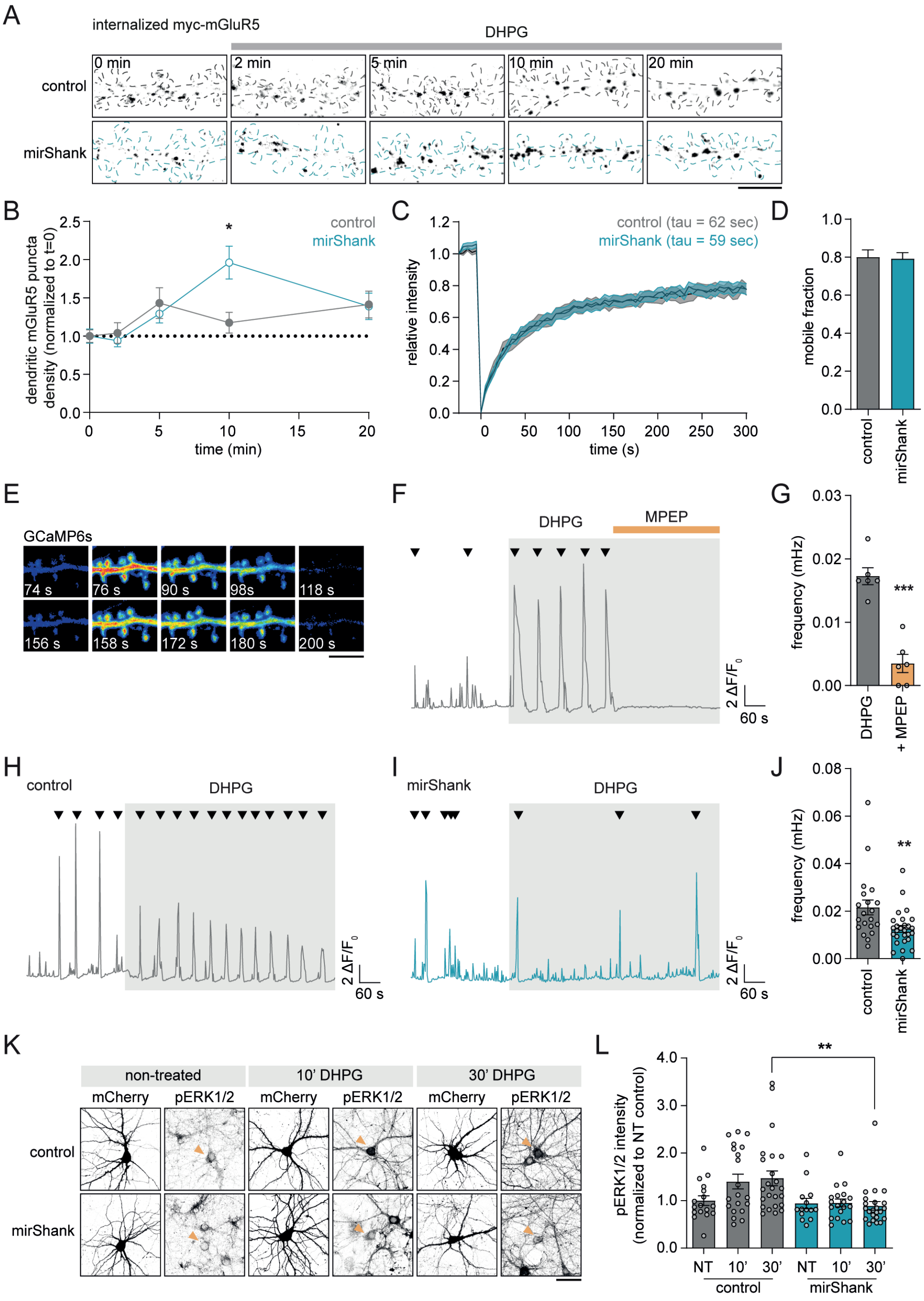
A
internalized myc-mGluR5
DHPG
0 min
2 min
5 min
10 min
20 min
control
mirShank
B
dendritic mGluR5 puncta density (normalized to t=0)
2.5
2.0
1.5
1.0
0.5
0.0
*
control
mirShank
0
5
10
15
20
time (min)
C
relative intensity
1.2
1.0
0.8
0.6
0.4
0.2
0.0
control (tau = 62 sec)
mirShank (tau = 59 sec)
0
50
100
150
200
250
300
time (s)
D
mobile fraction
1.0
0.8
0.6
0.4
0.2
0.0
control
mirShank
E
GCaMP6s
74 s
76 s
90 s
98s
118 s
156 s
158 s
172 s
180 s
200 s
F
DHPG
MPEP
2 ΔF/F$_0$
60 s
G
frequency (mHz)
0.03
0.02
0.01
0.00
***
DHPG
+ MPEP
H
control
DHPG
2 ΔF/F$_0$
60 s
I
mirShank
DHPG
2 ΔF/F$_0$
60 s
J
frequency (mHz)
0.08
0.06
0.04
0.02
0.00
**
control
mirShank
K
non-treated
10' DHPG
30' DHPG
mCherry
pERK1/2
mCherry
pERK1/2
mCherry
pERK1/2
control
mirShank
L
pERK1/2 intensity (normalized to NT control)
4.0
3.0
2.0
1.0
0.0
**
NT
10'
30'
NT
10'
30'
control
mirShank

Figure 4. Shanks control mGluR5-mediated calcium signaling and ERK1/2 activity. (A) Dendrite stained for internalized myc-mGluR5 at different time points after DHPG stimulation in control (grey outline; upper panels) and mirShank (blue outline; lower panels) neurons. Scale bar, 5 µm. (B) Quantification of internalized myc-mGluR5 puncta density in the dendritic shaft at different time points afHPG stimulation in control (n = 18 – 24) and mirShank (n = 18 – 27) neurons, normalized to t = 0 per condition. (C) FRAP analysis of Venus-mGluR5 in spines of control (grey; n = 38 spines) and mirShank (blue; n = 38 spines) neurons. (D) Quantification of the mobile fraction of Venus-mGluR5 in spines of control and mirShank neurons. (E) Example of a dendrite expressing GCaMP6s stimulated with DHPG. Scale bar, 5 µm. (F) Oscillatory response of GCaMP6s signal in response to the application of DHPG (grey; n = 22) and DHPG + MPEP (orange; n = 26). (G) Quantification of the frequency (mHz) of the GCaMP6s oscillations in response to DHPG and DHPG + MPEP (n = 6). (H) Oscillatory response of GCaMP6s signal in response to DHPG in control (grey), and (I) mirShank (blue) neurons. (J) Quantification of the frequency (mHz) of the GCaMP6s oscillations in response to DHPG in control (n = 20) and mirShank (n = 27) neurons. (K) Examples of control (upper panels) and mirShank (lower panels) neurons immuno-labeled for anti-pERK1/2 in non-treated (NT) and treated neurons with DHPG for 10 minutes (10’) or 30 minutes (30’). Orange arrowheads indicate the mCherry expressing control and mirShank neurons used for quantification. Scale bar, 50 µm. (L) Quantification of the average anti-pERK1/2 fluorescence intensity in the cell bodies of the transfected neurons of control (n = 17 – 24) and mirShank (n = 14 – 23) neurons with indicated treatment. Data is normalized to the average intensity of the non-treated control condition. Data are represented as mean ± SEM. * $P < 0.05$, ** $P < 0.01$ and *** $P < 0.001$.

internalization of mGluR5 in spines. While DHPG-induced mGluR5 internalization is greatly affected in Shank knockdown neurons, in the absence of stimulation the levels of mGluR5 remain relatively constant in both control and Shank knockdown neurons. This suggests that in the absence of Shanks constitutive internalization of mGluR5 is not affected and continues to replace surface receptors. Thus, in the absence of efficient PSD-EZ coupling, synaptic receptors now escape this local endocytic sink and become internalized and recycled at extrasynaptic sites, slowly depleting the synaptic pool of receptors. Indeed, we found a significant increase in agonist-induced mGluR5 internalization in dendrites, and a significant decrease in surface mGluR5 levels in spines of Shank knockdown neurons. This also suggests that dendritic internalization of mGluR5 is regulated independent of Shanks. Moreover, blocking dynamin activity did not alter dendritic mGluR5 internalization, indicating that internalization of dendritic receptors is regulated by different mechanisms. We consistently found a small reduction in SEP-mGluR5 signal in the absence of agonist, both in spines and dendrites. This could reflect constitutive internalization of mGluR5, but ongoing recycling and lateral diffusion of receptors make it hard to interpret this directly. Nevertheless, previous studies found that mGluR5 undergoes constitutive internalization at a similar rate, but that this process is independent of clathrin and dynamin activity (Fourgeaud et al., 2003), and has been suggested to be mediated by the caveolin-mediated internalization pathway (Francesconi et al., 2009). Altogether, our results are consistent with the notion that the EZ captures synaptic receptors through spatially restricted, clathrin-mediated endocytosis and recycling, allowing the synapse to autonomously control its receptor content (Czondor et al., 2012).

Importantly, the reduction in surface mGluR5 levels in spines in Shank knockdown neurons was functionally reflected in a decrease in mGluR5-mediated calcium responses and ERK1/2 activation. Our experiments were focused on mGluR5, but we cannot exclude that other synaptic receptors or ion channels undergo aberrant trafficking when the EZ is uncoupled from the PSD. Indeed, glutamatergic transmission in general is reduced in Shank knockdown neurons (Arons et al., 2012; Duffney et al., 2013; Verpelli et al., 2011), Shank knockout mouse models (Bozdagi et al., 2010; Duffney et al., 2015; Kouser et al., 2013; Schmeisser et al., 2012), and in neurons expressing ASD-associated Shank mutations (Lee et al., 2019). Thus, disrupting the link between the PSD and the EZ could have much broader effects on the composition of the synaptic membrane and glutamatergic transmission.

Our results indicate that all three Shank isoforms, which share a similar domain structure, recruit important components of the endocytic machinery to the PSD. The interaction between Shank and Homer1b/c confers a direct molecular link to the EZ through Dynamin3. Indeed, abrogating this interaction through directed mutation (our data) or through dominant-negative approaches (Lu et al., 2007), significantly impairs EZ positioning. Shank proteins also seem to recruit Dynamin2 to the EZ, which likely provides the GTPase activity necessary for vesicle scission. Interestingly, we found that the Cortactin-binding motif in SHANK2 was also required for efficient mGluR5 internalization. Cortactin can also bind Dynamin2 and 3 directly (Gray et al., 2003), and has been implicated in endocytosis and endo-lysomal sorting of AMPARs (Parkinson et al., 2018). Importantly, expression of the Shank triple knockdown construct leads to a strong reduction in total Shank levels, but leaves ~20% of total Shank levels intact (MacGillavry et al., 2016). Thus, we cannot exclude that remaining Shank proteins still recruit other interacting proteins that contribute to the trafficking of synaptic receptors.

Consistent with our results that Shank proteins control mGluR trafficking and function, recent studies show that deficits in social behavior caused by the loss of Shank function could be rescued by group I mGluR positive allosteric modulators (Bariselli et al., 2016; Vicidomini et al., 2017). However, even though deregulated receptor functioning at excitatory synapses has been implicated to underlie physiological deficits in many disease models, the molecular mechanisms underlying this have not been resolved. Our results indicate that Shank proteins do not directly anchor receptors at the synapse but provide a stable molecular framework that permits the local uptake and trafficking of receptors via the EZ thereby governing a stable pool of synaptic receptors. That the ASD-associated T1127M mutation in SHANK2 disrupts this process further underlines the relevance of understanding the functional relationship between Shank proteins and mGluR signaling in the context of human neurodevelopmental disorders.

STAR METHODS

Key Resources Table

REAGENT or RESOURCE	SOURCE	IDENTIFIER
Antibodies		
Mouse anti-c-Myc (9E10) Monoclonal Antibody	Santa Cruz Biotechnology	Cat# sc-40; RRID: AB_627268
Human anti-EEA1 Antibody (clone 4114)	M. Fritzler	N/A
Rabbit anti-mGluR5 Antibody	Millipore	Cat# 06-451; RRID: AB_2313604
Rabbit anti-phospho-ERK1/2 Antibody	Cell Signaling	Cat# 9101; RRID: AB_331646
Mouse anti-PSD-95 Antibody	Neuromab	Cat# 75-028; RRID: AB_2292909
Mouse anti-Clathrin Heavy Chain (X22) Monoclonal Antibody	Thermo Fisher Scientific	Cat# MA1-065; RRID: AB_2083179
Rabbit anti-Homer1 Antibody	Synaptic Systems	Cat# 160 006; RRID: AB_2631222
Mouse anti-alpha-tubulin	Sigma-Aldrich	Cat# T6074, RRID: AB_477582
Goat anti-Human IgG (H+L) Secondary Antibody, Alexa Fluor 568	Thermo Fisher Scientific	Cat# A-21090; RRID: AB_2535746
Goat anti-Mouse IgG (H+L) Secondary Antibody, Alexa Fluor 647	Thermo Fisher Scientific	Cat# A-21236; RRID: AB_2535805
Goat anti-Mouse IgG (H+L) Secondary Antibody, Alexa Fluor 488	Thermo Fisher Scientific	Cat# A-11029; RRID: AB_2534088
Goat anti-Rabbit IgG (H+L) Secondary Antibody, Alexa Fluor 488	Thermo Fisher Scientific	Cat# A-11034; RRID: AB_2576217
Swine anti-mouse HRP-conjugated	Agilent	Cat# P0260; RRID: AB_263692
Goat Anti-Rabbit IgG Secondary Antibody, IRDye 680LT	LI-COR Biosciences	Cat# 827-11081; RRID: AB_10795015
Goat Anti-Mouse IgG Secondary Antibody, IRDye 800CW	LI-COR Biosciences	Cat# 827-08364; RRID: AB_10793856
Bacterial and Virus Strains		
Escherichia coli: BL21DE3	N/A	N/A
Chemicals, Peptides, and Recombinant Proteins		
Lipofectamine 2000	Thermo Fisher Scientific	Cat# 11668019
(S)-3,5-DHPG	Tocris	Cat# 805
Dynasore	Tocris	Cat# 2897
MPEP hydrochloride	Tocris	Cat# 1212
Tetrodotoxin citrate	Tocris	Cat# 1069
Polyvinyl alcohol mounting medium with DABCO®, antifading (Mowiol)	Sigma Aldrich	Cat# 10981
HaloTag® AcidiFluor™ORANGE Ligand	GORYO Chemical	Cat# GC310-01
Experimental Models: Cell Lines		
Human embryonic kidney 239T (HEK293T)	ATCC	Cat# CRL-3216; RRID: CVCL_0063
Experimental Models: Organisms/Strains		
Rattus norvegicus (Wistar; HanRj:WI)	RGD, Janvier labs	Cat# 13792727;

		RRID: RGD_13792727
Oligonucleotides		
See Table S1 for miRNA targeting sequences of Shank1, 2 and 3	N/A	N/A
ΔPDZ: deleted Thr254 – Thr348 with forward primer: ATTATTGAGGAGAAGAGGAATCTGGACCCCG	This paper	N/A
ΔPDZ: deleted Thr254 – Thr348 with reverse primer: CTTCTCCTCAATAATGCAGTCA	This paper	N/A
ΔDYN: deleted Glu1114 – Ser113 with forward primer: TTTGACGCCGTCGCCGACTCTGGGATCGAGACCCTGTCTTCCGAAGGTG	This paper	N/A
ΔDYN: deleted Glu1114 – Ser113 with reverse primer: CACATTCTCTCCACCTTCGGAAGACAGGGTCTCGATCCCAGAGTCGG	This paper	N/A
T1127M: mutagenesis with forward primer: AGCGACCACCACCTCGAGATGACCAGCACTATCTCCACCG	This paper	N/A
T1127M: mutagenesis with reverse primer: CGGTGGAGATAGTGCTGGTCATCTCGAGGTGGTGGTCGCT	This paper	N/A
L1008P1009: duplication with forward primer: GTGATTTTGCCATTGCCATTCCGCATCCCTCC	This paper	N/A
L1008P1009: duplication with reverse primer: GGGATGCGGAATGGCAATGGCAAAATCACCGC	This paper	N/A
Recombinant DNA		
pRK5-Venus-mGluR5a	Dr. J. Perroy	N/A
pRK5-SEP-mGluR5a	This paper	N/A
pRK5-myc-mGluR5a	This paper	N/A
pRK5-Halo-mGluR5a	This paper	N/A
pRK5-SEP-mGluR1	This paper	clone image ID # 40080840
pSM155-Cer3	(MacGillavry et al., 2015)	N/A
pSM155-mCherry	This paper	N/A
pSM155-GFP	(MacGillavry et al., 2015)	N/A
pSM155-mirShank::Cer3	(MacGillavry et al., 2015)	N/A
pSM155-mirShank::mCherry	This paper	N/A
pSM155-mirShank::GFP	(MacGillavry et al., 2015)	N/A
pSM155-mirShank::mCherry-Shank1	This paper	N/A
pSM155-mirShank::mCherry-SHANK2	This paper and (MacGillavry et al., 2015)	N/A
pSM155-mirShank::mCherry-SHANK3	This paper	N/A
pSM155-mirShank::mCherry-SHANK2-ΔPDZ	This paper	N/A
pSM155-mirShank::mCherry-SHANK2-ΔDYN	This paper	N/A
pSM155-mirShank::mCherry-SHANK2-ΔCOR	This paper and	N/A

	(MacGillavry et al., 2015)	
pSM155-mirShank::mCherry-SHANK2-P1035L	This paper and (MacGillavry et al., 2015)	N/A
pSM155-mirShank::mCherry-SHANK2-T1127M	This paper	N/A
pSM155-mirShank::mCherry-SHANK2-Lpdup	This paper	N/A
pcDNA3.1- mCherry-Shank2	Dr. Simone Berkel (Berkel et al., 2012)	N/A
mCherry-Shank3	Dr. M. Schmeisser (Cochoy et al., 2015)	N/A
pEGFP-C2-GFP-Clathrin-light-Chain	Dr. Mike Ehlers	
pmCherry-N1-Homer1c-mCherry	(MacGillavry et al., 2013)	N/A
GFP-Rab5	(Hoogenraad et al., 2010)	N/A
GFP-Rab11	(Esteves da Silva et al., 2015)	N/A
TfR-SEP	(Hoogenraad et al., 2010)	N/A
GFP-Rab7	(Hoogenraad et al., 2010)	N/A
pEGFP-N3-LAMP1-mGFP	Dr. Esteban Dell'Angelica (Falcon-Perez et al., 2005)	http://n2t.net/addgene:34831; RRID: Addgene_34831
pEGFP-N1-Dynamin2-GFP	Dr. Pietro De Camilli (Ochoa et al., 2000)	N/A
pEGFP-N1-Dynamin2-K44A-GFP	Dr. Pietro De Camilli (Ochoa et al., 2000)	http://n2t.net/addgene:22301; RRID: Addgene_22301
pGP-CMV-GcaMP6s	Dr. Douglas Kim (Chen et al., 2013)	http://n2t.net/addgene:40753; RRID: Addgene_40753
pCAG_PSD95.FingR-eGFP-CCR5TC	Dr. Don Arnold (Gross et al., 2013)	http://n2t.net/addgene:46295; RRID: Addgene_46295
FUGW	Dr. David Baltimore	http://n2t.net/addgene:14883 ; RRID: Addgene_14883
FUGW-mirShank-GFP	This paper	N/A
p.MDG2	Didier Trono	http://n2t.net/addgene:12259; RRID: Addgene_12259
psPAX2	Didier Trono	http://n2t.net/addgene:12260; RRID: Addgene_12260
Software and Algorithms		
ImageJ	NIH	https://imagej.nih.gov/ij/; RRID: SCR_003070

Fiji	Fiji	http://fiji.sc; RRID: SCR_002285
GraphPad Prism 8	GraphPad	https://www.graphpad.com/scientific-software/prism/; RRID: SCR_002798
Adobe Illustrator CC 2017	Adobe	https://www.adobe.com/products/illustrator.html; RRID: SCR_010279
MATLAB 2018a	MATLAB	http://www.mathworks.com/products/matlab/; RRID: SCR_001622

Experimental Model and Subject Details

Animals

All animal experiments were performed in compliance with the guidelines for the welfare of experimental animals issued by the Government of The Netherlands (Wet op de Dierproeven, 1996) and European regulations (Guideline 86/609/EEC). All animal experiments were approved by the Dutch Animal Experiments Review Committee (Dier Experimenten Commissie; DEC), performed in line with the institutional guidelines of Utrecht University.

Primary neuronal cultures and transfections

Hippocampal cultures were prepared from embryonic day 18 (E18) Janvier Wistar rat brains (both genders) as described in (Cunha-Ferreira et al., 2018). Dissociated neurons were plated on coverslips coated with poly-L-lysine (37.5 μg/ml, Sigma-Aldrich) and laminin (1.25 μg/ml, Roche Diagnostics) at a density of 100,000 neurons per well of a 12-well plate. Cultures were grown in Neurobasal medium (NB) supplemented with 2% B27 (GIBCO), 0.5 mM glutamine (GIBCO), 15.6 μM glutamate (Sigma-Aldrich), and 1% penicillin/ streptomycin at 37°C in 5% CO2. At DIV14-18 neurons were transfected with indicated constructs using Lipofectamine 2000 (Invitrogen). Before transfection 260 μl conditioned medium was transferred to a new culture plate and replaced with 260 μl NB with 0.5 mM glutamine. For each well, 1.8 μg DNA was mixed with 3.3 μl Lipofectamine 2000 in 200 μl NB, incubated for 30 min at RT and added to the neurons. After 45 – 60 minutes, neurons were briefly washed with NB and transferred to the new culture plate with conditioned medium supplemented with 260 μl NB with B27, glutamine, penicillin/ streptomycin and kept at 37°C in 5% CO2 for 2-4 days (for overexpression) or 5-7 days (for Shank knockdown).

METHODS DETAILS

DNA constructs

The pRK5-SEP-mGluR5a, pRK5-Halo-mGluR5a and pRK5-myc-mGluR5a constructs were made using the pRK5-Venus-mGluR5a construct (a gift from Dr. Julie Perroy) as a template and the pRK5-SEP-mGluR1 construct was made by replacing mGluR5a with mGluR1 (clone image ID # 40080840). The human mCherry-SHANK2 expression plasmid was kindly provided by Dr. Simone Berkel (Berkel et al., 2012). The pSM155-GFP (or Cerulean3; Cer3), Shank triple-knockdown construct pSM155-mirShank-GFP (or Cer3), and mirShank::GFP-SHANK2 wild-type (:: to indicate that the Shank miRNAs and GFP-tagged human SHANK2 are expressed simultaneously from a single expression cassette), mirShank::GFP-SHANK2-ΔCOR, and mirShank::GFP-SHANK2-P1035L mutant rescue constructs are described in (MacGillavry et al., 2016). In these constructs GFP was replaced by mCherry (from pmCherry-N1, Invitrogen). To make the mirShank::mCherry-SHANK2-ΔDYN (lacking the 25-amino acid dynamin-binding domain; Glu1114 - Ser1138) (Okamoto et al., 2001), mirShank::mCherry-SHANK2-ΔPDZ (lacking the 95-amino acid PDZ domain, Thr254 - Thr348), mirShank::mCherry-SHANK2-L1008P1009dup and mirShank::mCherry-SHANK2-T1127M constructs, primers were designed containing the desired mutations and 10 – 15 bp overhangs for Gibson assembly (NEBuilder HiFi DNA assembly cloning kit). The rat Shank1 and human SHANK3 expression plasmids were a gift from Dr. Morgan Sheng and Dr. Michael Schmeisser (Cochoy et al., 2015), respectively, and used as a template to make the pSM155-mirShank::mCherry-Shank1 and pSM155-mirShank::mCherry-SHANK3 rescue constructs. Dynamin2-GFP and Dynamin2-K44A-GFP (Addgene plasmid # 22301) were a gift from Dr. Pietro De Camilli (Ochoa et al., 2000), and in both constructs GFP was replaced by mCherry. GFP-CLC (rat clathrin light chain A1) was a gift from Dr. Mike Ehlers, LAMP1-GFP was a gift from Dr. Esteban Dell’Angelica (Addgene plasmid # 34831) (Falcon-Perez et al., 2005), and pGP-CMV-GCaMP6s was a gift from Dr. Douglas Kim (Addgene plasmid # 40753) (Chen et al., 2013). pCAG-PSD95.FingR-eGFP-CCR5TC (PSDFingR-GFP) was a gift from Dr. Don Arnold (Addgene plasmid # 46295) (Gross et al., 2013). The following constructs have been described before: Homer1c-mCherry (MacGillavry et al., 2013), GFP-Rab5, GFP-Rab7, mRFP-TfR (Hoogenraad et al., 2010), and tdTomato-Rab11 (Esteves da Silva et al., 2015). FUGW was a gift from David Baltimore (Addgene plasmid # 14883) (Lois et al., 2002). FUGW-mirShank-GFP was generated by replacing GFP with the Shank triple-knockdown cassette from pSM155-mirShank-GFP. All constructs were verified by sequencing.

Lentiviral particles were generated by transfecting the transfer plasmid together with the packaging plasmids p.MDG2 (Addgene plasmid #12259) and psPAX2 (Addgene plasmid #12260) (gifts from Didier Trono) in HEK293T cells. The supernatant was collected two days after transfection and concentrated using tangential flow filtration (Amicon Ultra spin filters, Millipore #UFC910024).

Confocal imaging

Confocal images were taken with a Zeiss LSM 700 confocal laser-scanning microscope with a Plan-Apochromat 63x NA 1.40 oil objective. Images consist of a z-stack of 7-9 planes at 0.39 μm interval, and maximum intensity projections were generated for analysis and display. The pERK1/2 (Figure J and K) and anti-mGluR5 (Supplementary Figure 4B and C) images were taken with an EC Plan-Neofluar 40x NA 1.30 oil objective and consist of a z-stack of 9 planes at 0.67 μm interval to obtain maximum intensity projections of the entire neuron in the z-axis.

Antibody feeding assay

DIV18 neurons were transfected with myc-mGluR5 and endosomal markers as indicated and were live-labeled at DIV21 with mouse anti-c-myc (9E10, Santa Cruz Biotechnology, catalog # sc-40) diluted 1:200 in extracellular imaging buffer (120 mM NaCl, 3 mM KCl, 2 mM $CaCl_2$, 2 mM $MgCl_2$, 10 mM glucose, and 10 mM HEPES, pH adjusted to 7.35 with NaOH) for 30 minutes at RT, washed twice with imaging buffer, and incubated with 50 µM DHPG (Tocris) for the indicated time-points at 37°C. Cells were then fixed in 4% (w/v) paraformaldehyde (PFA) and 4% (w/v) sucrose in PBS for 10 minutes at RT, and washed three times with PBS supplemented with 100 mM glycine (PBS/Gly). To label the surface-expressed pool of receptors, cells were incubated with goat anti-mouse Alexa-647 (Thermo Fisher Scientific) diluted 1:200 in 5% (v/v) NGS in PBS/Gly for 30 minutes at RT, and washed three times with PBS/Gly. Then, to label the intracellular pool of receptors, cells were permeabilized with 0.25% (v/v) Triton X-100 and 5% (v/v) NGS in PBS/Gly for 5 minutes at RT, blocked with 10% (v/v) NGS in PBS/Gly for 30 minutes, and incubated with goat anti-mouse Alexa-488 (Thermo Fisher Scientific) diluted 1:200 in 5% (v/v) NGS in PBS/Gly for 30 minutes at RT. For co-labeling internalized mGluR5 with EEA1, cells were incubated with human anti-EEA1 (clone 4114; gift from M. Fritzler) diluted 1:500 in 5% (v/v) NGS in PBS/Gly for 2 hours at RT after the permeabilization and blocking steps, and detected with goat anti-human Alexa-568 (Thermo Fisher Scientific). Cells were washed three times with PBS/Gly, mounted in Mowiol mounting medium and imaged on a confocal system as described above.

For the Shank knockdown experiments DIV14 neurons were transfected with pSM155-Cer3 or mirShank::Cer3 together with myc-mGluR5 and Homer1c-mCherry. For the rescue experiments DIV14 neurons were transfected with indicated mirShank::mCherry-SHANK rescue constructs and myc-mGluR5. After 7 days (DIV21), neurons were live-labeled with anti-myc, stimulated with DHPG for 30 minutes, and the surface and internalized pools of myc-mGluR5 were visualized as described above.

For the density of internalized mGluR5 puncta in the dendritic shaft after treatment with DHPG for several points before fixation, DIV14 neurons were transfected with pSM155-mCherry or mirShank::mCherry and myc-mGluR5. After 7 days (DIV21), neurons were live-labeled with anti-myc, stimulated with DHPG for 0, 2, 5, 10 or 20 minutes, and the surface and internalized pools of myc-mGluR5 were visualized as described above.

Endocytic zone associated PSDs

For the Shank knockdown experiments DIV14 neurons were transfected with pSM155-Cer3 or mirShank::Cer3 together with GFP-CLC and Homer1c-mCherry. Alternatively, pSM155-Cer3 or mirShank::Cer3 transfected neurons were stained for endogenous clathrin with mouse anti-clathrin heavy chain (clone X22, Fisher Scientific) and Homer1, with rabbit anti-Homer1 (SySy), and visualized with goat anti-mouse Alexa-647 and goat anti-rabbit Alexa-488 antibodies. For the rescue experiments DIV14 neurons were transfected with indicated mirShank::mCherry-SHANK rescue constructs and GFP-CLC. After 7 days (DIV21), neurons were fixed with 4% PFA and 4% sucrose in PBS for 15 minutes, washed, mounted in Mowiol mounting medium and imaged on a confocal system as described above.

For the co-localization between the PSD and Homer1c in control and Shank knockdown neurons, DIV14 neurons were transfected with pSM155-Cer3 or mirShank::Cer3 together with Homer1c-mCherry and PSDFingR-GFP. For the rescue experiments DIV14 neurons were transfected with indicated mirShank::mCherry-SHANK2 rescue constructs and PSDFingR-GFP. After 7 days (DIV21) the neurons were fixed, mounted and imaged as described above.

Receptor recycling assay

Neurons were live labeled with anti-myc 1:200 in extracellular imaging buffer for 30 minutes at RT, washed twice with imaging buffer, and incubated with 50 µM DHPG for 30 minutes at 37°C to induce receptor internalization. Remaining surface-bound anti-myc antibodies were blocked by incubating with HRP-conjugated swine anti-mouse (Agilent) antibodies diluted 1:100 for 30 minutes at RT. Cells were then washed twice and returned to 37°C to allow receptor recycling for the indicated time points. The recycled receptor pool was then labeled with goat anti-mouse Alexa-647 diluted 1:200 in 5% (v/v) NGS in PBS/Gly for 30 minutes at RT. Cells were washed three times with PBS/Gly, mounted in Mowiol mounting medium and imaged on a confocal system as described above.

Endogenous mGluR5 protein levels

DIV14 neurons were transfected with pSM155-mCherry or mirShank::mCherry and stained for endogenous surface and intracellular mGluR5 with rabbit anti-mGluR5 (Chemicon, catalog #ab5675) diluted 1:500 in 0.1% (v/v) Triton X-100 and 5% (v/v) NGS in PBS/Gly overnight at 4°C, and visualized with goat anti-rabbit Alexa-488 diluted 1:250 in 0.1% (v/v) Triton X-100 and 5% (v/v) NGS in PBS/Gly for 1 hour at RT. Cells were washed three times with PBS/Gly, mounted in Mowiol mounting medium and imaged on a confocal system as described above.

ERK1/2 phosphorylation assay

Neurons were transfected with pSM155-mCherry or mirShank::mCherry at DIV14. Tetrodotoxin (2 µM; TTX) was added 12 hours before treatment. At DIV22 neurons were incubated with either 100 µM DHPG diluted in extracellular imaging buffer for 10 or 30 minutes, or with extracellular imaging buffer only for non-treated control neurons. After the indicated time points the neurons were fixed in 4% PFA and 4% sucrose in PBS for 10 minutes at RT, followed by a quick wash with PBS/Gly, incubated with ice cold methanol (MeOH) for 10 minutes at -20°C and washed three times with PBS/Gly. The pSM155-mCherry or mirShank::mCherry transfected neurons were stained for ERK1/2 phosphorylation with rabbit anti-pERK1/2 (Cell Signaling, catalog #9101) diluted in 0.1% (v/v) Triton X-100 and 5% (v/v) NGS in PBS/Gly overnight at 4°C , and visualized with goat anti-rabbit Alexa-A488 diluted in 0.1% (v/v) Triton X-100 and 5% (v/v) NGS in PBS/Gly for 1 hour at RT. Cells were washed three times with PBS/Gly, mounted in Mowiol mounting medium and imaged on a confocal system as described above.

Live-cell imaging

Live-cell imaging was performed on a spinning disk confocal system (CSU-X1-A1; Yokogawa) mounted on a Nikon Eclipse Ti microscope (Nikon) with Plan Apo VC

100x 1.40 NA, or Plan Apo 60x 1.30 NA oil objectives (Nikon) with excitation from Cobolt Calyspso (491 nm), and Jive (561 nm) lasers, and emission filters (Chroma). The microscope was equipped with a motorized XYZ stage (ASI; MS-2000), Perfect Focus System (Nikon), Evolve 512 EM-CCD camera (Photometrics), and was controlled by MetaMorph 7.7.6 software (Molecular Devices). Neurons were maintained in a closed incubation chamber (Tokai hit: INUBG2E-ZILCS) at 37°C in 5% CO2 in extracellular imaging buffer.

Live-cell imaging of SEP-tagged mGluR5

DIV14 neurons were transfected with SEP-mGluR5 or SEP-mGluR1 together with pSM155-mCherry, mirShank::mCherry, mirShank::mCherry-Shank1 rescue, mirShank::mCherry-SHANK2 rescue, mirShank::mCherry- SHANK3 rescue or mCherry-Shank2 overexpression constructs. After 7 days, live neurons were imaged on a spinning disk confocal system (described above). After a 2-minute base-line acquisition, internalization was induced by the addition of DHPG to a final concentration of 50 μM and the SEP-mGluR5 signal was imaged every 30 seconds for 30 minutes (61 frames). Dynasore (100 μM; Tocris) was added 2 minutes before acquisition. In the vehicle control extracellular imaging buffer was added to the incubation chamber after a 2-minute base-line acquisition in the same volume (40 μl to 360 μl) as DHPG. To control for photobleaching the SEP-mGluR5 signal was imaged every 5 minutes for 30 minutes (7 frames). Multiple Z-stacks (10 planes) were obtained, with 0.5 μm intervals to acquire 4.5 μm image stacks.

SEP pH sensitivity assay

DIV18 neurons were transfected with SEP-mGluR5 and imaged at DIV21 on a spinning disk confocal system (described above). First, neurons were maintained in extracellular imaging buffer with pH 7.35 to visualize the mGluR5 surface pool. Then, the buffer was exchanged for imaging buffer with pH 5.5 (identical to extracellular imaging buffer, except 10 mM HEPES was replaced by 15 mM MES). Then, the low-pH buffer was exchanged for a buffer with pH 7.35 containing ammonium chloride (NH4Cl) (identical to extracellular imaging buffer, except for 70 mM NaCl, 50 mM NH4Cl and 2 mM NaHCO3 instead of 120 mM NaCl). To evaluate the change in fluorescence upon exchanging the buffers, each neuron was imaged consecutively for all three conditions and 6 time points at 30 second intervals were obtained per condition. Multiple Z-stacks (10 planes) were obtained, with 0.5 μm intervals to acquire 4.5 μm image stacks per time point. For analysis, MAX intensity projections were used to assess the SEP-mGluR5 intensity for all 6 time points per condition and the change in fluorescence over time and different conditions was plotted.

Live-cell imaging of AcidiFluor ORANGE Halo-tagged mGluR5

DIV18 neurons were transfected with Halo-mGluR5 and psm155-GFP, and imaged at DIV21 on a spinning disk confocal system (described above). Surface Halo-mGluR5 was labeled with 1.5 μM HaloTag AcidiFluor ORANGE (Goryo Chemical, cat#-GC310) for 20 minutes at 37°C in 5% CO2. Neurons were rinsed in extracellular imaging buffer to remove unbound dye. Halo-mGluR5 labeled with AcidiFluor ORANGE was imaged in extracellular imaging buffer at 100 ms exposure and 2 second interval for 5 minutes using the 561 excitation laser. Timelapses were taken of a single z-plane.

After a 40 second baseline acquisition, internalization was induced by the application of DHPG to a final concentration of 100 μM. Then, after 280 seconds, imaging buffer was exchanged for a buffer with pH 7.35 containing NH_4Cl (described above) to quench the signal of internalized Halo-mGluR5 AcidiFluor ORANGE. Also, a Z-stack (10 planes) was obtained, with 0.5 μm intervals to acquire 4.5 μm image stacks of psm155-GFP, which was co-transfected for quantification purposes.

Fluorescence recovery after photobleaching

For fluorescence recovery after photobleaching (FRAP) experiments, DIV14 neurons were transfected with Venus-mGluR5 and pSM155-mCherry or mirShank::mCherry, and imaged on a spinning disk confocal system (described above). FRAP experiments were performed using the ILas2 system (Roper Scientific). Individual spines were photobleached with a targeted 488 nm laser and imaged every 5 seconds for fluorescence recovery for a period of 5 minutes.

Calcium imaging

DIV14 neurons were transfected with GCaMP6s together with pSM155-mCherry or mirShank::mCherry and imaged 5 – 7 days later. Calcium imaging was performed on a spinning disk confocal system (described above). GCaMP6s signal was imaged at 2 second intervals (0.5 Hz) with a z-stack stream (3 - 5 planes) at every time point. After 5 minutes baseline imaging, DHPG was added to 100 μM final concentration, and cells were imaged for another 5 - 10 minutes. MPEP (5 μM; Tocris) was added 5 minutes after application of DHPG.

Western blot and imaging

DIV10 neurons were infected with FUGW or FUGW-mirShank lentivirus for 10 days. Neurons were directly lysed in SDS sample buffer containing DTT. Lysates were subjected to Tris-Glycine SDS-PAGE followed by transfer on PVDF membranes. Blots were blocked in 2% BSA in PBS-T (0.05% Tween20) followed by primary and IRDye-conjugated secondary antibody incubation (in 2% BSA in PBS-T). Western blots were scanned using Odyssey infrared imaging system (Li-COR Biosciences).

Quantification and Statistical Analysis

Quantification of endocytic zone associated PSDs

To quantify the fraction of synapses with an associated endocytic zone, circular regions with a fixed diameter (0.69 μm) were centered on the Homer1c-mCherry or mCherry-SHANK2 clusters to indicate synaptic regions. These regions were then transferred to the GFP-CLC or anti-clathrin channel. A synapse was classified EZ-positive if the clathrin cluster overlapped partially or completely with the circular region. The fraction of EZ-positive synapses was calculated per neuron and averaged per condition over the total population of neurons. Furthermore, the density of clathrin puncta was determined along the dendrite (per 10 μm). To quantify the percentage of PSDFingR-GFP puncta overlapping with indicated mCherry constructs, puncta were selected with circular regions in the mCherry channel and transferred to the PSDFingR-GFP channel. It was classified as overlapping if the PSDFingR cluster overlapped partially or completely with the circular region. Furthermore, the puncta density of the indicated mirShank::mCherry-SHANK2 rescue constructs was determined along the dendrite (per 20 μm).

Quantification of internalized mGluR5 puncta in spines and dendrites
The number of PSDs associated with an internalized mGluR5 puncta was determined similar as the fraction of endocytic zone positive PSDs. The density of internalized mGluR5 puncta in the dendritic shaft was determined by semi-automatic quantification. The dendritic shaft (20 μm in length) was selected and a threshold was set for each image. The selection was converted to an inverted binary image and a particle analysis was used to detect internalized mGluR5 puncta with a minimum size of 0.01 μm^2. The baseline condition (t = 0) was similar between control and Shank knockdown neurons. Therefore, to show the relative increase in internalized mGuR5 puncta in the dendritic shaft over time the treatment conditions were normalized per batch to the average density of its corresponding baseline condition.

Quantification of SEP-mGluR5 internalization in spines and dendrites
MAX intensity projections of the Z-stacks were obtained and corrected for XY drift over time using the Fiji plugin "StackReg". To quantify the SEP-mGluR5 intensity over a time-period of 30 minutes circular regions of interest (spines or dendrites) were selected at t = -2 and the intensity was measured for all 61 time points. To obtain the change in relative fluorescence intensity ($\Delta F/F_0$) over time, background was subtracted and the intensity relative to t = -2 was computed. For visualization all values were subtracted by 1 and plotted at 1 minute intervals.

Quantification of AcidiFluor ORANGE Halo-tagged mGluR5 acidification in spines and dendrites
MAX intensity projections of the psm155-GFP Z-stacks were made and used to trace the neuron using Fiji software. This selection was then transferred to the AcidiFluor ORANGE Halo-mGluR5 channel to clearly indicate the outline of the neuron. A gaussian blur (sigma = 2) was applied to the AcidiFluor ORANGE images, and a total of 6 neurons from 2 batches were manually screened for acidification events. To test the pH sensitivity of AcidiFluor ORANGE, imaging buffer was exchanged for a buffer containing NH_4Cl which quenched the signal. Representative images are shown at 4-10 second intervals. To visualize the change in relative fluorescence intensity over time, values were plotted as $\Delta F/F_0$ for the spine and dendrite.

Quantification of spine enrichment
To assess the spine enrichment of surface mGluR5, the SEP-mGluR5 intensity at t = -2 min from the live-cell base-line acquisition was quantified in control, mirShank and mirShank::Shank1, mirShank::SHANK2 and mirShank::SHANK3 rescue neurons as relative spine intensity over relative dendritic shaft intensity. For each neuron circular regions were traced on multiple dendritic spines to measure spine intensity and for each selected spine a circular region in the dendrite at the base of the spine was measured as dendritic shaft intensity. Background intensity was subtracted.

Quantification of immunofluorescence of endogenous mGluR5
For the analysis of endogenous total mGluR5 levels a dendritic stretch of 20 μm was selected and traced in the mCherry channel using Fiji software. This selection

was then transferred to the anti-mGluR5 channel and the average intensity of the anti-mGluR5 fluorescence of the transfected neurons with indicated constructs was obtained. Per batch the average intensity was normalized to the average intensity of the control neurons.

Quantification of FRAP experiment

For FRAP analysis, the mean intensity of the bleached area was corrected for background values, as well as the bleaching that occurred during image acquisition. Data were normalized to control fluorescence averaged over 5 frames before bleaching. Individual recovery curves were fitted with a single-exponential function $I = A(1 – \exp(-Kt))$ to estimate the mobile fraction (A) and time constant tau.

Quantification of calcium experiment

For each neuron, the fluorescence intensity of GCaMP6s signal was measured in 10 - 20 ROIs along the dendrite, background subtracted and averaged. To obtain the mean amplitude and frequency of the calcium oscillations, events were detected with the MATLAB ‘PeakFinder’ function.

Quantification of ERK1/2 phosphorylation assay

For analysis the cell bodies were manually traced based on the mCherry channel using Fiji software. The average intensity of the anti-pERK1/2 fluorescence of the transfected neurons with indicated constructs was obtained for each condition and was normalized per batch to the average intensity of the non-treated control condition.

Statistical Analysis

Statistical significance was tested with a paired t-test (Figure 3L and 4G) or unpaired t-test (Figures 3C, and H, 4D, S3A and S4A, D and F) when comparing two groups with a normal distribution and a Mann Whitney test when comparing two groups without a normal distribution (Figure 4J and S3C). If multiple groups were compared (Figures 1D, 3D, F and J, S3G, H and J and S4B), statistical significance was tested with a one-way ANOVA followed by a Tukey’s multiple comparison when comparing the mean of each column to the mean of every other column or a Dunnet’s multiple comparison when comparing the mean of each column to the mean of a control column. When comparing multiple groups without a normal distribution, a Kruskall Wallis followed by a Dunn’s multiple comparison was performed (Figure S3F). To test for an effect of treatment over time between different groups with matched values in time (Figures 1G-L, 2B-F, S1B, C and I-L, S2C and D and 4C), statistical significance was tested with a repeated measures two-way ANOVA followed by a Tukey’s multiple comparison when comparing more than two groups. To test for an effect of treatment over time between different groups without matched factors (Figure 4B and L), statistical significance was tested with a two-way ANOVA followed by a Tukey’s multiple comparison when comparing more than two groups. The data table of Figure 2G contains some missing values, since during image acquisition some frames were out of focus and could not be taken into account for analysis, and a mixed effects ANOVA was performed. The effect was considered significant if the row factor (time or treatment), the column factor (condition) and the interaction (time x condition) effect were all significant (P-value below 0.05). In the text the P-values of the condition effects are reported. In the figures, * indicates significance based on the condition effect and when comparing more than two groups, * indicates significance based on the multiple comparison test. In all figures * was used to indicate a P-value < 0.05, ** for P < 0.01, and *** for P < 0.001. See Supplementary Table 2 for all P-values and statistical tests performed. Data are represented as mean ± SEM. Reported n is number of neurons, which are indicated as scatters in the bar graphs. Each experiment was replicated in cultures from at least 2 independent preparations. Statistical analysis and graphs were prepared in GraphPad Prism and figures were generated in Adobe Illustrator CC.

Data and Code Availability

The published article includes all datasets generated or analyzed during this study.

Lead Contact and Materials Availability

Plasmids generated in this study are available on request. Further information and requests for resources and reagents should be directed to and will be fulfilled by the Lead Contact, Harold MacGillavry (h.d.macgillavry@uu.nl).

ACKNOWLEDGMENTS

We would like to thank the MacGillavry lab for helpful discussions. This work was supported by the Netherlands Organization for Scientific Research (NWO-ALW-VENI to HDM and the Graduate Program of Quantitative Biology and Computational Life Sciences to NS), the Federation of European Biochemical Societies (FEBS Return-to-Europe Fellowship), the European Research Council (ERC-StG 716011), and the Brain and Behavior Research Foundation (NARSAD Young Investigator Award) to HDM.

AUTHOR CONTRIBUTIONS

Conceptualization, Methodology, Validation and Formal Analysis, N.S. and H.D.M., Investigation, N.S., L.C., M.W. and H.D.M., Resources, H.D.M., C.C.H. and T.A.B., Writing - Original Draft & Editing, N.S. and H.D.M., Writing - Review, C.C.H. and T.A.B., Visualization, N.S. and H.D.M., Supervision, H.D.M., Funding Acquisition, H.D.M.

REFERENCES

Arons, M.H., Thynne, C.J., Grabrucker, A.M., Li, D., Schoen, M., Cheyne, J.E., Boeckers, T.M., Montgomery, J.M., and Garner, C.C. (2012). Autism-Associated Mutations in ProSAP2/Shank3 Impair Synaptic Transmission and Neurexin-Neuroligin-Mediated Transsynaptic Signaling. J Neurosci 32, 14966-14978.

Bariselli, S., Tzanoulinou, S., Glangetas, C., Prevost-Solie, C., Pucci, L., Viguie, J., Bezzi, P., O'Connor, E.C., Georges, F., Luscher, C., and Bellone, C. (2016). SHANK3 controls maturation of social reward circuits in the VTA. Nat Neurosci 19, 926-934.

Berkel, S., Marshall, C.R., Weiss, B., Howe, J., Roeth, R., Moog, U., Endris, V., Roberts, W., Szatmari, P., Pinto, D., et al. (2010). Mutations in the SHANK2 synaptic scaffolding gene in autism spectrum disorder and mental retardation. Nat Genet 42, 489-491.

Berkel, S., Tang, W., Trevino, M., Vogt, M., Obenhaus, H.A., Gass, P., Scherer, S.W., Sprengel, R., Schratt, G., and Rappold, G.A. (2012). Inherited and de novo SHANK2 variants associated with autism spectrum disorder impair neuronal morphogenesis and physiology. Hum Mol Genet 21, 344-357.

Blanpied, T.A., Scott, D.B., and Ehlers, M.D. (2002). Dynamics and regulation of clathrin coats at specialized endocytic zones of dendrites and spines. Neuron 36, 435-449.

Bozdagi, O., Sakurai, T., Papapetrou, D., Wang, X., Dickstein, D.L., Takahashi, N., Kajiwara, Y., Yang, M., Katz, A.M., Scattoni, M.L., et al. (2010). Haploinsufficiency of the autism-associated Shank3 gene leads to deficits in synaptic function, social interaction, and social communication. Mol Autism 1, 15.

Chen, T.W., Wardill, T.J., Sun, Y., Pulver, S.R., Renninger, S.L., Baohan, A., Schreiter, E.R., Kerr, R.A., Orger, M.B., Jayaraman, V., et al. (2013). Ultrasensitive fluorescent proteins for imaging neuronal activity. Nature 499, 295-300.

Choi, K.Y., Chung, S., and Roche, K.W. (2011). Differential binding of calmodulin to group I metabotropic glutamate receptors regulates receptor trafficking and signaling. J Neurosci 31, 5921-5930.

Cochoy, D.M., Kolevzon, A., Kajiwara, Y., Schoen, M., Pascual-Lucas, M., Lurie, S., Buxbaum, J.D., Boeckers, T.M., and Schmeisser, M.J. (2015). Phenotypic and functional analysis of SHANK3 stop mutations identified in individuals with ASD and/or ID. Mol Autism 6, 23.

Cunha-Ferreira, I., Chazeau, A., Buijs, R.R., Stucchi, R., Will, L., Pan, X., Adolfs, Y., van der Meer, C., Wolthuis, J.C., Kahn, O.I., et al. (2018). The HAUS Complex Is a Key Regulator of Non-centrosomal Microtubule Organization during Neuronal Development. Cell Rep 24, 791-800.

Czondor, K., Mondin, M., Garcia, M., Heine, M., Frischknecht, R., Choquet, D., Sibarita, J.B., and Thoumine, O.R. (2012). Unified quantitative model of AMPA receptor trafficking at synapses. Proc Natl Acad Sci U S A 109, 3522-3527.

Dhami, G.K., and Ferguson, S.S. (2006). Regulation of metabotropic glutamate receptor signaling, desensitization and endocytosis. Pharmacol Ther 111, 260-271.

Duffney, L.J., Wei, J., Cheng, J., Liu, W., Smith, K.R., Kittler, J.T., and Yan, Z. (2013). Shank3 deficiency induces NMDA receptor hypofunction via an actin-dependent mechanism. J Neurosci 33, 15767-15778.

Duffney, L.J., Zhong, P., Wei, J., Matas, E., Cheng, J., Qin, L., Ma, K., Dietz, D.M., Kajiwara, Y., Buxbaum, J.D., and Yan, Z. (2015). Autism-like Deficits in Shank3-Deficient Mice Are Rescued by Targeting Actin Regulators. Cell Rep 11, 1400-1413.

Esteves da Silva, M., Adrian, M., Schatzle, P., Lipka, J., Watanabe, T., Cho, S., Futai, K., Wierenga, C.J., Kapitein, L.C., and Hoogenraad, C.C. (2015). Positioning of AMPA Receptor-Containing Endosomes Regulates Synapse Architecture. Cell Rep 13, 933-943.

Fourgeaud, L., Bessis, A.S., Rossignol, F., Pin, J.P., Olivo-Marin, J.C., and Hemar, A.

(2003). The metabotropic glutamate receptor mGluR5 is endocytosed by a clathrin-independent pathway. J Biol Chem 278, 12222-12230.
Francesconi, A., Kumari, R., and Zukin, R.S. (2009). Regulation of group I metabotropic glutamate receptor trafficking and signaling by the caveolar/lipid raft pathway. J Neurosci 29, 3590-3602.
Gray, N.W., Fourgeaud, L., Huang, B., Chen, J., Cao, H., Oswald, B.J., Hemar, A., and McNiven, M.A. (2003). Dynamin 3 is a component of the postsynapse, where it interacts with mGluR5 and Homer. Curr Biol 13, 510-515.
Gross, G.G., Junge, J.A., Mora, R.J., Kwon, H.B., Olson, C.A., Takahashi, T.T., Liman, E.R., Ellis-Davies, G.C., McGee, A.W., Sabatini, B.L., et al. (2013). Recombinant probes for visualizing endogenous synaptic proteins in living neurons. Neuron 78, 971-985.
Hoogenraad, C.C., Popa, I., Futai, K., Martinez-Sanchez, E., Wulf, P.S., van Vlijmen, T., Dortland, B.R., Oorschot, V., Govers, R., Monti, M., et al. (2010). Neuron specific Rab4 effector GRASP-1 coordinates membrane specialization and maturation of recycling endosomes. PLoS Biol 8, e1000283.
Isa, M., Asanuma, D., Namiki, S., Kumagai, K., Kojima, H., Okabe, T., Nagano, T., and Hirose, K. (2014). High-throughput screening system to identify small molecules that induce internalization and degradation of HER2. ACS Chem Biol 9, 2237-2241.
Kawabata, S., Tsutsumi, R., Kohara, A., Yamaguchi, T., Nakanishi, S., and Okada, M. (1996). Control of calcium oscillations by phosphorylation of metabotropic glutamate receptors. Nature 383, 89-92.
Kessels, M.M., Engqvist-Goldstein, A.E., Drubin, D.G., and Qualmann, B. (2001). Mammalian Abp1, a signal-responsive F-actin-binding protein, links the actin cytoskeleton to endocytosis via the GTPase dynamin. J Cell Biol 153, 351-366.
Kouser, M., Speed, H.E., Dewey, C.M., Reimers, J.M., Widman, A.J., Gupta, N., Liu, S., Jaramillo, T.C., Bangash, M., Xiao, B., et al. (2013). Loss of predominant Shank3 isoforms results in hippocampus-dependent impairments in behavior and synaptic transmission. J Neurosci 33, 18448-18468.
Lee, J.H., Lee, J., Choi, K.Y., Hepp, R., Lee, J.Y., Lim, M.K., Chatani-Hinze, M., Roche, P.A., Kim, D.G., Ahn, Y.S., et al. (2008). Calmodulin dynamically regulates the trafficking of the metabotropic glutamate receptor mGluR5. Proc Natl Acad Sci U S A 105, 12575-12580.
Lee, K., Vyas, Y., Garner, C.C., and Montgomery, J.M. (2019). Autism-associated Shank3 mutations alter mGluR expression and mGluR-dependent but not NMDA receptor-dependent long-term depression. Synapse 73, e22097.
Lois, C., Hong, E.J., Pease, S., Brown, E.J., and Baltimore, D. (2002). Germline transmission and tissue-specific expression of transgenes delivered by lentiviral vectors. Science 295, 868-872.
Lu, J., Helton, T.D., Blanpied, T.A., Racz, B., Newpher, T.M., Weinberg, R.J., and Ehlers, M.D. (2007). Postsynaptic positioning of endocytic zones and AMPA receptor cycling by physical coupling of dynamin-3 to Homer. Neuron 55, 874-889.
Lüscher, C., and Huber, K.M. (2010). Group 1 mGluR-dependent synaptic long-term depression: mechanisms and implications for circuitry and disease. Neuron 65, 445- 459.
MacGillavry, H.D., Kerr, J.M., Kassner, J., Frost, N.A., and Blanpied, T.A. (2016). Shank-cortactin interactions control actin dynamics to maintain flexibility of neuronal spines and synapses. Eur J Neurosci 43, 179-193.
MacGillavry, H.D., Song, Y., Raghavachari, S., and Blanpied, T.A. (2013). Nanoscale scaffolding domains within the postsynaptic density concentrate synaptic AMPA receptors. Neuron 78, 615-622.

Macia, E., Ehrlich, M., Massol, R., Boucrot, E., Brunner, C., and Kirchhausen, T. (2006). Dynasore, a cell-permeable inhibitor of dynamin. Dev Cell 10, 839-850.

Mao, L., Yang, L., Tang, Q., Samdani, S., Zhang, G., and Wang, J.Q. (2005). The scaffold protein Homer1b/c links metabotropic glutamate receptor 5 to extracellular signal-regulated protein kinase cascades in neurons. J Neurosci 25, 2741-2752.

McNiven, M.A., Kim, L., Krueger, E.W., Orth, J.D., Cao, H., and Wong, T.W. (2000). Regulated interactions between dynamin and the actin-binding protein cortactin modulate cell shape. J Cell Biol 151, 187-198.

Naisbitt, S., Kim, E., Tu, J., Xiao, B., Sala, C., Valtschanoff, J., Weinberg, R., Worley, P., and Sheng, M. (1999). Shank, a novel family of postsynaptic density proteins that binds to the NMDA receptor/PSD-95/GKAP complex and cortactin. Neuron 23, 569-582.

Nash, M.S., Schell, M.J., Atkinson, P.J., Johnston, N.R., Nahorski, S.R., and Challiss, R.A. (2002). Determinants of metabotropic glutamate receptor-5-mediated Ca2+ and inositol 1,4,5-trisphosphate oscillation frequency. Receptor density versus agonist concentration. J Biol Chem 277, 35947-35960.

Ochoa, G.C., Slepnev, V.I., Neff, L., Ringstad, N., Takei, K., Daniell, L., Kim, W., Cao, H., McNiven, M., Baron, R., and De Camilli, P. (2000). A functional link between dynamin and the actin cytoskeleton at podosomes. J Cell Biol 150, 377-389.

Okamoto, P.M., Gamby, C., Wells, D., Fallon, J., and Vallee, R.B. (2001). Dynamin isoform-specific interaction with the shank/ProSAP scaffolding proteins of the postsynaptic density and actin cytoskeleton. J Biol Chem 276, 48458-48465.

Parkinson, G.T., Chamberlain, S.E.L., Jaafari, N., Turvey, M., Mellor, J.R., and Hanley, J.G. (2018). Cortactin regulates endo-lysosomal sorting of AMPARs via direct interaction with GluA2 subunit. Sci Rep 8, 4155.

Petrini, E.M., Lu, J., Cognet, L., Lounis, B., Ehlers, M.D., and Choquet, D. (2009). Endocytic trafficking and recycling maintain a pool of mobile surface AMPA receptors required for synaptic potentiation. Neuron 63, 92-105.

Qualmann, B., Boeckers, T.M., Jeromin, M., Gundelfinger, E.D., and Kessels, M.M. (2004). Linkage of the actin cytoskeleton to the postsynaptic density via direct interactions of Abp1 with the ProSAP/Shank family. J Neurosci 24, 2481-2495.

Racz, B., Blanpied, T.A., Ehlers, M.D., and Weinberg, R.J. (2004). Lateral organization of endocytic machinery in dendritic spines. Nat Neurosci 7, 917-918.

Rosendale, M., Jullie, D., Choquet, D., and Perrais, D. (2017). Spatial and Temporal Regulation of Receptor Endocytosis in Neuronal Dendrites Revealed by Imaging of Single Vesicle Formation. Cell Rep 18, 1840-1847.

Scheefhals, N., and MacGillavry, H.D. (2018). Functional organization of postsynaptic glutamate receptors. Mol Cell Neurosci 91, 82-94.

Schmeisser, M.J., Ey, E., Wegener, S., Bockmann, J., Stempel, A.V., Kuebler, A., Janssen, A.L., Udvardi, P.T., Shiban, E., Spilker, C., et al. (2012). Autistic-like behaviours and hyperactivity in mice lacking ProSAP1/Shank2. Nature 486, 256-260.

Tu, J.C., Xiao, B., Naisbitt, S., Yuan, J.P., Petralia, R.S., Brakeman, P., Doan, A., Aakalu, V.K., Lanahan, A.A., Sheng, M., and Worley, P.F. (1999). Coupling of mGluR/Homer and PSD-95 complexes by the Shank family of postsynaptic density proteins. Neuron 23, 583-592.

Verpelli, C., Dvoretskova, E., Vicidomini, C., Rossi, F., Chiappalone, M., Schoen, M., Di Stefano, B., Mantegazza, R., Broccoli, V., Bockers, T.M., et al. (2011). Importance of Shank3 protein in regulating metabotropic glutamate receptor 5 (mGluR5) expression and signaling at synapses. J Biol Chem 286, 34839-34850.

Vicidomini, C., Ponzoni, L., Lim, D., Schmeisser, M.J., Reim, D., Morello, N., Orellana, D., Tozzi, A., Durante, V., Scalmani, P., et al. (2017). Pharmacological enhancement of mGlu5 receptors rescues behavioral deficits in SHANK3 knock-out mice. Mol Psychiatry 22, 689-702.

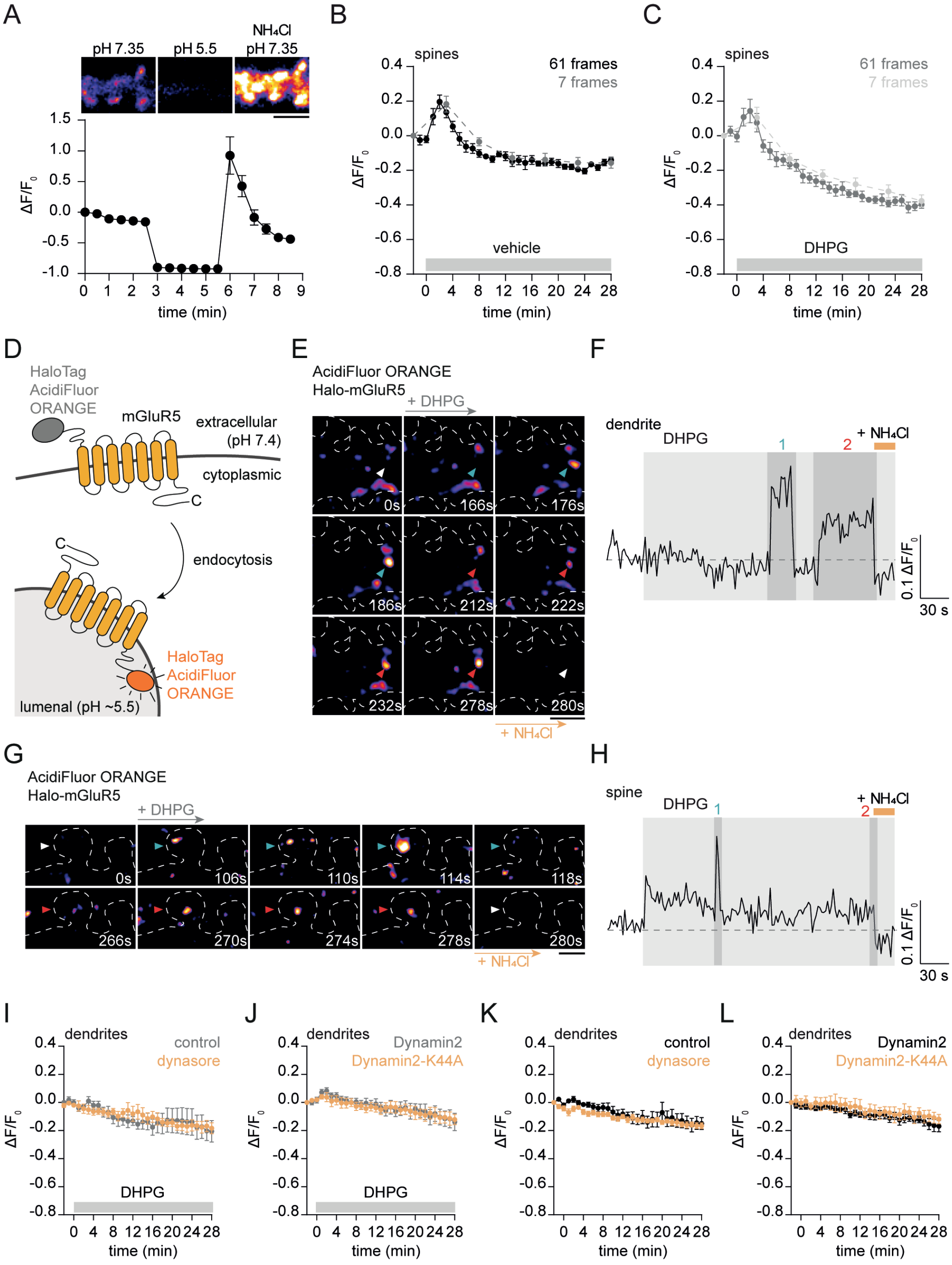
A
pH 7.35
pH 5.5
NH₄Cl pH 7.35
ΔF/F₀
1.5
1.0
0.5
0.0
-0.5
-1.0
0 1 2 3 4 5 6 7 8 9
time (min)
B
spines
61 frames
7 frames
vehicle
0.4
0.2
0.0
-0.2
-0.4
-0.6
-0.8
0 4 8 12 16 20 24 28
time (min)
C
spines
61 frames
7 frames
DHPG
time (min)
D
HaloTag
AcidiFluor
ORANGE
mGluR5
extracellular
(pH 7.4)
cytoplasmic
C
endocytosis
C
HaloTag
AcidiFluor
ORANGE
lumenal (pH ~5.5)
E
AcidiFluor ORANGE
Halo-mGluR5
+ DHPG
0s
166s
176s
186s
212s
222s
232s
278s
280s
+ NH₄Cl
F
dendrite
DHPG
1
2
+ NH₄Cl
0.1 ΔF/F₀
30 s
G
AcidiFluor ORANGE
Halo-mGluR5
+ DHPG
0s
106s
110s
114s
118s
266s
270s
274s
278s
280s
+ NH₄Cl
H
spine
DHPG
1
2
+ NH₄Cl
0.1 ΔF/F₀
30 s
I
dendrites
control
dynasore
DHPG
time (min)
J
dendrites
Dynamin2
Dynamin2-K44A
DHPG
time (min)
K
dendrites
control
dynasore
time (min)
L
dendrites
Dynamin2
Dynamin2-K44A
time (min)

Figure S1, related to Figure 1. Characterization of SEP-mGluR5 fluorescence and evaluation of dendritic internalization. (A) Surface SEP-mGluR5 fluorescence intensity in imaging buffer with pH 7.35 (t = 0 - 3 min), is quenched at pH 5.5 (t = 3 – 6 min) and increased in fluorescence upon the application of imaging buffer containing NH_4Cl with pH 7.35 (t = 6 min) visualizing both surface and intracellular SEP-mGluR5 (n = 6). Scale bar, 2 μm. (B and C) Quantification of SEP-mGluR5 intensity in spines over a 30-minute time period comparing the loss of SEP-mGluR5 intensity when imaged every 5 minutes (7 frames; dashed light grey line; n = 12) and when imaged every 30 seconds (61 frames; solid black line; n = 8) after application with vehicle (B) and after DHPG stimulation (7 frames; dashed light grey line; n = 12 and 61 frames; solid dark grey line; n= 6) (C). The data sets from 61 frames shown in B and C are also shown in Figure 1G, as these figures describe different aspects of the same experiment. (D) Schematic of Halo-tag labeled with AcidiFluor ORANGE fused to mGluR5 to reveal acidification of Halo- mGluR5-containing endocytic vesicles. (E and G) Representative image of a dendrite expressing Halo-mGluR5 labeled with AcidiFluor ORANGE stimulated with DHPG (at t = 40 s) showing two acidification events, and quenching of the signal upon application of imaging buffer containing NH_4Cl with pH 7.35 (t = 280 s) at the dendritic shaft (E) and in a spine (G). Arrowheads indicate two acidification events (1; blue and 2; red). Scale bars, 2 μm. (F and H) $\Delta F/F_0$ trace of the Halo-mGluR5 signal intensity, showing the baseline (t = 0 – 40 s), application of DHPG (t = 42 – 178 s; light grey), the acidification events shown in E and G (dark grey) and the application of NH_4Cl (t = 280 – 300 s; orange) at the dendritic shaft shown in E (indicated by arrowhead) (F) and in the spine shown in G (indicated by arrowhead) (H). (I and J) Quantification of SEP-mGluR5 intensity in dendrites over time after DHPG stimulation comparing the time course of SEP-mGluR5 intensity in control neurons (grey; n = 6) with neurons pre-treated with dynasore (orange; n = 6) (I) and in neurons co-transfected with Dyn2 (grey; n = 6) with neurons co-transfected with the dominant negative Dyn2-K44A (orange; n = 6) (J). (K and L) Quantification of SEP-mGluR5 intensity in dendrites over time without the addition of DHPG comparing the time course of SEP-mGluR5 intensity in control neurons (black; n = 6) with neurons pre-treated with dynasore (orange; n = 8) (K) and in neurons co-transfected with Dyn2 (grey; n = 6) with neurons co- transfected with the dominant negative Dyn2-K44A (orange; n = 6) (L). Data are represented as mean ± SEM.

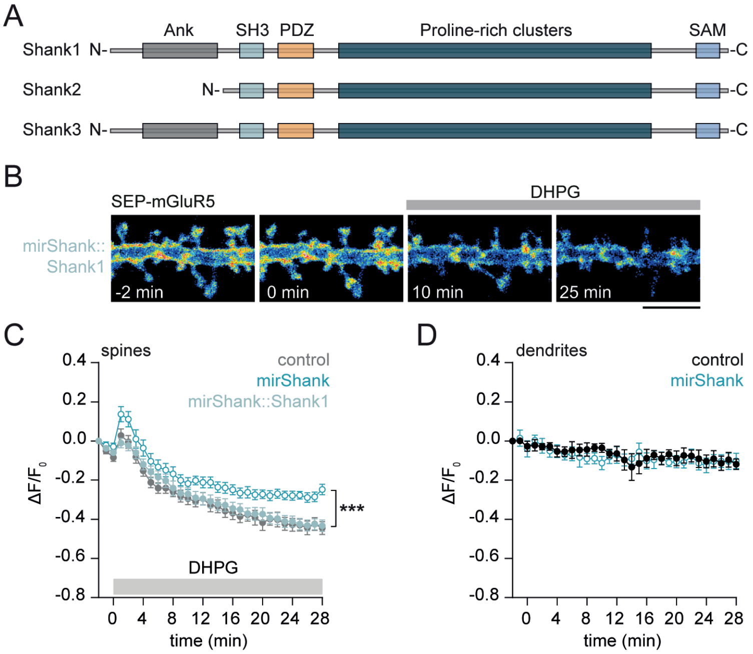

Figure S2, related to Figure 2. Re-expression of Shank1 rescues agonist-induced mGluR5 internalization in spines. (A) Domain structure of Shank1, Shank2 and Shank3. (B) Representative live-cell time-lapse image of SEP-mGluR5 before and after DHPG stimulation (added at t = 0 min) in mirShank::Shank1 neurons. Scale bar, 5 µm. (C) Quantification of SEP-mGluR5 intensity in spines over time after the addition of DHPG comparing the time course of SEP-mGluR5 intensity in control (grey; n = 14), mirShank (blue; open circles; n = 17) and mirShank::Shank1 rescue neurons (shade of blue; closed circles; n = 22). (D) Quantification of SEP-mGluR5 intensity in dendrites over time without the addition of DHPG comparing the time course of SEP-mGluR5 intensity in control (black; n = 5) and mirShank neurons (blue; n = 5).Data are represented as mean ± SEM. ***, indicates $P < 0.001$.

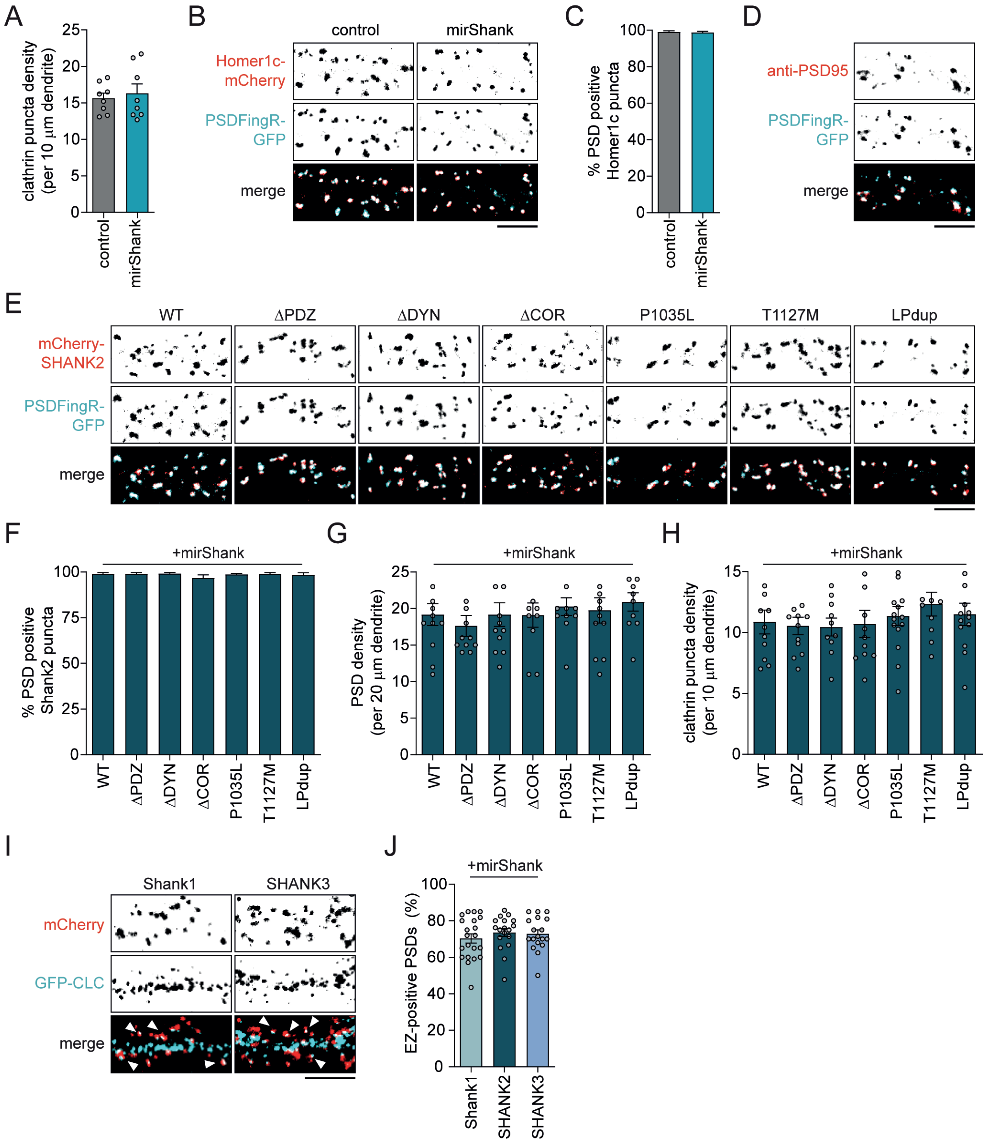

Figure S3, related to Figure 3. Clathrin puncta density in dendrites, mGluR5 spine enrichment and synaptic targeting of SHANK2 mutants. (A) Quantification of the density of GFP-CLC puncta along the dendrite (per 10 µm) in control (n = 8) and mirShank (n=8) neurons. (B) Representative images of dendrites co-expressing PSDFingR-GFP (cyan) and Homer1c-mCherry (red) in control and mirShank neurons. Scale bar, 5 µm. (C) Quantification of the percentage of Homer1c-mCherry puncta positive for PSDFingR-GFP, a marker of the PSD, in control (n = 10) and mirShank (n = 11) neurons. (D) Co-localization of PSDFingR-GFP (cyan) and immuno-labeled anti-PSD-95 (red). Scale bar, 5 µm. (E) Representative images of dendrites co-expressing mCherry-tagged SHANK2 rescue constructs (red) and PSDFingR-GFP (cyan). Scale bar, 5 µm. (F) Quantification of the percentage of mCherry-tagged WT and mutant SHANK2 puncta positive for PSDFingR-GFP, a marker of the PSD (WT: n = 12, Δ PDZ: n = 11, ΔDYN: n = 12, ΔCOR: n = 10, P1035L: n = 11, T1127M: n = 12, LPdup: n = 10). (G) Quantification of the density of PSDs, marked by PSDFingR-GFP, along the dendrite (per 20 µm) in neurons co-expressing the mCherry-tagged SHANK2 rescue constructs (WT: n = 12, Δ PDZ: n = 11, ΔDYN: n = 12, ΔCOR: n = 10, P1035L: n = 11, T1127M: n = 12, LPdup: n = 10). (H) Quantification of the density of GFP-CLC puncta along the dendrite (per 10 μm) in neurons co-expressing mCherry-tagged SHANK2 rescue constructs (WT: n = 11, Δ PDZ: n = 12, ΔDYN: n = 10, ΔCOR: n = 11, P1035L: n = 15, T1127M: n = 10, LPdup: n = 13). (I) Representative images of dendrites co-expressing mCherry-tagged Shank1, SHANK2 and SHANK3 rescue constructs (red) and GFP-CLC (cyan). Scale bar, 5 μm. (J) Quantification of the percentage of EZ-positive PSDs in neurons co-expressing mCherry-tagged Shank1 (n = 21), SHANK2 (n = 18) and SHANK3 (n = 18) rescue constructs. Data are represented as mean ± SEM.

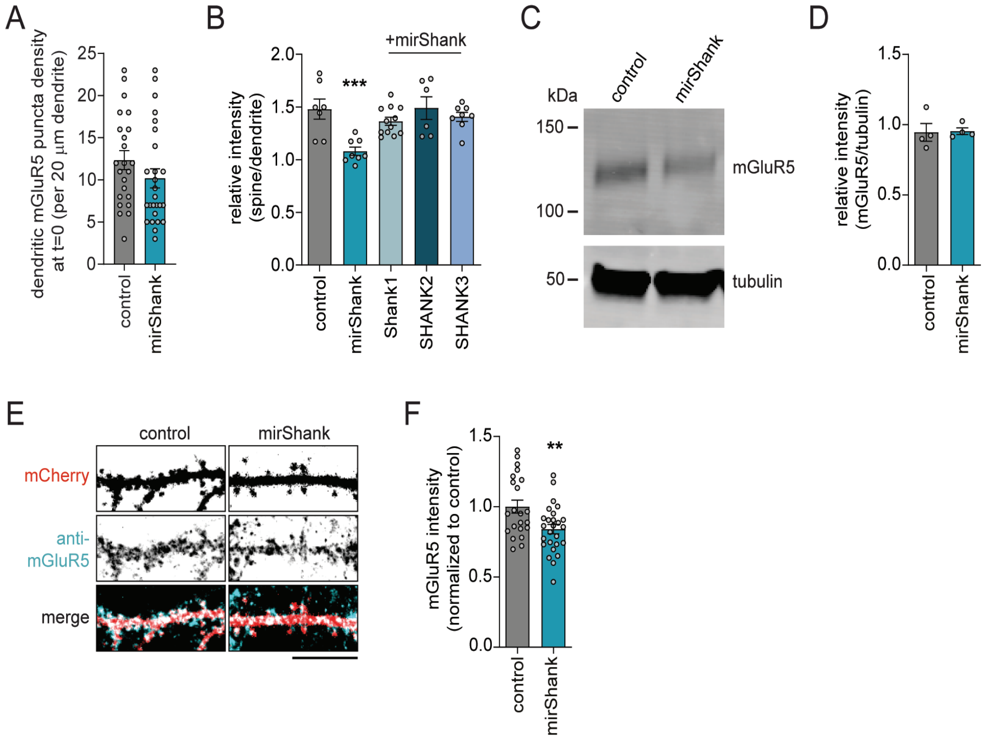

Figure S4, related to Figure 4. Shank proteins control surface and total expression of mGluR5. (A) Quantification of internalized myc-mGluR5 puncta density in dendrites of control (n = 23) and mirShank neurons (n = 26) at t = 0. (B) Quantification of SEP-mGluR5 intensity in spines over dendritic shaft of control (n = 7), mirShank (n = 8), mirShank::Shank1 (n = 12), mirShank::SHANK2 (n = 6) and mirShank::SHANK3 (n = 9) rescue neurons. (C) Western blot analysis of total lysates of neurons infected with GFP and GFP::mirShank and immuno-labelled for anti-mGluR5; tubulin was used as a loading control. (D) Quantification of anti-mGluR5 over tubulin intensity in control and mirShank neurons (n = 3). (E) Representative images of dendrites immuno-labeled for anti-mGluR5 (cyan) in mCherry-tagged control and mirShank neurons (red). Scale bar, 10 µm. (F) Quantification of anti-mGluR5 intensity along the dendrite (20 µm) in control (n = 20) and mirShank (n = 27) neurons, normalized to the average intensity of anti-mGluR5 fluorescence in the control condition. Data are represented as mean ± SEM. **, indicates P < 0.01 and ***, indicates P < 0.001.

4

Dynamics and nanoscale organization of the postsynaptic endocytic zone at excitatory synapses

Lisa A.E. Catsburg, Manon Westra, Annemarie M. L. van Schaik,
Harold D. MacGillavry

Department of Cell Biology, Neurobiology and Biophysics at the Faculty of
Science of Utrecht University in Utrecht, the Netherlands

Under review, eLife
Preprint available on BioArxiv : doi 10.1101/2021.02.18.431766

ABSTRACT

At postsynaptic sites of neurons, a prominent clathrin-coated structure, the endocytic zone (EZ), controls the trafficking of glutamate receptors and is essential for synaptic plasticity. Despite its importance, little is known about how this clathrin structure is organized to mediate endocytosis. We used live-cell and super-resolution microscopy techniques to reveal the dynamic organization of this poorly understood clathrin structure. We found that a subset of endocytic proteins only transiently appeared at postsynaptic sites. In contrast, other proteins, including Eps15, intersectin1L, and β2-adaptin, were persistently enriched and partitioned at the edge of the EZ. We found that uncoupling the EZ from the synapse led to the loss of most of these components, while disrupting the actin cytoskeleton or AP2-membrane interactions did not alter EZ positioning. We conclude that the EZ is a stable, highly organized molecular platform where components are differentially recruited and positioned to orchestrate the endocytosis of synaptic receptors.

INTRODUCTION

Clathrin-mediated endocytosis is the principal mechanism for the internalization of membrane components, and is essential for cellular homeostasis, intercellular signaling and nutrient uptake in mammalian cells (Kaksonen and Roux, 2018; McMahon and Boucrot, 2011; Mettlen et al., 2018). This process involves the tightly-controlled initiation and maturation of clathrin-coated pits that is mediated by the sequential recruitment of clathrin, cargo and endocytic adaptor proteins (Cocucci et al., 2012; Taylor et al., 2011). Apart from these well-characterized, small (~100 nm) and short-lived (<120 sec) clathrin coats, numerous electron and (live-cell) light microscopy studies have revealed that clathrin can assemble into a remarkably large variety of membrane-attached structures (Grove et al., 2014; Heuser, 1980; Leyton-Puig et al., 2017; Saffarian et al., 2009; Sanan and Anderson, 1991). In fact, the lifetime, size and morphology of clathrin assemblies at the membrane diverge enormously between cell types and even within cells. Clathrin structures varying from 100 nm up to 1 µm with lifetimes ranging from seconds to tens of minutes have been reported. The origins and functional relevance of this striking heterogeneity remain to be elucidated.

This heterogeneity is particularly evident in neurons that contain a divergent population of clathrin structures distributed over their immense and complex plasma membrane. At postsynaptic sites, a clathrin-coated structure referred to as the endocytic zone (EZ) is stably associated with the postsynaptic density (PSD) (Blanpied et al., 2002; Lu et al., 2007), via a Shank-Homer1c-Dynamin3 interaction (Lu et al., 2007; Rosendale et al., 2017). Disrupting the PSD-EZ interaction severely affects glutamate receptor levels at synapses. Particularly, the ionotropic AMPA-type glutamate receptors (Petrini et al., 2009; Rosendale et al., 2017) and metabotropic glutamate receptors (Scheefhals et al., 2019) have been found to undergo trafficking mediated by the EZ, while transferrin receptors are not preferentially internalized near the synapse (Rosendale et al., 2017). It has been proposed that once internalized at the EZ, glutamate receptors enter the local recycling mechanism, that retains receptors in intracellular pools that can recycle back to the synaptic membrane in an activity-dependent manner (Park et al., 2006). Indeed, the local recycling of receptors via the EZ is essential for synaptic plasticity as uncoupling the EZ from the PSD depletes synaptic AMPA receptors and aborts activity-induced trafficking of receptors to the synaptic membrane during long-term potentiation (Lu et al., 2007; Petrini et al., 2009). Importantly, disruptions in EZ structure and function have been associated with the development of neuronal disorders such as autism spectrum disorder and Parkinson's disease (Cortese et al., 2016; Scheefhals et al., 2019).

Despite the clear functional importance of the EZ for synaptic transmission and plasticity in neurons, the molecular organization and how this organization contributes to its function is poorly understood. In electron microscopy studies, clathrin-coated structures have been observed within dendritic spines (Petralia et al., 2003; Tao-Cheng et al., 2011) at an approximate distance of 100-600 nm from the PSD, coinciding with an enrichment of adaptor proteins such as dynamin2 and AP2 (Rácz et al., 2004). However, fundamental information on the spatial distribution and dynamics of endocytic proteins relative to the EZ and how these proteins contribute to EZ organization is missing. Here, we resolved the spatial and temporal organization of clathrin-coated structures in dendrites and spines using live-cell imaging and super-resolution microscopy. We found that the postsynaptic EZ contains a unique and stable assembly of endocytic proteins, that is highly organized at the nanoscale level. Based on these findings, we propose that the EZ is a highly distinct clathrin-coated structure that operates as a preassembled platform for endocytosis of synaptic components to sustain efficient synaptic transmission and plasticity.

RESULTS

Heterogenous morphology of clathrin-coated structures in dendrites

To visualize clathrin-coated structures in mature cultured hippocampal neurons (DIV16-21), GFP-clathrin light-chain-A (GFP-CLCa) was co-transfected with Homer1c-mCherry as a marker of excitatory synapses. We found a large variety of clathrin-coated structures distributed throughout the entire neuron (Figure 1A). In dendrites, a high density of clathrin structures was found in the shaft and the majority of dendritic spines contained a distinct EZ, defined as a clathrin puncta closely associated with the PSD (75 ± 5%), consistent with previous observations (Blanpied et al., 2002; Lu et al., 2007; Scheefhals et al., 2019). Importantly, labelling endogenous CLCa using a CRISPR/Cas9-based approach (Willems et al., 2020) resulted in comparable distribution of clathrin structures (Supplement Figure 1A-C). To resolve clathrin-coated structures in dendrites at high spatial resolution, we used stimulated emission depletion (STED) microscopy, allowing quantitative analyses of clathrin structure morphology (Figure 1B). Notably, STED resolved individual structures at much higher resolution than confocal, often resolving distinct substructures within clathrin patches that appeared homogenous in confocal microscopy (Figure 1C). PSDs associated with more than one clathrin structure were also observed (Figure 1B, C). We found that 59 ± 5% of the PSDs were associated with one clathrin structure, while 14 ± 2% and 5.4 ± 0.8% were associated with two or three clathrin structures, respectively (Figure 1C). Next, we analyzed the morphology of dendritic clathrin structures and found a large range of sizes from as small as 0.01 μm^2 up to 0.43 μm^2 (Figure 1E). On average, the area of PSD-associated clathrin structures was lower, albeit not statistically different from the average area of clathrin structures found in the shaft (area clathrin structures in shaft: 0.045 ± 0.003 μm^2, spine: 0.038 μm^2 ± 0.002, $P > 0.1$) . However, the variability in sizes of clathrin structures in the shaft, was much larger than in spines

(CV shaft: 1.3; spines: 0.84), with larger structures exclusively found in the shaft and not in spines (Figure 1D, E; range in width/length shaft: 0.15 µm to 1.7 µm, spine: 0.084 µm to 0.78 µm). Indeed, large clathrin structures were regularly observed in the shaft, approximately ~3 per 20 µm of dendrite (data not shown). Thus, dendrites contain a large variation of clathrin-marked structures, with PSD-associated EZs being a distinct, homogenous sub-population of clathrin structures in dendritic spines. Studies in non-neuronal cells often classify clathrin structures as flat lattices based on size and shape. Compared to small, circular clathrin structures, presumably representing endocytic pits or intracellular vesicles, lattices are defined as large and irregularly shaped clathrin structures (Grove et al., 2014; Leyton-Puig et al., 2017; Saffarian et al., 2009). We generated scatterplots of the circularity and area of individual dendritic clathrin structures to test if we could find a similar classification (Figure 1E). However, there was no correlation between size and circularity in dendritic clathrin structures (R2 = 0.006). Also, we did not observe a clear differentiation in clathrin structures using this approach, suggesting that clathrin-coated structures in dendrites form a highly heterogeneous population that cannot be classified based on these morphological parameters. Altogether, these data highlight the morphological heterogeneity of clathrin-coated structures in neuronal dendrites.

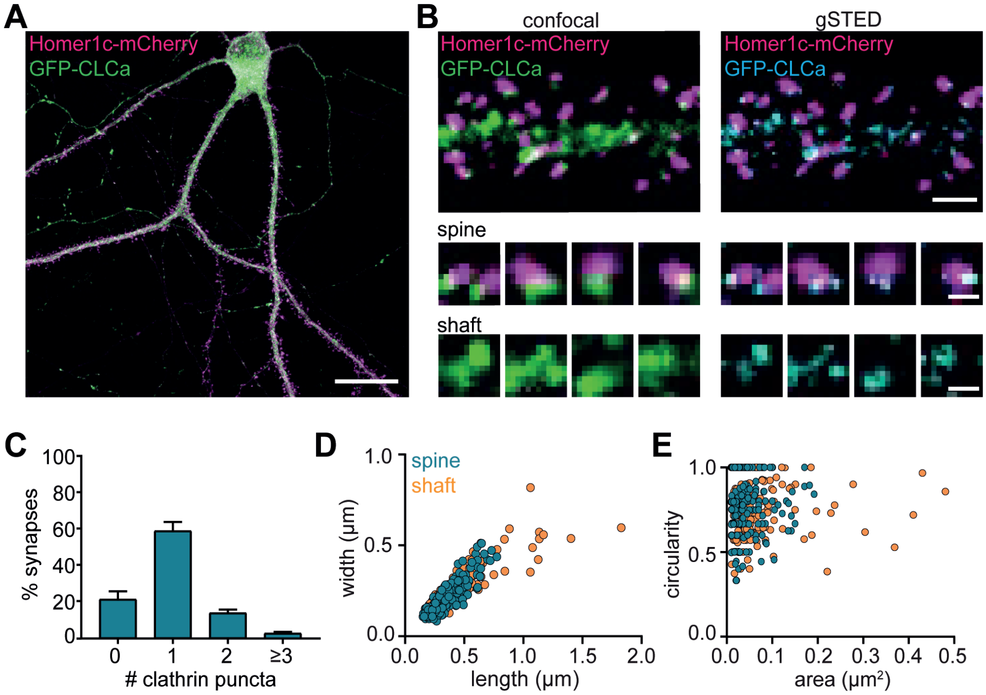

Figure 1. Heterogenous morphology of clathrin-coated structures in dendrites. (A) Example image of neuron expressing Homer1c-mCherry and GFP-CLCa. Scale bar: 20 µm. (B) Comparison of confocal and gSTED images of dendrite expressing Homer1c-mCherry and GFP-CLCa. Scale bars dendrite: 2 µm, zooms: 500 nm. (C) Number of clathrin-coated structures per PSD per neuron, represented as mean ± SEM (N = 12 neurons). (D) Scatterplot of the length (µm) and width (µm) of clathrin-coated structures in the dendritic shaft and associated with Homer1c based on ferret dimensions (spine: n = 248, shaft: n = 301). (E) Circularity ratio plotted against area (µm^2) (spine: n = 248, shaft: n = 301).

Clathrin dynamics at the EZ are distinct from clathrin-coated structures in the dendritic shaft

To study the dynamic properties of clathrin-coated structures in both spines and dendritic shaft we next performed live-cell imaging of GFP-CLCa in dendrites. We first investigated the dynamics of clathrin-coated structures on short time intervals by imaging at 0.2 Hz for 5 minutes. To differentiate stationary from moving particles we used a Fourier analysis-based filtering on kymographs (Mangeol et al., 2016). The dendritic shaft predominantly contained stationary clathrin-coated structures, however smaller anterograde and retrograde moving puncta were also observed (Figure 2A). Interestingly, these fast-moving particles were small (IQR: 0.013 – 0.065 μm^2) most likely reflecting intracellular vesicle transport. Within the stationary pool in the shaft, we observed a few distinct clathrin-coated structures. The two most frequently observed structures were larger, high-intensity structures that either remained fluorescently stable over the entire course of imaging (CV fluorescence intensity = 0.09, Figure 2B: upper panel), or showed large fluctuations in fluorescence intensity (CV = 0.16, Figure 2B: lower panel), perhaps indicating a more dynamic structure. In rare cases transient budding of clathrin from these structures was observed, reminiscent of endocytic pit formation. In spines, the EZ appeared much more stable than dendritic clathrin structures, with little fluctuations in GFP-CLCa intensity (CV: 0.02, Figure 2C: upper panel). Strikingly, we were able to pick up, what seemed to be the budding of individual vesicles from the EZ (Figure 2C, lower panel). On average, the fluctuations in intensity of clathrin structures in shaft and spines were significantly different, with much lower fluctuations found in spines (shaft CV: 0.06 ± 0.004, spine CV: 0.02 ± 0.001, $p < 0.001$) (Figure 2D). Longer acquisitions of 20 minutes at 30-second intervals showed that the clathrin-coated structures in spines had a considerably higher average lifetime compared to clathrin-coated structures in the shaft (average lifetime spines: 10 ± 0.7 minutes, shaft: 6.0 ± 0.3 minutes, $p < 0.001$) (Figure 2E). Indeed, 68.1 ± 6.0% of PSDs remained associated with at least one clathrin structure that was present for the entire 20 minutes, confirming that the EZ is stably coupled to the PSD (Blanpied et al., 2002; Lu et al., 2007; Scheefhals et al., 2019). In contrast, in the dendritic shaft, only a small fraction (~15%) of clathrin-coated structures was long-lived (>17.5 minutes) and the median lifetime of all events was ~2.5 minutes, indicating that the majority of clathrin structures in the dendritic shaft are transient structures (Figure 2E).

The relatively long lifetime and small fluctuations in intensity of clathrin at the EZ might suggest a considerably lower turnover of clathrin at the EZ compared to shaft structures. To determine the turnover of clathrin at stable dendritic structures we used fluorescence recovery after photobleaching (FRAP) of GFP-CLCa (Figure 2F). A relatively long baseline of two minutes was acquired to make sure that only stationary structures would be included in the analysis. We determined that in stable shaft structures GFP-CLCa recovered relatively fast (tau: 13.0 min) to 75.8 ± 10% in 20 minutes (Figure 2G, H), indicating a high level of clathrin exchange at these structures. In contrast to the high turnover of stationary structures in the shaft, the EZ showed relatively low levels of turnover (tau: 36.2 min) and total recovery (38.2 ± 5.2% after 20 minutes) (Figure 2G, H), suggesting little exchange of clathrin at the EZ. Taken together, these live-cell imaging experiments show that clathrin-coated

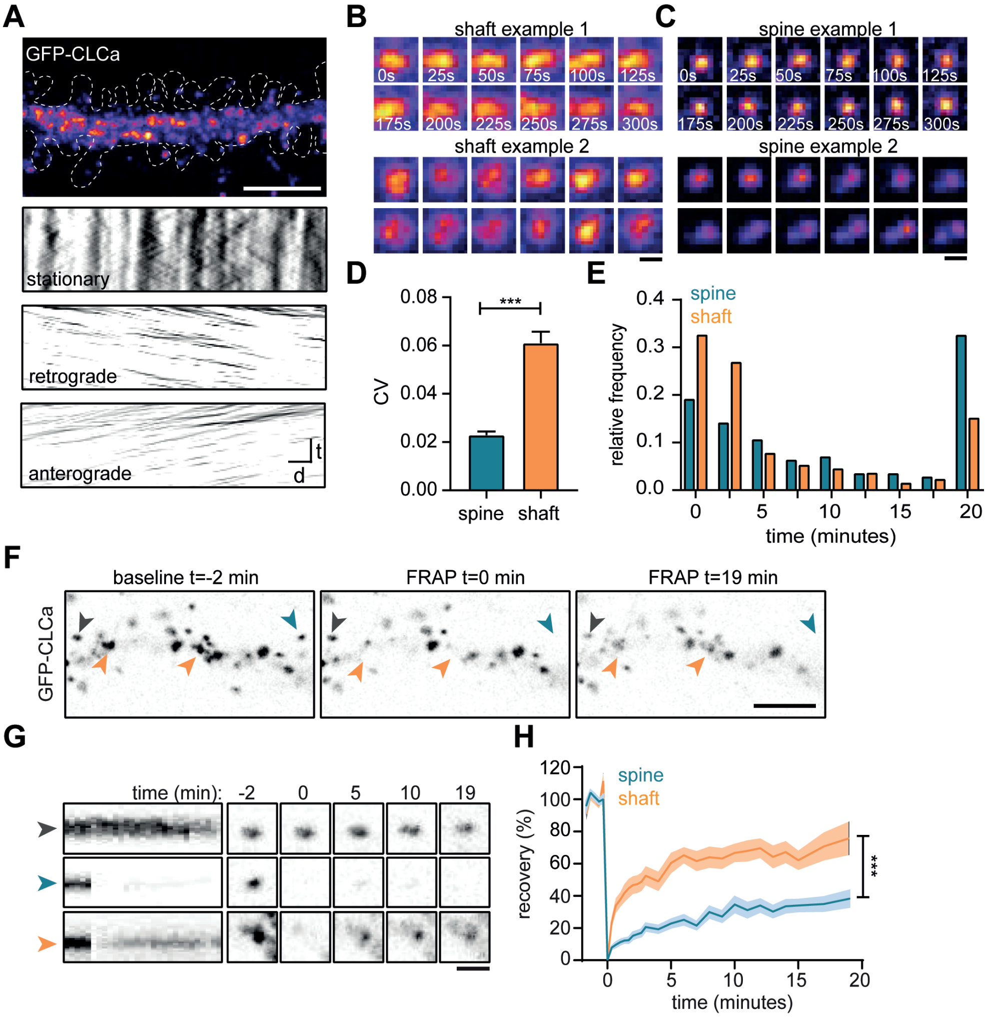

Figure 2. The EZ is dynamically distinct from shaft clathrin-coated structures. (A) Representative dendrite expressing GFP-CLCa, scale bar: 5 µm, and kymographs of clathrin-coated structures in the dendritic shaft only, separated in stationary (upper panel), retrograde (middle panel) and anterograde (lower panel) particles. Scale: time t, on the y-axis is 5 minutes, and distance d on x-axis is 20 µm. (B) Two examples of intensity fluctuations in stationary dendritic shaft structures. Scale bar: 1 µm. (C) Two examples of intensity fluctuations in spine structures. Scale bar: 1 µm. (D) Fluctuations in intensity plotted as the coefficient of variance (CV) between shaft and spine (spine: n = 48, shaft: n = 49, $p < 0.001$). Data represented at mean ± SEM. (E) Histogram of the lifetime of clathrin-coated structures in shaft and spine (spine: n = 171, shaft n = 769), data represented as fraction. (F) Example images of GFP-CLCa before (left panel), directly after FRAP (middle panel) and recovery (right panel), scale bar: 5 µm. Grey arrow indicates control, unbleached region, blue indicated bleached EZ, orange indicates bleached stationary dendritic shaft structures. (G) Kymograph and example images of the structures indicated in F. Kymograph shows 22-minute acquisition, scale bar: 1 µm. (H) Percentage of recovery in shaft (orange, n = 14) and spine (blue, n= 30).

structures in the dendritic shaft are morphologically and dynamically highly diverse, and that the EZ in dendritic spines contains a stable accumulation of clathrin that is very similar from spine to spine, thereby differentiating itself from all other clathrin-coated structures.

Nanoscale organization of the endocytic zone in dendritic spines

To further resolve the spatial organization of the EZ, we next used single-molecule localization microscopy (SMLM). Homer1c-mCherry and GFP-CLCa were co-transfected as before and labelled with primary and secondary antibodies to perform two-color dSTORM imaging and reconstruct high-density localization maps of the distribution of clathrin molecules within the EZ and relative to the PSD (Figure 3A). We used DBScan to define clusters of Homer1c molecules, outlining the PSD and the associated clathrin clusters, marking the EZ (Figure 3B). We found that the centroid of the EZ was generally located within 100 nm from the border of the PSD (Figure 3C) with an average border-to-centroid distance from PSD to EZ of 10.6 ± 7.8 nm, confirming that the EZ is closely linked to the PSD and well within a distance that can be linked by scaffold proteins (Lu et al., 2007). On average the area of the EZ was 35.0 ± 2.0 x10^3 nm^2 (Figure 3E), and 224.6 ± 10.4 nm in length and 146.5 ± 5.2 nm in width (Figure 3D). Moreover, the dimensions (length and width) of individual structures were positively correlated ($R^2 = 0.58$). Interestingly, we often found that PSDs were associated with multiple clathrin structures, similar as to what we observed with gSTED imaging (Figure 1B, D). We noted that two distinct populations could be observed based on morphological characteristics anddistinguished between the primary and secondary clathrin structure based on size. The largest was classified as the primary structure and we found that this structure most likely corresponds to the EZ, as these were also the most closely linked to the PSD (Supplement Figure 2A, B). The secondary, smaller structures were between 50 and 100 nm in diameter (Supplement Figure 2C), similar to the reported size of endocytic vesicles (Kirchhausen and Harrison, 1981; Pearse and Crowther, 1987). These smaller structures also appeared more circular and further away from the PSD (Supplement figure 2B, D), further suggesting that these smaller secondary structures are endocytic vesicles that perhaps budded off from the edge of the EZ.

Endocytic proteins are differentially retained at perisynaptic sites

Apart from clathrin, only a few other endocytic components have been suggested to be part of the EZ. Among these proteins are synaptotagmin-3 (Awasthi et al., 2018), PICK1 (Maria Fiuza et al., 2017) and CPG2 (Cottrell et al., 2004). Moreover, the presence of dynamin2 and AP2 at the site of clathrin-coated pits in spines suggest that these proteins could also be part of the EZ (Rácz et al., 2004). However, it remains unknown whether these and other endocytic proteins are stably accumulated at the EZ, or whether these are perhaps transiently recruited only during endocytic events. To begin to address this, we first determined the localization of 12 well-known endocytic proteins using confocal microscopy and live-cell imaging. Among these proteins are the well-known F-BAR and N-BAR proteins like FCHO1, syndapin-1 (Sdp1), syndapin- 2 (Sdp2) and amphiphysin (Amph), β2-adaptin, a subunit of the membrane proteins AP2, scission protein dynamin2 (Dyn2) and other adaptor proteins like Eps15, PICALM, intersectin-1 long (Itsn1L) and epsin-2 (Epsn2). In

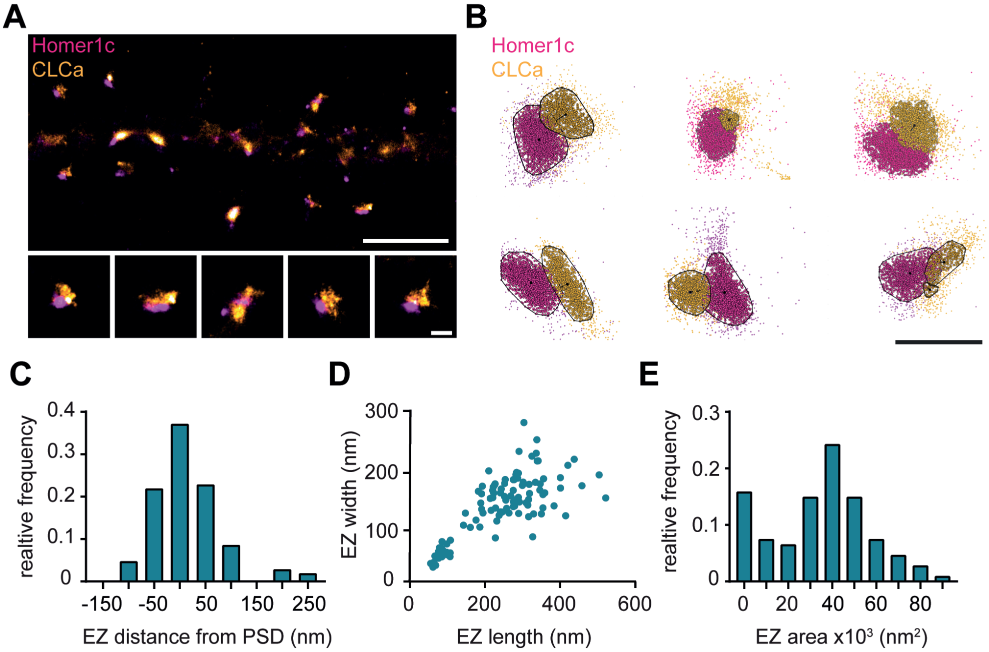

Figure 3. Nanoscale organization of the endocytic zone. (A) SMLM image of dendrite expressing Homer1c-mCherry and GFP-CLCa labelled with CF568 and A647 respectively and zooms of individual EZs. Scale bar upper panel: 2 µm, zooms: 250 nm. (B) Individual molecules of Homer1c (magenta) and CLCa (orange) are outlined using DBScan. Black dot and line indicate center of the EZ (dot) and distance to the border of the PSD (line). Scale bar: 500 nm. (C) Histogram of the border (Homer1c) to center (CLCa) distance in nm. (D) Scatterplot of the FWTM length (nm) and FWTM width (nm) of the EZ. (E) Histogram of the area of the EZ plotted as x103 nm^2. (C-E) n = 107.

addition, we included HIP1R and CPG2 that can couple the endocytic machinery to the actin cytoskeleton (Chen and Brodsky, 2005; Engqvist-Goldstein et al., 2001; Loebrich et al., 2016; Wilbur et al., 2008). We found that most of these proteins localized at perisynaptic sites in a punctate manner, similar to clathrin (Figure 4B). Sdp1, Sdp2 and Amph showed a more diffuse signal within the spine and dendritic shaft. For Amph, clear puncta associated with the PSD could be detected occasionally, however Sdp1 and Sdp2 did not seem to be enriched in distinct puncta and were not further analyzed. In this experiment we found that 66.8 ± 6.9% of PSDs was associated with GFP-CLCa (Figure 4A, C). We found that the fraction of PSDs associated with HIP1R, β2-adaptin, Dyn2, CPG2, Eps15, and Itsn1L was similar to the percentage of clathrin-associated PSDs. In contrast, PICALM, Epsn2, Amph and FCHO1 were less frequently found in association with the PSD (Figure 4B, C).Thus, HIP1R, β2-adaptin, Dyn2, CPG2, Eps15 and Itsn1L appear associated with the PSD and could be intrinsic components of the EZ. To validate that the localization of the stable proteins was not the result of overexpression, we endogenously tagged Eps15, Itsn1 and Dyn2 using the CRISPR/Cas9 based approach (Willems et al., 2020). We attempted to generate a KI for multiple AP2 subunits, but were not able to get a proper KI. We found similar distribution and perisynaptic localization of these

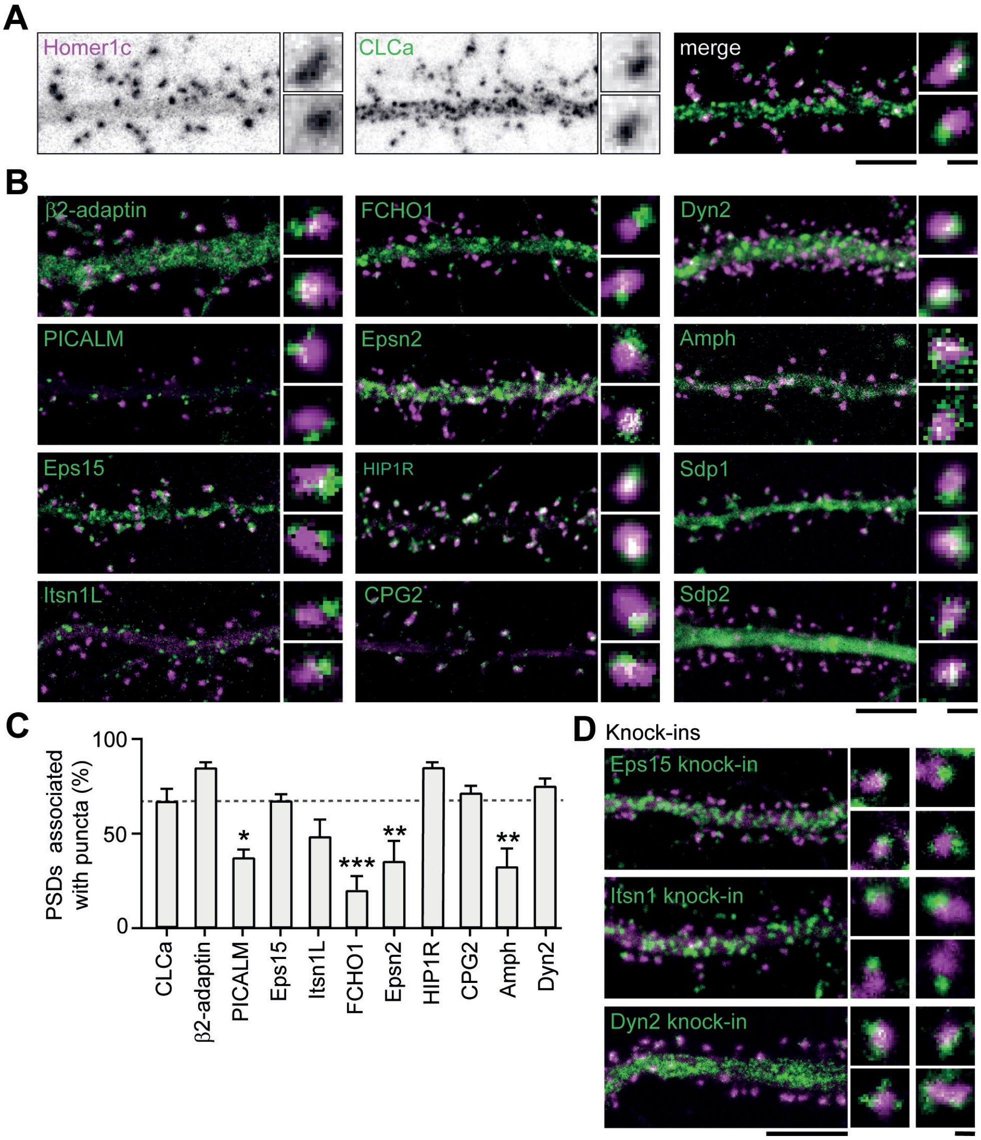
A
Homer1c
CLCa
merge
B
β2-adaptin
FCHO1
Dyn2
PICALM
Epsn2
Amph
Eps15
HIP1R
Sdp1
Itsn1L
CPG2
Sdp2
C
PSDs associated with puncta (%)
100
50
0
CLCa
β2-adaptin
PICALM
Eps15
Itsn1L
FCHO1
Epsn2
HIP1R
CPG2
Amph
Dyn2
*
***
**
**
D
Knock-ins
Eps15 knock-in
Itsn1 knock-in
Dyn2 knock-in

Figure 4. Endocytic accessory proteins localize to the perisynapse. (A) Example images of dendrites expressing Homer1c-mCherry and GFP-CLCa visualized as black and white images (left, middle panel), and merge (right panel). (B) Example images of neurons co-expressing tagged endocytic proteins relative to Homer1c. (A-B) Scale bars: 5 μm, zoom dimensions: 1 μm. (C) Percentage of synapses associated with endocytic proteins, represented as mean ± SEM. Relative to Homer1c-CLCa association ($n = 8$), PICALM-mCherry ($n = 6$, $p < 0.05$), FCHO1-mCherry ($n = 6$, $p < 0.001$), Epsn2-mCherry ($n = 9$, $p < 0.01$) and Amph-mCherry ($n = 6$, $p < 0.01$) were significantly less often associated with the PSD, while β2-adaptin- GFP ($n = 6$), GFP-Eps15 ($n = 5$), GFP-Itsn1L ($n = 5$), HIP1R-GFP ($n = 9$), GFP-CPG2 ($n = 5$), Dyn2-GFP ($n = 5$) were not different from GFP-CLCa. (D) Example images of neurons expressing Homer1c-ALFA labelled with Cy3 (magenta) and endogenously GFP-tagged endocytic proteins using KI (green). Scale bar: 5 μm, zoom: 500 nm. (E) Data represented as mean ± SEM.

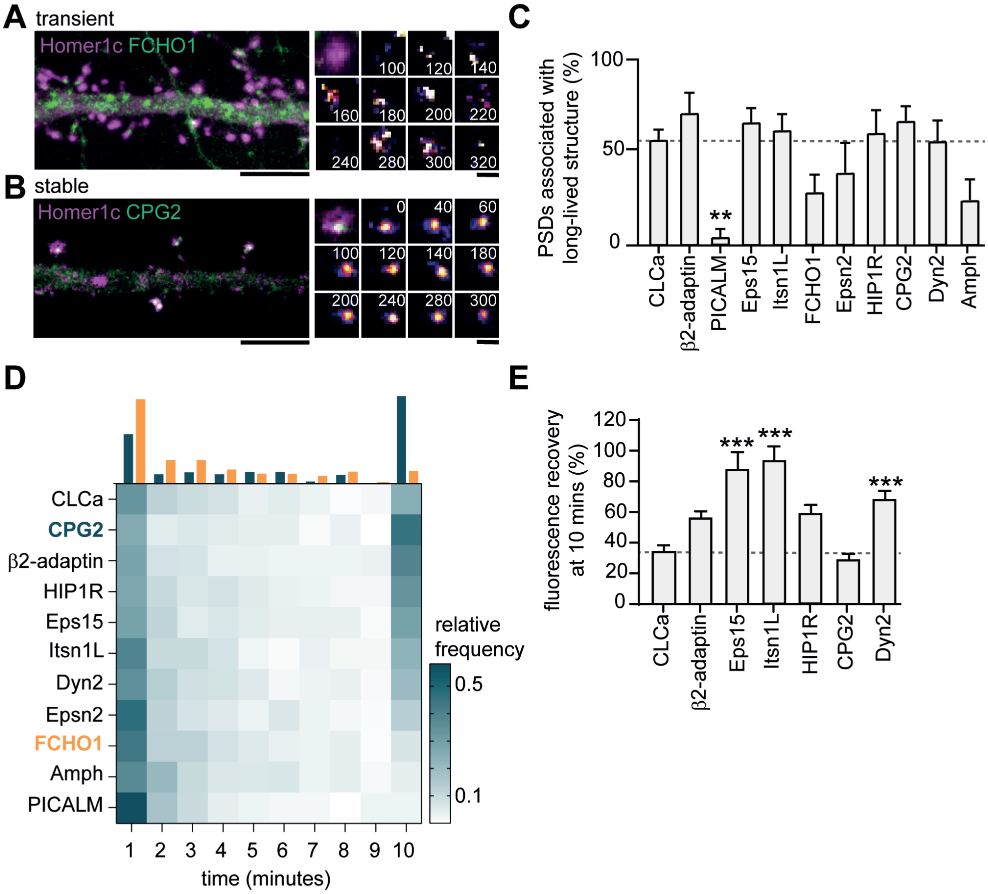

Figure 5. Endocytic proteins are differentially associated with the PSD. (A) Example image of FCHO1 (green) that is transiently associated with Homer1c (magenta). Zooms show temporal recruitment of FCHO1. Scale bar: 5 µm, zoom: 500 nm. (B) Example image of CPG2 that is stably associated with Homer1c. Zooms show temporal dynamics of CPG2. Scale bar: 5 µm, zoom: 500 nm. (C) Percentage of synapses that contain at least one stable structure (persisting for >9 minutes). Only PICALM-mCherry (n = 5, $p < 0.01$) was significantly less often stably associated with the PSD compared to GFP-CLCa (N = 6). β2-adaptin-GFP (N = 6), GFP-Eps15 (N = 6), GFP-Itsn1L (N = 6), FCHO1-mCherry (N = 5), Epsn2-mCherry (N = 5), HIP1R-GFP (N = 6), GFP-CPG2 (N = 8), Amph-mCherry (N = 5), Dyn2-GFP (N = 7), were not different from GFP-CLCa. (D) Heatmap visualizing the frequency distribution of the lifetime of endocytic proteins associated with the PSD. The histogram on top is an example of FCHO1 (orange) that is mostly short-lived, and CPG2 (blue) that is mostly stable, plotted as relative frequency. (E) Summary graph of the recovery 10 minutes after FRAP for GFP-Eps15 (n = 23 , $p < 0.001$), GFP-Itsn1L (n = 20, $p < 0.001$), HIP1R-GFP (n = 44, $p < 0.01$), Dyn2-GFP (n = 51, $p < 0.001$) had significantly higher turnover compared to GFP-CLCa (n = 32). GFP-CPG2 (n = 22) and β2-adaptin GFP (n = 13) were not different compared to GFP-CLCa. Data plotted as mean ± SEM.

proteins compared to overexpression (Figure 4D, Supplement Figure 3A). Similarly, endogenous labelling using antibodies showed that Eps15, Itsn1 and Dyn2 are indeed located at the perisynapse (Supplement Figure 3B). Next, to test whether these endocytic proteins were stably associated with the PSD we performed time-lapse experiments on neurons co-expressing Homer1c and a fluorophore-tagged endocytic protein. Neurons were imaged for 10 minutes at 20-second time intervals. We found very distinct behaviors in the dynamics of endocytic proteins. While some proteins only transiently occurred at perisynaptic sites (e.g., FCHO1; Figure 5A), other proteins appeared stable over the entire duration of the acquisition (e.g., CPG2; Figure 5B). Consistent with our previous observations in fixed neurons (Figure 4C), the percentage of PSDs associated with a clear endocytic protein structure for the entire duration of the acquisition was high for HIP1R, β2-adaptin, Dyn2, CPG2, Eps15 and Itsn1L, and much lower for PICALM, FCHO1, Epsn2 and Amph (Figure 5C). From these live-cell acquisitions we determined the lifetime of events where these proteins were enriched at perisynaptic sites. Interestingly, when plotted as histograms, a clear bimodal distribution of lifetimes was observed (Figure 5D). Endocytic proteins accumulated either briefly (<3 min) or appeared persistent (>9 minutes) at perisynaptic sites (Figure 5D). These data also indicated that HIP1R, β2-adaptin, Dyn2, CPG2, Eps15 and Itsn1L are stable components that are generally long-lived (Figure 5D). In contrast, the average lifetimes of FCHO1 (2.74 ± 1.7 min), PICALM (1.73 ± 0.2 min), Epsn2 (3.00. ± 0.2 min), and Amph (2.73 ± 1.7 min) at perisynaptic sites were significantly lower compared to the average lifetime of CLCa. Notably, the lifetime of these short-lived events is comparable to the duration of endocytic events (~2 minutes), suggesting that these proteins are transiently recruited upon the induction of endocytosis. To determine the turnover of the long-lived endocytic proteins at perisynaptic sites we performed FRAP experiments. Except for CPG2, all endocytic proteins showed considerably higher turnover than clathrin (percentage of recovery after 10 minutes CPG2: 29.4 ± 3.7%, HIP1R: 59.2 ± 5.2%, β2-adaptin: 56.7 ± 3.8%, Eps15: 88.1 ± 3.8, Itsn1L: 93.9 ± 8.7) (Figure 5E, Supplement Figure 4A-F). Taken together, these experiments reveal that apart from clathrin, HIP1R, β2-adaptin, Dyn2, CPG2, Eps15, and Itsn1L are also integral components of the perisynaptic EZ, while PICALM, FCHO1, Epsn2 and Amph only appear transiently at perisynaptic sites, perhaps to initiate or facilitate endocytosis.

Endocytic proteins have distinct spatial organization relative to the clathrin coat at the EZ

The presence of multiple endocytic adaptor proteins and their stable retention at perisynaptic sites suggests that these proteins might be an integral part of the EZ. First, we applied two-color gSTED on Halo-CLCa co-transfected with the stably retained endocytic proteins fused to GFP and stained for endogenous Homer1b/c to localize the PSD. We indeed found that Eps15, Itsn1L, Dyn2, β2-adaptin and HIP1R all colocalize with clathrin next to the PSD (Supplement Figure 5A-C). Next, to dissect the spatial organization of endocytic proteins relative to the clathrin structure at the EZ we used two-color SMLM. Halo-CLCa was co-transfected with a GFP-tagged endocytic protein to efficiently label and acquire high-density localization maps in two channels. Strikingly, we found that β2-adaptin, Eps15, and Itsn1L were often distributed in smaller patches around and sometimes within the EZ marked by CLCa (Figure 6A-C). HIP1R showed a more homogenous distribution and often colocalized with the EZ entirely and even surrounding the EZ (Figure 6D). Dyn2 showed an overall more homogenous distribution, similar to HIP1R (Figure 6E).

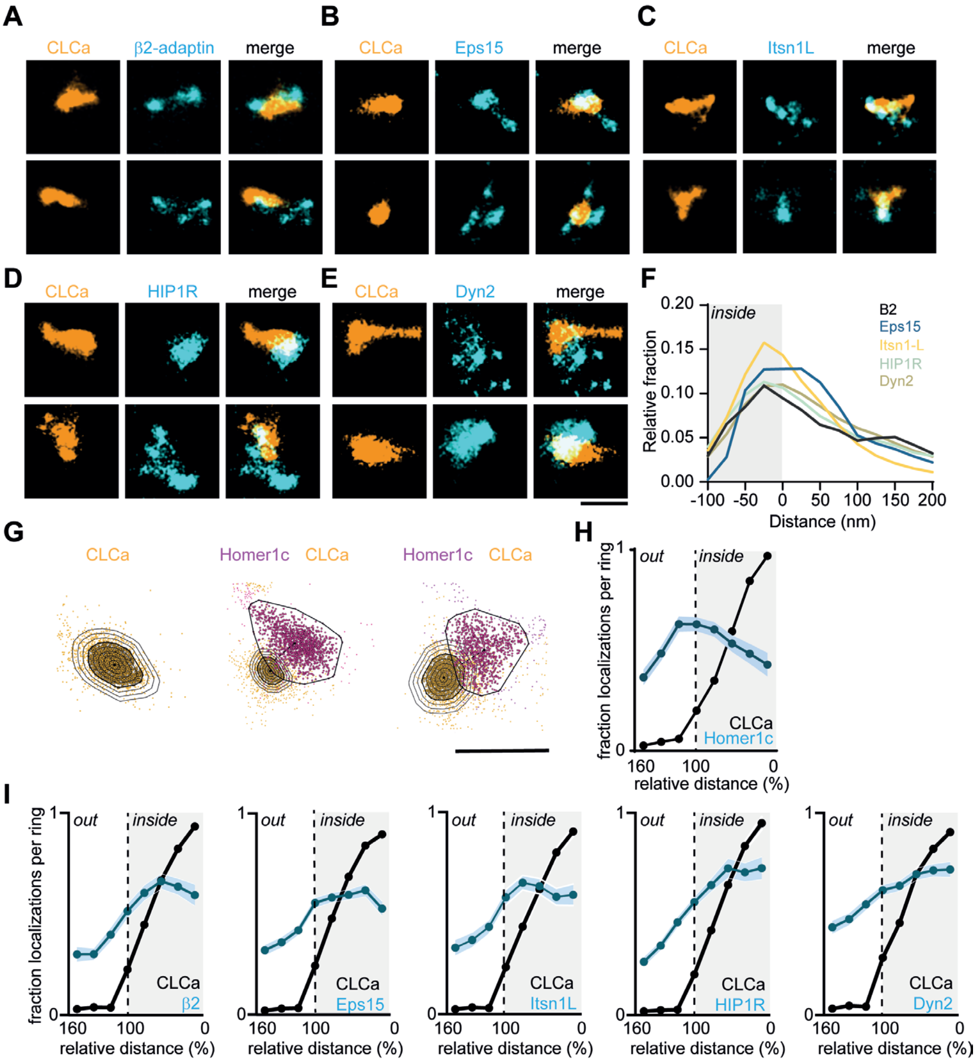

Figure 6. Endocytic proteins have distinct spatial organization relative to the clathrin structure marking the EZ (A-E) High resolution example images of Halo-CLCa labelled with JF647 (orange) co-expressed with endocytic proteins fused to GFP labelled with CF568 (cyan). Scale bar: 500 nm. (F) Histogram visualizing the relative frequency of the distance of individual localizations relative to the border of CLCa. (G) Example plots of CLCa with rings based on the size of the structure (left panel), and example plots of individual CLCa and Homer1c localization. Scale bar: 500 nm. (F) Fraction of localizations per ring. Dotted line depicts the border of CLCa (Homer1c n = 65, CLCa n = 66). (I) Fraction of localizations per ring. Dotted line depicts the border of CLCa. β2-adaptin (n = 87), GFP-Eps15 (n = 126), GFP-Itsn1L (n = 58), GFP-HIP1R (n = 72), GFP-Dyn2 (n = 82).

However, we also found examples where Dyn2 localized in small clusters at the edge of the EZ. To analyze these distributions quantitatively, we manually selected regions around clathrin structures in dendritic spines for further analysis. We then used

DBScan to determine the outline of the EZ marked by CLCa. We first mapped the absolute distance of localizations to the border of the EZ averaged over a population of EZs and found that all the endocytic proteins analyzed here peaked within 25 nm from the edge of the clathrin structure (Figure 6F). However, since individual EZs can vary in size, we next mapped the density of endocytic proteins in rings that were set in size relative to the clathrin structure. For each EZ, we defined 8 incremental rings that were scaled with proportion to the outline of the EZ and binned the density of localizations within each of these rings (Figure 6G).

As expected, when plotting the relative fraction of Halo-CLCa localization within the rings, we found that the density of clathrin molecules was highest in the center (0-20% ring), gradually decreased towards the outer ring (80-100%) and dropped to close to zero in the rings surrounding the EZ (100-160% rings) . In contrast, when we plotted the relative density of Homer1c localizations relative to CLCa, we found a clear separation of these distributions (Figure 6H), further validating the analysis. When analyzing the endocytic adaptor proteins relative to the EZ, we again found that the relative density of Eps15, β2-adaptin and Itsn1L peaked within the EZ, but close to the edge of the EZ (Figure 6I). The profiles of HIP1R and Dyn2 localizations (Figure 6G) showed less clear peaks, indicating a more homogenous distribution of these proteins within the EZ.

Interactions with the PSD, but not with the membrane or actin cytoskeleton are required for the perisynaptic localization of the EZ

The differential dynamics and nanoscale organization of endocytic proteins at perisynaptic clathrin structures suggests that the EZ is a highly organized structure where several endocytic proteins are assembled. The mechanisms that retain the EZ at this particular position, however, are not fully understood. The EZ is coupled to the PSD via Shank-Homer-Dyn3 interactions (Lu et al., 2007; Petrini et al., 2009; Scheefhals et al., 2019). In addition, we now identified several new EZ components that can couple to the plasma membrane, e.g., via AP2, or the actin cytoskeleton, e.g., via CPG2 and HIP1R (Loebrich et al., 2016; Saffarian et al., 2009), suggesting that these modes of interaction could also contribute to the positioning of the EZ. To test this, we interfered with several of these connections. First, we tested whether Shank knockdown (KD), which we showed previously uncouples the EZ from the PSD (Scheefhals et al., 2019), also leads to the loss of these newly identified EZ components (Figure 7A, B). Indeed, we found that Shank-KD did not only reduce the number of clathrin-positive PSDs as found before (0.5 ± 0.1 relative to control), but also reduced the association of the PSD with other endocytic proteins (Figure 7B). We found that Shank-KD significantly reduced Homer1c-Eps15 (0.63 ± 0.1), Homer1c-Itsn1L (0.6 ± 0.1) and Homer1c-β2-adaptin (0.55 ± 0.1) coupling compared to control (Figure 7B). Interestingly, HIP1R (0.89 ± 0.04), Dyn2 (0.91 ± 0.1) and CPG2 (0.86 ± 0.1) were not uncoupled from the PSD (Figure 7B). Together, these findings show that PSD-EZ coupling via Shank proteins is necessary for the integrity of the EZ. Next, to test if other mechanisms contribute to EZ maintenance we tested whether alterations in actin dynamics, membrane binding capacity or depleting specific EZ components would lead to a reduction of EZs (Figure 7C). Interestingly, we found that disrupting the integrity of the actin cytoskeleton did not result in a clear reduction of the PSD-EZ association. The actin depolymerization drug Latrunculin B

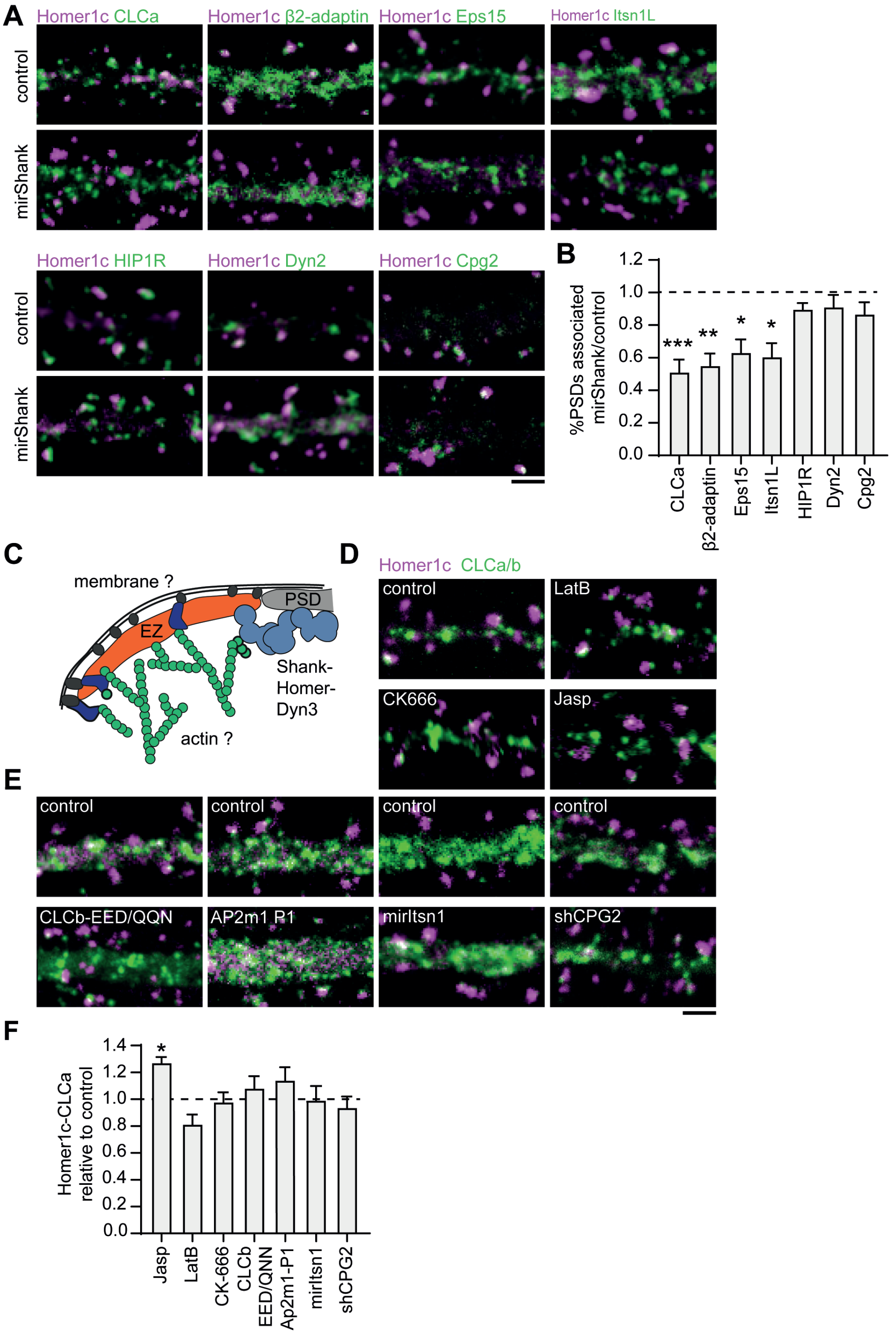
A
Homer1c CLCa
Homer1c β2-adaptin
Homer1c Eps15
Homer1c Itsn1L
control
mirShank
Homer1c HIP1R
Homer1c Dyn2
Homer1c Cpg2
control
mirShank
B
%PSDs associated mirShank/control
1.2
1.0
0.8
0.6
0.4
0.2
0.0
***
**
*
*
CLCa
β2-adaptin
Eps15
Itsn1L
HIP1R
Dyn2
Cpg2
C
membrane ?
PSD
EZ
Shank-Homer-Dyn3
actin ?
D
Homer1c CLCa/b
control
LatB
CK666
Jasp
E
control
control
control
control
CLCb-EED/QQN
AP2m1 P1
mirItsn1
shCPG2
F
Homer1c-CLCa relative to control
1.4
1.2
1.0
0.8
0.6
0.4
0.2
0.0
*
Jasp
LatB
CK-666
CLCb EED/QNN
Ap2m1-P1
mirItsn1
shCPG2

Figure 7. Interactions with the PSD, but not with the membrane or actin cytoskeleton are required for positioning of the EZ. (A) Example images of dendrites expressing Homer1c-ALFA and endocytic proteins fused to GFP co-expressed with control or mirShank-mCherry construct. Scale bar: 2 μm. (B) Fraction of PSDs associated with an EZ after Shank-KD relative to control plotted as mean ± SEM. GFP-CLCa (N = 8, $p < 0.001$), β2-adaptin (N = 10, $p < 0.01$), Eps15 (N = 12, $p < 0.05$), Itsn1L (N = 10, $p < 0.05$), HIP1R (N = 11 $p > 0.05$), Dyn2 (N = 12, $p > 0.05$), CPG2 (N = 13, $p > 0.05$). (C) Illustration of possible mechanisms that could maintain the EZ adjacent to the PSD. (D) Example images of dendrites co-expressing Homer1c-ALFA and GFP-CLCa in dendrites treated with LatB, CK666 or Jasp. Scale bar: 2 μm. (E) Example images of dendrites expressing control constructs, CLCb-EED/QQN (left panel) and AP2m1-P1 (middle panel), or Itsn1 KD construct (mirItsn1; right panel). Scale bar: 2 μm. (F) Fraction of EZ-associated PSDs relative to control, plotted as mean ± SEM. Jasp (N = 4), LatB (N = 8), CK666 (N = 12), CLCb-EED/QQN (N = 7), AP2m1-P1 (N = 5), mirItsn1 (N = 11), shCPG2 (N = 8).

slightly decreased the PSD-EZ association (0.81 ± 0.1), but this was not statistically significant. The Arp2/3 inhibitor CK-666 (0.98 ± 0.1) also did not significantly alter PSD-EZ association (Figure 7D, F), suggesting that disrupting actin dynamics does not disrupt positioning of the EZ. Jasplakinolide, an F-actin stabilizing drug, resulted in significantly more PSD-EZ association compared to control (1.27 ± 0.04, $p<0.05$). To test specific EZ-actin interactions, we assessed whether the binding of clathrin to HIP1R is necessary for EZ maintenance. Overexpression of a clathrin-light chain mutant that is unable to bind HIP1R (GFP-CLCb-EED/QQN) (Chen and Brodsky, 2005; Poupon et al., 2008), did not affect the localization of the EZ (Figure 7E, F), further indicating that coupling to the actin cytoskeleton is not a primary mechanism for maintaining the EZ. The third mechanism that could allow the perisynaptic localization of the EZ involves interactions with the plasma membrane. To address this, we overexpressed an AP2m1 mutant that is unable to interact with PIP2 and was shown to hamper receptor internalization (Raman et al., 2014), but we found no change in the fraction of EZ-positive PSDs (1.1 ± 0.1), suggesting that coupling to the membrane via AP2 does not affect EZ maintenance (Figure 7E, F). Lastly, we checked if removing specific stable endocytic components would affect EZ positioning. Itsn1L is multi-domain scaffold protein that interacts with several endocytic proteins to orchestrate endocytosis and could thus have a central role as scaffold in the EZ. However, Itsn1L knockdown did not alter the fraction of EZ-positive PSDs (Figure 7E, F). In addition, CPG2 that couples the actin cytoskeleton to the membrane, does not actively maintain the EZ near the PSD, as shCPG2 did not affect PSD-EZ coupling (Figure 7E). Altogether, based on these mechanistic experiments, we conclude that the EZ is assembled from a distinct set of endocytic proteins and is maintained and positioned primarily by interactions with the PSD.

DISCUSSION

Neurons contain a large variety of clathrin structures. A particularly important clathrin structure in neurons, the postsynaptic EZ, is characterized by the stable accumulation of clathrin associated with the PSD. Localized endocytosis of synaptic receptors at the EZ is essential for the maintenance and activity-directed changes in the composition of the synaptic membrane. However, despite vigorous investigation of clathrin-coated structures in various cell types, the molecular composition and organization of the EZ has remained largely elusive. Here, we present evidence that the EZ is a highly unique clathrin structure. We found that a defined arsenal of endocytic proteins is differentially retained at the EZ and highly organized at the nanoscale level with respect to the clathrin assembly.

Our data show that the postsynaptic EZ can be clearly distinguished from other dendritic clathrin assemblies. Clathrin-coated structures in the dendritic shaft form a highly heterogenous population, including small, fast-moving particles, as well as larger stationary structures. This heterogeneity in clathrin-coated structures resembles those found in other cell types, where a large variety of clathrin assemblies have been identified. Often, small clathrin structures represent transient endocytic pits or intracellular vesicles while the large patches are stable, membrane-attached structures (Grove et al., 2014; Leyton-Puig et al., 2017; Saffarian et al., 2009). Indeed, we found that the small structures in the dendritic shaft are often transient or moving, most likely representing endocytic pits or cargo vesicles, while the larger assemblies are stationary but still undergo dynamic exchange of clathrin. The function of these larger dendritic patches remains unknown. In dendritic spines, we found that the morphological characteristics of the EZ are highly similar from spine to spine, with much less variation in size and dynamics than observed for clathrin structures in the dendritic shaft. Moreover, the EZ appeared as a long-lived and fluorescently stable clathrin structure with relatively low exchange of clathrin, in line with previous studies (Blanpied et al., 2002; Petrini et al., 2009; Rosendale et al., 2017; Scheefhals et al., 2019). Together, these results indicate that based on the morphological and dynamic behavior of clathrin, the EZ can be distinguished from other clathrin assemblies found in the dendritic shaft.

The EZ has been postulated as a primary site for endocytosis of synaptic membrane proteins to sort these components in the local recycling machinery and effectively retain these at the synaptic membrane (Blanpied et al., 2002). Indeed, several studies have unequivocally demonstrated that in the absence of the EZ endocytic trafficking of glutamate receptors is severely affected, leading to the net loss of membrane-expressed receptors and consequential deregulated glutamatergic signaling (Cortese et al., 2016; Lu et al., 2007; Nakano-Kobayashi et al., 2014; Petrini et al., 2009; Scheefhals et al., 2019). Formation of endocytic vesicles containing synaptic receptors has also been directly visualized in close proximity to the PSD (Rosendale et al., 2017), supporting the endocytic capacity of the EZ. In our live-cell experiments, we occasionally observed the formation of a secondary clathrin structure from the larger, primary clathrin structure. Further, super-resolution imaging allowed us to resolve the EZ at higher resolution and we often found that PSDs were associated with more than one clathrin structure, with the secondary, smaller structure often having a size similar to those described for clathrin-coated vesicles (Kirchhausen et al., 2014). These secondary structures were often 200 - 250 nm away from the border of the PSD, i.e., more distant from the PSD than the EZ that was closely (within ~30 nm) associated. Similarly, EM studies showed that clathrin coated vesicles bud off from the membrane preferentially at 100 - 600 nm from the PSD (Rácz et al., 2004). Thus, although we did not reach sufficient resolution to unequivocally resolve clathrin-coated pits associated with the EZ, our data is consistent with the idea that endocytic pits bud off at the edge of the EZ.

Importantly, our findings significantly expand on the notion that the EZ is a perisynaptic site of endocytosis by identifying several key endocytic proteins that reside at the EZ. Based on our live-cell imaging, quantitative super-resolution imaging and mechanistic studies we conclude that the early-phase endocytic proteins β2-adaptin, Eps15, and Itsn1L are stable EZ residents that localize preferentially at the edge of the EZ, which is surprisingly similar to findings on flat clathrin lattices in non-neuronal cells (Sochacki et al., 2017). The accumulation of the AP-2 complex and its binding partner Eps15 at the periphery of the EZ likely contributes to the efficient capture of cargoes, i.e., synaptic membrane proteins, and their local uptake via endocytosis. Itsn1 is a multi-domain scaffold protein that coordinates different aspects of endocytosis(Pechstein et al., 2010) (Hussain et al., 2001)(Evergren et al., 2007). Thus, Itsn1 could have a central organizing role at the EZ. Consistently, we recently reported that Itsn1 knockdown abrogates mGluR-mediated AMPAR trafficking (van Gelder et al., 2020). The results presented here show that Itsn1 knockdown does not alter the location or overall morphology of the EZ indicating that while Itsn1 has likely an important role in coordinating endocytosis at the EZ, Itsn1 does not seem to directly support the maintenance of this clathrin structure. Furthermore, removing Shank proteins, which has been shown before to uncouple clathrin from the PSD (Lu et al., 2007; Scheefhals et al., 2019), specifically uncoupled these early-phase proteins, further indicating that these proteins are indeed stable residents and coupled to the EZ, likely to facilitate endocytosis .

The later-phase proteins HIP1R,Dyn2 and CPG2 were also stably associated with the EZ, but this association seemed independent of PSD-EZ coupling via Shank. Interestingly, both Dyn2 and HIP1R were more widely distributed, indicating that they are not directly coupled to the EZ . Indeed, in most cases, we found that the distribution of Dyn2 at the EZ was diffuse, but the clear differential localization patterns between different EZs may indicate that dynamin relocates to the EZ upon endocytosis as has been suggested before (Rosendale et al., 2017). Unfortunately for CPG2, we were not able to obtain sufficient localization maps and cannot draw any conclusions about the nanoscale organization of CPG2 at the EZ. Although, previous studies have shown that CPG2 couples the actin cytoskeleton to the membrane upon endocytosis. Together with our findings that HIP1R and Dyn2 are more homogenously distributed relative to the EZ suggests that these later-phase proteins are not directly coupled to the EZ under basal conditions but rather reside in close proximity, likely via other interactions.

Finally, we found that PICALM, FCHO1, Epsn2 and Amph were associated with the EZ to a much lesser extent and appeared only transiently at perisynaptic sites. Interestingly, Amph, Epsn2 and FCHO1 are BAR proteins, and preferentially bind curved membranes. Thus, perhaps these proteins are only transiently recruited to the EZ upon induction of endocytosis and the associated increase in membrane curvature. Taken together, we show that different classes of endocytic proteins, both early- and late-phase proteins are associated with the EZ.

We and other have consistently found that the EZ is coupled to the PSD via a Shank-Homer1c-Dynamin-3 interaction (Lu et al., 2007; Scheefhals et al., 2019). However, it is likely that other mechanisms are in place to stabilize the EZ, but how this association is established remains unknown. Several proteins that we identified here as EZ components could couple the EZ to the membrane. For example, the AP2 complex directly binds clathrin heavy chain and phosphatidylinositol 4,5-biphosphate (PIP2) (Beacham et al., 2019; Gaidarov and Keen, 1999; Kadlecova et al., 2017;

Mettlen et al., 2018; Owen et al., 2000; Shih et al., 1995; Traub et al., 1999) and we found that β2-adaptin was stably associated with the EZ. However, we found that expression of a dominant-negative form of AP2mu2 that cannot bind PIP2 did not abrogate EZ positioning. Another candidate, PICALM can also simultaneously bind PIP2 and clathrin (Ford et al., 2001), but we found that PICALM was only transiently associated with the PSD and is thus unlikely to form a stable intermediate between the EZ and the membrane. Thus, either these components are not involved in coupling the EZ to the membrane or membrane anchoring is not a prerequisite for EZ positioning.

The actin cytoskeleton is prominent in dendritic spines and supports many aspects of synaptic transmission and plasticity. Several endocytic proteins that we found enriched at the EZ could link the EZ to the actin cytoskeleton. For instance, both HIP1R and CPG2 are actin-binding proteins, and were enriched in dendritic spines and associated with the PSD. Notably, these results are consistent with previous studies that found that CPG2 localizes to the EZ (Cottrell et al., 2004; Nedivi, 1999) and is essential for glutamate receptor trafficking (Loebrich et al., 2016; Loebrich et al., 2013). In fact, of all the proteins that we analyzed in the current study, CPG2 was the most persistently associated with the PSD, and appeared to be even more stable than clathrin, suggesting that CPG2 could have a function in stabilizing and maintaining the EZ. However, removing CPG2 did not disrupt PSD-EZ positioning, suggesting that the potential role of CPG2 in stabilizing the EZ is perhaps secondary to PSD-EZ coupling via Shank, or that CPG2 is not involved in EZ maintenance.HIP1R directly binds clathrin light-chain and physically links clathrin to F-actin (Chen and Brodsky, 2005; Engqvist-Goldstein et al., 2001; Wilbur et al., 2008), to promote actin polymerization at endocytic sites. Moreover, HIP1R has been shown before to be involved in maintaining stable clathrin structures (Grove et al., 2014; Saffarian et al., 2009). Surprisingly however, neither disruption of the actin cytoskeleton with pharmacological compounds, nor interfering with the HIP1R-CLC association significantly disrupted the localization or integrity of the EZ. Thus, the actin cytoskeleton is most likely involved in facilitating endocytosis at the EZ, but does not seem to have a prime structural role in maintaining or positioning the EZ.

Taken all together, we found that the EZ is a highly organized clathrin structure where endocytic proteins are differentially retained and stabilized. This distinct organization likely facilitates the efficient capture and endocytosis of synaptic membrane proteins close to the PSD. These findings motivate further investigation into the molecular composition, the mechanisms that control the recruitment and activation of individual EZ components and the coupling of the EZ to the intracellular endosomal system. Elucidating these aspects of the EZ will contribute to a better understanding of this subcellular structure in neurons that is so critical for the maintenance and activity-dependent modulation of neuronal synapses.

MATERIALS AND METHODS

Animals

All animal experiments were performed in compliance with the guidelines for the welfare of experimental animals issued by the Government of the Netherlands (Wet op de Dierproeven, 1996) and European regulations (Guideline 86/609/EEC). All animal experiments were approved by the Dutch Animal Experiments Review

Committee (Dier Experimenten Commissie; DEC), performed in line with the institutional guidelines of Utrecht University.

Primary hippocampal cultures and transfection

Hippocampal cultures were prepared from brain of embryonic day 18 (E18) Wistar rats (both genders) as described before (Scheefhals et al., 2019). Dissociated hippocampal neurons were plated on coverslips coated with poly-L-lysine (37.5 µg/ml, Sigma-Aldrich) and laminin (1.25 µg/ml, Roche Diagnostics) at a density of 100,000 neurons per well of a 12-well plate. Cultures were allowed to settle in Neurobasal medium (NB) supplemented with 2% B27 (GIBCO), 0.5 mM glutamine (GIBCO), 15.6 mM glutamate (Sigma-Aldrich), and 1% penicillin/streptomycin at 37ºC in 5% CO2. After 24 hours halve of the NB medium was refreshed with BrainPhys medium (BP) supplemented with SM1 supplement (Stemcell Technologies) and 1% penicillin/streptomycin, and kept at 37ºC in 5% CO_2. Refreshment were done weekly replacing halve of the medium with fresh supplemented BP medium. At DIV11-16 neurons were transfected with indicated constructs using Lipofectamine 2000 (Invitrogen). Before transfection 300 µl conditioned medium was transferred to a new culture plate. For each well, 1.8 µg DNA was mixed with 3.3 µl Lipofectamine 2000 in 200 µl BP, incubated for 30 minutes at room temperature and added to the neurons. After 1 to 1.5 hours, neurons were briefly washed with BP and transferred to the new culture plate with conditioned medium with an additional 500 µl supplemented BP and kept at 37ºC in 5% CO_2 for 4-6 days. For the knock-ins, transfection was done at DIV 3 using the Homer-ALFA CamKII construct together with 200 ng of the indicated knock-ins.

DNA constructs

GFP-CLCa was a gift from Dr. Blanpied. Halo-CLCa was obtained by replacing the GFP from GFP-CLCa for a Halo-tag using Gibson assembly (NEBbuilder HiFi DNA assembly cloning kit). GFP-CPG2 was obtained by replacing the HA-tag in the HA-CPG2 construct (gift from Dr. Nedivi) using Gibson assembly. GFP-Intersectin Long (Addgene plasmid # 47395) and GFP-CLCb (EED/QQN) (Addgene plasmid # 47422) were a gift from Peter McPherson. FCHO1-pmCherryC1 (Addgene plasmid # 27690), Epsin2-pmCherryC1 (Addgene plasmid # 27673), CALM-pmCherryN1 (Addgene plasmid # 27691), Amph1-pmCherryN1 (Addgene plasmid # 27692) and Syndapin2-pmCherryC1 (Addgene plasmid # 27681) were a gift from Christien Merrifield. FKBP-β2-adaptin-GFP (Wood et al., 2017) and HIP1R-GFP-FKBP (Addgene plasmid # 100752) were a gift from Stephen Royle. The AP2m1 patch 1 mutant (AP2m1-P1-HA) was a gift from Dr. Richmond (Raman et al., 2014). GFP-Syndapin I was a gift from Dr. Robinson. GFP-Eps15 was a gift from Dr. Van Bergen en Henegouwen. shCPG2 was a gift from Dr. Nedivi. The following constructs have been described before: Homer1c-mCherry, Homer1c-GFP, Dynamin2-GFP (Scheefhals et al., 2019), pSM155-mirItsn-GFP (van Gelder et al., 2020) , GFP-CLCa knock-in construct (Willems et al., 2020). Homer-ALFA construct was cloned by replacing mCherry for the ALFA tag (Gotzke et al., 2019) and the CMV promotor was replaced by a CamKII promotor using Gibson assembly. The knock-ins for GFP-Eps15, GFP-Itsn1 and GFP-Dyn2 were cloned as described previously Willems et al., 2020).

Immunocytochemistry and HaloTag labelling

Neurons were fixed between DIV16-21 with 4% paraformaldehyde (PFA, EM grade) diluted in PEM buffer (80 mM PIPES, 5 mM EGTA, 2 mM MgCl2, pH 7.4) for 10 minutes at 37ºC and washed three times with PBS supplemented with 100 mM glycine (PBS-gly). Then, neurons were permeabilized and blocked with 10% normal goat serum (NGS) and 0.01% Triton X-100 (TX) in PBS-gly for 30 minutes at 37ºC. For STED imaging, GFP and mCherry containing constructs were enhanced with corresponding polyclonal anti-GFP (1:2000, MBL) and anti-mCherry (1:1000, Clonetech) antibodies diluted in PBS-gly supplemented with 5% NGS and 0.01% TX, for an overnight at 4ºC. The next day, coverslips were washed three times in PBS-gly and anti-GFP was further labelled with ATTO647N (1:500, Sigma) and anti-mCherry was labelled with CF568 (1:500, Sigma) for 2 hours at room temperature (RT), washed and mounted in Mowiol (Sigma). For SMLM on Homer-mCherry and GFP-CLCa the same procedure was used as described above, but anti-GFP was labelled with Alexa-647-conjugated secondary antibodies (Life Technologies). After two hours, coverslips were washed three times and kept in PBS until further use. For SMLM on Halo-CLCa combined with various endocytic proteins fused to GFP, we first performed live-labeling with Halo-JF646 (1:1000, Promega) for 15 minutes at RT. To label endocytic proteins, GFP was labelled with a monoclonal anti-GFP (1:1000, Thermo Fisher) and labelled with a corresponding CF568-conjugated secondary antibody (1:500, Sigma). Although the localization density obtained for Halo-CLCa labelled with JF646 was lower compared to GFP-CLCa labelled with primary and secondary antibodies, no difference in CLCa morphology was observed (Supplement Figure 2). For the KIs, the GFP tagged proteins were enhanced using polyclonal GFP antibody described above and further labelled with Alexa488 (1:500, Life Technologies). During the incubation of the secondary antibody Homer1c-ALFA was labelled with Cy3-conjugated FluoTAG X4 anti-ALFA (1:500 Fluotag X4, Nanotag). For the endogenous antibody labelling the same protocol was used as described above, using anti-Eps15 (1:400,Cell Technologies), anti-Itsn1 (1:400) and anti-Dyn2 (1:400, BD transduction), further labelled with Alexa488. Homer1c-ALFA was labelled with Cy3 during the secondary antibody labelling.

Confocal imaging

Confocal images were acquired with a Zeiss LSM 700 confocal laser-scanning microscope using a Plan-Apochromat 63x NA 1.40 oil objective. Images consist of a z-stack of 5-9 planes at 0.37-μm interval, and maximum intensity projections were generated in Fiji (Schindelin et al., 2012) for analysis and display.

STED imaging

Gated STED (gSTED) images were taken with the Leica TCS SP83x microscope using a HC PL APO 100x/NA 1.4 oil immersion STED WHITE objective. The 488 nm pulsed white laser (80 MHz) was used to excite Alexa-488, 561 nm to excite CF568, and the 647 nm to excite JF646 and ATTO647N labeled proteins. JF646 and ATTO647N were depleted with the 775-nm pulsed depletion laser, and for depleting CF568 the 660-nm pulsed depletion laser was used. The internal Leica HyD hybrid detector was set at time gate between 0.3 and 6 ns. Images were taken with a pixel size lower than 40 nm, and Z-stacks were acquired. Maximum intensity projections were generated in Fiji (Schindelin et al., 2012) for analysis and display.

Live-cell imaging

Live-cell imaging was performed on a spinning disk confocal system (CSU-X1-A1; Yokogawa) mounted on a Nikon Eclipse Ti microscope (Nikon) with Plan Apo VC 100x 1.40 NA with excitation from Cobolt Calyspso (491 nm), and Jive (561 nm) lasers, and emission filters (Chroma). The microscope was equipped with a motorized XYZ stage (ASI; MS-2000), Perfect Focus System (Nikon), Evolve 512 EM-CCD camera (Photometrics), and was controlled by MetaMorph 7.7.6 software (Molecular Devices). Neurons were maintained in a closed incubation chamber (Tokai hit: INUBG2E-ZILCS) at 37ºC in extracellular imaging buffer. For high frequency live-cell imaging (Figure 2A-D) images of GFP-CLCa were taken every 5 seconds for 5 minutes. For long-term live-cell imaging of Homer1c and CLCa (Figure 2E), images were taken every 30 seconds for 20 minutes. Lastly, imaging Homer1c and endocytic proteins fused to either mCherry or GFP was done taking images every 20 seconds for 10 minutes. In all the above-mentioned experiments Z-stacks of 5-9 planes were acquired, with varying step sizes per neuron. Also Homer1c-mCherry was only imaged in the first and last frame. Maximum intensity images were analyzed in Fiji, by manually drawing same-size ROIs around individual puncta associated with PSDs. To measure lifetimes of clathrin and endocytic proteins we used the TrackMate plugin (Tinevez et al., 2017).

Fluorescence recovery after photobleaching

FRAP experiments were performed on the spinning disk confocal system as described above, using the ILas2 system (Roche scientific). A baseline of 2 minutes with a 20-second interval was taken, followed by photobleaching of individual puncta with a targeted laser. The recovery of fluorescence of GFP-CLCa was imaged for 3 minutes with 20-second interval, followed by 12 minutes with 60-second interval, and 4 minutes with 120-second interval, resulting in a total recovery time of 19 minutes. For imaging the recovery of the endocytic proteins an acquisition of 10 minutes was taken (2-minute baseline, 3 minutes with 20-second interval and 7 minutes with 60-second interval). For acquiring FRAP images, a single Z-plane was taken. Fluorescence intensity was measured in Fiji, by manually drawing same-size ROIs around puncta. For analysis, acquisitions were corrected for drift. For each ROI, the mean intensity was measured for every time point and corrected for background and bleaching. Normalized intensities were plotted over time. Individual curves were fitted with a single-exponential function $I = A(1 - \exp(-Kt))$ to estimate the mobile fraction (A) and time constant tau.

Single-molecule localization microscopy and analysis

dSTORM data was acquired on the Nanoimager S from ONI (Oxford Nanoimaging Ltd.), equipped with a 100x, 1.4NA oil immersion objective, an XYZ closed-loop piezo stage, and four laser lines: 405-nm, 471-nm, 561-nm and 640-nm. Fluorescence emission was detected using a sCMOS camera (ORCA Flash 4, Hamamatsu). Stacks of 10,000 images were acquired at 20 Hz in TIRF mode. Samples were imaged in PBS containing 10 - 50 mM MEA, 5% w/v glucose, 700 µg/ml glucose oxidase, and 40 µg/ml catalase. Data was processed in NimOS software from ONI. Before

each imaging session, a bead sample calibration was performed to align the two channels, achieving a channel mapping precision smaller than 8 nm. Images were rendered in ONI software and loaded into Fiji. Here, ROIs of 1 x 1 µm were drawn around individual EZ. The ROI sets were imported in Matlab (2018b) for analysis.
First, tracking was performed on the localization data to merge localizations that were detected in more than two consecutive frames as described in (Willems et al., 2020) . Next, a localization cutoff of 15 nm was taken to further analyze the localization data. A DBScan was performed to define the borders of Homer1c and CLCa in figure 4, using an epsilon of 0.2 and minimum number of localizations of 100. For figure 6, an epsilon of 0.35 and minimum number of localizations of 50 was used. For figure 6, rings were applied to reveal the relative distribution of endocytic proteins to the EZ. Rings were calculated as a percentage of the 100% polyshape given by the DBScan. Inwards, 5 rings were created: 0-20, 20-40, 40-60, 60-80, 80-100; and outwards 3 rings were created: 100-120, 120-140, 140-160. Then, the number of localizations for each of the endocytic proteins were calculated per ring. The fraction of these localizations per EZ, were plotted against the fraction of the area of the ring and normalized to 1.

Pharmacology

For all the following experiments DIV15-16 neurons were used. Latruncalin B (20 µM, Bioconnect), Jasplakinolide (20µM, Tocris) and CK-666 (400µM, Sigma), were incubated in preheated extracellular imaging buffer for 30 minutes at 37ºC. After incubation, the neurons were immediately fixed as described before.

Quantification of EZ-associated synapses

For the Shank knockdown experiments DIV14 neurons were transfected with pSM155-mCherry or pSM155-mirShank-mCherry together with Homer1c-ALFA and indicated construct. Homer1c-ALFA was labelled with JF646-conjugated FluoTAG X4 anti-ALFA (1:500 Fluotag X4, Nanotag). In the experiments manipulating actin dynamics, Homer-mCherry and GFP-CLCa expressing neurons were incubated with Latrunculin B (20 µM, Bioconnect), CK666 (400 µM, Tocris) or Jasplakinolide (20 µM, Tocris) in E4 for 30 minutes at 37˚C and fixed immediately after. As a control E4 containing DMSO was used. GFP-CLCa or GFP-CLCb-EED/QQN were co-expressed with Homer1c-mCherry. pSM155-mirItsn and shCPG2 were co-expressed with Homer1c-mCherry and Halo-CLCa labelled with JF646. AP2m1-WT or AP2m1-P1-HA was co-expressed with Homer1c-mCherry and GFP-CLCa. To quantify the fraction of synapses with an associated EZ or puncta of endocytic protein, circular regions with a fixed diameter (0.69-0.89 µm) were centered on the Homer1c signal to outline synaptic regions. These regions were then transferred to the GFP-CLC or tagged endocytic protein channel. A synapse was classified positive if the endocytic protein cluster overlapped partially or completely with the circular region. The fraction of positive synapses was calculated per cell and averaged per condition over the total population of neurons. Data plotted is normalized to the average of the control.

Statistical analysis

Statistical significance was tested using a student's t-test when comparing two groups. When comparing multiple groups statistical significance was tested using a one-way ANOVA followed by a Tukey or Dunnett’s multiple comparison post-hoc test. All the statistical tests with a p-value below 0.05 were considered significant. In all figures, significance is indicated as follows: $p < 0.05$ is indicated by *, $p < 0.01$ by **, and $p < 0.001$ by ***. Analysis was performed on neurons originating from at least two individual batches of hippocampal neurons. Number of neurons used for analysis is indicated as N, number of spines or clathrin-coated structures is represented as n.

ACKNOWLEGDEMENTS

We would like to thank all members of the MacGillavry lab for support and discussions. This work was supported by the Netherlands Organization of Scientific Research (NWO-ALWOP. 191 to H.D.M).

AUTHOR CONTRIBUTION

Conceptualization, Methodology, Validation & Format Analysis: L.A.E.C and H.D.M; Investigation: L.A.E.C., M.W., A.M.L.S; Resources: H.D.M; Writing and Editing: L.A.E.C and H.D.M; Supervision: H.D.M; Funding: H.D.M

DECLARATION OF INTEREST

Authors declare no competing interests.

REFERENCES

Anggono, V., Koc-Schmitz, Y., Widagdo, J., Kormann, J., Quan, A., Chen, C.M., Robinson, P.J., Choi, S.Y., Linden, D.J., Plomann, M., et al. (2013). PICK1 interacts with PACSIN to regulate AMPA receptor internalization and cerebellar long-term depression. Proc Natl Acad Sci U S A 110, 13976-13981.

Awasthi, A., Ramachandran, B., Ahmed, S., Benito, E., Shinoda, Y., Nitzan, N., Heukamp, A., Rannio, S., Martens, H., Barth, J., et al. (2018). Synaptotagmin-3 drives AMPA receptor endocytosis, depression of synapse strength, and forgetting. Science, eaav1483-eaav1483.

Beacham, G.M., Partlow, E.A., and Hollopeter, G. (2019). Conformational regulation of AP1 and AP2 clathrin adaptor complexes. Traffic 20, 741-751.

Blanpied, T.A., Scott, D.B., and Ehlers, M.D. (2002). Dynamics and regulation of clathrin coats at specialized endocytic zones of dendrites and spines. Neuron 36, 435-449.

Chen, C.Y., and Brodsky, F.M. (2005). Huntingtin-interacting protein 1 (Hip1) and Hip1-related protein (Hip1R) bind the conserved sequence of clathrin light chains and thereby influence clathrin assembly in vitro and actin distribution in vivo. J Biol Chem 280, 6109-6117.

Cocucci, E., Aguet, F., Boulant, S., and Kirchhausen, T. (2012). The first five seconds in the life of a clathrin-coated pit. Cell 150, 495-507.

Cortese, G.P., Zhu, M., Williams, D., Heath, S., and Waites, C.L. (2016). Parkin Deficiency Reduces Hippocampal Glutamatergic Neurotransmission by Impairing AMPA Receptor Endocytosis. J Neurosci 36, 12243-12258.

Cottrell, J.R., Borok, E., Horvath, T.L., and Nedivi, E. (2004). CPG2: A brain- and synapse-specific protein that regulates the endocytosis of glutamate receptors. Neuron 44, 677-690.

Engqvist-Goldstein, A.E., Warren, R.A., Kessels, M.M., Keen, J.H., Heuser, J., and Drubin, D.G. (2001). The actin-binding protein Hip1R associates with clathrin during early stages of endocytosis and promotes clathrin assembly in vitro. The Journal of cell biology 154, 1209-1223.

Evergren, E., Gad, H., Walther, K., Sundborger, A., Tomilin, N., and Shupliakov, O. (2007). Intersectin is a negative regulator of dynamin recruitment to the synaptic endocytic zone in the central synapse. J Neurosci 27, 379-390.

Ford, M.G., Pearse, B.M., Higgins, M.K., Vallis, Y., Owen, D.J., Gibson, A., Hopkins, C.R., Evans, P.R., and McMahon, H.T. (2001). Simultaneous binding of PtdIns(4,5)P2 and clathrin by AP180 in the nucleation of clathrin lattices on membranes. Science 291, 1051-1055.

Gaidarov, I., and Keen, J.H. (1999). Phosphoinositide-AP-2 interactions required for targeting to plasma membrane clathrin-coated pits. J Cell Biol 146, 755-764.

Gotzke, H., Kilisch, M., Martinez-Carranza, M., Sograte-Idrissi, S., Rajavel, A., Schlichthaerle, T., Engels, N., Jungmann, R., Stenmark, P., Opazo, F., et al. (2019). The ALFA-tag is a highly versatile tool for nanobody-based bioscience applications. Nat Commun 10, 4403.

Grove, J., Metcalf, D.J., Knight, A.E., Wavre-Shapton, S.T., Sun, T., Protonotarios, E.D., Griffin, L.D., Lippincott-Schwartz, J., and Marsh, M. (2014). Flat clathrin lattices: stable features of the plasma membrane. Molecular biology of the cell 25, 3581-3594.

Henne, W.M., Boucrot, E., Meinecke, M., Evergren, E., Vallis, Y., Mittal, R., and McMahon, H.T. (2010). FCHo proteins are nucleators of clathrin-mediated endocytosis. Science 328, 1281-1284.

Heuser, J. (1980). Three-dimensional visualization of coated vesicle formation in fibroblasts. J Cell Biol 84, 560-583.

Hussain, N.K., Jenna, S., Glogauer, M., Quinn, C.C., Wasiak, S., Guipponi, M., Antonarakis, S.E., Kay, B.K., Stossel, T.P., Lamarche-Vane, N., et al. (2001). Endocytic protein intersectin-l regulates actin assembly via Cdc42 and N-WASP. Nat Cell Biol 3, 927-932.

Kadlecova, Z., Spielman, S.J., Loerke, D., Mohanakrishnan, A., Reed, D.K., and Schmid, S.L. (2017). Regulation of clathrin-mediated endocytosis by hierarchical allosteric activation of AP2. J Cell Biol 216, 167-179.

Kaksonen, M., and Roux, A. (2018). Mechanisms of clathrin-mediated endocytosis. Nature Reviews Molecular Cell Biology 19, 313-326.

Kirchhausen, T., and Harrison, S.C. (1981). Protein organization in clathrin trimers. Cell 23, 755-761.

Kirchhausen, T., Owen, D., and Harrison, S.C. (2014). Molecular structure, function, and dynamics of clathrin-mediated membrane traffic. Cold Spring Harb Perspect Biol 6, a016725.

Leyton-Puig, D., Isogai, T., Argenzio, E., Van Den Broek, B., Klarenbeek, J., Janssen, H., Jalink, K., and Innocenti, M. (2017). Flat clathrin lattices are dynamic actin-controlled hubs for clathrin-mediated endocytosis and signalling of specific receptors. Nature Communications 8.

Loebrich, S., Benoit, M.R., Konopka, J.A., Cottrell, J.R., Gibson, J., and Nedivi, E. (2016). CPG2 recruits endophilin B2 to the cytoskeleton for activity-dependent endocytosis of synaptic glutamate receptors. Current Biology 26, 296-308.

Loebrich, S., Djukic, B., Tong, Z.J., Cottrell, J.R., Turrigiano, G.G., and Nedivi, E. (2013). Regulation of glutamate receptor internalization by the spine cytoskeleton is mediated by its PKA-dependent association with CPG2. Proceedings of the National Academy of Sciences of the United States of America 110, E4548-4556.

Lu, J., Helton, T.D., Blanpied, T.A., Rácz, B., Newpher, T.M., Weinberg, R.J., and Ehlers, M.D. (2007). Postsynaptic Positioning of Endocytic Zones and AMPA Receptor Cycling by Physical Coupling of Dynamin-3 to Homer. Neuron 55, 874-889.

Mangeol, P., Prevo, B., and Peterman, E.J. (2016). KymographClear and KymographDirect: two tools for the automated quantitative analysis of molecular and cellular dynamics using kymographs. Mol Biol Cell 27, 1948-1957.

Maria Fiuza, C.M.R.G.T.P.A.M.B.N.H., Marcio Baptista, I.M., and Jonathan, G.H. (2017). PICK1 regulates AMPA receptor endocytosis via direct interaction with AP2 a-appendage and dynamin. The Rockefeller University Press J Cell Biol.

McMahon, H.T., and Boucrot, E. (2011). Molecular mechanism and physiological functions of clathrin-mediated endocytosis. Nature Reviews Molecular Cell Biology 12, 517-533.

Mettlen, M., Chen, P.H., Srinivasan, S., Danuser, G., and Schmid, S.L. (2018). Regulation of Clathrin-Mediated Endocytosis. Annu Rev Biochem 87, 871-896.

Nakano-Kobayashi, A., Tai, Y., Nadif Kasri, N., and Van Aelst, L. (2014). The X-linked mental retardation protein OPHN1 interacts with Homer1b/c to control spine endocytic zone positioning and expression of synaptic potentiation. J Neurosci 34, 8665-8671.

Nedivi, E. (1999). Molecular analysis of developmental plasticity in neocortex. Journal of neurobiology 41, 135-147.

Owen, D.J., Vallis, Y.F., Pearse, H.T., McMahon, and Evans, P.R. (2000). Structure and function of the B2-adaptin appendage domain.

Park, M., Salgado, J.M., Ostroff, L., Helton, T.D., Robinson, C.G., Harris, K.M., and Ehlers, M.D. (2006). Plasticity-induced growth of dendritic spines by exocytic trafficking from recycling endosomes. Neuron 52, 817-830.

Pearse, B.M., and Crowther, R.A. (1987). Structure and assembly of coated vesicles. Annu

Rev Biophys Biophys Chem 16, 49-68.

Pechstein, A., Bacetic, J., Vahedi-Faridi, A., Gromova, K., Sundborger, A., Tomlin, N., Krainer, G., Vorontsova, O., Schafer, J.G., Owe, S.G., et al. (2010). Regulation of synaptic vesicle recycling by complex formation between intersectin 1 and the clathrin adaptor complex AP2. Proc Natl Acad Sci U S A 107, 4206-4211.

Petralia, R.S., Wang, Y.X., and Wenthold, R.J. (2003). Internalization at glutamatergic synapses during development. Eur J Neurosci 18, 3207-3217.

Petrini, E.M., Lu, J., Cognet, L., Lounis, B., Ehlers, M.D., and Choquet, D. (2009). Endocytic trafficking and recycling maintain a pool of mobile surface AMPA receptors required for synaptic potentiation. Neuron 63, 92-105.

Poupon, V., Girard, M., Legendre-Guillemin, V., Thomas, S., Bourbonniere, L., Philie, J., Bright, N.A., and McPherson, P.S. (2008). Clathrin light chains function in mannose phosphate receptor trafficking via regulation of actin assembly. Proceedings of the National Academy of Sciences of the United States of America 105, 168-173.

Rácz, B., Blanpied, T.A., Ehlers, M.D., and Weinberg, R.J. (2004). Lateral organization of endocytic machinery in dendritic spines. Nature Neuroscience 7, 917-918.

Raman, D., Sai, J., Hawkins, O., and Richmond, A. (2014). Adaptor protein2 (AP2) orchestrates CXCR2-mediated cell migration. Traffic 15, 451-469.

Reider, A., Barker, S.L., Mishra, S.K., Im, Y.J., Maldonado-Baez, L., Hurley, J.H., Traub, L.M., and Wendland, B. (2009). Syp1 is a conserved endocytic adaptor that contains domains involved in cargo selection and membrane tubulation. EMBO J 28, 3103-3116.

Rosendale, M., Julli, D., Choquet, D., and Perrais, D. (2017). Spatial and Temporal Regulation of Receptor Endocytosis in Neuronal Dendrites Revealed by Imaging of Single Vesicle Formation. Cell Reports 18, 1840-1847.

Saffarian, S., Cocucci, E., and Kirchhausen, T. (2009). Distinct Dynamics of Endocytic Clathrin-Coated Pits and Coated Plaques. PLoS Biology 7, e1000191-e1000191.

Sanan, D.A., and Anderson, R.G. (1991). Simultaneous visualization of LDL receptor distribution and clathrin lattices on membranes torn from the upper surface of cultured cells. J Histochem Cytochem 39, 1017-1024.

Scheefhals, N., Catsburg, L.A.E., Westerveld, M.L., Blanpied, T.A., Hoogenraad, C.C., and MacGillavry, H.D. (2019). Shank Proteins Couple the Endocytic Zone to the Postsynaptic Density to Control Trafficking and Signaling of Metabotropic Glutamate Receptor 5. Cell Rep 29, 258-269 e258.

Schindelin, J., Arganda-Carreras, I., Frise, E., Kaynig, V., Longair, M., Pietzsch, T., Preibisch, S., Rueden, C., Saalfeld, S., Schmid, B., et al. (2012). Fiji: an open-source platform for biological-image analysis. Nat Methods 9, 676-682.

Shih, W., Gallusser, A., and Kirchhausen, T. (1995). A clathrin-binding site in the hinge of the beta 2 chain of mammalian AP-2 complexes. J Biol Chem 270, 31083-31090.

Sochacki, K.A., Dickey, A.M., Strub, M.-P., and Taraska, J.W. (2017). Endocytic proteins are partitioned at the edge of the clathrin lattice in mammalian cells. Nature Cell Biology 19.

Tao-Cheng, J.H., Crocker, V.T., Winters, C.A., Azzam, R., Chludzinski, J., and Reese, T.S. (2011). Trafficking of AMPA receptors at plasma membranes of hippocampal neurons. J Neurosci 31, 4834-4843.

Taylor, M.J., Perrais, D., and Merrifield, C.J. (2011). A High Precision Survey of the Molecular Dynamics of Mammalian Clathrin-Mediated Endocytosis. 9.

Tinevez, J.Y., Perry, N., Schindelin, J., Hoopes, G.M., Reynolds, G.D., Laplantine, E., Bednarek, S.Y., Shorte, S.L., and Eliceiri, K.W. (2017). TrackMate: An open and extensible platform for single-particle tracking. Methods 115, 80-90.

Traub, L.M., Downs, M.A., Westrich, J.L., and Fremont, D.H. (1999). Crystal structure of the alpha appendage of AP-2 reveals a recruitment platform for clathrin-coat assembly. Proc Natl Acad Sci U S A 96, 8907-8912.

van Gelder, C.A., Penning, R., Veth, T., Catsburg, L.A., Hoogenraad, C.C., MacGillavry, H.D., and Altelaar, M. (2020). Temporal quantitative proteomics of mGluR-induced protein translation and phosphorylation in neurons. Mol Cell Proteomics.

Widagdo, J., Fang, H., Jang, S.E., and Anggono, V. (2016). PACSIN1 regulates the dynamics of AMPA receptor trafficking. Nature Publishing Group.

Wilbur, J.D., Chen, C.Y., Manalo, V., Hwang, P.K., Fletterick, R.J., and Brodsky, F.M. (2008). Actin binding by Hip1 (huntingtin-interacting protein 1) and Hip1R (Hip1-related protein) is regulated by clathrin light chain. J Biol Chem 283, 32870-32879.

Willems, J., de Jong, A.P.H., Scheefhals, N., Mertens, E., Catsburg, L.A.E., Poorthuis, R.B., de Winter, F., Verhaagen, J., Meye, F.J., and MacGillavry, H.D. (2020). ORANGE: A CRISPR/Cas9-based genome editing toolbox for epitope tagging of endogenous proteins in neurons. PLoS Biol 18, e3000665.

Wood, L.A., Larocque, G., Clarke, N.I., Sarkar, S., and Royle, S.J. (2017). New tools for hot-wiring clathrin-mediated endocytosis with temporal and spatial precision. The Journal of cell biology, jcb.201702188-jcb.201702188.

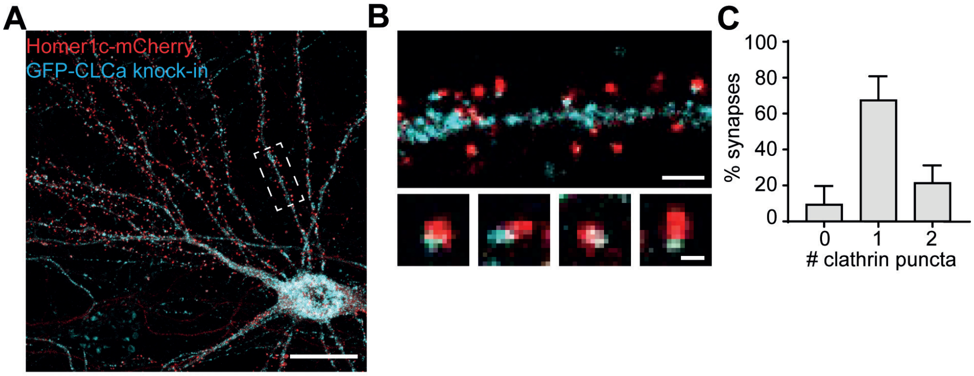
A
Homer1c-mCherry
GFP-CLCa knock-in
B
C
100
80
60
40
20
0
% synapses
0
1
2
# clathrin puncta

Supplementary Figure 1. Distribution of endogenously tagged CLCa in neurons. (A) Example image of neuron expressing Homer1c-mCherry and GFP-CLCa knock-in construct. Scale bar: 20 µm. (B) Example image of clathrin-coated structures in the dendrite (upper panel) and zooms of individual synapses associated with an EZ (lower panel). Scale bars: 2 µm, zooms: 500 nm. (C) Quantification of the average number of clathrin-coated structures per synapse, plotted as mean ± SEM (n = 6).

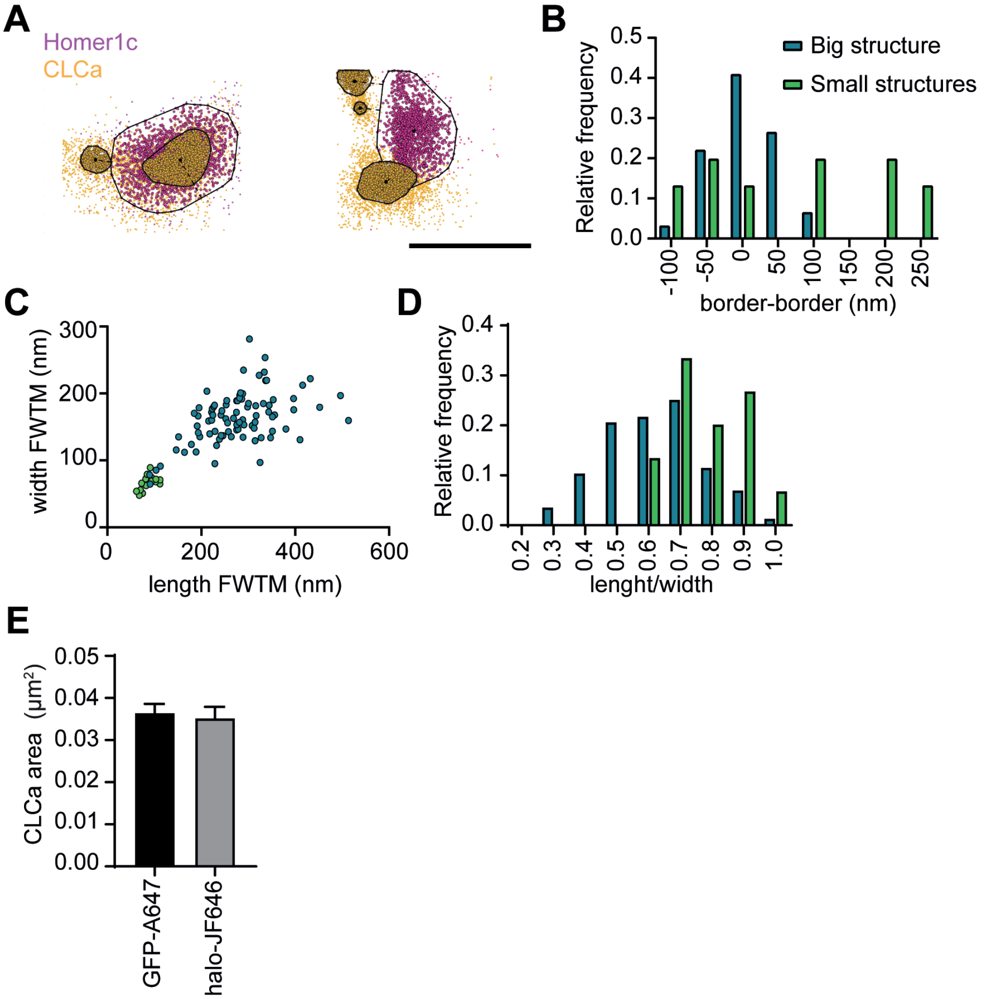

Supplementary Figure 2. SMLM reveals nanoscale scale architecture of PSD-associated CLCa structures. (A) Example plots visualizing the individual localizations obtained for Homer1c (magenta) and CLCa (orange). Two or more individual CLCa structures can be observed per PSD. Scale bar: 500 nm. (B-D) Data visualized in these plots is the same data represented in Figure 3, but here a distinction was made between PSDs containing one (blue) or two (green) CLCa structures is made. (B) Histogram of the distance from the border of the PSD to the border of CLCa structures. (C) Scatterplot showing the dimensions of larger (blue) CLCa structures, most likely representing the EZ, and smaller CLCa structures (green) (big structures: n = 92, small structures: n = 13). (D) Histogram showing circularity ratio of CLCa structures. (E) Comparison of the average area of CLCa puncta labelled with different strategies (GFP-CLCa labelled with monoclonal GFP and CF568, Halo-CLCa labelled with halo-JF646), plotted as mean ± SEM (GFP-CF568: n = 103, Halo-JF646: n = 50).

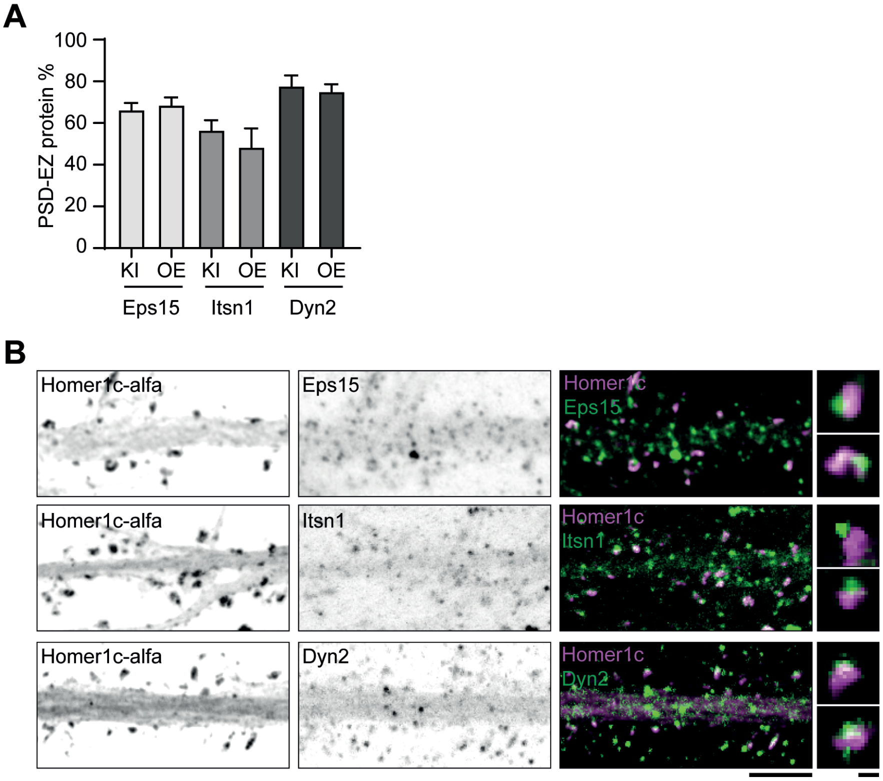

Supplementary Figure 3. Endogenously labeling of endocytic proteins in neurons. (A) Quantification of the average number of EZ proteins puncta per synapse after overexpression (OE) or knock-in (KI). OE data represented is a copy from the data shown in figure 4C. KI Eps15 (N = 8), KI Itsn1 (N = 9), KI Dyn2 (N = 7). Data is plotted as mean ± SEM. (B) Example images (confocal) of Homer1c-ALFA labelled with Cy3 and endogenous labelling of EZ proteins using antibodies. Scalebar: 5µm, zoom: 500 nm.

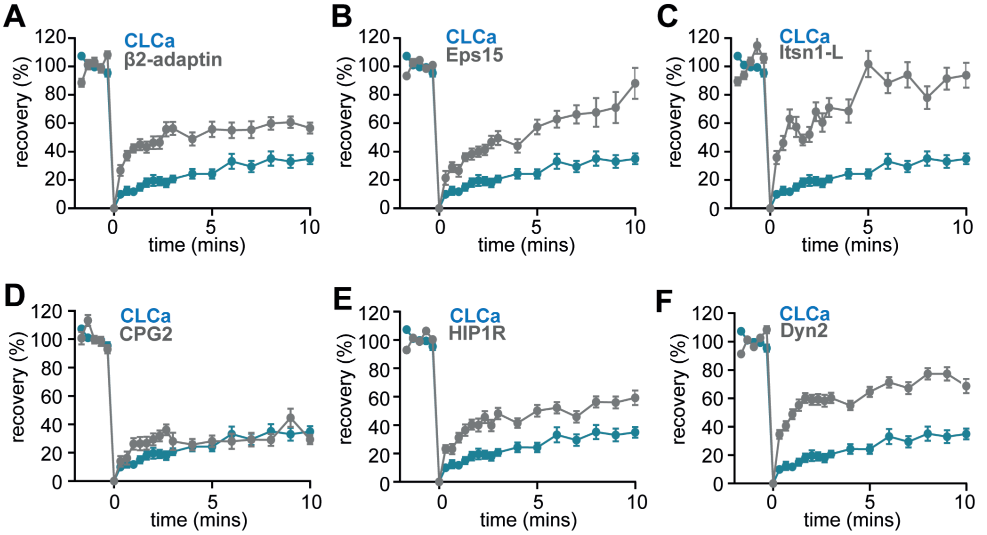

Supplementary Figure 4. FRAP curves of endocytic proteins compared to CLCa. (A-G) FRAP curves of endocytic proteins (grey) and CLCa (blue) after bleaching on t = 0 for (A) β2-adaptin (n = 13), (B) Eps15 (n = 23), (C) Itsn1L (n = 20), (D) CPG2 (n = 22), (E) HIP1R (n = 44) and (F) Dyn2 (n = 51). All graphs show the same CLCa (n = 32) data for comparison. All data is plotted as mean ± SEM.

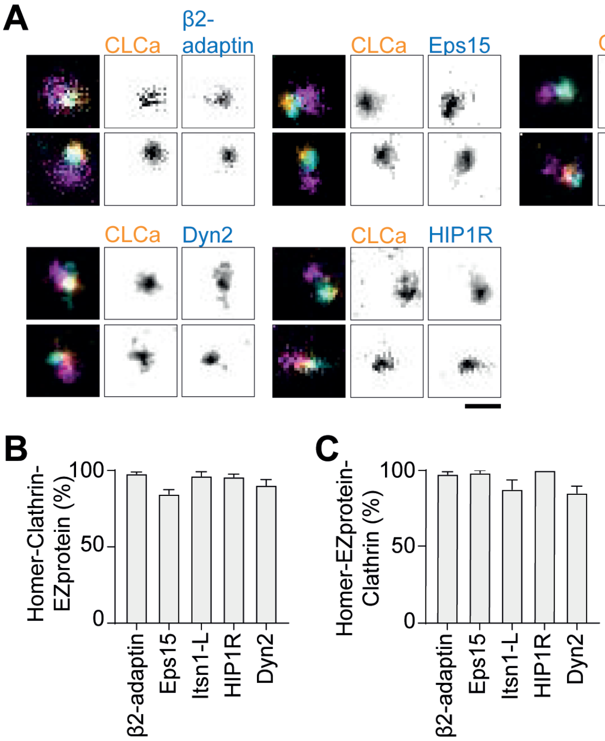

Supplementary Figure 5. Endocytic proteins colocalize with the EZ. (A) Examples of endogenous Homer1b/c (eHomer1b/c) labelled with anti-Homer1 antibody (magenta), combined with Halo-CLCa labelled with JF646 (orange) and co-expressed with endocytic proteins fused to GFP labelled with CF568 (cyan). eHomer1b/c was imaged using confocal, for CLCa and endocytic proteins gSTED was applied. Scale bar: 500 nm. (B) Percentage of eHomer1c-associated CLCa puncta overlapping with endocytic protein signal. (C) Percentage of eHomer1c-associated endocytic protein puncta overlapping with CLCa signal. Bar graphs show mean ± SEM, normalized to the average of the representative controls described in method section.

5

Activity-dependent alterations in the molecular organization of the postsynaptic endocytic zone

Lisa A.E. Catsburg, Harold D. MacGillavry

Department of Cell Biology, Neurobiology and Biophysics at the Faculty of Science of Utrecht University in Utrecht, the Netherlands

ABSTRACT

At excitatory synapses, the postsynaptic endocytic zone (EZ) regulates the local internalization of glutamate receptors and is vital for synaptic plasticity. Uncoupling of the EZ from the postsynaptic density (PSD) blocks receptor recycling and impairs the induction of long-term potentiation (LTP). However, while activity-dependent alterations in synaptic structure are well studied, whether the EZ undergoes reorganization in response to changes in synaptic activity remains unknown. Here, we found that in hippocampal neurons PSD-EZ coupling is correlated to spine morphology. Mature, mushroom spines more often contained a PSD associated with an EZ than immature thin spines, suggesting that PSD-EZ coupling is connected to maturation or activity history of individual synapses. Indeed, we found that chemical LTP (cLTP) induced long-lasting reorganization of the EZ. In contrast, long-term depression (LTD) induced by activation of group I mGluRs (mGluR-LTD) induced a rapid, transient increase in the number of clathrin-coated structures per PSD, while NMDA receptor-dependent cLTD (NMDA-LTD) did not. Interestingly, also chronic changes in network activity did not affect EZ organization. The mechanisms and functional implications underlying the structural reorganization of the EZ upon synaptic plasticity have yet to be determined, but we propose that activity-directed plasticity of the EZ tunes the endocytic capacity of individual synapses.

INTRODUCTION

At glutamatergic synapses, activity-dependent alterations in synaptic strength are accompanied by changes in size, shape and synaptic content (Matsuzaki et al., 2001; Meyer et al., 2014; Nusser et al., 1998). Long-term potentiation (LTP) induces rapid spine expansion followed by synaptic growth, while long-term depression (LTD) is associated with spine shrinkage (Straub and Sabatini, 2014). Apart from synaptic growth, LTP induces dramatic changes in molecular composition of the postsynaptic density (PSD) to facilitate the expression of synaptic plasticity (Bosch et al., 2014; Meyer et al., 2014). While spine volume and structural changes are important effectors of synaptic plasticity, ultimately the density of AMPA receptors in the PSD determines synaptic strength. During LTP, AMPA receptors are recruited to the PSD, while LTD is associated with the removal and internalization of AMPA receptors (Anggono and Huganir, 2012; Bredt and Nicoll, 2003; Malinow and Malenka, 2002; Shepherd and Huganir, 2007). Understanding the mechanisms that regulate activity-dependent membrane trafficking of AMPA receptors has therefore been subject of intense investigation.

The endocytic zone (EZ) is a clathrin-marked structure that is physically coupled to PSD and facilitates local endocytosis of postsynaptic AMPA receptors (Blanpied et al., 2002; Lu et al., 2007; Rosendale et al., 2017). Receptors that are internalized via the EZ, enter a local recycling compartment that allows receptors to recycle back to the PSD, for example during LTP (Petrini et al., 2009). The localized endocytosis via the EZ is therefore critical for synaptic transmission, and uncoupling of the EZ from the PSD results in the loss of synaptic AMPA receptors and impaired LTP (Lu et al., 2007; Petrini et al., 2009). While changes in spine morphology, synapse structure and AMPA receptor trafficking during synaptic plasticity are extensively studied, whether the EZ itself undergoes activity-dependent alterations is not known. Early studies on the EZ showed that several LTD protocols did not lead to disappearance of the EZ, suggesting that clathrin remains tightly associated to the EZ after LTD (Blanpied et al., 2002). However, whether reorganization within the EZ occurred, could not be determined due to the use of diffraction-limited microscopy techniques. Here, we used super-resolution microscopy to resolve the EZ at high spatial resolution in hippocampal neurons. We found that the association of the EZ with the PSD was already apparent during early development but steadily increased and most prevalent in mushroom-type spines. For the first time we show that the EZ is subjected to molecular reorganization during synaptic activity. While, chemical LTP (cLTP) resulted in long-lasting reorganization of the EZ, mGluR receptor LTD led to a transient reorganization. Interestingly, NMDA receptor LTD did not affect EZ organization. .Similarly, we show that homeostatic plasticity does not affect EZ organization.Based on these findings, we propose that EZ appearance during early development is coupled to PSD maturation. At mature neurons, the is EZ reorganized in response to synaptic activation.

RESULTS

The appearance of PSD-associated CCS is coupled to PSD formation

To visualize the distribution and appearance of endogenous clathrin-coated structures (CCS) during development we generated a GFP-CLCa knock-in at DIV3 and fixed the neurons at different timepoints. We co-expressed Homer1c-mCherry to visualize the PSD. From DIV7 to DIV11 the dendritic shaft primarily contained small circular CCS, and CLCa appeared relatively diffuse compared to later timepoints (Figure 1A). From DIV14 to DIV18 large dendritic CLCa assemblies started to appear and seemed to gradually increase in number over time (Figure 1A, data not shown). Next, to see the appearance of PSD-associated CCS, we quantified the number of Homer1c puncta associated with a CCS (Figure 1A). Interestingly, while the number of PSDs per 20 μm increased five-fold from DIV7 to DIV16 (DIV7: 5.2 ± 1.2 %, DIV16: 26 ± 2%) (Figure 1B), the percentage of PSDs associated with a CCS only increased by 28% during the same period (DIV7: 55 ± 8%, DIV16: 83.1 ± 4.5%) (Figure 1C). Nevertheless, the PSD-CCS association significantly increased from DIV7 to DIV14 and DIV16, with over 80% of PSD associated with a CCS from DIV14 onwards. Thus, synaptogenesis seems to be accompanied with the formation of the EZ.

PSD-EZ association is most prevalent in mushroom spines

During development newly formed spines are thought to develop from immature, thin spines to mature mushroom spines (Runge et al., 2020; Sala et al., 2008). To test if PSD-CCS association is correlated with spine morphology, we expressed GFP as a cell fill together with Homer1c-mCherry and CLCa-Halo labelled with JF646. First, we classified spines in four different groups: filopodia-like spines that are characterized by long thin protrusions; thin spines characterized by a long thin neck with slight thickening at the top; stubby spines that have no discernable spine neck and mushroom spines characterized by a short thin neck and a large spine head (Figure 1D, E). At DIV16, thin (35.4 ± 3.8%) and mushroom-type spines (39.5 ± 0.6%) were the most prevalent in our dissociated hippocampal neurons, while stubby spines were less prevalent (21.8 ± 3.3%) and filopodia-like spines were nearly absent (2.1 ± 0.7%). Next, we quantified the percentage of spines containing Homer1c, CLCa or both. We found that thin, stubby and mushroom spines all

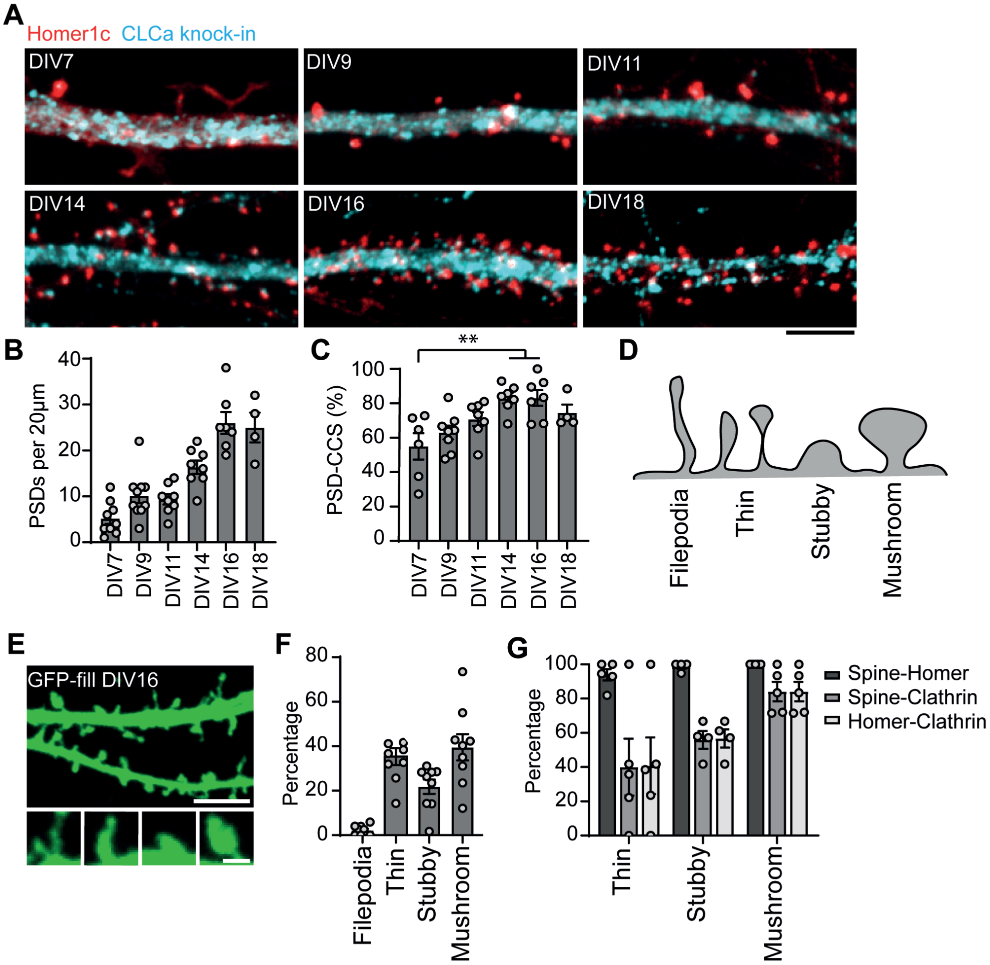

Figure 1. The appearance of PSD-associated CCS is associated with PSD formation, and most prevalent in mushroom-type spines. (A) Example confocal images of neurons expressing Homer1c-mCherry (red) together with GFP-CLCa-KI (cyan) over time. Scale bar: 5 µm. (B) Density of PSDs at different timepoints during development (N = 4-9). (C) PSD-CCS association at different timepoints during development. PSD-CCS association significantly increased from DIV7 till DIV14 and DIV16 (N = 4-8, $p < 0.01$). (D) Illustration of different spine morphologies. (E) Example image of a neuron expressing GFP as a cell fill at DIV16. Zooms represent the different spine types analyzed. Scale bar: 5 µm, zoom: 1 µm. (F) Percentage of spines classified in the different spine morphology groups in DIV16 neurons (N = 9). (G) Percentage of spines containing a Homer1c puncta (dark grey), a CLCa puncta (middle grey) and Homer1c-CLCa (light grey) (N = 5).

contained a clear Homer1c puncta, indicating the presence of a PSD within these spines (Figure 1G). Interestingly, approximately half of the thin (39.9 ± 16.6%) and stubby (55.8 ± 5.2%) spines contained a CLCa puncta. Similarly, half of the thin (40.7 ± 16.5%) and stubby (56.6 ± 5.4%) spines were marked by both Homer1c and CLCa, showing that CLCa in spines is always associated with a PSD.In mushroom spines, that are thought to represent mature and active synapses, the presence of CLCa and Homer1c-CLCa association was most frequently observed, with 84.2 ± 7.3% of PSDs containing CLCa puncta.

cLTP induces splitting of the EZ at mature synapses

To test if synaptic activity leads to changes in PSD-EZ coupling we induced chemical LTP (cLTP) at DIV16, in neurons co-expressing Homer1c-mCherry and GFP-CLCa. Neurons were stimulated for 5 minutes with 200 mM glycine in Mg2+-free buffer, and allowed to recover for 25 minutes, after which neurons were fixed and GFP-CLCa was labelled with Atto647N for gSTED imaging. Interestingly, we found that not the number of PSDs containing an EZ increased but that the number of PSDs associated with two or more CCSs significantly increased (control: 17.6 ± 2.8%, cLTP: 29.1 ± 2.7%, $p < 0.01$) (Figure 2A, B). This effect was completely blocked by AP5, an NMDA receptor antagonist, suggesting that the appearance of multiple CCSs associated with PSDs after cLTP was triggered by NMDA receptor activation. Moreover, the size of the PSD correlated to the number of associated CCSs under basal conditions, with larger PSDs more frequently associated with multiple CCSs than smaller PSDs (Figure 2C). To see whether the presence of multiple CCSs per PSD was transient or was a long-lasting effect we fixed neurons at different timepoints, and observed that the increase in the number of CCSs per PSD was stable, even up to 120 minutes after induction of cLTP (Figure 2D).

The increase in CCSs associated with PSDs could be due to recruitment of new clathrin or due to the splitting of the pre-exisiting CCS. To differentiate between these possibilities, we used live-cell gSTED to observe changes over time within individual synapses after cLTP (Figure 2E). Indeed, we found that cLTP induced structural alterations of the EZ (Figure 2E). In some cases multiple CCSs could be observed 5 minutes after cLTP, however these structures rapidly disappeared, perhaps indicating the formation of transient endocytic vesicles. Other examples clearly showed more structural reorganization of the EZ 5 minutes after cLTP, that resulted in multiple CCSs associated with the PSD after 30 minutes. Interestingly, this seemingly splitting of the PSD was associated with an increase in PSD area. PSDs that were not associated with multiple CCSs after 30 minutes remained the same size (Figure 2F). These results suggest that splitting of the EZ preferentially occurs in PSDs that are strongly potentiated by the cLTP protocol. Finally, to further test that the observed effect was due to splitting and not due to new recruitment of CLCa, we used confocal imaging and analyzed the intensity and total area of CLCa per spine after cLTP induction. Indeed, we found that CLCa area was not different between control and cLTP (Control: 0.06 ± 0.007, cLTP: 0.05 ± 0.009). Similarly, live-cell confocal imaging showed that CLCa intensity was not changed after cLTP (Figure 2G, E), indicating that there is no recruitment of new clathrin molecules to the EZ. Interestingly, we found under basal conditions that when PSDs were associated with multiple CCSs, both these CCSs were associated with other endocytic proteins, including ß2-adaptin, Eps15, Hip1R, Intersectin (Itsn1L) and dynamin2 (Dyn2) (Supplement figure 1A, B).

mGluR-LTD but not NMDA-LTD transiently increases the number of CCS per PSD

Next, we tested whether apart from protocols that potentiate synapses, long-term

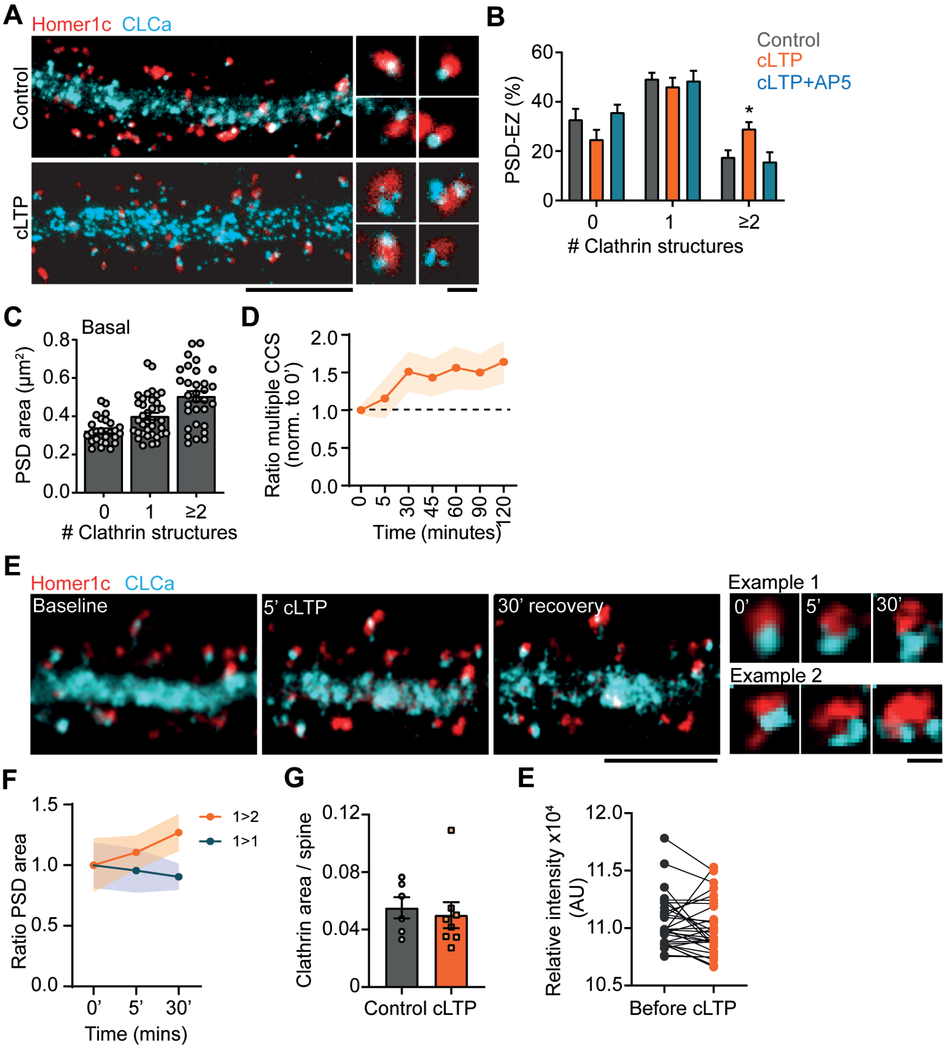

Figure 2: cLTP induced multiple CCSs per PSD. (A) Example images of Homer1c-mCherry (red, confocal) and GFP-CLCa labelled with Atto647N (cyan, gSTED) under basal conditions (upper panel) and 25 minutes after cLTP induction (lower panel). Scale bar: 5 µm, zoom: 500 nm. (B) Quantification of the number of CCSs per PSD under basal control conditions (grey), after cLTP (orange) and cLTP in the presence of AP5 (blue) (Control: 17.6 ± 2.8%, LTP: 29.1 ± 2.7%, $p < 0.05$) (N = 8-11). (C) Bar graph with individual values showing the correlation between PSD area and the number of CCS per PSD (n = 26-36). (D) Timeline showing the relative number of PSDs associated with multiple CCS normalized to timepoint 0 (n = 8-13). (E) Example image of live-cell gSTED on GFP-CLCa-JF646 overlayed with confocal image of Homer1c-mCherry. Zooms show examples of morphological alterations of the EZ after cLTP induction. Scale bar: 5 µm, zoom: 500 nm. (F) PSD area before (0'), directly after cLTP (5') and after recovery (30'). The orange line shows individual PSDs that were associated with one CCS at timepoint 0 and two at timepoint 30, the blue line shows PSD that have one CCS throughout the time of imaging. Area is normalized to timepoint 0 (n = 5). (G) CLCa area per spine, measured using confocal imaging (N = 6-8). (F) Relative intensity of CLCa per spine, before and after cLTP (n = 31).

synaptic depression is also associated with structural changes in the EZ. We therefore compared two distinct paradigms to induce LTD: one triggered by NMDAR activation (NMDA-LTD) and one induced by activation of group I mGluRs (mGluR-LTD). First, neurons were incubated with NMDA for 5 minutes or DHPG for 10 minutes, and were allowed to recover up to 30 minutes. We found no significant differences in the number of CCS associated with PSDs after 30 minutes with both protocols (Figure 3A, B). A slight reduction in PSD-EZ association and increase in the number of PSDs lacking an EZ was observed in both groups, however these results were not significant (Figure 3B). Thus, cLTD does not seem to induce long-lasting structural alterations of the EZ as we observed for cLTP. However, since both forms of LTD rely on AMPAR endocytosis, we considered that perhaps the EZ undergoes transient alterations or alterations on a shorter timescale after the induction of cLTD. To test this, we fixed neurons at different timepoints: before, during and immediately after the induction of cLTD and after the recovery time. Surprisingly, we found that DHPG induced a transient, two-fold increase in the number of PSDs associated with multiple CCSs after 5 minutes (control: 0.95 ± 0.14, 5’ DHPG: 2.1 ± 0.35), that recovered to control levels after 10 minutes (Figure 3C, D). However, this effect was not observed after NMDA application. Furthermore, we found that the mGluR5 antagonist MPEP effectively blocked the effect of DHPG, however, the protein translation inhibitor anisomycin did not block the increase in the number of CCS per PSD after 5 minutes DHPG, although the increase in the number of CCSs per PSDs after DHPG + anisomycin was not significant compared to control. Intriguingly, we did not find reorganization of other endocytic proteins after DHPG (supplement figure 2B, C).

Forms of homeostatic plasticity does not alter the PSD-EZ association

To test if protocols that induce homeostatic plasticity change PSD-EZ association we incubated neurons with AP5 and CNQX to block NMDA and AMPA receptor mediated transmission, and TTX to block sodium channels for five days. Both paradigms result in homeostatic plasticity and synaptic upscaling (Chowdhury and Hell, 2018; Fong et al., 2015; Wang et al., 2012). We found that these chronic changes in network activity did not alter the number of CCSs per PSD. A slight increase in the number of PSDs lacking an EZ was observed after chronic TTX treatment, however these results were not significant. The size of the PSD was significantly increased after CNQX/AP5 and TTX compared to control, suggesting that synaptic upscaling did occur (control: 0.24 ± 0.013 μm^2, CNQX/AP5: 0.35 ± 0.022 μm^2, TTX: 0.34 ± 0.032 μm^2, $p < 0.01$). Thus, in contrast to LTP and LTD, homeostatic plasticity paradigms do not seem to alter PSD-EZ coupling.

DISCUSSION

Changes in synaptic activity are associated with prominent alterations in spine morphology, synaptic content and synapse organization. While synaptic organization in developing and mature neurons has been studied in detail over the past decades, whether perisynaptic regions undergo alterations during activity is not known. In particular, the postsynaptic EZ, that is vital for proper synaptic function by facilitating local endocytosis and recycling of synaptic components is poorly understood. Although, the critical function of the EZ is broadly acknowledged, whether PSD-EZ

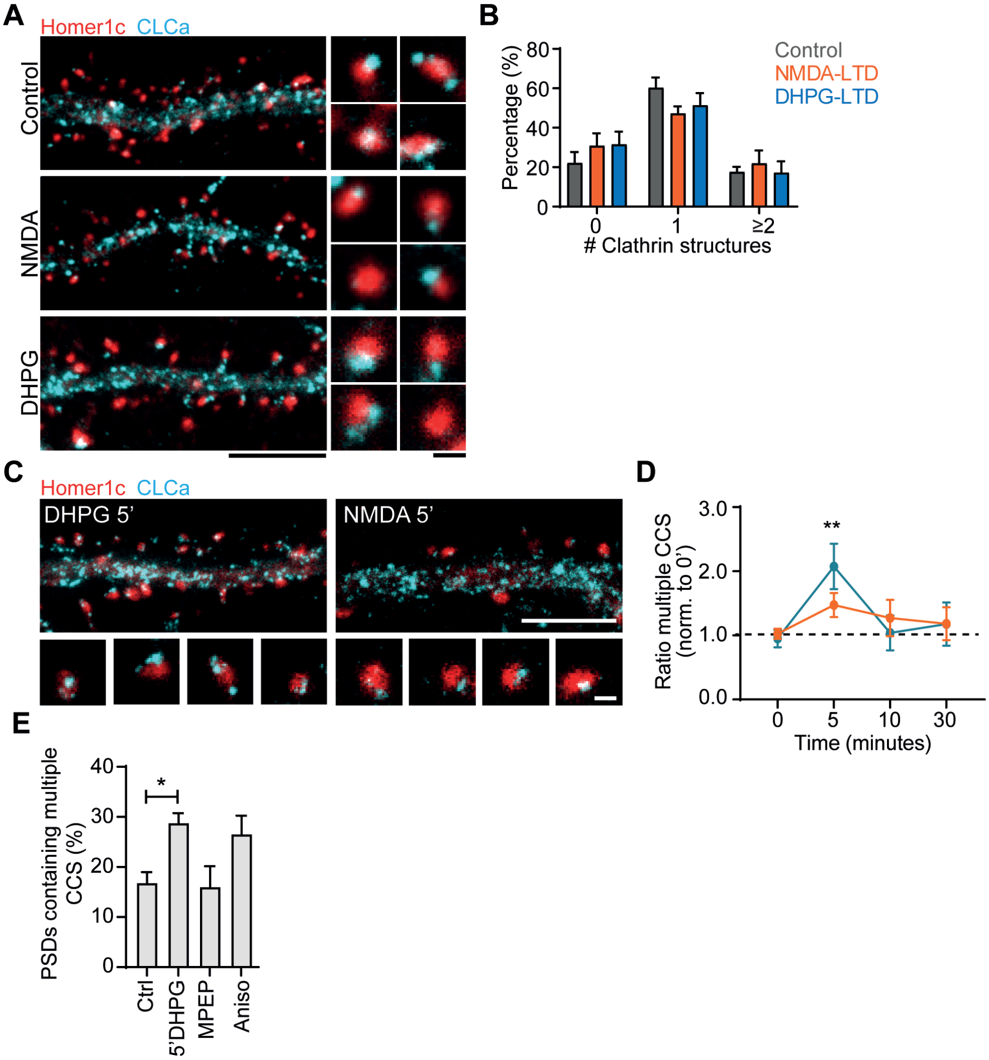

Figure 3: mGluR-LTD but not NMDA-LTD transiently increases the number of CCS per PSD. (A) Example images of Homer1c-mCherry (red, confocal) co-expressed with GFP-CLCa labelled with Atto647N (cyan, gSTED), under basal control conditions (upper panel), after NMDA application (middle panel) and after DHPG (lower panel). Scale bar: 5 μm, zoom: 500 nm. (B) Quantification of the number of CCS per PSD (N = 7-10). (C) Example images after 5 minutes DHPG (left) and NMDA (right). Scale bar: 5 μm, zoom: 500 nm. (D) Relative number of PSDs associated with multiple CCS after DHPG (blue) and NMDA (orange). DHPG significantly increases the number of PSDs associated with multiple CCS after 5 minutes (N = 11-19, $p < 0.01$), NMDA-LTD did not significantly affect PSD-CCS association (N = 5-13, $p > 0.05$). (E) Percentage of PSDs containing multiple CCS. 5 minutes DHPG significantly increased the number of PSDs containing multiple CCS (N = 9, $p < 0.05$). MPEP effectively blocked this effect (N = 10), while anisomycin did not completely block this effect (N = 11), however the data is not significant.

coupling is altered or whether the EZ undergoes structural alterations in response to synaptic activity has not been studied extensively. Here, we show that cLTP induces the appearance of multiple clathrin structures that remain closely associated to the PSD for up to 120 minutes after induction. In contrast, cLTD did not result in long-lasting alterations, however mGluR-LTD, but not NMDA-LTD resulted in a transient two-fold increase in the number of CCSs per PSD.

Our data shows that CCSs are prevalent throughout development, however, the appearance and morphology changes over time. During early development CCSs appear as small circular structures in the dendritic shaft, most likely representing transient clathrin-coated pits (Blanpied et al., 2002), while in the later stages large CCSs dominate the dendritic shaft, likely representing stable membrane features (Blanpied et al., 2002; Grove et al., 2014; Saffarian et al., 2009). In spines, we found that the number of PSDs rapidly increases over time, however already early in development half of the PSDs were associated with clathrin. Moreover, we also found that PSD-CCS association was most prevalent in mushroom-type spines, suggesting that the appearance of PSD associated CCS is linked to synaptic activity and maturation stage. Whether these specific CCSs were stably associated with the PSD early in development was not determined, and live-cell imaging should determine whether these CCSs are indeed stable EZs.

We found that 5 minutes cLTP followed by 25 minutes recovery was sufficient to effectively increase the size of Homer1c puncta in a subset of PSDs. Homer1c was previously described to be rapidly recruited after LTP, indicating effective LTP induction in a subset of our PSDs (Meyer et al., 2014). This subset was specifically associated with multiple CCSs per PSD, that originate from EZ splitting. Interestingly, both CCSs obtained from EZ splitting remained close to the PSD up to 120 minutes after cLTP, suggesting that both structures are stable. Moreover, we found that PSDs associated with multiple CCS were often associated with multiple endocytic protein puncta. For example, ß2-adaptin, Eps15, Hip1R, Intersectin1-long and Dynamin2 were frequently observed at both CCSs, suggesting that the entire EZ was reorganized. However, whether the second structure is truly stable and coupled to the PSD, resembling the EZ, is yet to be determined. The novel observation of EZ splitting during cLTP raises many questions and potential targets for new research. A previous electron microscopy study showed that cLTP results in PSD perforation that results in the presence of multiple clathrin-coated pits associated with perforated PSDs (Puchkov et al., 2011), perhaps indicating increased endocytic capacity of potentiated synapses. Future studies should investigate whether LTP is accompanied by an increase in endocytic capacity to perhaps accompany enhanced receptor trafficking and recycling.

Interestingly, we found that LTD did not lead to the disappearance of the EZ, but rather induced a transient increase in the number of CCSs per PSD. The transient nature of these CCSs might suggest that these structures represent endocytic vesicles. Interestingly, this effect was specificcaly observed after mGluR-LTD, but not NMDA-LTD. Previous studies showed endocytosis in close proximity to the PSD after NMDA-LTD, however it was not determined whether the endocytosis took place at the EZ (Rosendale et al., 2017). Although, mGluR-LTD and NMDA-LTD are fundamentally distinct processes, and differences in underlying mechanisms might explain the differential findings. For instance, a recent study showed that

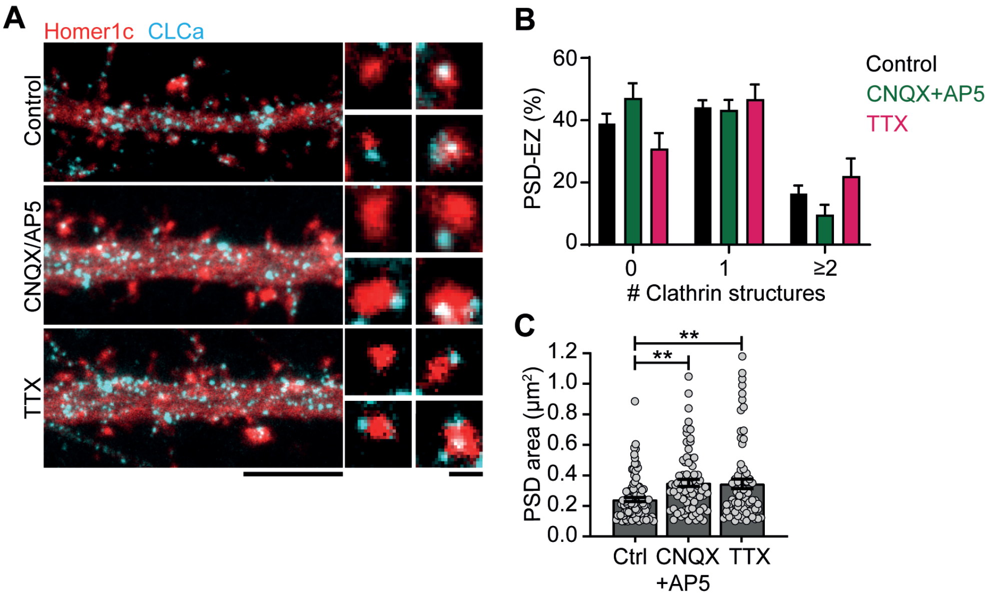

Figure 4: Homeostatic plasticity does not alter PSD-EZ association. (A) Example images of Homer1c-mCherry (red, confocal) co-expressed with GFP-CLCa labelled with Atto647N (cyan, gSTED), under basal control conditions (upper panel), after CNQX+AP5 application (middle panel) and after TTX (lower panel). Scale bar: 5 μm, zoom: 500 nm. (B) Quantification of the number of CCS per PSD (N = 9-13). (C) PSD area in the different conditions. CNQX+AP5 (0.35 ± 0.022 μm^2, n = 76, $p < 0.01$) and TTX (0.34 ± 0.032 μm^2, n = 72, $p < 0.01$) significantly increased the size of the PSD compared to control (0.24 ± 0.013 μm^2, n = 103).

LTD results in significant spine shrinkage, while DHPG did not change spine volume (Thomazeau et al., 2020). Interestingly, even though chronic silencing of network activity increased PSD size, the number of PSDs associated with multiple CCSs was not increased. The mechanisms underlying the expression of homeostatic plasticity are fundamentally different from those of Hebbian plasticity (Turrigiano, 2012). For example, while both LTP and LTD depend on PICK1 to recruit AMPA receptors to the EZ and regulate recycling, homeostatic plasticity is unaffected by loss of PICK1 (Anggono et al., 2011). Moreover, chronic blockage of activity reduces the levels of PICK1, while AMPA receptor recycling is enhanced, suggesting that AMPA receptor trafficking during homeostatic plasticity is not facilitated by the EZ. Therefore it is plausible that EZ organization is not altered during homeostatic plasticity and further highlights the specific role for the EZ during Hebbian forms of plasticity.

Interestingly, the fact that homeostatic plasticity does not lead to alterations in PSD-EZ association suggests that the absence of NMDA and AMPA receptor-mediated transmission does not remove the EZ from the PSD. These observations might be contradicting our earlier hypothesis that EZ appearance is coupled to PSD formation, which highly depends on synaptic activity (De Roo et al., 2008). However, homeostatic plasticity was induced starting at DIV11. At that point already 60% of PSDs are associated with an EZ, suggesting that perhaps lack of NMDA and AMPA receptor-mediated transmission does not actively remove existing EZ, but might affect the appearance of new EZ. Future research should determine whether absence of trafficking, for example by removing AMPA receptors using knock-down strategies leads to removal of the EZ.

To conclude, in contrast to earlier findings that the EZ is optical stable, we found that synaptic activity induces structural reorganization of the EZ. These preliminary observations trigger many questions and open up many possibilities for future research. Gaining insight into the molecular mechanisms of EZ reorganization during LTP would greatly contribute to our understanding of synaptic plasticity.

MATERIALS AND METHODS

Animals

All animal experiments were performed in accordance to the guidelines for the welfare of experimental animals issued by the Government of the Netherlands (Wet op de Dierproeven, 1996) and European regulations (Guideline 86/609/EEC). All animal experiments were approved by the Dutch Animal Experiments Review Committee (Dier Experimenten Commissie; DEC), and performed in line with the institutional guidelines of Utrecht University.

Primary hippocampal cultures and transfection

Hippocampal cultures were prepared from brain of embryonic day 18 (E18) Wistar rats (both genders) as described before (Scheefhals et al., 2019). Dissociated hippocampal neurons were plated on coverslips coated with poly-L-lysine (37.5 µg/ml, Sigma-Aldrich) and laminin (1.25 µg/ml, Roche Diagnostics) at a density of 100,000 neurons per well of a 12-well plate. Cultures were allowed to settle in Neurobasal medium (NB) supplemented with 2% B27 (GIBCO), 0.5 mM glutamine (GIBCO), 15.6 mM glutamate (Sigma-Aldrich), and 1% penicillin/streptomycin at 37ºC in 5% CO_2. After 24 hours halve of the NB medium was refreshed with BrainPhys medium (BP) supplemented with SM1 supplement (Stemcell Technologies) and 1% penicillin/streptomycin, and kept at 37ºC in 5% CO_2. Refreshment were done weekly replacing halve of the medium with fresh supplemented BP medium. At DIV3 (for knock-in experiments) or DIV11 (overexpression) neurons were transfected with indicated constructs using Lipofectamine 2000 (Invitrogen). Before transfection 300 µl conditioned medium was transferred to a new culture plate. For each well, 1.8 µg DNA was mixed with 3.3 µl Lipofectamine 2000 in 200 µl BP, incubated for 30 minutes at room temperature and added to the neurons. After 1 to 1.5 hours, neurons were briefly washed with BP and transferred to the new culture plate with conditioned medium with an additional 500 µl supplemented BP and kept at 37ºC in 5% CO_2 for 4-6 days.

DNA constructs

The following constructs were a gift: GFP-CLCa (Dr. Blanpied), FKBP-β2-adaptin-GFP and HIP1R-GFP-FKBP (Dr. Royle) (Wood et al., 2017), GFP-Intersectin Long (Dr. McPherson), GFP-Eps15 (Dr. van Bergen Henegouwen). The following constructs have been described before: Homer1c-mCherry and Dynamin2-GFP (Scheefhals et al., 2019), Halo-CLCa (Catsburg et al. 2021, preprint), GFP-CLCa knock-in (Willems et al., 2020), Psm155-GFP (MacGillavry et al., 2013).

Immunocytochemistry and HaloTag labelling

Neurons were fixed between DIV7-18 with 4% paraformaldehyde (PFA, EM grade) diluted in PEM buffer (80 mM PIPES, 5 mM EGTA, 2 mM MgCl2, pH 7.4) for 10 minutes at 37ºC and washed three times with PBS supplemented with 100 mM glycine (PBS-gly). Then, neurons were permeabilized and blocked with 10% normal goat serum (NGS) and 0.01% Triton X-100 (TX) in PBS-gly for 20-30 minutes at 37 ºC. The GFP-CLCa knock-in was enhanced with ATTO488-conjugated FluoTAG X4 anti-GFP (1:500 Fluotag X4, Nanotag). For gSTED imaging, GFP-CLCa was enhanced with monoclonal anti-GFP (1:1000, Thermo Fisher) and further labelled with ATTO647N (1:500, Sigma), or ATTO647N-conjugated FluoTAG X4 anti-GFP (1:500, Nanotag) was used. Antibodies and nanobodies were diluted in PBS-gly supplemented with 5% NGS and 0.01% TX, for an overnight at 4ºC or 1 hour at room temperature, respectively. Samples labelled with the nanobody were washed three times with PBS-gly and mounted in Mowiol (Sigma). Samples labelled with antibody were washed the next day as described for the nanobody, and further labelled with ATTO647N (1:500, Sigma) for 2 hours at room temperature, washed and mounted as described above. Endogenous Homer1c was labelled with anti-Homer1b/c (1:1000, MBL), using the same protocol as anti-GFP labelling. For the Halo labelling, neurons were live-labelled with Halo-JF646 (1:1000, Promega) in prewarmed extracellular imaging buffer (EB) for 15 minutes at 37 ºC.

Confocal imaging

Confocal images were acquired with a Zeiss LSM 700 confocal laser-scanning microscope using a Plan-Apochromat 63x NA 1.40 oil objective. Images consist of a z-stack of 5-9 planes at 0.37-μm interval, and maximum intensity projections were generated in Fiji (Schindelin et al., 2012) for analysis and display.

(Live-cell) gSTED imaging

Gated STED (gSTED) images were taken with the Leica TCS SP83x microscope using a HC PL APO 100x/NA 1.4 oil immersion gSTED WHITE objective. For live-cell gSTED the neurons were kept in a prewarmed cabinet and imaged in EB. Three sequential gSTED images were taken, at the represented timepoints. For both fixed and live samples, the 488 nm pulsed white laser (80 MHz) was used to excite Alexa-488, 561 nm to excite mCherry, and the 647 nm to excite JF646 and ATTO647N labeled proteins. JF646 and ATTO647N were depleted with the 775-nm pulsed depletion laser. The internal Leica HyD hybrid detector was set at time gate between 0.3 and 6 ns. Images were taken with a pixel size lower than 50 nm, and a z-stacks of 8-14 planes at 0.28-μm interval was acquired. Maximum intensity projections were generated in Fiji (Schindelin et al., 2012) for analysis and display.

Live-cell confocal imaging

Live-cell imaging was performed on a spinning disk confocal system (CSU-X1-A1; Yokogawa) mounted on a Nikon Eclipse Ti microscope (Nikon) with Plan Apo VC 100x 1.40 NA with excitation from Cobolt Calyspso (491 nm), and Jive (561 nm) lasers, and emission filters (Chroma). The microscope was equipped with a motorized XYZ stage (ASI; MS-2000), Perfect Focus System (Nikon), Evolve 512 EM-CCD camera (Photometrics), and was controlled by MetaMorph 7.7.6 software

(Molecular Devices). Neurons were maintained in a closed incubation chamber (Tokai hit: INUBG2E-ZILCS) at 37 ºC in EB. Images were taken every 30 seconds for 15 minutes, including 1 minute baseline, 5 minutes LTP and 9 minutes recovery. Z-stacks of 5-9 planes were acquired, with varying step sizes per neuron. Maximum intensity images were analyzed in Fiji. Analysis was done by manually drawing same-size ROIs around individual clathrin puncta associated with PSDs. Intensity and area of GFP-CLCa was measured using the integrated intensity and particle analysis respectively.

Plasticity experiments

All plasticity experiments were performed in prewarmed EB at 37 ºC. cLTP was induced with 300 µM glycine (Sigma) and 25 µM bicuculin (Tocris) in magnesium-free EB for 5 minutes. Neurons were allowed to recover in regular EB for the indicated timepoints before being fixed. For blocking cLTP, 300 µM AP5 was added during cLTP induction and the recovery period. NMDA-LTD was induced with 20 µM NMDA (Tocris) in EB for 5 minutes, followed by a recovery period as indicated in the figures. For mGluR-LTD, neurons were incubated with 100 µM DHPG for 10 minutes. For the timeline experiment DHPG remained on for the full 30 minutes or shorter when indicated. CNQX (Tocris), AP5 (Tocris) and TTX (Tocris) were used at 10, 300 and 1 µM, respectively. The drugs were added to the medium directly after transfection and incubated for 5 days. The medium was refreshed after 72 hours with fresh drugs to account for the half-life of the drugs.

Statistical analysis

Statistical significance was tested using a student's t-test when comparing two groups. When comparing multiple groups statistical significance was tested using a one-way ANOVA followed by a Tukey or Dunnett's multiple comparison post-hoc test. All the statistical tests with a p-value below 0.05 were considered significant. In all figures, significance is indicated as follows: $p < 0.05$ is indicated by *, $p < 0.01$ by **, and $p < 0.001$ by ***. Analysis was performed on neurons originating from at least two individual batches of hippocampal neurons. Number of neurons used for analysis is indicated as N, number of spines, PSDs or clathrin-coated structures is represented as n.

REFERENCES

Anggono, V., Clem, R.L., and Huganir, R.L. (2011). PICK1 loss of function occludes homeostatic synaptic scaling. J Neurosci 31, 2188-2196.

Anggono, V., and Huganir, R.L. (2012). Regulation of AMPA receptor trafficking and synaptic plasticity. Curr Opin Neurobiol 22, 461-469.

Blanpied, T.A., Scott, D.B., and Ehlers, M.D. (2002). Dynamics and regulation of clathrin coats at specialized endocytic zones of dendrites and spines. Neuron 36, 435-449.

Bosch, M., Castro, J., Saneyoshi, T., Matsuno, H., Sur, M., and Hayashi, Y. (2014). Structural and molecular remodeling of dendritic spine substructures during long-term potentiation. Neuron 82, 444-459.

Bredt, D.S., and Nicoll, R.A. (2003). AMPA receptor trafficking at excitatory synapses. Neuron 40, 361-379.

Chowdhury, D., and Hell, J.W. (2018). Homeostatic synaptic scaling: molecular regulators of synaptic AMPA-type glutamate receptors. F1000Res 7, 234.

De Roo, M., Klauser, P., Mendez, P., Poglia, L., and Muller, D. (2008). Activity-dependent PSD formation and stabilization of newly formed spines in hippocampal slice cultures. Cereb Cortex 18, 151-161.

Fong, M.F., Newman, J.P., Potter, S.M., and Wenner, P. (2015). Upward synaptic scaling is dependent on neurotransmission rather than spiking. Nat Commun 6, 6339.

Grove, J., Metcalf, D.J., Knight, A.E., Wavre-Shapton, S.T., Sun, T., Protonotarios, E.D., Griffin, L.D., Lippincott-Schwartz, J., and Marsh, M. (2014). Flat clathrin lattices: stable features of the plasma membrane. Molecular biology of the cell 25, 3581-3594.

Lu, J., Helton, T.D., Blanpied, T.A., Rácz, B., Newpher, T.M., Weinberg, R.J., and Ehlers, M.D. (2007). Postsynaptic Positioning of Endocytic Zones and AMPA Receptor Cycling by Physical Coupling of Dynamin-3 to Homer. Neuron 55, 874-889.

MacGillavry, H.D., Song, Y., Raghavachari, S., and Blanpied, T.A. (2013). Nanoscale scaffolding domains within the postsynaptic density concentrate synaptic AMPA receptors. Neuron 78, 615-622.

Malinow, R., and Malenka, R.C. (2002). AMPA receptor trafficking and synaptic plasticity. Annu Rev Neurosci 25, 103-126.

Matsuzaki, M., Ellis-Davies, G.C., Nemoto, T., Miyashita, Y., Iino, M., and Kasai, H. (2001). Dendritic spine geometry is critical for AMPA receptor expression in hippocampal CA1 pyramidal neurons. Nat Neurosci 4, 1086-1092.

Meyer, D., Bonhoeffer, T., and Scheuss, V. (2014). Balance and stability of synaptic structures during synaptic plasticity. Neuron 82, 430-443.

Nusser, Z., Lujan, R., Laube, G., Roberts, J.D., Molnar, E., and Somogyi, P. (1998). Cell type and pathway dependence of synaptic AMPA receptor number and variability in the hippocampus. Neuron 21, 545-559.

Petrini, E.M., Lu, J., Cognet, L., Lounis, B., Ehlers, M.D., and Choquet, D. (2009). Endocytic trafficking and recycling maintain a pool of mobile surface AMPA receptors required for synaptic potentiation. Neuron 63, 92-105.

Puchkov, D., Leshchyns’ka, I., Nikonenko, A.G., Schachner, M., and Sytnyk, V. (2011). NCAM/spectrin complex disassembly results in PSD perforation and postsynaptic endocytic zone formation. Cereb Cortex 21, 2217-2232.

Rosendale, M., Julli, D., Choquet, D., and Perrais, D. (2017). Spatial and Temporal Regulation of Receptor Endocytosis in Neuronal Dendrites Revealed by Imaging of Single Vesicle Formation. Cell Reports 18, 1840-1847.

Runge, K., Cardoso, C., and de Chevigny, A. (2020). Dendritic Spine Plasticity: Function and Mechanisms. Front Synaptic Neurosci 12, 36.

Saffarian, S., Cocucci, E., and Kirchhausen, T. (2009). Distinct Dynamics of Endocytic

Clathrin-Coated Pits and Coated Plaques. PLoS Biology 7, e1000191-e1000191.

Sala, C., Cambianica, I., and Rossi, F. (2008). Molecular mechanisms of dendritic spine development and maintenance. Acta Neurobiol Exp (Wars) 68, 289-304.

Scheefhals, N., Catsburg, L.A.E., Westerveld, M.L., Blanpied, T.A., Hoogenraad, C.C., and MacGillavry, H.D. (2019). Shank Proteins Couple the Endocytic Zone to the Postsynaptic Density to Control Trafficking and Signaling of Metabotropic Glutamate Receptor 5. Cell Rep 29, 258-269 e258.

Schindelin, J., Arganda-Carreras, I., Frise, E., Kaynig, V., Longair, M., Pietzsch, T., Preibisch,S., Rueden, C., Saalfeld, S., Schmid, B., et al. (2012). Fiji: an open-source platform for biological-image analysis. Nat Methods 9, 676-682.

Shepherd, J.D., and Huganir, R.L. (2007). The cell biology of synaptic plasticity: AMPA receptor trafficking. Annu Rev Cell Dev Biol 23, 613-643.

Straub, C., and Sabatini, B.L. (2014). How to grow a synapse. Neuron 82, 256-257.

Thomazeau, A., Bosch, M., Essayan-Perez, S., Barnes, S.A., De Jesus-Cortes, H.,and Bear, M.F. (2020). Dissociation of functional and structural plasticity of dendritic spines during NMDAR and mGluR-dependent long-term synaptic depression in wild-type and fragile X model mice. Mol Psychiatry.

Turrigiano, G. (2012). Homeostatic synaptic plasticity: local and global mechanisms for stabilizing neuronal function. Cold Spring Harb Perspect Biol 4, a005736.

Wang, G., Gilbert, J., and Man, H.Y. (2012). AMPA receptor trafficking in homeostatic synaptic plasticity: functional molecules and signaling cascades. Neural Plast 2012, 825364.

Willems, J., de Jong, A.P.H., Scheefhals, N., Mertens, E., Catsburg, L.A.E., Poorthuis, R.B., de Winter, F., Verhaagen, J., Meye, F.J., and MacGillavry, H.D. (2020). ORANGE: A CRISPR/Cas9-based genome editing toolbox for epitope tagging of endogenous proteins in neurons. PLoS Biol 18, e3000665.

Wood, L.A., Larocque, G., Clarke, N.I., Sarkar, S., and Royle, S.J. (2017). New tools for hot-wiring; clathrin-mediated endocytosis with temporal and spatial precision. The Journal of cell biology, jcb.201702188-jcb.201702188.

6

General Discussion

Lisa A.E. Catsburg

Department of Cell Biology, Neurobiology and Biophysics at the Faculty of Science of Utrecht University in Utrecht, the Netherlands

Endocytosis and recycling of glutamate receptors are critical for proper synaptic communication. At glutamatergic synapses, these processes are facilitated by the postsynaptic endocytic zone (EZ). Although the functional importance of the EZ is evident, fundamental insights about the EZ i.e. its components and organization and dynamics are lacking. Moreover, how the EZ is built to sustain endocytosis, is not known. Therefore, the aim of this thesis was to uncover these fundamental properties of the EZ. To summarize, in Chapter 2 we reviewed our current understanding about the mechanisms of AMPA-type glutamate receptor trafficking. In Chapter 3 we showed that not only ionotropic glutamate receptors but also metabotropic glutamate receptors (mGluRs) undergo EZ-mediated endocytosis and recycling. In Chapter 4 novel components of the EZ were identified, and revealed their spatiotemporal organization that likely contributes to endocytic efficiency. In Chapter 5 preliminary work showed that these EZ components are reorganized is response to synaptic activity. In the current chapter, I discuss the key findings of this thesis, place them into a broader context, and provide recommendations for future research and perspectives.

Novel insights into endocytic zone-mediated receptor trafficking

Glutamate receptor trafficking is a highly coordinated and critical process for proper synaptic function. At glutamatergic synapses, the EZ plays a critical role in receptor trafficking as it facilitates local internalization via clathrin-mediated endocytosis (CME) and local recycling (Blanpied et al., 2002; Lu et al., 2007; Petrini et al., 2009). However, what determines whether receptors are targeted for EZ-mediated endocytosis? Moreover, whether the EZ facilitates internalization of specific content, or is a general hub for endocytosis, is not fully understood. For example, the transferrin receptor, that controls AMPA receptor trafficking (Liu et al., 2016), is internalized via CME, but not specifically in the spine. While AMPA receptors, that are also internalized via CME, are internalized in close proximity to the PSD, most likely at the EZ (Rosendale et al., 2017). Similarly, NMDA receptor-containing clathrin-coated vesicles have been observed inside the spine, suggesting local endocytosis of glutamate receptors. (Cottrell et al., 2004; Rosendale et al., 2017; Wu et al., 2017). Moreover, in Chapter 3 we show that endocytosis of metabotropic glutamate receptor 5 (mGluR5) is facilitated by the EZ (Scheefhals et al., 2019). Together, this implies that specifically synaptic glutamate receptors traffic via the EZ. However, what mechanisms determine, where, when and how receptors are internalized have remained largely elusive.

Nevertheless, while internalization of AMPARs after NMDA application results in recycling, AMPA application targets AMPARs to lysosomal compartments (Ehlers, 2000), suggesting that the type of stimulus determines the trafficking pathway. Moreover, in the past decade several studies have found key proteins that regulate the specific internalization via the EZ. PICK1 was shown to competitively bind AMPARs and recruit them to the EZ (Anggono et al., 2013; Lin and Huganir, 2007; Maria Fiuza et al., 2017). For mGluR5, ß-arrestin and Siah1 have been shown to target mGluR5 to AP2 enriched membranes, which we found in chapter 4 to be located in the EZ (Dale et al., 2001; Ferguson et al., 1996; Ko et al., 2012; Moriyoshi et al., 2004; Pula et al., 2004). These observations suggest that receptors are specifically marked and targeted for EZ-mediated endocytosis, and it is likely that different types of activation initiate the binding of specific proteins that facilitate EZ targeting. Interestingly, PICK1 binds AMPARs both after agonist stimulation and constitutively, which coincides with the general notion that AMPARs are targeted to the EZ after both agonist stimulation and constitutively (Anggono and Huganir, 2012; Carroll et al., 1999; Dale et al., 2001). In contrast, ß-arrestin and Siah1 only bind mGluR5 after agonist stimulation. Indeed, in Chapter 3 we found that EZ-mediated internalization of mGluR5 is mostly agonist-induced, and even though mGluR5 traffics constitutively (Fourgeaud et al., 2003; Francesconi et al., 2009), this might not be facilitated by the EZ.

Remarkably, similar to AMPARs, mGluR5 endocytosed via the EZ is more likely to enter the recycling pathway rather than being sorted for degradation (Chapter 3). Moreover, we show that in the absence of an EZ, mGluR5 is lost from the perisynaptic region. These data highlight the importance of the EZ in facilitating recycling, and receptors endocytosed via the EZ are most likely recycled back the synaptic membrane and escape the degradation pathway. Such a local recycling mechanism of synaptic components is especially important in dendritic spines, that are isolated from the main dendritic branch and highly compartmentalized. Here, structures like the EZ are needed to facilitate compartmentalized recycling.

However, to date many questions remain. For example, what proportion of receptors is targeted for EZ-mediated endocytosis? It is estimated that under basal conditions approximately 60 AMPAR are located in the PSD (Cheng et al., 2006; Sheng and Hoogenraad, 2007). However, the number of receptors internalized during LTD and whether all of them are internalized at the EZ or only a few are targeted for recycling is not known. Finally, the EZ is crucial for synaptic function and facilitates local trafficking of specific receptors. However, to date mechanistic insights about the mechanisms that mediate receptor trafficking after CME is still lacking. For example, to what extent are receptors recycled after EZ-mediated endocytosis? More specifically, are all receptors internalized via de EZ recycled or is Is there still a pool degraded? Moreover, what regulates these specific processes remains to be solved. It would be interesting for future studies to address specific trafficking pathways and be able to map what stimuli or components regulate the targeting into a specific trafficking pathway.

Does endocytosis take place at the endocytic zone?

Perhaps the most important and longstanding question in the field of the EZ that remains to be answered is: does endocytosis take place at the EZ? Because the EZ is marked by a stable accumulation of clathrin, it is assumed that the route for internalization via the EZ is CME. However, although it is generally acknowledged that the EZ facilitates endocytosis, whether the EZ is the key location for endocytosis or is merely a reservoir for endocytic components, is not clear. Nevertheless, several studies have shown that CME of glutamate receptors takes place in close proximity to the PSD (Blanpied et al., 2002; Lu et al., 2007; Petrini et al., 2009; Rácz et al., 2004; Rosendale et al., 2017). Moreover, we found that specifically proteins involved in the early phases of CME are stably enriched and coupled to the EZ (Chapter 4), suggesting that initiation of CME occurs at the EZ itself. However evidence for actual endocytosis at the EZ itself remains highly circumstantial.

We and others have tried to visualize endocytosis at the EZ, but this has been proven challenging. Classically, CME is visualized by measuring the accumulation and disappearance of clathrin and other endocytic proteins such as dynamin-2 at endocytic sites (Grove et al., 2014; Saffarian et al., 2009; Taylor et al., 2011). However, due to the uniquely stable characteristics of clathrin at the EZ (Chapter 4) (Blanpied et al., 2002; Rosendale et al., 2017), visualizing disappearance of clathrin from the EZ is not possible. Similarly, in Chapter 4 we show that dynamin-2 is stably enriched at the EZ and can therefore not be used to visualize endocytosis. Nevertheless, while disappearance of clathrin from the EZ could not be observed, using super-resolution we frequently found the presence of multiple clathrin structures associated with the PSD, indicating that clathrin-coated vesicles could have budded of from the EZ. Interestingly, cLTD transiently increased the number of these clathrin structures, indeed suggesting that these secondary structures could represent vesicle formation (Chapter 4). Moreover, the size of the secondary structures was often well within the range of sizes reported for synaptic vesicles and the dimensions of these structures are similar to the dimension of clathrin-coated pit formation observed with EM (Kirchhausen et al., 2014; Rácz et al., 2004). However, these observations were done using STED and SMLM microscopy that significantly increase spatial resolution but lack temporal resolution. Ideally, these experiments would be repeated using live-cell super-resolution imaging to obtain both high spatial and temporal resolution to observe whether those secondary clathrin structures after cLTD originate from the EZ, exhibit vesicle-like dynamics and contain internalized receptors.

Other methods to visualize endocytosis at the EZ could also be developed. To date, the closest study to answer whether endocytosis takes place at the EZ itself, elegantly combined pH-sensitive fluophores with acid washing to visualize endocytosis in close proximity to the PSD (Rosendale et al., 2017). Despite that this study demonstrated endocytosis in close proximity to the PSD, this study could not reveal the exact location of vesicle formation relative to the EZ. Therefore, novel approaches that allow high spatial and temporal resolution need to be developed, ideally in combination with pH-sensitive fluophores. Coupling pH-sensitive fluophores to different types of receptors would allow us to visualize the location of receptors as they pass through different cellular compartments e.g. membrane, endosomes and lysosomes. However, the current availability of pH-sensitive fluorophores is limited. Two types of pH-sensitive fluophores exist, the most well-known is superecliptic pHluorin (SEP), a GFP variant that is fluorescent at neutral pH conditions (pH 7.4) and quenched in low pH (< pH 6). The second type of fluophores are quenched at neutral pH, but fluorescent at low pH (e.g., the AcidiFluor probe used in Chapter 2). SEP is often used to study internalization of membrane components by measuring the disappearance of SEP fluorescence (Chapter 2). However, the downside is that the exact location of internalization cannot be observed. Similarly, AcidiFluor allows visualization of vesicle acidification, but at the time vesicles reach sufficiently low pH to increase the fluorescence of AcidiFluor, these vesicles are classified as a late endosome or lysosome, making it nearly impossible to visualize early and recycling endosomes. Thus, there is a great need for pH-sensitive fluophores that are able to detect small changes in pH in the range of pH 6.4-7.0, to visualize cargoes in early and recycling endosomes. Tagging glutamate receptors with such pH-sensitive fluophores, would then allow visualization of the exact localization of internalization and the route these receptors take after endocytosis. Ideally, this would be done using super-resolution imaging, to exactly pinpoint the location of vesicle formation. However, it might take a long time to develop such fluophores, and other methods for visualizing endocytosis at the EZ should be thought of. For example, in Chapter 4 we show that apart from stable proteins, several proteins are transiently recruited to perisynaptic sites. If these proteins are only recruited upon vesicle formation these could be used as a marker for endocytosis. However, initial experiments failed to show that these proteins are indeed recruited upon cLTD. Nevertheless, further optimization is required and it is still possible that these transient proteins can be used as marker for visualizing endocytosis.

An alternative, intriguing model could be that endocytosis does not occur at the EZ, but that the EZ functions to retain receptors in the perisynaptic region. This notion would be in line with previous studies, showing that caveolae-type endocytosis might not actually induce endocytosis, but rather function to retain and immobilize receptors at specific locations (see chapter 1: general introduction) (Sinha et al., 2011). Here, the EZ would trap receptors and initiate membrane curvature to restrict receptors from diffusing across the membrane, but vesicle formation is halted and cutting from the membrane is prevented. This intriguing hypothesis would explain some findings, like the optical stability of clathrin at the EZ. Moreover, a study showed that indeed glutamate receptors are rapidly immobilized and captured at the EZ (Petrini et al., 2009), and while clathrin pits are frequently observed with EM (Puchkov et al., 2011; Rácz et al., 2004), an actual accumulation of clathrin near the PSD has never been observed using EM. Nevertheless, several arguments contradict this hypothesis. For example, in Chapter 4 we show that not only clathrin but many other proteins critical for the initiation of CME are enriched in the EZ, highly suggesting that endocytosis takes place at the EZ. Moreover, removal of glutamate receptors from the membrane has been shown on multiple occasions, even in close proximity to the synapse, indicating endocytosis. Also, clathrin-coated vesicles containing glutamate receptors inside the spine have been observed (Cottrell et al., 2004), however whether these vesicles actually originate from the EZ could not be determined.

In conclusion, while circumstantial evidence highly suggests that endocytosis takes place at the EZ itself, directly visualizing endocytosis at the EZ is impossible at this point, due to technical limitations. Future studies should focus on creating novel optical approaches that combine super-resolution imaging with pH-sensitive molecules. These techniques would not only significantly contribute to our understanding about the EZ, but would aid the entire field of endocytosis.

The spatiotemporal organization of the endocytic zone contributes to endocytic efficiency

Clathrin-coated structures come in all sizes, shapes and exhibit different dynamics. Most studies looking into the mechanisms of CME are performed in yeast or relatively flat mammalian cells. In yeast, only one type of CME exists, namely canonical-type endocytosis. Canonical CME is transient, meaning that components of the endocytic machinery are recruited to the membrane upon endocytosis (Taylor et al., 2011). In mammalian cells, a second type called non-canonical CME coexists and has been a topic of interest in the past decade. Non-canonical CME is characterized by large flat clathrin-coated structures that are stably associated with the membrane (Grove et al., 2014; Leyton-Puig et al., 2017; Saffarian et al., 2009; Sochacki et al., 2017). Similar to clathrin, other endocytic components are stably enriched and have distinct localizations at these flat lattices. Here, receptors are recruited to -and captured by the flat lattice, where endocytosis is then initiated from the edge of the structure (Grove et al., 2014; Sochacki et al., 2017). Many of the characteristics described for flat clathrin lattices can be found in the EZ as well. For example, the clathrin structure at the EZ is remarkably stable (Chapter 4), as well as other endocytic components that are stably retained at the EZ (Chapter 4). Moreover, the enrichment of specific endocytic proteins at the edge of the clathrin structure is very similar to the localization of endocytic proteins described at flat clathrin lattices (Sochacki et al., 2017). Together, these observations suggest that the EZ is organized as a lattice-like structure. However, whether the ultrastructure of the EZ is indeed similar to that of flat clathrin lattices can only be determined with electron microscopy (EM). Early studies show the presence of clathrin-coated vesicles and pits in close proximity to the PSD (Rácz et al., 2004), but an actual flat lattice has never been observed. To date, flat lattices can only be observed using a specific EM technique that requires unroofing of cells. While this has been done on immortalized cells such COS7 and HeLa cells, the three-dimensional structure of neurons makes unroofing challenging. Nevertheless, a recent paper described unroofing of axons and indeed found flat lattices, which might suggest that it would be possible to unroof dendrites as well (Vassilopous et al. 2019).

Nonetheless, it could be argued that a flat clathrin lattice would be the preferred type of clathrin structure at the perisynapse. A preassembled flat clathrin lattice could contribute to efficient endocytosis, by capturing receptors and allowing compartmentalized trafficking. Indeed, receptors that are uncoupled from the PSD rapidly diffuse across the membrane until they reach the EZ, where they are immobilized (Petrini et al., 2009). Endocytic proteins at the edge of the EZ likely facilitate this immobilization or capture. Moreover, the enrichment of endocytic proteins at the edge of the clathrin structure likely could contribute to clathrin-coated vesicles formation from the edge of the flat lattice. Indeed, in HeLa cells endocytic vesicles are formed from the edge of the flat lattice (Grove et al., 2014; Sochacki et al., 2017). Moreover, in neurons clathrin-coated pits have been observed within 600 nm from the PSD (Rácz et al., 2004), which is in line with our measurements on the location of the EZ and its edge region.

However, some differences have been found as well. For example, the stability of flat lattices in cells like HeLa, is highly controlled by the actin cytoskeleton (Grove et al., 2014; Leyton-Puig et al., 2017; Saffarian et al., 2009), while interfering with the actin cytoskeleton does not affect the presence of the EZ (Chapter 4). However, in neurons, the EZ is tightly coupled to the PSD via a shank-homer1c-dynamin-3 interaction. This PSD-EZ coupling appears to be the primary mechanism for retaining the EZ near the PSD, and could diminish the need for the actin cytoskeleton for maintenance. To further elucidate actin contribution, it would be necessary to determine whether altering actin dynamics affects EZ stability. Another, more physical concern could be raised as well. The energetically favored conformation of clathrin is a dome-like assembly. Therefore, flat clathrin lattices have to be actively kept in a flat conformation. If neither membrane interactions nor actin cytoskeleton are involved in maintenance of the EZ (Chapter 4), how would clathrin be kept in a flat lattice-like structure at the EZ? Moreover, flat lattices require a flat membrane surface to form, but spines are highly curved, which would make a stable flat clathrin conformation physically impossible. Perhaps, this is the reason why clathrin structures in early development are transient, and are only stabilized at mature synapses (Blanpied et al., 2002). The early stages of development are characterized by immature filopodia and thin spines (Matsuzaki et al., 2001; Meyer et al., 2014; Nusser et al., 1998; Straub and Sabatini, 2014), that would physically not allow for a flat lattice to form and stabilize. As spines mature, they grow in size leaving enough space and perhaps a relatively flat surface for stable lattices to form.

Emerging role for plasticity-induced changes in EZ organization

Synaptic plasticity is accompanied by structural changes in spine morphology and synapse organization (Biederer et al., 2017; MacGillavry et al., 2013; Matsuzaki et al., 2001; Meyer et al., 2014; Nusser et al., 1998; Opazo et al., 2012; Tang et al., 2016). However, whether the EZ is subjected to organizational changes during plasticity has not been studied in detail. Early studies showed that cLTD did not affect the presence and stability of clathrin at the EZ, suggesting that clathrin remains tightly localized to the EZ during LTD (Blanpied et al., 2002). One study has shown that LTP induced reorganization of the PSD that was accompanied by the presence of multiple clathrin-coated pits per PSD (Puchkov et al., 2011), however whether this is the results of EZ splitting or new recruitment of clathrin was not determined.

Interestingly, in Chapter 5 we show that cLTP induces splitting of clathrin at the EZ. Moreover, when multiple clathrin structures were observed both of these structures often associated with other endocytic proteins, suggesting that not only clathrin is reorganized, but rather the entire EZ. A similar observation for clathrin was done after mGluR-LTD, however the timescale of reorganization is different (Chapter 4). While mGluR-LTD induces reorganization of clathrin within 5 minutes and appears to be back at baseline after 10 minutes, the effects of cLTP are long lasting. Moreover, cLTD did not alter the organization of endocytic proteins, suggesting that the mechanisms of reorganization are different during LTD and LTP. It is plausible that during LTD the reorganization observed represents vesicle formation, while the reorganization during LTP is an adaptive mechanism to accompany changes in endocytic rate. However, whether this means that during LTP endocytic rate is increased or whether it is an adaptive mechanism for future endocytosis is not known.

Based on our current understanding, it seems unlikely that LTP increases endocytic rate, as LTP is associated with an increase in the number of receptors at the synapse. However, a recent paper based on computational modelling suggested that the endocytic flux during LTP is significantly higher compared to LTD, and the increase in the number of receptors can be explained by a high exocytic flux (Sumi and Harada, 2020). This intriguing hypothesis could explain why the EZ splits in two, as it would adjust to the increased endocytic rate. Moreover, as discussed before, at flat lattices, vesicles are formed at the edge region. Therefore, to accompany possible changes in endocytic rate the EZ might split to significantly increase its edge region thereby increasing endocytic capacity. It would be interesting to see whether LTP indeed induces internalization using a similar assay described in Chapter 3, figure

1. If there is indeed endocytosis during LTP, then what content is endocytosed? Sumi et al. proposes that AMPAR are endocytosed during LTP, but another study revealed that in response to LTP, calcium-activated potassium channels (SK2) are internalized, perhaps via the EZ (Lin et al., 2008; Sumi and Harada, 2020).

Alternatively, EZ splitting could be the result of multi-synaptic spine formation. Multi-synaptic spines are spines that contain multiple PSDs, and are often observed after LTP induction (Berry and Nedivi, 2017; Puchkov et al., 2011; Toni et al., 1999; Toni et al., 2001). This reformation of the PSD is associated with the presence of multiple CCS per spine (Puchkov et al., 2011). Future experiments, should reveal if in our model multi-synaptic spines appear after LTP by visualizing presynaptic sites and super-resolution imaging to resolve the PSD itself.

In conclusion, different plasticity paradigms seem to differentially affect the organization of the EZ. Future studies should look into the possibility that LTP is accompanied by EZ-mediated endocytosis, and should elucidate which components are internalized and how they are trafficked during LTP.

Concluding remarks

In the past decades the underlying mechanisms of receptor trafficking have emerged. While the critical function for the EZ in facilitating receptor trafficking is widely acknowledged, how the EZ is built to sustain endocytosis is not fully understood. In this thesis, we have used a multitude of advanced microscopy techniques and revealed the molecular architecture of the EZ and its functional processes. These novel fundamental insights greatly contribute to our understanding of how the EZ could facilitate local endocytosis and recycling of synaptic glutamate receptors. The current challenge lies within the development of new techniques that allow us to directly visualize endocytic processes in neurons. The ability to visualize endocytosis at the EZ or surrounding regions would provide exciting advances in the field of EZ research. These techniques would allow us to get an in depth understanding of what receptor is internalized via which mechanism after specific activity paradigms. This will be especially powerful in combination with high spatial -and temporal resolution imaging techniques to exactly pinpoint the location of internalization and recycling. Together, these advances would greatly contribute to our understanding of synapse biology and the mechanisms of neuronal communication, that are so important for all brain functions.

REFERENCES

Anggono, V., and Huganir, R.L. (2012). Regulation of AMPA receptor trafficking and synaptic plasticity. Curr Opin Neurobiol 22, 461-469.

Anggono, V., Koc-Schmitz, Y., Widagdo, J., Kormann, J., Quan, A., Chen, C.M., Robinson, P.J., Choi, S.Y., Linden, D.J., Plomann, M., et al. (2013). PICK1 interacts with PACSIN to regulate AMPA receptor internalization and cerebellar long-term depression. Proc Natl Acad Sci U S A 110, 13976-13981.

Berry, K.P., and Nedivi, E. (2017). Spine Dynamics: Are They All the Same? Neuron 96, 43-55.

Biederer, T., Kaeser, P.S., and Blanpied, T.A. (2017). Transcellular Nanoalignment of Synaptic Function. Neuron 96, 680-696.

Blanpied, T.A., Scott, D.B., and Ehlers, M.D. (2002). Dynamics and regulation of clathrin coats at specialized endocytic zones of dendrites and spines. Neuron 36, 435-449.

Carroll, R.C., Beattie, E.C., Xia, H., Luscher, C., Altschuler, Y., Nicoll, R.A., Malenka, R.C., and von Zastrow, M. (1999). Dynamin-dependent endocytosis of ionotropic glutamate receptors. Proc Natl Acad Sci U S A 96, 14112-14117.

Cheng, D., Hoogenraad, C.C., Rush, J., Ramm, E., Schlager, M.A., Duong, D.M., Xu, P., Wijayawardana, S.R., Hanfelt, J., Nakagawa, T., et al. (2006). Relative and absolute quantification of postsynaptic density proteome isolated from rat forebrain and cerebellum. Mol Cell Proteomics 5, 1158-1170.

Cottrell, J.R., Borok, E., Horvath, T.L., and Nedivi, E. (2004). CPG2: A brain- and synapse-specific protein that regulates the endocytosis of glutamate receptors. Neuron 44, 677-690.

Dale, L.B., Bhattacharya, M., Seachrist, J.L., Anborgh, P.H., and Ferguson, S.S. (2001). Agonist-stimulated and tonic internalization of metabotropic glutamate receptor 1a in human embryonic kidney 293 cells: agonist-stimulated endocytosis is beta-arrestin1 isoform-specific. Mol Pharmacol 60, 1243-1253.

Ehlers, M.D. (2000). Reinsertion or Degradation of AMPA Receptors Determined by Activity-Dependent Endocytic Sorting. Neuron 28, 511-525.

Ferguson, S.S., Downey, W.E., 3rd, Colapietro, A.M., Barak, L.S., Menard, L., and Caron, M.G. (1996). Role of beta-arrestin in mediating agonist-promoted G protein-coupled receptor internalization. Science 271, 363-366.

Fourgeaud, L., Bessis, A.S., Rossignol, F., Pin, J.P., Olivo-Marin, J.C., and Hemar, A. (2003). The metabotropic glutamate receptor mGluR5 is endocytosed by a clathrin-independent pathway. J Biol Chem 278, 12222-12230.

Francesconi, A., Kumari, R., and Zukin, R.S. (2009). Regulation of group I metabotropic glutamate receptor trafficking and signaling by the caveolar/lipid raft pathway. J Neurosci 29, 3590-3602.

Grove, J., Metcalf, D.J., Knight, A.E., Wavre-Shapton, S.T., Sun, T., Protonotarios, E.D., Griffin,L.D., Lippincott-Schwartz, J., and Marsh, M. (2014). Flat clathrin lattices: stable features of the plasma membrane. Molecular biology of the cell 25, 3581-3594.

Kirchhausen, T., Owen, D., and Harrison, S.C. (2014). Molecular structure, function, and dynamics of clathrin-mediated membrane traffic. Cold Spring Harb Perspect Biol 6, a016725.

Ko, S.J., Isozaki, K., Kim, I., Lee, J.H., Cho, H.J., Sohn, S.Y., Oh, S.R., Park, S., Kim, D.G., Kim, C.H., et al. (2012). PKC phosphorylation regulates mGluR5 trafficking by enhancing binding of Siah-1A. J Neurosci 32, 16391-16401.

Leyton-Puig, D., Isogai, T., Argenzio, E., Van Den Broek, B., Klarenbeek, J., Janssen, H., Jalink, K., and Innocenti, M. (2017). Flat clathrin lattices are dynamic actin-controlled hubs for clathrin-mediated endocytosis and signalling of specific receptors. Nature Communications 8.

Lin, D.T., and Huganir, R.L. (2007). PICK1 and phosphorylation of the glutamate receptor 2 (GluR2) AMPA receptor subunit regulates GluR2 recycling after NMDA receptor-induced internalization. J Neurosci 27, 13903-13908.

Lin, M.T., Lujan, R., Watanabe, M., Adelman, J.P., and Maylie, J. (2008). SK2 channel plasticity contributes to LTP at Schaffer collateral-CA1 synapses. Nat Neurosci 11, 170-177.

Liu, K., Lei, R., Li, Q., Wang, X.X., Wu, Q., An, P., Zhang, J., Zhu, M., Xu, Z., Hong, Y., et al. (2016). Transferrin Receptor Controls AMPA Receptor Trafficking Efficiency and Synaptic Plasticity. Sci Rep 6, 21019.

Lu, J., Helton, T.D., Blanpied, T.A., Rácz, B., Newpher, T.M., Weinberg, R.J., and Ehlers, M.D. (2007). Postsynaptic Positioning of Endocytic Zones and AMPA Receptor Cycling by Physical Coupling of Dynamin-3 to Homer. Neuron 55, 874-889.

MacGillavry, H.D., Song, Y., Raghavachari, S., and Blanpied, T.A. (2013). Nanoscale scaffolding domains within the postsynaptic density concentrate synaptic AMPA receptors. Neuron 78, 615-622.

Maria Fiuza, C.M.R.G.T.P.A.M.B.N.H., Marcio Baptista, I.M., and Jonathan, G.H. (2017). PICK1 regulates AMPA receptor endocytosis via direct interaction with AP2 a-appendage and dynamin. The Rockefeller University Press J Cell Biol.

Matsuzaki, M., Ellis-Davies, G.C., Nemoto, T., Miyashita, Y., Iino, M., and Kasai, H. (2001). Dendritic spine geometry is critical for AMPA receptor expression in hippocampal CA1 pyramidal neurons. Nat Neurosci 4, 1086-1092.

Meyer, D., Bonhoeffer, T., and Scheuss, V. (2014). Balance and stability of synaptic structures during synaptic plasticity. Neuron 82, 430-443.

Moriyoshi, K., Iijima, K., Fujii, H., Ito, H., Cho, Y., and Nakanishi, S. (2004). Seven in absentia homolog 1A mediates ubiquitination and degradation of group 1 metabotropic glutamate receptors. Proc Natl Acad Sci U S A 101, 8614-8619.

Nusser, Z., Lujan, R., Laube, G., Roberts, J.D., Molnar, E., and Somogyi, P. (1998). Cell type and pathway dependence of synaptic AMPA receptor number and variability in the hippocampus. Neuron 21, 545-559.

Opazo, P., Sainlos, M., and Choquet, D. (2012). Regulation of AMPA receptor surface diffusion by PSD-95 slots. Curr Opin Neurobiol 22, 453-460.

Petrini, E.M., Lu, J., Cognet, L., Lounis, B., Ehlers, M.D., and Choquet, D. (2009). Endocytic trafficking and recycling maintain a pool of mobile surface AMPA receptors required for synaptic potentiation. Neuron 63, 92-105.

Puchkov, D., Leshchyns’ka, I., Nikonenko, A.G., Schachner, M., and Sytnyk, V. (2011). NCAM/spectrin complex disassembly results in PSD perforation and postsynaptic endocytic zone formation. Cereb Cortex 21, 2217-2232.

Pula, G., Mundell, S.J., Roberts, P.J., and Kelly, E. (2004). Agonist-independent internalization of metabotropic glutamate receptor 1a is arrestin- and clathrin-dependent and is suppressed by receptor inverse agonists. J Neurochem 89, 1009-1020.

Rácz, B., Blanpied, T.A., Ehlers, M.D., and Weinberg, R.J. (2004). Lateral organization of endocytic machinery in dendritic spines. Nature Neuroscience 7, 917-918.

Rosendale, M., Julli, D., Choquet, D., and Perrais, D. (2017). Spatial and Temporal Regulation of Receptor Endocytosis in Neuronal Dendrites Revealed by Imaging of Single Vesicle Formation. Cell Reports 18, 1840-1847.

Saffarian, S., Cocucci, E., and Kirchhausen, T. (2009). Distinct Dynamics of Endocytic Clathrin-Coated Pits and Coated Plaques. PLoS Biology 7, e1000191-e1000191.

Scheefhals, N., Catsburg, L.A.E., Westerveld, M.L., Blanpied, T.A., Hoogenraad, C.C., and MacGillavry, H.D. (2019). Shank Proteins Couple the Endocytic Zone to the Postsynaptic Density to Control Trafficking and Signaling of Metabotropic Glutamate Receptor 5. Cell Rep 29, 258-269 e258.

Sheng, M., and Hoogenraad, C.C. (2007). The postsynaptic architecture of excitatory synapses: a more quantitative view. Annu Rev Biochem 76, 823-847.

Sinha, B., Koster, D., Ruez, R., Gonnord, P., Bastiani, M., Abankwa, D., Stan, R.V., Butler-Browne, G., Vedie, B., Johannes, L., et al. (2011). Cells respond to mechanical stress by rapid disassembly of caveolae. Cell 144, 402-413.

Sochacki, K.A., Dickey, A.M., Strub, M.-P., and Taraska, J.W. (2017). Endocytic proteins are partitioned at the edge of the clathrin lattice in mammalian cells. Nature Cell Biology 19.

Straub, C., and Sabatini, B.L. (2014). How to grow a synapse. Neuron 82, 256-257.

Sumi, T., and Harada, K. (2020). Mechanism underlying hippocampal long-term potentiation and depression based on competition between endocytosis and exocytosis of AMPA receptors. Sci Rep 10, 14711.

Tang, A.H., Chen, H., Li, T.P., Metzbower, S.R., MacGillavry, H.D., and Blanpied, T.A. (2016). A trans-synaptic nanocolumn aligns neurotransmitter release to receptors. Nature 536, 210-214.

Taylor, M.J., Perrais, D., and Merrifield, C.J. (2011). A High Precision Survey of the Molecular Dynamics of Mammalian Clathrin-Mediated Endocytosis. 9.

Toni, N., Buchs, P.A., Nikonenko, I., Bron, C.R., and Muller, D. (1999). LTP promotes formation of multiple spine synapses between a single axon terminal and a dendrite. Nature 402, 421-425.

Toni, N., Buchs, P.A., Nikonenko, I., Povilaitite, P., Parisi, L., and Muller, D. (2001). Remodeling of synaptic membranes after induction of long-term potentiation. The Journal of neuroscience : the official journal of the Society for Neuroscience 21, 6245-6251.

Wu, Y., Chen, C., Yang, Q., Jiao, M., and Qiu, S. (2017). Endocytosis of GluN2B-containing NMDA receptors mediates NMDA-induced excitotoxicity. Mol Pain 13, 1744806917701921.

&

Addendum

Nederlandse samenvatting
Curriculum vitae
List of publications
Acknowledgements

NEDERLANDSE SAMENVATTING

Neuronen communiceren door informatie te sturen via het axon en te ontvangen via de dendrieten. De plek waar neuronen contact met elkaar maken en communiceren, wordt een synaps genoemd. Hier communiceren neuronen met behulp van neurotransmitters, die vanuit presynaptische intracellulaire vesikels vrijkomen in de synaptische spleet. Neurotransmitters worden vervolgens gedetecteerd door postsynaptische receptoren die het signaal doorgeven. De efficiëntie van signaaloverdracht kan sterk variëren tussen synapsen en afhankelijk van de activiteit kan de sterkte van synapsen precies worden gemoduleerd. De mogelijkheid van synapsen om sterker en zwakker te worden heet synaptische plasticiteit en is belangrijk voor het vermogen van het brein om te leren en te onthouden. Verandering in synaptische sterkte worden onder andere gereguleerd door het aantal receptoren op het postsynaptische membraan aan te passen. De hoeveelheid receptoren in een postsynaps wordt bepaald door membraantransport processen, waarbij receptoren zich bewegen tussen het oppervlakte van het neuron en intracellulaire compartimenten.

Glutamaterge synapsen zijn geïsoleerd van de rest van de dendriet, waardoor membraantransport lokaal kan worden gereguleerd. Hierbij speelt de postsynaptische endocytic zone (EZ) een cruciale rol door lokaal endocytose van receptoren te faciliteren. De EZ is een structuur gevormd door clathrine eiwitten die stabiel gekoppeld is aan de postsynaptische dichtheid (PSD), een netwerk van eiwitten die nauw verbonden zijn met het postsynaptische membraan. Deze koppeling maakt lokale endocytose mogelijk en ontkoppeling resulteert in verlies van receptoren op het synaptische membraan, wat plasticiteit belemmert. Receptoren die via de EZ worden geïnternaliseerd, gaan een lokaal recyclingmechanisme binnen, waardoor zij terug gebracht kunnen worden naar het synaptische membraan. Hoewel de functie en cruciale rol van de EZ voor synaptische plasticiteit erkent worden, hoe de EZ is opgebouwd om lokale endocytose te kunnen faciliteren is niet bekend.

In het huidige proefschrift maken we gebruik van een groot aantal fluorescentie microscopietechnieken en visualiseren we hoe de EZ is opgebouwd om endocytose te faciliteren. In het eerste deel focussen wij ons op de functie van de EZ. In hoofdstuk 2 beschrijven wij onze huidige kennis over de mechanismen van glutamaatreceptor transport, specifiek de AMPA receptor. We beschrijven hoe AMPA receptoren door de ontwikkeling heen getransporteerd worden en hoe membraan transport in volwassen synapsen via de EZ wordt gereguleerd. In hoofdstuk 3 tonen wij aan dat niet alleen AMPA receptoren, maar ook een ander klasse glutamaatreceptor, namelijk mGluR5, via de EZ endocytose en recycling ondergaat. We laten zien dat de lokale endocytose van mGluR5 mogelijk wordt gemaakt door Shank-eiwitten, die de EZ aan de PSD koppelen. Deze resultaten bieden inzicht in de functie van de EZ als middelpunt voor het reguleren van lokale endocytose en recyclen van glutamaatreceptoren.

In het tweede deel van het proefschrift richten wij ons op de architectuur en dynamiek van de EZ. Wij concentreren ons vooral op het eiwit clathrine, dat tot nu toe wordt beschreven als het belangrijkste eiwit van het EZ. Omdat clathrine de belangrijkste component is van clathrine-gemedieerde endocytose (CME), nemen wij aan dat dit het mechanisme is van endocytose in de EZ. Inderdaad, in hoofdstuk

4 laten wij zien dat eiwitten betrokken bij CME, stabiel verrijkt zijn in de EZ. Daarnaast zien wij dat de EZ zeer nauwkeurig is georganiseerd, waarbij endocytische eiwitten die betrokken zijn bij het initiëren van CME, zich aan de rand van de clathrin structuur bevinden. Deze typische organisatie is vergelijkbaar met bevindingen van clathrine structuren in niet-neuronale cellen. In deze cellen is aangetoond dat de lokalisatie aan de rand van de clathrine structuur ervoor zorgen dat receptor gevangen kunnen worden en endocytose aan de rand van de clathrin structuur wordt geïnitieerd. In hoofdstuk 5, laten we vervolgens zien dat synaptische activiteit de organisatie van de EZ verandert. Tijdens synaptische verzwakking zien wij twee clathrine structuren geassocieerd met de PSD. De aanwezigheid van twee structuren is echter van korte duur, wat mogelijk suggereert dat er endocytose plaats vindt en de tweede structuur een vesikel is. Echter, de meest verrassende bevinding is dat tijdens het sterker worden van een synaptische connectie de EZ zich lijkt te splitsen. Deze reorganisatie is van lange duur, wat suggereert dat beide structuren stabiel zijn. In recente literatuur wordt de hypothese gesteld dat tijdens het versterken van een synaptische connectie de hoeveelheid receptoren dat wordt geïnternaliseerd verhoogd is. Onze bevindingen zouden deze hypothese ondersteunen. Om de endocytische capaciteit te verhogen moet de EZ in twee splitsen om zo te kunnen voldoen aan de verhoogde hoeveelheid endocytose.

De bevindingen in dit proefschrift bieden nieuwe fundamentele inzichten in hoe de EZ is opgebouwd om endocytose van glutamaatreceptoren te faciliteren. Deze inzichten geven ons een breder begrip van synaps biologie en kunnen toekomstig onderzoek naar de mechanismen van receptor transport ondersteunen.

CURRICULUM VITAE

Lisa Adrianne Elisabeth Catsburg was born on the 26th of August 1993 in Zeist, the Netherlands. In 2010 she finished her high school education (HAVO) at the Christelijk Lyceum Zeist. Because of her broad interest in biology and chemistry she decided to study Life Sciences and Chemistry, at the University of Applied sciences in Utrecht. After one year she focused her studies on Life Science and Zoology for the remaining 3 years. During her studies she was engaged in extracurricular activities, as she was the secretary of a study-related student society, member of the educational committee and chairman of an activity committee within the student society. In 2014, she went abroad for an internship at the university of Lille, France, where she investigated the underlying mechanisms and onset of brain disease. This internship was finished successfully, after which she obtained her bachelor degree. That same year she started as a zoological research technician at the Amsterdam Medical Center in the department of reproductive biology. Motived by her specific interesting in brain disease, she continued her education in 2015, at the University of Amsterdam with a master in Molecular Neuroscience. During her first internship she applied molecular techniques to study the onset of a degenerative eye disease using stem cells, in the lab of prof. dr. Arthur Bergen at the Amsterdam Medical Center. This internship was followed by a second internship in the lab of dr. Harm Krugers at the University of Amsterdam, where she studied the effect of stress hormones on memory formation and consolidation. In 2017, she obtained her Master's degree after finishing a writing assignment under the supervision of dr. Harold MacGillavry at Utrecht University. That same year she started her PhD in the group of dr. Harold MacGillavry at the department of Cell biology, Neurobiology and Biophysics at Utrecht University, of which the results are presented in the current thesis.

LIST OF PUBLICATIONS

2021 **Dynamics and nanoscale organization of the postsynaptic endocytic zone at glutamatergic synapses** – Lisa A.E. Catsburg, Manon Westra, Annemarie van Schaik, Harold D. Macgillavry – Under review - preprint available on BioRxiv: DOI 10.1101/2021.02.18.431766

2020 **Temporal quantitative proteomics of mGluR-induced protein translation and phosphorylation in neurons** - Charlotte AGH van Gelder, Renske Penning, Tim S Veth, Lisa A.E. Catsburg, Casper C Hoogenraad, Harold D MacGillavry, Maarten Altelaar. DOI: 10.1074/mcp.ra120.002199

2020 **ORANGE: A CRISPR/Cas9-based genome editing toolbox for epitope tagging of endogenous proteins in neurons** - Jelmer Willems, Arthur P. H. de Jong, Nicky Scheefhals, Eline Mertens, Lisa A. E. Catsburg, Rogier B. Poorthuis, Fred de Winter, Joost Verhaagen, Frank J. Meye, Harold D. MacGillavry. DOI: 10.1371/journal.pbio.3000665

2019 **AMPA receptor trafficking in the developing and mature glutamatergic synapse. Synapse Development and Maturation** – Comprehensive developmental neuroscience. Elsevier. Page: 507-525 - Lisa A.E. Catsburg and Harold D. MacGillavry. DOI: 10.1017/CBO9781107415324.004

2019 **Shank proteins couple the endocytic zone to the postsynaptic density to control trafficking and signaling of metabotropic glutamate receptor 5** - Nicky Scheefhals, Lisa A.E. Catsburg, Margriet L. Westerveld, Thomas A. Blanpied, Casper C. Hoogenraad, Harold D. MacGillavry. DOI: 10.1016/j.celrep.2019.08.102

2018 **A practical blueprint to systematically study life-long health consequences of novel medically assisted reproductive treatments** - Mulder CL, Serrano JB, Catsburg LAE, Roseboom TJ, Repping S, van Pelt AMM - Human Reproduction. DOI: 10.1093/humrep/dey070

2017 **Effect of corticosterone on mild auditory fear conditioning and extinction; role of sex and training paradigm** - Lesuis SL, Catsburg LAE, Lucassen PJ, Krugers HJ. DOI: 10.1101/lm.047811.118

2017 **Stem cell derived retinal pigment epithelium: The role of pigementation as maturation marker and gene expression profile comparison with human endogenous retinal pigment epithelium** - Bennis A, Jacobs JG, Catsburg LAE, Ten Brink JB, Koster C, Schlingemann RO, van Meurs J, Gorgels TGMF, Moerland PD, Heine VM, Bergen AA. DOI: 10.1007/s12015-017-9754-0

2017 **Long-term health in recipients of transplanted in vitro propagated spermatogonial stem cells** - Mulder CL, Catsburg LAE, Zheng Y, de Winter- Korver CM, van Daalen SKM, van Wely M, Pals S, Repping S, van Pelt AMM. DOI: 10.1093/humrep/dex348

ACKNOWLEDGEMENTS

En dan ben ik ineens aangekomen bij het schrijven van het dankwoord. Het voelt als de dag van gister dat ik vol energie begon aan het avontuur van promoveren. Want ja, een avontuur was het zeker, en zoals bij elk avontuur weet je van tevoren nooit goed wat je te wachten staat. Maar wat ben ik trots op alles wat ik de afgelopen 4 jaar heb behaald. Ik heb ervaren dat wetenschap veel meer is dan alleen onderzoek doen. Het is veelzijdig en hard werk dat om een hoop creativiteit, goede communicatie en doorzettingsvermogen vraagt, en laten we eerlijk zijn, vaak ook gewoon een hoop geluk. Maar misschien wel het belangrijkste zijn de mensen die het allemaal mogelijk maken en met wie je de ervaring deelt. Daarom wil ik hieronder iedereen bedanken die op zijn of haar eigen manier mij heeft geholpen de afgelopen jaren.

Als eerst wil ik Harold bedanken. Ik heb het al eerder gezegd, maar ik had mijzelf geen fijner lab kunnen wensen. Als jij nieuwe mensen zoekt voor het lab, kijk jij niet alleen naar cv, skills en motivatie maar weet je ook precies de mensen eruit te pikken die goed in de groep passen. Dit heeft ervoor gezorgd dat er altijd een hele fijne en open sfeer hing in het MacGillavry lab en we hebben met z’n allen een hoop plezier gehad. Daarnaast heb ik ontzettend veel van je geleerd. Waar mijn verhaallijnen vaak alle kanten op gingen, wist jij duidelijke structuur aan te brengen. Ook heb je mij laten inzien dat onderzoek niet alleen om grote doorbraken gaat, maar dat juist die kleine stapjes belangrijk zijn, en het ook zeker waard zijn om enthousiast van te worden. Ik wens je heel erg veel succes met je geweldige lab en ik hoop nog veel van je te horen!

Lukas, ik ben je erg dankbaar voor je hulp tijdens mijn hele promotie traject. Je kritische blik en vragen tijdens mijn presentaties hebben mij erg geholpen met het nadenken over mijn projecten. Ook je opmerking tijdens mijn commissie meeting afgelopen jaar is mij erg bijgebleven. Je zei namelijk tegen mij: sta met overtuiging achter wat je zegt en uitlegt, je mag wel wat meer lef tonen. Deze opmerking is mij erg bijgebleven en ik hoop dat ik dit heb kunnen toepassen in dit proefschrift en duidelijk zal worden tijdens mijn verdediging.

Ook wil ik de rest van mijn promotie commissie bedanken. Anna & Corette, bedankt voor het lezen van mijn proefschrift en voor jullie scherpe blik op mijn onderzoek tijdens de maandag en vrijdag meetings. Helmut Kessels, Elly Hol en Judith Klumperman, bedankt voor het nauwkeurig lezen en beoordelen van mijn proefschrift. David Perrais, thank you for reading my dissertation and joining us during the defense. I look forward to our discussion.

To everyone in MacGillavry lab I would like to say: you have made the past 4 years amazing, and thanks for all the fun times! From lunches, coffee breaks, walks and borrels, I could always count on you to have a great time. I also truly appreciate our work discussions, where there were critical views, but it was also allowed to make mistakes (in my case, say stupid or non-cohesive things). Nicky, ik kijk met heel veel plezier terug aan onze de tijd dat we nog naar het lab kwamen en ik altijd letterlijk bij jou aan kon kloppen. Die praatdeur was echt zo handig. Bij jou kon ik altijd terecht met mijn vragen en voor een eerlijke mening over mijn posters, thesis cover en ook data. Wij konden altijd goed discussiëren over de data en het samenwerken tijdens de revisies was echt ontzettend leuk! Daarnaast was je niet alleen een hele fijne collega, maar ben ik ook een vriendin rijker! Ik heb erg genoten van het tripje naar Lausanne, de vele koffie wandelingen en borrels, bedankt voor alles. Gelukkig zijn die momenten niet voorbij en ik weet zeker dat wij elkaar nog vaak gaan zien. Als laatste natuurlijk bedankt voor het zijn van mijn paranimf, het is fijn om te weten dat ik naar mijn verdediging toe iemand naast me heb staan die altijd eerlijk zal zijn en mij af en toe een scheutje zelfvertrouwen kan geven. Manon, als eerst bedankt voor al het scripten dat je voor mij hebt gedaan. Het paper had niet bestaan zonder jou, want wat jij kan in matlab had ik je nooit na kunnen doen! Ik heb daar echt zoveel bewondering voor! En laten we de glamorous Lab Girls niet vergeten! Wat hebben we daar een lol mee gehad, dit was echt fantastisch en zal ik nooit vergeten! Daarnaast waren onze koffie en lunch wandelingen naar de plaatselijke kinderboerderij waar we de jonge geitjes en biggetje bewonderden altijd gezellig. Ik hoop ook zeker dat wij elkaar nog vaak blijven zien, en laten we de lunch wandelingen er in ieder geval inhouden! Heel veel succes met de laatste lootjes, je kunt het! Jelmer, ik heb heel veel bewondering hoe jij het hele crispr project hebt aangepakt. Je bent er zo creatief mee aan de slag gegaan en vind het knap hoe je de vaak toch lastige techniek heel duidelijk uit kunt leggen. Bedankt dat ik altijd bij je terecht kon met vragen over technieken en experimenten. Ook heb ik vaak met je, en ook om je kunnen lachen. 6 burrito’s! Heel veel succes met het afronden van de laatste dingen! Anna, thank you for your always critical view on my data. You were always able to quickly see the flaws in my experiments and were not shy to tell me that. I truly appreciate that, because it helped a lot with optimizing the experiments and shaping the story to what it is now! But most important, thank you for getting me familiar with the Polish kitchen! I still miss that potato dish (I forgot the name, but it is delicious!) and Polish chocolate. I wish you all the best in Germany and your future career! I am sure you will succeed in everything you are going to do! Arthur, ik heb veel bewondering voor je creativiteit. Je weet experimenten, technieken en presentaties altijd een hele leuke en ingenieuze twist te geven. Ook was jij altijd degene die de meest basale maar zeer belangrijke vragen stelde tijdens presentaties, zoals ‘maar wat is het doel van dit experiment’ of ‘wat verwacht je van hiervan’. Hoewel ik altijd een beetje zenuwachtig werd van deze vragen, hebben ze me erg geholpen met het structureren van het onderzoek en nadenken over de vervolg stappen. Ik wens je heel veel succes met de volgende stappen in je carrière. Yolanda, you are a very open and easy to talk to person and I really like that. You always made me feel like it was okay to ask questions that in my mind felt like a stupid one. I really admire how you try to embrace the Dutch culture and language and try new words every day. Your accent is really good by the way, keep it up! Also, I wish you all the best with the next steps in your career, and I hope we will see each other in the future! Wouter, wat een ambitie heb jij, het is echt bewonderingswaardig. Waar ik vaak denk ‘nee dit kan niet, of nee dit is te moeilijk’ zie jij oneindige mogelijkheden. Ik denk dat dit jou heel ver gaat brengen tijdens je PhD en je carrière daarna! Heel veel succes met alles dat je nog gaat ondernemen! Niels, ik vond het erg leuk dat jij je kennis vanuit alzheimer perspectief meenam naar het lab, dit zorgde vaak voor een ander soort discussie en heeft mij erg geholpen om wat meer translationeel na te denken over mijn project. Ik wens je heel veel succes met je onderzoek!

Thank you to all the members and group leaders of the Cellbiology, Neurobiology and Biophysics department that I haven't mentioned yet. Casper, wij hebben elkaar in totaal 3 keer ontmoet de afgelopen 4 jaar. Tijdens mijn sollicitatie gesprek, de overname van de neuron culture en het gala. Toch wil ik jou ook bedanken voor het geven van deze kansen, en ik wens je heel veel plezier en succes verder in San Francisco. Ginny, thank you for your feedback on my projects during my committee meeting last year, and our conversations during the neuron culture. I wish you all the best and success with your fast growing lab!

Dieudonnée, Jessica, Feline, Xingxiu and Nazmiye, you were amazing office mates. Always in for a chat, office cleanup, and I loved our attempt to green up the office and grow our own food. Those moments I really missed while working at home! Most of us have moved on already and it is fun to see how everyone is doing something completely different now! I wish all of you a lot of luck with everything you are doing! Nazmiye, I really enjoyed our walks, diners and lunches, I hope we can keep doing those things and keep seeing each other! Good luck with all your projects, including your curtains, haha. Robbelien, dezelfde master, departement voor onze PhD en nu allebei in verwachting! Wat is het leuk om deze dingen met jou te kunnen delen. Ik wens je heel veel succes met de laatste lootjes en heel veel geluk in jullie nieuwe huis en met Poppy! Ik kan niet wachten om haar te ontmoeten!

Anne, Roderick, Klara, Marijn, Daphne, Lotte, Carlijn, Dennis, Robin, Sybren, Peter-Jan, Cyntha bedankt voor alle gezelligheid tijdens de wine en cheese avonden en in de Belgische bier bar tijdens de Dutch Biophysics en Dutch Neuroscience conferentie. Heel veel succes met het afronden van de projecten en jullie postdocs. PJ, bedankt voor de fijne samenwerking tijdens het MAP project, ik vond het samenwerken erg leuk en heb er een hoop van geleerd. Ik wens je heel veel plezier bij Jansen! Max, heel veel succes met al je projecten en je grootste project: de neuron culture (grapje, het valt reuze mee). Amélie, Martin, Eitan, Wilco, thank you for all the fun times during the lunches, borrels and many beers on conferences and your openness to discuss data. To all other members of the department: I wish all of you the best with your PhD's or postdoc projects and good luck with all future endeavors.

En degene die ik absoluut niet mag vergeten zijn zij die deze afdeling draaiende houden! Phebe, ik zie jou echt als het stabiele middelpunt van de afdeling. Het is zo fijn wat jij allemaal regelt, en ik hoop dat je weet hoeveel dit gewaardeerd wordt. Ook bedankt voor al je ah pannen en glazen zegels haha, ik heb er nog heel veel plezier van! Ik wens je heel veel plezier en ook succes in deze nog steeds gekke tijd op het lab. Ik hoop dat jullie snel weer terug mogen komen naar het lab en de gezelligheid weer als van oudst zal worden. Bart, het is verfrissend om iemand te hebben die van alles een flauwe grap probeert te maken. Jou flauwe grappen en serie/film ideeën op de vroege maandag ochtend maakte de neuron culture altijd iets om naar uit te kijken en ook tijdens de lockdown was het erg gewaardeerd. Ilya, thank you for everything you taught me about microscopes. Your expertise helped me lot with understanding those difficult setups. Eugene, thank you for our discussions on how to process data or which plugins to use to analyze very specific data.

To the neuron culture team, thank you for being such an amazing team to work with. It was truly a pleasure to organize everything around the culture, but all of you made

it happen! To me it always felt like every Monday morning allowed for 3 hours quality time to get to know each other better and talk about so much random stuff. Thank you for that! A special thanks to Dieudonnée for teaching me everything regarding the culture, and good luck to Max with organizing the cultures in the future!

Ook heel veel dank aan de mensen met wie ik heb mogen samenwerken van andere departementen. Charlotte, bedankt voor je inpunt en nieuwe inzichten over proteomics. Het is een prachtig paper geworden met veel waardevolle informatie, waar ik ook veel inzichten uit heb gehaald voor mijn project. Jan, ik vond het samenwerken met jou erg leuk. Nadenken hoe we twee technieken goed konden samen brengen was aan het begin een uitdaging. Maar het was ontzettend leuk om te zien dat het na wat trial en error toch gelukt is! Helaas kwam de lockdown en hebben het project niet af kunnen maken, maar ik heb er alsnog heel veel van geleerd en kijk er positief op terug.

Ook wil even aandacht besteden aan de studenten die hard hebben meegeholpen. Annemarie, Julia, Laura, Tim, Asha, Daan en Luuk ontzettend bedankt voor jullie harde en goede inzet. Een groot deel van jullie werk is terug te vinden in dit proefschrift en word binnenkort zelfs gepubliceerd. Ik hoop dat ik jullie nieuwe dingen heb kunnen leren tijdens jullie stage en jullie een leuke tijd hebben gehad. Ik heb in ieder geval heel veel van jullie geleerd, heel erg bedankt daarvoor.

Margit, Jasper, Lars, Nielsiieeeh, Tim, Femke, Sterre en Bas, op jullie kan ik altijd rekenen voor een leuke, gezellige en gekke avond waar ik even niet aan het onderzoek hoefde te denken. Van spelletjes spelen en vals spelen tot weekendjes weg naar Ierland, Polen en Slovenië, ik zal ze nooit vergeten, en het zullen ook zeker niet de laatste zijn! Nog even extra aandacht voor Margit. We kennen elkaar inmiddels al 11 jaar! Samen begonnen aan onze bachelor, samen een master en PhD, nu beide bij NWO, en zijn we elkaars paranimf. Het lijkt wel alsof wij hetzelfde leven leiden en daar ben ik zo blij mee. Jij snapt altijd waar ik het over heb en begrijpt bepaalde frustratie en blijdschap als geen ander! Ik ga onze onze PPP (pizza w(h)ine en PhD) avonden met whiteboard missen. Deze avonden hebben altijd weer bewezen dat wijn alles beter maakt! Cheers op onze volgende avonturen! Keshia en Arne, ook jou Keshia ken ik inmiddels 11 jaar. Onze vriendschap heeft z'n ups en down gekend maar we weten elkaar altijd weer te vinden, en ik ben heel erg blij met een vriendin als jij. Onze reizen, stap avonden en diner dates waren altijd een heerlijke afleiden van het werkende leven. Johanna, ik vind het echt jammer dat je nu al een lange tijd aan de andere kant van de wereld woont, maar ik snap het wel! Jij gaat altijd voor hetgeen dat je wilt en dat bewonder ik aan jou! We hebben veel meegemaakt, van studie en de vele feestjes, tot huisgenoten. Ik hoop dat we elkaar binnenkort weer kunnen zien en net zulke gezellige tijden kunnen beleven als vroeger. Evan, hoewel we elkaar niet heel vaak zien, wil ik ook jou bedanken voor de gezelligheid op de momenten dat we gaan lunchen, dineren of wandelen. Sofia, we hebben elkaar tijdens onze laatste master stage ontmoet en het klikte meteen. Ik ben heel blij met een vriendin als jij, altijd eerlijk, open en je staat altijd voor iedereen klaar. Ik ben heel trots op jou, en vind het zo knap dat je bij Philips aan de slag bent gegaan. Je gaat nooit een uitdaging uit de weg. Ik hoop dat wij nog een hoop wijn en kaas avonden gaan hebben, proost! Céline, wij kennen elkaar al 16 jaar en hebben zoveel leuke momenten meegemaakt! Ik vind onze vriendschap heel bijzonder, want ookal zien we elkaar niet vaak, wanneer we elkaar zien is het weer als vroeger en altijd zo vertrouwd! Ik wens jou en Lisanne heel geluk samen! En Lisanne, bedankt dat je me tijdens mijn stress om de thesis cover hebt geholpen!

Carla en Benno, bedankt dat jullie mij zo fijn hebben ontvangen in jullie familie. Jullie warmte en openheid liet mij meteen op mijn gemak voelen en ik wil jullie bedanken voor al jullie support de afgelopen jaren.

Lieve papa, mama, Jesse en Caroline. Waar ik altijd erg veel plezier in heb gehad is het uitleggen wat ik aan het onderzoeken ben, en naarmate mijn uitleg vorderde ik jullie langzaam in gedachten zag afdwalen. Hoewel jullie nooit echt goed hebben begrepen wat ik nou precies doe (I don’t blame you) vond ik het erg leuk dat jullie het toch elke keer weer probeerde en er interesse in toonde. Heel erg bedankt voor alles dat jullie voor mij hebben gedaan en dat jullie er altijd voor mij zijn.

De laatste maar misschien wel de belangrijkste, lieve Mitch. Ik krijg tranen in mijn ogen nu ik aan dit stukje begin. Dit zijn deels hormonen, maar ook omdat ik mij realiseer hoeveel wij hebben meegemaakt de afgelopen jaren en hoeveel mooie momenten er nog gaan komen. Ik ben je zo dankbaar dat je er de afgelopen jaren voor mij was. Je hebt me zien huilen van frustratie en zien lachen van enthousiasme. Ik wil je bedanken voor je eeuwige geduld en je altijd nuchtere kijk op dingen, dit laatste hielp mij altijd erg dingen te relativeren op de moeilijke momenten. Bedankt dat je het PhD avontuur samen met mij bent aangegaan, en ik kan niet wachten op het volgende avontuur dat wij samen met ons kleine meisje gaan beleven.

Lisa